The Use of iPSC-derived Neurons to Investigate the Role of Clusterin Trafficking in Alzheimer's Disease

Evangeline Monroe Foster

Brasenose College
University of Oxford
DPhil Psychiatry
Hilary Term 2021

Thesis submitted for the Degree of Doctor of Philosophy

Supervisors: Prof. Noel Buckley, Prof. Simon Lovestone and Dr. Menelas Pangalos

Abstract

Clusterin's role in neurodegeneration and Alzheimer's disease (AD) remains unclear. Clusterin (CLU) protein expression and trafficking are altered in response to stress; the treatment of rodent neurons with beta-amyloid (Aβ) increases intracellular retention and reduces secretion of clusterin proteins. *CLU* knockdown in rodent neurons provides protection against Aβ-induced toxicity including cell death indicating clusterin may mediate Aβ toxicity.

Although traditionally referred to as a highly glycosylated and secreted protein, clusterin can also be found intracellularly. However, the biogenesis, structure, and functional importance of these intracellular proteins remains debated.

In this thesis, CRISPR/Cas9 genome engineering was used to remove exon 2 from *CLU*, since this exon contains the endoplasmic reticulum (ER) signal peptide required for the generation of glycosylated, secreted clusterin proteins. This generated heterozygous and homozygous exon 2 knockout (KO) iPSC lines. These were then differentiated into neurons and treated with Aβ to compare cellular and genetic responses of KO and control cells.

The data demonstrated that heterozygous KO neurons responded similarly to control neurons when treated with Aβ, displaying both cell death and neurite retraction indicating no altered sensitivity. Furthermore, Aβ treatment, and not neuronal genotype, was identified as the largest contributor to gene expression changes measured by RNA-Seq. In contrast, homozygous exon 2 KO was sufficient to generate intracellular, non-glycosylated clusterin proteins, and prevent secretion. This manifested as reduced sensitivity to Aβ: neurons displayed cell death but no evidence of neurite damage indicating exon 2 KO provides partial protection to iPSC-neurons.

Acknowledgements

Firstly, I would like to offer my gratitude to my supervisors, Prof. Noel Buckley, Prof. Simon Lovestone, Dr. Elena Ribe and Dr Menelas Pangalos. I am incredibly grateful to you for your support, guidance, and wisdom. I feel lucky to have been part of the Lovestone-Buckley lab for so many years, and to have worked with an amazing team of scientists and people. A special thanks must go to the past and present members of the Mechanisms Team led by Elena Ribe: Helen Rowland, Adrià Dangla Valls, Francesca Nicholls, Caroline Woffindale, Anne Hedegaard and Jacqueline Robbins – thank you for always being a welcome sight in the dark basement office.

Mene, I would like to formally thank you and your team at AstraZeneca for all your generous support, help and your ongoing interest in my DPhil, but also in me as a scientist. I credit my visits to Cambridge and Gothenburg in helping me find my confidence to speak about my research. I am also indebted to the kindness of Nigel and Françoise Jones and the generous Valat-Jones Scholarship that was awarded to me. I will forever look back at our meetings with pride and I appreciate the time you both took in supporting me in my DPhil.

Thank you to Prof. Richard Wade-Martins and his team for sharing their amazing iPSC facility with me, and for making me feel part of their lab. Particularly I would like to thank Bryan Ng, Dayne Beccano-Kelly and Brent Ryan for all the hilarious times we have shared in the iPSC facility. I would also like to show my appreciation to Dr. Philip Hublitz for his hard work on this but especially in teaching me so much about CRISPR/Cas9 and to never be afraid of asking questions.

My DPhil experience would be nothing without my friends. Thank you to all those who have been there especially when iPSCs were not behaving (which was often). This

past year has been a challenging one for friendships, but I am so grateful to all the Zoom parties and quizzes we have shared especially when I was writing my thesis. Thank you, to all my friends in London, Oxford, and Durham but especially to Sebastian Birtles, William Glass, Ricky Sengupta, Jack Campbell, Jack Evans, Melissa Bedard, Harry Morgan, Melis Anaturk, Roshaan Koneswaran, Aoife McCourt, Trent Taylor, Catherine Harrison, Sophie Terret, Maura McKeon, and Samantha Gibson. I look forward to a time we can all get together and celebrate all our achievements. I owe a huge debt of gratitude and love to Jiorgos Kourelis. You listened to all my concerns, worries and anxieties over the years and have supported me no matter what. Your passion for science and research spurred me on and I will be grateful for everything that you taught me. I hope I taught you a thing or two about iPSCs and clusterin.

And last, but no means least, I am immensely grateful to my entire family who have supported me in everything I have done. To my siblings, Elliot, Julienne, and Darren, thank you for all your support, hugs, and food. I am grateful for all you have done, especially this last year. To my parents Helen, and Stephen, thank you for supporting me through school and the many degrees that followed. To my father, Stephen, thank you for always encouraging me to read more and giving me my first Neuroscience book, which sparked my interest in studying the brain and its diseases. Lastly, I would like to thank my mother, Helen, who spent many weekends travelling to London and Oxford for retail therapy and reading my numerous applications, CVs, and cover letters. You must have been very glad that I did not ask you to proofread my thesis. Without you both, I would not be the person I am today.

Dedication

I would like to dedicate my thesis to the memory of my mother, Helen Patricia Foster. You taught me to always be kind, think of others and to believe in myself. I hope I have made you proud. Thank you for everything, love you always.

Collaborations

I would like to thank Dr. Philip Hublitz for designing the CRISPR/Cas9 sgRNA used in the generation of the heterozygous exon 2 KO iPSC line. Dr Hublitz ran the Surveyor Nuclease Assay (Chapter 2, sections 2.2.2.1, 2.2.2.2) and bacterial transformations and sequencing of the heterozygous exon 2 knockout iPSC line (Chapter 2, section 2.2.5.3). Dr Hublitz provided figures 3.2B-C and figure 3.7.

I would also thank Dr. Marco Fernandes from the Translational Neuroscience and Dementia Research team for performing the RNA-Seq analysis included in Chapter 5 and for providing the methods (Chapter 2, section 2.2.6.7) and figures (figures 5.5-5.7) included in this thesis.

I am grateful to the team at Synthego who generated and performed the quality control on the homozygous exon 2 knockout iPSC line used in Chapter 6. Methods and figures included in Chapter 6 were provided by Synthego (Chapter 2, section 2.2.2.12, and figures 6.1-6.3).

Declaration Statement

I declare that this thesis is entirely my own work, and except where otherwise stated describes my own research. Content included in Chapter 1 section 1.1 has been adapted from previously published research paper I co-authored alongside Adria DV. This includes modifications of Chapter 1, figures 1.1 and 1.2, which I made for the publication (Foster et al., 2019).

Word count: 43,169

Table of contents

ABSTRACT **2**

ACKNOWLEDGEMENTS **3**

DEDICATION **5**

COLLABORATIONS **6**

DECLARATION STATEMENT **7**

TABLE OF CONTENTS **8**

LIST OF FIGURES **11**

LIST OF TABLES **13**

LIST OF ABBREVIATIONS **14**

1 INTRODUCTION **17**

1.1 CLUSTERIN 17
1.1.1 Overview *17*
1.1.2 Clusterin species and trafficking *18*
1.1.3 Clusterin in cell death and survival pathways *23*
1.2 ALZHEIMER'S DISEASE (AD) 26
1.2.1 Overview *26*
1.2.2 Aβ and AD *26*
1.2.3 CLU and AD risk *29*
1.2.4 Clusterin and Aβ deposition *31*
1.2.5 Clusterin and WNT signalling *33*
1.2.6 Astrocytes, clusterin and AD *34*
1.2.7 Tau, AD and clusterin *36*
1.3 CRISPR/CAS9 39
1.3.1 Overview *39*
1.3.2 CRISPR/Cas adaptive immune system in bacteria *40*
1.3.3 The CRISPR/Cas9 system *41*
1.3.4 DNA repair mechanisms *43*
1.3.5 Off-target editing *44*
1.4 HUMAN INDUCED PLURIPOTENT STEM CELL TECHNOLOGY 46
1.4.1 Overview *46*
1.4.2 Differentiation of human iPSCs into cortical neurons *48*
1.4.3 iPSC models of AD *50*
1.5 AIMS 54

2 MATERIALS AND METHODS **55**

2.1 MATERIALS 55
2.1.1 Cell culture reagents *55*
2.1.2 Mammalian cells *56*
2.1.3 Media formulations *57*
2.1.4 Coating reagents and conditions *58*
2.2 METHODS 59
2.2.1 Human iPSC culture *59*
2.2.2 CRISPR/Cas9 genome engineering *61*
2.2.3 Aβ treatments *74*
2.2.4 Extraction of gDNA for sequencing *75*
2.2.5 PCR and sequencing *76*
2.2.6 RNA analysis *79*
2.2.7 Protein analysis *84*
2.2.8 Imaging *90*

3 OPTIMISATION OF CRISPR/CAS9 PROTOCOLS AND GENERATION OF THE EXON 2 +/- IPSC LINE 97

3.1 INTRODUCTION 97
3.2 RESULTS 100
3.2.1 Generating an optimised CRISPR/Cas9 protocol for excision of CLU exon 2 in human iPSCs 100
3.2.2 Generation and confirmation of a heterozygous exon 2 knockout human iPSC line..... 108
3.2.3 Confirmation of exon 2 +/- pluripotency and the generation of cortical neurons..... 114
3.3 DISCUSSION 118
3.3.1 All factors tested influence Cas9 cleavage efficiency 118
3.3.2 A single heterozygous exon 2 knockout iPSC line was generated from CTR iPSCs 120
3.3.3 Exon 2 +/- iPSCs retain pluripotency and can be differentiated into MAP2 positive neurons 121

4 CHARACTERISING CLUSTERIN MRNA AND PROTEIN EXPRESSION IN EXON 2 +/- IPSCS 122

4.1 INTRODUCTION 122
4.2 RESULTS 124
4.2.1 CLU transcript expression is altered in exon 2 +/- iPSCs..... 124
4.2.2 Expression of total CLU mRNA is similar in exon 2 +/- and CTR iPSCs 126
4.2.3 Clusterin antibodies detect human clusterin in iPSC samples 127
4.2.4 Intracellular clusterin protein immunoreactivity is reduced in exon 2 +/- iPSCs 130
4.2.5 Secretion of clusterin is not altered in exon 2 +/- iPSCs 131
4.2.6 Intracellular and secreted clusterin proteins are glycosylated in human iPSCs 133
4.2.7 Abundance of nuclear and cytoplasmic proteins is not altered in exon 2 +/- iPSCs 134
4.2.8 Non-glycosylated clusterin species exist in the cytoplasm but not the nucleus of iPSCs..... 139
4.3 DISCUSSION 141
4.3.1 Expression of clusterin mRNA and protein is altered in exon 2 +/- iPSCs 141
4.3.2 Immunoreactivity and abundance of non-glycosylated clusterin species is not altered in exon 2 +/- iPSCs..... 142

5 AB_{25-35} TREATMENT OF CTR AND EXON 2 +/- IPSC-NEURONS 144

5.1 INTRODUCTION 144
5.2 RESULTS 145
5.2.1 Exon 2 +/- iPSC-neurons express CLU variant 1 Δ exon 2 transcripts but CTR iPSC-neurons do not 145
5.2.2 Expression of total CLU mRNA is unaltered by CLU exon 2 editing in iPSC-neurons 147
5.2.3 $Aβ_{25-35}$ induces cell death in CTR and exon 2 +/- iPSC-neurons..... 148
5.2.4 $Aβ_{25-35}$ induces neurite damage in CTR and exon 2 +/- iPSC-neurons..... 152
5.2.5 Changes in gene expression in exon 2 +/- iPSC-neurons is similar to that of CTR iPSC-neurons after treatment with $Aβ_{25-35}$ 158
5.3 DISCUSSION 164
5.3.1 $Aβ_{25-35}$ does not alter the expression of CLU variant 1 Δ exon 2 transcripts..... 164
5.3.2 Exon 2 +/- iPSC-neurons respond similarly to CTR iPSC-neurons after treatment with $Aβ_{25-35}$ 165

6 CHARACTERISATION OF EXON 2 -/- IPSCS AND IPSC-NEURON RESPONSE TO AB 167

6.1 INTRODUCTION 167
6.2 RESULTS 169
6.2.1 Generation and quality control of exon 2 -/- iPSCs 169
6.2.2 Exon 2 -/- iPSCs express CLU variant 1 Δ exon 2 transcripts and total CLU transcript expression is reduced 172
6.2.3 Exon 2 -/- iPSCs generate intracellular but not secreted clusterin proteins 175
6.2.4 Clusterin trafficking is altered in exon 2 -/- iPSCs..... 178
6.2.5 Exon 2 -/- iPSC-neurons can be differentiated into neurons 180
6.2.6 $Aβ_{25-35}$ alters trafficking of glycosylated clusterin but not the expression of non-glycosylated clusterin 182
6.2.7 Exon 2 -/- iPSC-neurons exhibit less cell death than CTR iPSC-neurons following treatment with $Aβ_{25-35}$ 187
6.2.8 Exon 2 -/- iPSC-neurons do not display neurite damage following $Aβ_{25-35}$ treatment..... 190

6.3 DISCUSSION 203
6.3.1 Expression of CLU mRNA transcripts and clusterin proteins is altered in exon 2 -/- iPSCs 203
6.3.2 Generating and characterisation of exon 2 -/- iPSC-neurons 204
6.3.3 Aβ$_{25-35}$ treatment alters trafficking of glycosylated clusterin but does not alter abundance of non-glycosylated clusterin species 204
6.3.4 Exon 2 -/- iPSC-neurons are partially protected from Aβ$_{25-35}$ induced toxicity 205

7 DISCUSSION 208

7.1.1 Overview 208
7.1.2 Exon 2 is required for the generation of glycosylated clusterin species 208
7.1.3 Clusterin trafficking facilitates Aβ induced toxicity in human neurons 212
7.1.4 Non-glycosylated clusterin species do not mediate Aβ induced toxicity 215
7.1.5 RNA-Seq analysis can be used to identify novel genes and pathways mediating Aβ toxicity 216
7.1.6 Using neuron models to study clusterin in AD 217
7.1.7 Limitations of using iPSCs to study AD 219
7.1.8 Concluding remarks and summary diagram 225

REFERENCES 227

List of figures

Figure 1.1. CLU mRNA splicing. 20
Figure 1.2. Clusterin gene and protein structure..... 21
Figure 1.3. Schematic diagram of APP processing. 29
Figure 1.4. Schematic diagram of the CRISPR/Cas9 system. 42
Figure 1.5. Cellular DNA repair mechanisms. 44
Figure 2.1. CTR and exon 2 +/- iPSC cultures following thawing. 59
Figure 3.1. Schematic diagram of the dual sgRNA approach used to excise CLU exon 2. 100
Figure 3.2. Surveyor Nuclease Assay confirms 5' and 3' sgRNA efficiently recruit Cas9 in HEK293T cells. 102
Figure 3.3. A heterozygous natural variant was identified in CLU intron 2 in CTR iPSCs. 104
Figure 3.4. Cell density, Cas9 concentration and RNP concentration influence the efficiency of Cas9 cleavage at the CLU exon 2 locus. 108
Figure 3.5. Clone 30 iPSCs are edited at the CLU exon 2 locus. 110
Figure 3.6. Clone 30 cells are heterozygously edited at the CLU exon 2 locus. 111
Figure 3.7. Sequencing following bacterial transformation confirms Clone 30 iPSCs are a heterozygous exon 2 knockout iPSC line (exon 2 +/-). 113
Figure 3.8. CTR and exon 2 +/- iPSCs express pluripotency markers OCT4 and NANOG. 115
Figure 3.9. CTR and exon 2 +/- iPSCs can be differentiated into neurons positive for neuronal marker MAP2 and cortical marker CTIP2. 117
Figure 4.1. Expression of CLU variant 2 is significantly reduced in exon 2 +/- iPSCs. 125
Figure 4.2. CLU mRNA transcript variant 1 Δ exon 2 expression is significantly higher in exon 2 +/- iPSCs than in CTR iPSCs. 126
Figure 4.3. Expression of total CLU mRNA is similar between exon 2 +/- and CTR iPSCs. 127
Figure 4.4. Clusterin antibodies are suitable for detecting human clusterin in iPSC samples. 129
Figure 4.5. Clusterin antibodies are specific to clusterin. 130
Figure 4.6. Intracellular clusterin immunoreactivity is significantly lower in exon 2 +/- iPSCs. 131
Figure 4.7. Secretion of clusterin is comparable between exon 2 +/- and CTR iPSCs. 132
Figure 4.8. Intracellular and secreted clusterin species are glycosylated. 134
Figure 4.9. Clusterin proteins are identified in the cytoplasm of human iPSCs. 136
Figure 4.10. Clusterin proteins are present in the nucleus of human iPSCs. 138
Figure 4.11. Glycosylated and non-glycosylated clusterin species are found in the cytoplasm of human iPSCs. Nuclear clusterin proteins are glycosylated. 140
Figure 5.1. Exon 2 +/- iPSC-neurons express CLU variant 1 Δ exon 2 transcripts. Expression is not altered by $A\beta_{25-35}$. 146
Figure 5.2. Heterozygous exon 2 KO does not alter the expression of total CLU mRNA in human iPSCs. 148
Figure 5.3. Exon 2 +/- iPSC-neurons exhibit similar amounts of death as CTR iPSC-neurons following treatment with 20μM $A\beta_{25-35}$ for 24 hours. 151
Figure 5.4. Exon 2 +/- iPSC-neurons exhibit similar retraction of neurite processes as CTR iPSC-neurons following treatment with 20μM $A\beta_{25-35}$ for 24 hours. 156
Figure 5.5. A heatmap of FPKM expression values in 4 conditions. 161
Figure 5.6. Volcano plots for comparisons between CTR and exon 2 +/- iPSC-neurons. 162
Figure 5.7. KEGG pathway analysis identifies pathway enrichment in 3 of the 4 group comparisons between CTR and exon 2 +/- iPSC-neurons. 163
Figure 6.1. A4 and D1 iPSCs are homozygous exon 2 knockout lines. 170
Figure 6.2. A4 and D1 iPSCs express pluripotency markers OCT4 and SSEA4. 171
Figure 6.3. A4 and D1 iPSCs have no chromosomal abnormalities following CRISPR/Cas9 editing. 172
Figure 6.4. Exon 2 -/- iPSCs express CLU variant 1 Δ exon 2 transcripts but no other CLU mRNA variants. 174
Figure 6.5. Total CLU mRNA expression is significantly reduced in exon 2 -/- iPSCs. 175
Figure 6.6. Intracellular clusterin abundance is significantly reduced in exon 2 -/- iPSCs. Exon 2 -/- iPSCs do not secrete clusterin proteins. 177
Figure 6.7. Trafficking of intracellular clusterin is altered in exon 2 -/- iPSCs. 179
Figure 6.8. Exon 2 -/- iPSCs can be differentiated into neurons comparable to those generated from CTR iPSCs. 182

FIGURE 6.9. $A\beta_{25-35}$ TREATMENT ALTERS TRAFFICKING OF GLYCOSYLATED CLUSTERIN BUT DOES NOT ALTER ABUNDANCE OF NON-GLYCOSYLATED CLUSTERIN SPECIES. 184
FIGURE 6.10. EXON 2 -/- IPSC-NEURONS DO NOT SECRETE CLUSTERIN. $A\beta_{25-35}$ TREATMENT REDUCES CLUSTERIN SECRETION IN CTR IPSC-NEURONS. 186
FIGURE 6.11. 20μM $A\beta_{25-35}$ TREATMENT INDUCES CELL DEATH OF HUMAN IPSC-NEURONS. EXON 2 -/- IPSC-NEURONS DISPLAY LESS DEATH THAN CTR IPSC-NEURONS. 189
FIGURE 6.12. EXON 2 -/- IPSC-NEURONS ARE PROTECTED AGAINST NEURITE DAMAGE INDUCED BY 20μM $A\beta_{25-35}$ TREATMENT. 196
FIGURE 6.13. $A\beta_{1-42}$ DOES NOT INDUCE NEURITE DAMAGE IN HUMAN IPSC-NEURONS. 201
FIGURE 7.1. SCHEMATIC DIAGRAM FOR THE GENERATION OF INEURONS DIRECTLY FROM SOMATIC CELLS AND THE PROGRAMMING OF IPSCS FOLLOWED BY NEURONAL DIFFERENTIATION. 225
FIGURE 7.2. DIAGRAM SUMMARISING RESULTS OBTAINED IN CHAPTER 7 226

List of tables

Table 2.1. iPSC lines for experimental use 57
Table 2.2. sgRNA sequences generated by Dr. Hublitz for editing CLU exon 2. 61
Table 2.3. Primers used to amplify CLU exon 2 locus. 65
Table 2.4. Dilution preparations of Cas9 nuclease for transfection (volumes given per well of cells). 67
Table 2.5. Volumes required for sgRNA preparation (volumes given per well of cells) 68
Table 2.6. sgRNA sequences used to generate the exon 2 -/- iPSC line. 73
Table 2.7. Primer sequences used to identify exon 2 -/- iPSCs following transfection. 73
Table 2.8. Primer sequences used to confirm excision of exon 2 by Sanger Sequencing. 74
Table 2.9. Primer sequences used to amplify gDNA for separation of CLU alleles by agarose gel electrophoresis. 77
Table 2.10. List of RT-qPCR primers. 81
Table 2.11. Sample preparation for western blotting. 88
Table 2.12. List of primary antibodies used in western blotting. 89
Table 2.13. List of secondary antibodies used in western blotting. 90
Table 2.14. List of primary antibodies used in confocal microscopy. 92
Table 2.15. List of secondary antibodies used in confocal microscopy. 93
Table 4.1. RT-qPCR quantification of CLU mRNA transcript variants in CTR and exon 2 +/- iPSCs. 124
Table 5.1. RT-qPCR quantification of CLU mRNA transcript variants in iPSC-neurons. 145
Table 5.2. Key changes in CTR and exon 2 +/- iPSC-neurons in response to $A\beta_{25-35}$ treatment. 157
Table 6.1. RT-qPCR quantification of CLU mRNA transcript variants in CTR and exon 2 -/- iPSCs. 173
Table 6.2. Key changes in exon 2 -/- iPSCs compared to CTR iPSCs. 180
Table 6.3. Key changes in exon 2 -/- iPSC-neurons compared to CTR iPSC-neurons. 187
Table 6.4. Key changes in CTR and exon 2 -/- iPSC-neurons in response to 20μM $A\beta_{25-35}$ treatment. 192

List of abbreviations

Aβ	Amyloid β/β-amyloid
AD	Alzheimer's disease
ACM	Astrocyte conditioned media
AICD	Amyloid intracellular domain
APOE	Apolipoprotein E
APP	Amyloid precursor protein
AraC	Cytosine Arabinoside
BACE1	β-site APP cleaving enzyme 1
BAX	Bcl-2-associated X protein
BMP	Bone morphogenic protein
Bp	Base pair
BSA	Bovine serum albumin
BIN1	Bridging integrator 1
BME	β-mercaptoethanol
BMP	Bone morphogenetic protein
Cas	Cas associated protein
cDNA	Complementary DNA
CAA	Cerebral amyloid angiopathy
CLU	Clusterin
CNS	Central nervous system
CRISPR	Clustered regularly interspaced short palindromic repeats
crRNA	CRISPR RNA
CSF	Cerebrospinal fluid
C_T	Cycle threshold
CTIP2	COUP-TF-interacting protein 2
CTR	Control
CUX1	Cut Like Homeobox 1
DAPI	4',6-diamidino-2-phenylindole
DKK1	Dickkopf-related protein 1
DMSO	Dimethyl sulfoxide
DMEM	Dulbecco's Modified Eagle's Medium
DNA	Deoxyribonucleic acid
dNTPs	Deoxyribonucleotide triphosphate
DPBS	Dulbecco's phosphate-buffered saline
dsODNs	Double stranded oligonucleotides
DSB	Double stranded break
E8	Essential 8 Medium
EDTA	Ethylenediaminetetraacetic acid
EGR1	Early growth response protein 1
ER	Endoplasmic reticulum
EtOH	Ethanol
ET/HD	Ethidium homodimer

fAD	Familial AD
FBF2	Basic fibroblast growth factor
FBS	Fetal bovine serum
FW	Forward
gDNA	Genomic DNA
GAPDH	Glyceraldehyde-3-phosphate dehydrogenase
GFAP	Glial fibrillary acidic protein
GOI	Gene of interest
gRNA	Guide RNA
GWAS	Genome Wide Association Studies
HBSS	Hanks' Balanced Salt Solution
HDR	Homology directed repair
HFIP	1,1,1,3,3,3-hexafluoropropanol-2-ol
HGPS	Hutchinson-Gilford progeria syndrome
HKG	Housekeeper gene
iPSC	Induced pluripotent stem cells
kDa	Kilodaltons
KLF10	Kruppel-like factor 10
KO	Knockout
LB	Laemelli buffer
LRP1/2	Low density lipoprotein receptor-related protein 1/2
LTP	Long term potentiation
MCI	Mild cognitive impairment
mRNA	Messenger RNA
MAP2	Microtubule-associated protein-2
NANOG	Nanog Homeobox
NCBI	National Center for Biotechnology Information
NFTs	Neurofibrillary tau tangles
NHEJ	Non-homology end joining
NIM	Neural Induction Media
NLS	Nuclear localisation signals
NMM	Neural Maintenance Media
NPC	Neural precursor cell
N-PER	Neuronal Protein Extraction Reagent
Nt	Nucleotide
OCT4	Octamer-binding transcription factor 4
P/S	Penicillin-streptomycin
PAM	Protospacer adjacent motif
PBS	Phosphate buffered saline
pCLU	Clusterin precursor protein
PCR	Polymerase chain reaction
PFA	Paraformaldehyde
PSEN	Presenilin

QC	Quality control
Ri	Rock inhibitor
RNA	Ribonucleic acid
RNAi	RNA interference
RNP	Ribonucleotide protein
R. T	Room temperature
RT-qPCR	Reverse transcription quantitative polymerase chain reaction
RV	Reverse
sAD	Sporadic AD
sAPPβ	Soluble APPβ
SDS	Sodium dodecyl sulfate
SEM	Standard error of the mean
SHH	Sonic hedgehog
SMAD	SMA/MAD homology
SNP	Single nucleotide polymorphism
SOX2	Sex determining region-Y-box-2
SSB	Single stranded break
SSEA4	Stage-specific embryonic antigen-4
SVZ	Subventricular zone
sgRNA	Single guide RNA
S100β	S100 calcium-binding protein β
T_m	Primer melting temperature
TALENS	Transcription activator-like effector nucleases
TBR1	T-box brain 1
TBST	Tris-buffered saline with Tween-20 detergent
tracrRNA	Trans-activating CRISPR RNA
TREM-2	Triggering receptor expressed on myeloid cells 2
TUJ1	β III Tubulin
VZ	Ventricular zone
WNT	Wingless/Integrated
WT	Wild-type
ZFN	Zinc-finger nucleases

1 Introduction

1.1 Clusterin

1.1.1 Overview

Clusterin (CLU) is a diverse and multifunctional glycoprotein that is expressed in a variety of tissues including the human brain (de Silva et al., 1990; Rizzi et al., 2009). Much of the work previously conducted on clusterin has focused on its role as a chaperone protein (Humphreys et al., 1999), however, increasing interest has been placed on clusterin's roles in cell death and survival pathways (Kim et al., 2012; Scaltriti, Bettuzzi, et al., 2004a; Scaltriti, Santamaria, et al., 2004b; Takase et al., 2008; Trougakos et al., 2004, 2009; Zhang et al., 2005).

There is a multitude of evidence implicating a crucial role of clusterin in Alzheimer's disease (AD). Clusterin expression is upregulated in the hippocampus and cortex of AD brains, where it co-localises with Aβ plaques (May et al., 1990). Additionally, clusterin is upregulated in the cerebrospinal fluid (CSF) of AD patients (Nilselid et al., 2006) and increased plasma clusterin is associated with hippocampal atrophy and rate of AD progression (Thambisetty et al., 2010, 2011). Several risk genes have now been identified that alter an individual's risk of developing AD later in life, including *APOE* (apolipoprotein E) and *BIN1* (bridging integrator 1). Furthermore, in 2009, two independent Genome Wide Association Studies (GWAS) identified *CLU* as the third most significant genetic risk factor for AD establishing a direct link between clusterin and AD development (Harold et al., 2009; Lambert et al., 2009).

Despite the evidence implicating clusterin in AD, the contribution clusterin plays in the development and pathogenesis of AD is still unclear. Furthermore, it remains debated

whether the increased expression of clusterin in AD brains occurs because of AD development or is directly contributing to AD pathogenesis.

1.1.2 Clusterin species and trafficking

Traditionally, clusterin is referred to as a highly glycosylated and secreted protein but numerous studies have also identified the presence of intracellular clusterin in cellular compartments including the nucleus, cytoplasm and mitochondria (Herring et al., 2019; Leskov et al., 2003; Nizard et al., 2007; Prochnow et al., 2013). However, the transcriptional origin, biogenesis, and functional importance of intracellular clusterin species is debated. The majority of clusterin generated by cells is glycosylated and secreted and arises from the translation of *CLU* mRNA transcript NM_001831.3, otherwise known as *CLU* variant 1 (Prochnow et al., 2013). *CLU* is made up of nine exons (***Figure 1.1***) and three alternative exon 1s have been identified (known as exon 1a, b and c) (Prochnow et al., 2013), which give rise to three distinct *CLU* mRNA transcript variants all containing exon 2. Located within exon 2 is the endoplasmic reticulum (ER) signal peptide that is required for the generation of mature, cleaved, glycosylated and secreted CLU proteins (Wong et al., 1993). Additionally, two nuclear localisation signals (NLS) have been identified in exon 3 and exons 8/9, which transports clusterin to the nucleus (Leskov et al., 2003).

The biogenesis of secreted clusterin is well described (Kapron et al., 1997; Lakins et al., 1998; Rohne et al., 2014; Sabatte et al., 2011; Urban et al., 1987; Wong et al., 1993; Yang et al., 2000) and begins with the translation of *CLU* mRNA variant 1 from exon 2 to generate clusterin preproprotein. Clusterin preproprotein is then trafficked to the ER and Golgi apparatus, where it is cleaved, phosphorylated and glycosylated (Rohne et al., 2016).

Cleavage results in the generation of a heterodimeric protein composed of an α chain and a β chain that are linked by 5 disulphide bonds (Kapron et al., 1997; Urban et al., 1987; Wong et al., 1993). Inside the ER, the ER signal peptide is removed to generate an N-terminal truncated protein. Mature clusterin is then secreted from cells as a heterodimeric 75-80kDa protein consisting of two chains of ~35/40kDa each (Choi-Miura & Oda, 1996; Jenne & Tschopp, 1989; Kirszbaum et al., 1992) (***Figure 1.2***).

In comparison, although several studies have reported the existence of intracellular clusterin in cells, its biogenesis and origin are not well characterised. Leskov et al., identified a *CLU* mRNA variant lacking exon 2 (*CLU* variant 1 Δ exon 2) (Leskov et al., 2003), which generates non-glycosylated clusterin species that reside in the nucleus and cytoplasm of cells (Leskov et al 2003). These proteins are approximately 50/55kDa in size (Leskov et al 2003). However, although the expression of *CLU* variant 1 Δ exon 2 transcripts has been described in some cells (Leskov et al., 2003), expression was demonstrated to be very low in several cell lines (Prochnow et al., 2013) and was not identified in others (Andersen et al., 2007). Therefore, the functional relevance of *CLU* variant 1 Δ exon 2 transcripts and non-glycosylated clusterin species remains unclear.

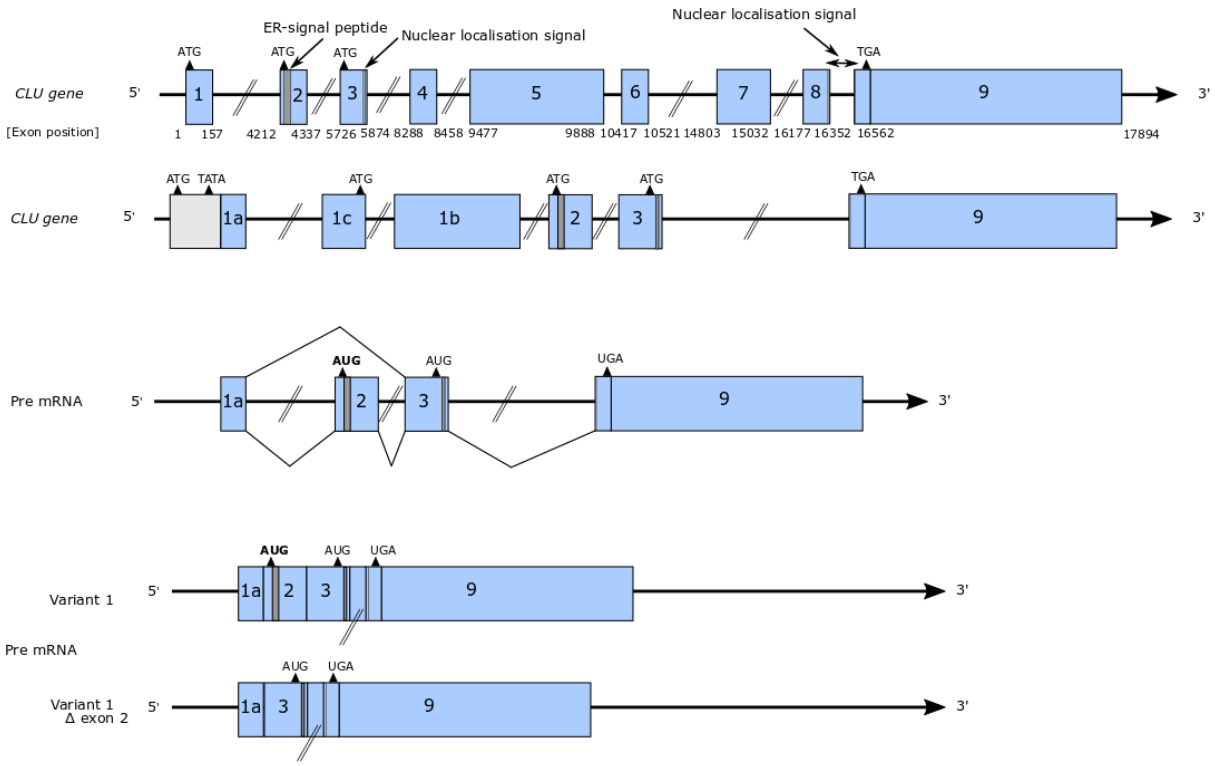


Figure 1.1. CLU mRNA splicing.

CLU is located on chromosome 8 and consists of 9 exons, of which 8 are coding. Located in exon 2 is the ER signal peptide that is essential for the secretion of clusterin from cells and the generation of mature, cleaved, and glycosylated clusterin species. Two nuclear localisation signals (NLS) are located exon 3 and spanning exons 8-9, which direct clusterin to the nuclei. Three alternative exon 1s (referred to as exons 1a, b and c) have been identified in CLU and various CLU mRNA transcripts have also been described. Each alternative exon 1 is spliced alongside exon 2 to generate full-length CLU mRNA transcripts. The majority of CLU expressed by cells is CLU variant 1 that contains exon 1a. Additionally, another variant referred to as CLU variant 1 Δ exon 2 has been demonstrated in cells, this lacks the ER signal peptide since exon 2 is omitted from the mRNA transcript. This figure has been adapted from publication (Foster et al., 2019).

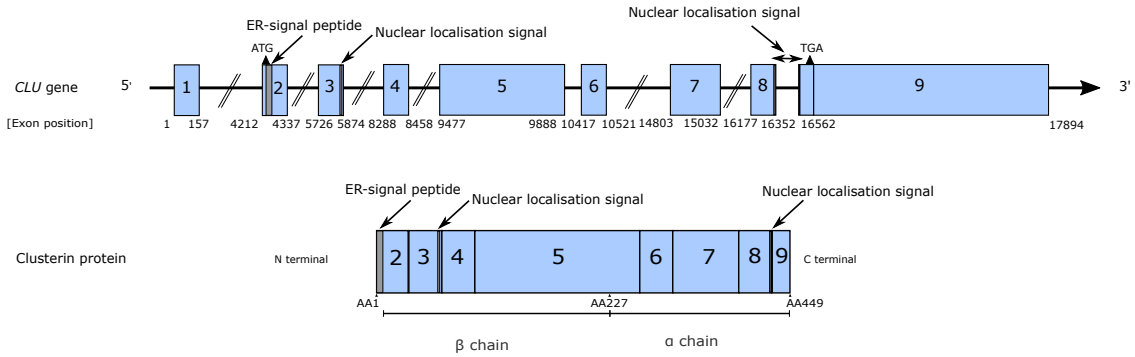


Figure 1.2. Clusterin gene and protein structure.

Translation of CLU mRNA variant 1 is initiated within exon 2 generating an immature preproprotein that contains exons 2-8. This preproprotein contains the ER signal peptide located in exon 2 that controls the trafficking of clusterin preproprotein to the ER and Golgi apparatus where it is phosphorylated, glycosylated, and cleaved. Two additional cleavage events take place, first immediately after the ER signal peptide to generate a truncated N-terminal protein and another between amino acid residues 227 and 228 to generate the α and β chains of clusterin. Mature clusterin now exists as a heterodimeric protein that is highly glycosylated and is secreted from cells. This figure has been adapted from publication (Foster et al., 2019).

In addition to non-glycosylated intracellular clusterin species, several studies have demonstrated the existence of intracellular clusterin species that are glycosylated. This includes mature, glycosylated and cleaved clusterin (Nizard et al., 2007) and an immature 60kDa form that is glycosylated but not cleaved (Zhang et al., 2005). However, it remains unclear what triggers the intracellular retention of these proteins. Several mechanisms have been postulated to explain the localisation of glycosylated clusterin species intracellularly including the premature release of clusterin from the ER/Golgi apparatus prior to secretion (Nizard et al., 2007) and the uptake of clusterin from the extracellular space into cells following binding to cell surface receptors (Ghiso et al., 1993). However, in both cases, it is not clear what triggers these mechanisms or their biological function. Interestingly, a number of studies have demonstrated increased retention of glycosylated

clusterin following cellular stress (Li et al., 2013; Nizard et al., 2007; O'Sullivan et al., 2003; Zhang et al., 2014). This suggests premature release or uptake of clusterin may be triggered by cell stress and death inducing factors such as proteasomal inhibition (Prochnow et al., 2013) and ER stress (Nizard et al., 2007), although it is not known if this is a protective response or facilitates cellular stress.

Clusterin trafficking is altered by $A\beta_{25-35}$ treatment of rodent neurons *in vitro*; secretion is reduced while intracellular retention is increased in the absence of altered *CLU* expression (Killick et al., 2014). This suggests altered clusterin trafficking may mediate Aβ induced toxicity in rodent neurons. This was further supported by the demonstration that *CLU* knockdown protects rodent neurons against Aβ induced cell death (Killick et al., 2014). Furthermore, several *CLU* mutations enriched in AD cohorts (Bettens et al 2012), were demonstrated to alter the trafficking and subcellular localisation of clusterin demonstrating a potential mechanism by which *CLU* variants may increase the risk of developing AD (Bettens et al., 2015; Zhou et al., 2014). Interestingly, several of these AD *CLU* mutations were found in *CLU* exon 5 or 6, clustered close to the location of the cleavage site that generates the β and α chains of clusterin. Three mutations were confirmed to be non-synonymous and alter the amino acid sequence of clusterin (Bettens et al 2012). For example, mutation p.I303NfsX13 results in the insertion of a premature stop codon, which was predicted to produce an unstable transcript that would be degraded (Bettens et al 2012). This variant also altered the subcellular localisation of clusterin proteins, resulting in an increased abundance in the ER and an absence in the Golgi apparatus (Bettens et al 2015). The p.R338W substitution mutation (C>T) was identified in the disulphide rich region near to the β and α chains of mature clusterin

(Bettens et al 2012) and reduced clusterin secretion while increasing intracellular retention (Bettens et al 2015).

Interestingly, clusterin trafficking is also altered in astrocytes cultured *in vitro* following treatment with $A\beta_{1-42}$ (Nuutinen et al., 2007). The altered trafficking of clusterin was suggested to arise from clusterin's role in mediating Aβ uptake and clearance by astrocytes. This occurred in the absence of cell death suggesting clusterin trafficking is altered to protect cells and is not toxic to astrocytes. These studies have demonstrated that clusterin trafficking *in vitro* is altered by Aβ, however, it is unclear whether this promotes Aβ induced toxicity, or is a protective mechanism. Interestingly, the relationship between Aβ and clusterin trafficking has not been explored in human iPSC-neurons.

1.1.3 Clusterin in cell death and survival pathways

Clusterin has been demonstrated to promote both cell death and provide cytoprotection. These opposing roles of clusterin may arise from the existence of different clusterin species with differing cellular localisations, however, this is very much unexplored in the context of neurodegeneration and most studies have focused on these roles of clusterin in cancer. To explore the cytoprotection conferred by glycosylated clusterin species, Zhang et al., overexpressed glycosylated clusterin to explore how this would alter the sensitivity of cells to a chemotherapeutic agent (Zhang et al., 2005). Cells overexpressing clusterin demonstrated reduced cell death following treatment suggesting glycosylated clusterin species protect cells against apoptosis (Zhang et al., 2005). The authors confirmed that this protection was mediated by immature 60kDa clusterin and not mature clusterin proteins. However, the origin of the 60kDa clusterin species is unclear (Nizard et al., 2007). In agreement, Trougakos et al., demonstrated that glycosylated clusterin species in the cytoplasm of cells bind and stabilise Ku70-BAX complexes to inhibit cell death (Trougakos

et al., 2009). This was further demonstrated by the depletion of glycosylated clusterin species by the use of RNA interference targeting *CLU* exon 2, which resulted in increased cell death and reduced cell growth in cancer cells in the absence of stress (Trougakos et al., 2009). In healthy cells, Ku70 binds to BAX to form a stable complex that blocks the translocation of BAX to the mitochondria (Green, 2004; Moldoveanu et al., 2014). Therefore, proteins that stabilise Ku70-BAX complexes inhibit cell death by reducing BAX translocation to the mitochondria where it would promote apoptosis.

Interestingly, other studies have demonstrated a pro-apoptotic role of clusterin, which is thought to be attributed to non-glycosylated clusterin species. Non-glycosylated clusterin species bind to Ku70 proteins promoting cell death (Leskov et al., 2003; Yang et al., 2000). This prevents the formation Ku70-BAX complexes and facilitates the translocation of BAX to the mitochondria to induce apoptosis. The interaction of Ku70 with clusterin was not demonstrated with secreted clusterin, thus, demonstrating a difference in binding partners between the clusterin species (C.-R. Yang et al., 1999). Leskov et al., confirmed the generation of the 55kDa clusterin species arises from the translation of *CLU* variants lacking exon 2 (*CLU* variant 1 Δ exon 2) and represent non-glycosylated clusterin species located in the nucleus and cytoplasm of cells that is induced following ionising radiation treatment (Leskov et al 2003). Overexpression of ~55kDa clusterin species is sufficient to induce cell death and reduces cell growth in unstressed cells indicating that this clusterin species promotes apoptosis (Yang et al., 2000). A number of studies have demonstrated induction of clusterin expression in the nuclei of cells following increased cell death (O'Sullivan et al., 2003; Scaltriti et al., 2004b), although it remains unclear if the translocation of clusterin to the nucleus arises as a result of death, or if the translocation itself triggers cell death. However, O'Sullivan et al., demonstrated the localisation of

nuclear clusterin in dying cells following DNA fragmentation, indicating nuclear clusterin translocation occurs following the initiation of cell death and may contribute but not trigger apoptosis (O'Sullivan et al., 2003). Another study by Trougakos et al., demonstrated intracellular clusterin may promote or reduce cell death depending on cell type and type of stress (Trougakos et al., 2005). Therefore, it remains unclear how clusterin may promote cell death and provide protection in cells, and what role clusterin plays in the loss of neurons observed in AD brains.

The studies mentioned here indicate intracellular, glycosylated clusterin species protect cells. Interestingly, this contrasts the studies mentioned in ***1.1.2*** that demonstrated increased retention of glycosylated clusterin may mediate Aβ induced cell death. Therefore, it is unclear how clusterin species may contribute to AD development and pathogenesis. Furthermore, little is known of the role of the non-glycosylated clusterin species in neurons and their potential role in Aβ induced toxicity and AD. Given that previous studies have demonstrated a role of non-glycosylated clusterin proteins in facilitating response to cell stress and cell death, it is the aim of this thesis to explore the role of these proteins in Aβ induced toxicity *in vitro*. Specifically, the contribution of glycosylated clusterin proteins and non-glycosylated clusterin proteins will be explored in iPSC-derived neurons to determine how clusterin mediates Aβ induced toxicity in human cells.

1.2 Alzheimer's disease (AD)

1.2.1 Overview

AD is the most common cause of dementia among the elderly, causing between 50-75% of cases (National Institute on Aging, 2019). Improvements in medical care combined with increased life expectancies has resulted in higher incidence rates of AD. Decades of research have improved our understanding of this disease, but much remains unclear, and although there are treatments that can temporarily relieve symptoms there none that can prevent AD onset or slow its progression. Therefore, there is a need to generate better models and methods of studying AD to elucidate pathways and mechanisms contributing to AD risk, development, and pathogenesis.

AD is characterised by cortical atrophy (Ray & Zhang, 2010), synaptic dysfunction (DeKosky & Scheff, 1990; Terry et al., 1991) and progressive cognitive decline (Wilson et al., 1999). Pathologically, AD brains are characterised by the accumulation of Aβ resulting in the formation of extracellular plaques and the intracellular accumulation of hyperphosphorylated tau protein resulting in the formation of neurofibrillary tau tangles (NFTs) (Braak & Braak, 1991; Kosik et al., 1986; Wood et al., 1986).

1.2.2 Aβ and AD

Amyloid Cascade Hypothesis

Although a number of theories have been generated to explain AD, the prevailing theory is the Amyloid Cascade Hypothesis (Hardy & Higgins, 1992; Musiek & Holtzman, 2015; Selkoe & Hardy, 2016). The Amyloid Cascade Hypothesis suggests Aβ is the triggering factor in the development of AD. Specifically, an increase in Aβ production and/or a reduction in Aβ clearance results in increased Aβ levels, Aβ deposition and the formation of Aβ plaques. This downstream leads to the loss of synapses, tau hyperphosphorylation and the

formation of NFTs and ultimately cell death. This hypothesis identified Aβ as the key pathological protein initiating AD.

Major support for the Amyloid Cascade Hypothesis comes from genetic studies involving patients with familial forms of AD, also known as fAD (Hardy & Higgins et al 1992). Mutations have been identified in fAD families in genes coding presenilin 1 (*PSEN1*), presenilin 2 (*PSEN2*) and amyloid precursor protein (*APP*) (Goate et al., et al 1991; Murrell et al., 1991; Mullan., et al 1992; Sherrington et al., 1995; Levy-Lahad et al., 1995; Bertram, 2005; Cruts et al., 2012; *Mutations | ALZFORUM*, n.d.; Tanzi & Bertram, 2005). *APP*, *PSEN1* and *PSEN2* encode proteins involved in the generation of Aβ, supporting the notion that Aβ plays a key role in AD development.

APP processing

Aβ is produced by the sequential cleavage of the transmembrane protein APP by a number of secretase enzymes in either the non-amyloidogenic or amyloidogenic pathway (Haass et al., 2012; Zhang et al., 2011) (***Figure 1.3***). In the non-amyloidogenic pathway, α secretase first cleaves APP within the Aβ domain, thus preventing the formation of Aβ peptides. APP cleavage by α secretase generates soluble APPα (sAPPα) that is secreted from cells, and the 83 amino acid c terminal fragment called CTF83, which is membrane bound. CTF83 is then further cleaved by γ secretase producing P3 peptide and the APP intracellular domain (AICD). It is the amyloidogenic pathway that results in the formation of Aβ peptides. First, APP is cleaved by β secretase often referred to as BACE1, which represents the main form of β secretase found in the brain (Vassar et al., 1999). This generates a 99 amino acid c terminal fragment called CTF99 that remains in the membrane and soluble APPβ (sAPPβ). The CTF99 fragment is further cleaved by γ secretase to generate Aβ peptides of varying lengths due to the presence of different

cleavage sites (Sanders, 2006; Xuemin Xu, 2009). The cleavage of the transmembrane domain of APP by γ secretase produces Aβ peptides of varying lengths depending on the position at which γ secretase cleavages. It is a shift in the species of Aβ peptides generated in the brain that is thought to contribute to AD pathogenesis. The CTF99 fragment will undergo ε-cleavage generating membrane bound Aβ peptides and cytosolic AICD. Then γ secretase will reduce the length of the Aβ peptides generated in a process called tripeptide cleavage where γ secretase cleaves the Aβ peptides and removes 3 amino acid residues at a time. Typically, $A\beta_{40}$ is generated from the tripeptide cleavage of $A\beta_{49}$ > $A\beta_{46}$ > $A\beta_{43}$> $A\beta_{40,}$ in comparison, $A\beta_{42}$ is generated from the tripeptide cleavage of $A\beta_{48}$ > $A\beta_{45}$ > $A\beta_{42}$ (Takami et al., 2009). The predominant species of Aβ generated is the $A\beta_{40}$ species, while it is the less dominant $A\beta_{42}$ species that is thought to be toxic, more prone to aggregation and mediates Aβ plaque formation in AD (Burdick et al., 1992). Several fAD mutations have been demonstrated to be found in the Aβ sequence (Massi et al., 2002) and near to the γ secretase cleavage sites (De Jonghe et al., 2001; Suzuki et al., 1994) resulting in the increased production of $A\beta_{42}$ compared to $A\beta_{40}$ (Citron et al., 1997; Scheuner et al., 1996; Tanzi & Bertram, 2005; Weggen & Beher, 2012, Szaruga et al., 2017). Data from fAD genetic studies thereby provide evidence for a central role of Aβ in AD and provide support for the Amyloid Cascade Hypothesis. Further support arises from Down's Syndrome studies; individual's with Down's Syndrome are born with extra material of chromosome 21, commonly they possess an extra full copy of this chromosome (Lejeune et al., 1959). These individuals also have an increased risk of developing AD, which is suggested to arise due to the increased expression of *APP*, which is located within chromosome 21 (Cataldo et al., 2004; Head et al., 2012).

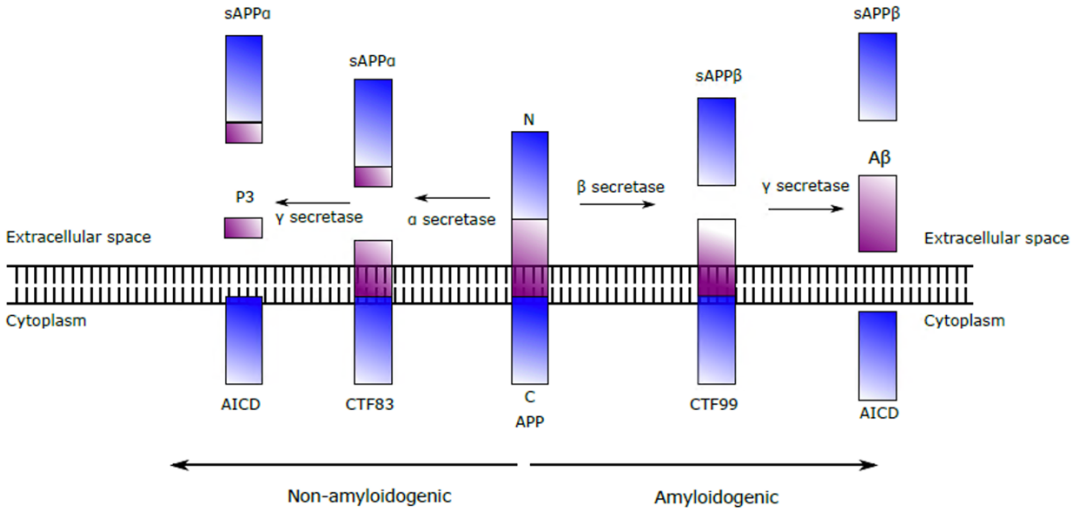


Figure 1.3. Schematic diagram of APP processing.

APP is a transmembrane protein that is cleaved by secretase enzymes in either the non-amyloidogenic or the amyloidogenic pathway. In the non-amyloidogenic pathway, α secretase cleaves APP within the Aβ domain of APP to generate soluble APPα (sAPPα) that is secreted from cells. Additionally, the cleavage of APP by α secretase generates the c terminal fragment CTF83 that is found membrane bound. CTF83 is then cleaved by γ secretase to generate P3 peptide and the APP intracellular domain (AICD) that is found intracellularly. In contrast, if APP is first cleaved by β secretase, soluble APPβ (sAPPβ) is generated and the c terminal fragment CTF99. CTF99 is then cleaved by γ secretase generating AICD and Aβ. The generation of Aβ peptides is via the non-amyloidogenic pathway.

1.2.3 *CLU* and AD risk

As mentioned in ***1.1.1*** there is a multitude of evidence implicating clusterin in AD and a great deal of research has focused on identifying clusterin's role in AD by focusing on clusterin as a genetic risk factor and its relationship with Aβ.

Most AD cases are not caused by a distinct genetic mutation and arises because of a combination of environmental and genetic risk factors. This form of AD is referred to as sporadic AD (sAD). The most significant genetic risk factor for sAD is the *APOE* genotype. There are three different isoforms of *APOE*: *E2*, *E3* and *E4* and possession of an *E4* allele

significantly increases risk of sAD while *E2* significantly reduces sAD risk (Brousseau et al., 1994; Corder et al., 1994; Roses & Saunders, 1994). However, it remains unclear exactly how *APOE* genotype influences AD risk. Numerous genetic studies have now been carried out identifying a number of other genetic sAD risk factors (Carrasquillo et al., 2010; Harold et al., 2009; Lambert et al., 2009, 2013; Naj et al., 2011; Seshadri et al., 2010). In 2009, *CLU* was identified as the third most significant genetic risk factor for sAD (Harold et al., 2009; Lambert et al., 2009). Lambert et al., identified several *CLU* single nucleotide polymorphisms (SNPs) in healthy individuals associated with increased AD risk (rs11136000, rs93318888, and rs2279590). The most commonly occurring *CLU* SNP identified is SNP rs11136000 (Carrasquillo et al., 2010; Harold et al., 2009; Lambert et al., 2009, 2013; Naj et al., 2011; Shuai et al., 2015; S. Zhang et al., 2015, 2016; Zhu et al., 2017). The C allele of rs11136000 increases AD risk (Bertram et al., 2007) and is carried by over 80% of Caucasians (Lambert et al., 2009). Rs11136000 is the most researched *CLU* AD SNP and is associated with brain atrophy (Haight et al., 2018; Thambisetty et al., 2012), mild cognitive impairment (MCI) (Cai et al., 2016) and reduced performance on memory tasks in healthy individuals (Lancaster et al., 2015). However, it is still not known how this SNP increases AD risk. In 2013, the spot of the top *CLU* AD risk SNP was replaced by the newly identified *CLU* SNP rs9331896 (Lambert et al., 2013). Rs9331896 is located in *CLU* intron 2 and exists in linkage disequilibrium with other *CLU* AD SNPs including rs11136000 (Lambert et al., 2013). Interestingly, the majority of the *CLU* SNPs associated with increased sAD risk are located within introns and therefore may alter the *CLU* splicing and protein abundance (Cai et al., 2016; Padhy et al., 2014, 2017; Szymanski et al., 2011; Tan et al., 2016; Xing et al., 2012). However, no functional variant in *CLU* has been identified (Bettens et al., 2010). In 2012, a number of coding mutations in *CLU* exons were identified

in AD patients (Bettens et al., 2012), and a potential functional phenotype of these mutations was later identified (Bettens et al., 2015; Zhou et al., 2014). As discussed in *1.1.2* these mutations increase intracellular clusterin retention while reducing clusterin secretion. However, the functional consequences for most *CLU* variants have not been explored, or the data are inconsistent. It is therefore imperative for research to begin to identify mechanisms by which clusterin contributes to AD risk.

1.2.4 Clusterin and Aβ deposition

Clusterin interacts with Aβ (Ghiso et al., 1993), preventing its aggregation *in vitro* (Matsubara et al., 1996) and alters Aβ solubility and aggregation *in vivo* (Wojtas et al., 2017). Additionally, clusterin directly contributes to the clearance of Aβ through the blood brain barrier and the blood-CSF barrier (Zlokovic, 1996), although the mechanisms are not well described. These studies indicate that clusterin promotes clearance and prevents aggregation and deposition of Aβ, thus, clusterin is a protective protein and prevents Aβ induced pathology. However, data from *in vivo* animal studies appear to suggest that clusterin facilitates the formation of Aβ pathology. DeMattos et al., demonstrated that fibrillar Aβ load was reduced in PDAPP transgenic mice (mice express human APP carrying the fAD Swedish mutation) in the absence of clusterin (DeMattos et al., 2002, 2004) indicating clusterin facilitates the fibrillization of Aβ in these mice. However, Aβ aggregation was increased in the same mice when both *APOE* and *CLU* were knocked out indicating a relationship exists between these proteins that regulates Aβ aggregation and metabolism (DeMattos et al., 2004). The potential protection observed by DeMattos et al., therefore suggests a redundant or compensatory mechanism by APOE in the absence of clusterin (DeMattos et al., 2002). In another study, clusterin was knocked out of APP/PS1 mice (transgenic mice bearing both an *APP* and a *PSEN1* mutation) and demonstrated a

shift in Aβ deposition from the brain parenchyma to the cerebral blood vessels (Wojtas et al., 2017). This change in deposition was associated with reduced neuritic dystrophy but increased cerebral amyloid angiopathy (CAA). This study therefore demonstrated that clusterin facilitates the formation of dystrophic neurites found around Aβ plaques and the loss of clusterin can directly influence the localisation of Aβ deposition *in vivo*. However, these studies also demonstrate that clusterin knockout (KO) may produce detrimental effects given the shift in Aβ deposition resulting in increased CAA.

Interestingly, a recent study by the same group overexpressed clusterin in the astrocytes of APP/PS1 mice (Wojtas et al., 2020a). This overexpression reduced both the total amount of Aβ but also fibrillar Aβ in the cortex and hippocampus (Wojtas et al., 2020a).This is therefore in disagreement with older studies that demonstrated clusterin facilitates Aβ fibrillization *in vivo*, since clusterin overexpression in astrocytes reduced Aβ fibrillization. More surprisingly, the same study demonstrated increased Aβ plaque load and neuritic dystrophy when clusterin expression was reduced in APP/PS1 mice (Wojtas et al., 2020a). This study therefore appears to indicate that clusterin (of astrocytic origin) is protective and thus, the effect of clusterin may be dependent on its origin (neuronal vs astrocytic), the genetic background of the animals used, and the amount of clusterin expressed. Previously, it was suggested that the molar ratio between clusterin and Aβ is crucial in determining clusterin's role in Aβ pathology (Yerbury et al., 2007). However, this relationship still is not well characterised.

Although interesting, these studies have demonstrated clusterin's effect on Aβ deposition in mice expressing fAD mutations, but it is unclear if the same effects would be demonstrated in mice expressing sAD mutations or wild-type (WT) mice, given that they do not endogenously develop Aβ plaques or pathology. Furthermore, these *in vivo* animal

studies focused solely on Aβ associated pathologies, and there is a lack of behavioural characterisation including cognitive or motor function changes.

Some studies have attempted to determine how clusterin may influence behavioural changes *in vivo*. Qi et al., infused clusterin into the brains of 5xfAD transgenic mice (Qi et al., 2018). These mice develop AD pathology at an early age due to their expression of five AD-linked mutations (three in *APP* and two in *PSEN1*). Clusterin infusion into the brains of these mice improved cognitive function, reduced plaque development and reduced CAA (Qi et al., 2018). Another group also explored the effect of clusterin on preventing Aβ induced cognitive deficits in WT rats. In agreement, co-injection of $A\beta_{1-42}$ oligomers and clusterin into the hippocampi of rats prevented $A\beta_{1-42}$ induced cognitive deficits and neuron loss (Cascella et al., 2013). These studies suggest a role of clusterin in protecting against Aβ induced toxicity. However, Oh et al., bred 5xfAD transgenic mice and clusterin KO mice to study the influence of clusterin in AD pathologies and memory deficits. Mice lacking clusterin developed fewer Aβ plaques and demonstrated improved learning and memory function compared to 5xfAD transgenic expressing clusterin (Oh et al., 2019). Interestingly, after 10 months of ageing the differences were lost and plaque deposition was similar between 5xfAD mice with and without clusterin. Clusterin may therefore mediate early stages of Aβ pathology, however, the loss of clusterin is not sufficient to prevent the development of Aβ pathology in aged mice. Many of these studies have used fAD genetic mouse models, which although recapitulate many features of AD, it is unclear how much they can be translated to work conducted on sAD.

1.2.5 Clusterin and WNT signalling

Clusterin has also been implicated in WNT signalling in relation to Aβ. WNT proteins are secreted glycoproteins that activate WNT/β catenin signalling. Canonical WNT signalling

stabilises β-catenin regulating signal transduction pathways and regulate cell survival (S. Chen et al., 2001) and cell proliferation (Pei et al., 2012; Teo & Kahn, 2010). Activation of WNT/ β-catenin signalling inhibits β secretase therefore preventing cleavage of APP in the amyloidogenic pathway (***Figure 1.3***) (Parr et al., 2015; Tapia-Rojas et al., 2016). This also inhibits tau phosphorylation by its inhibitory effects on GSK-3β activity (Caricasole, 2004; Scali et al., 2006). An imbalance of WNT signalling is observed in ageing and AD, with components of WNT signalling deregulated including a downregulation of WNT and β-catenin and an increase in canonical WNT antagonist, *DKK1*, resulting in the promotion of the WNT/PCP pathway (Palomer et al., 2019). *In vitro*, treatment of rodent neurons with Aβ increases the expression of *DKK1* (Caricasole, 2004; Killick et al., 2014; Purro et al., 2012) and *DKK1* expression has been demonstrated to be essential for Aβ induced tau hyperphosphorylation (Caricasole, 2004) and synapse loss (Purro et al., 2012). Furthermore, it was demonstrated in rodent neurons that treatment with Aβ and DKK1 protein activate a common pathway, the WNT-PCP pathway, which results in upregulation of a number of transcription factors including *ERG1* and *KLF10,* which were demonstrated to be essential for Aβ induced cell death and tau phosphorylation (Killick et al., 2014). Interestingly, clusterin was demonstrated to regulate the induction of *DKK1* expression by $A\beta_{25-35}$ in rodent neurons; silencing of *CLU* prevented the induction of *DKK1* expression and prevented downstream Aβ induced toxicity including cell death (Killick et al., 2014). These studies demonstrate that the activation of the WNT-PCP pathway may be key in regulating Aβ induced toxicity in neurons, and this is regulated by *CLU*.

1.2.6 Astrocytes, clusterin and AD

Astrocytes are a type of glial cell and are the most abundant cell type in the human CNS where they regulate synaptogenesis (Baldwin & Eroglu, 2017), neuronal activity and

synaptic function (Mederos et al., 2018) and neuroinflammation (Colombo & Farina, 2016). Following injury or disease, astrocytes become reactive, and their molecular, functional and morphological properties are altered in a process called reactive astrogliosis (Pekny & Pekna, 2014). Although a protective mechanism in the short term, chronic and abnormal astrogliosis can be detrimental and is linked to diseases including AD. In fact, astrogliosis increases during AD progression linking abnormal astrocytic response and AD pathogenesis (Serrano-Pozo et al., 2011). There is evidence supporting both a protective and toxic function of astrocytes in AD. Reactive astrocytes are found closely associated with Aβ plaques and may provide a protective barrier between neurons and the Aβ plaques (Rossner et al., 2005; Wyss-Coray et al., 2003) and engulf dystrophic neurites reducing damage (Gomez-Arboledas et al., 2018). Therefore, reactive astrocytes may promote protection; indeed, reducing astrocyte activation worsens Aβ plaque pathology in AD mice (Kraft et al., 2013). However, astrocytes were shown to gradually accumulate $A\beta_{1-42}$ positive material resulting in cell lysis and the formation of astrocytic plaques suggesting astrocytes may contribute to Aβ pathology (Nagele et al., 2003).

Additionally, it remains unclear whether astrocytes contribute to Aβ burden or have a crucial role in its metabolism and clearance. Numerous studies have shown that astrocytes express receptors and enzymes involved in the degradation of Aβ (Cahoy et al., 2008; Ries & Sastre, 2016) and both rodent and human astrocytes actively take up the peptide (Koistinaho et al., 2004; Mulder et al., 2014; Nielsen et al., 2009, 2010; Pihlaja et al., 2008, 2011; Wyss-Coray et al., 2003), demonstrating astrocytes may play a key role in reducing Aβ deposition. However, reactive astrocytes express enzymes required to generate Aβ suggesting astrocytic reactivity may actually be pro-amyloidogenic and contribute to Aβ load (Grolla et al., 2013; Veeraraghavalu et al., 2014).

Although neurons express and secrete clusterin, astrocytes are the primary source of clusterin in the human brain (Morgan et al., 1995; Pasinetti et al., 1994; Pasinetti & Finch, 1991) and their role in mediating Aβ deposition and clearance may be mediated through clusterin. Indeed, Nuutinen et al., demonstrated $A\beta_{1-42}$ is taken up by astrocytes *in vitro* resulting in increased intracellular abundance and reduced clusterin secretion in the absence of astrocytic cell death (Nuutinen et al., 2007). This study demonstrates altered clusterin trafficking in response to $A\beta_{1-42}$, which may result from clusterin mediating the uptake of Aβ in astrocytes. Although not well described, clusterin may form a complex with Aβ to facilitate clearance, which may be mediated by the megalin receptor or LRP2, which is expressed by both neurons and astrocytes (Bell et al., 2007; Hammad et al., 1997; Kounnas et al., 1995). Interestingly, the previously mentioned study by Wojtas et al., demonstrated protective effects when clusterin is overexpressed in astrocytes of APP/PS1 mice (Wojtas et al., 2020a). Although not explored, this may suggest a role in astrocytic clusterin in promoting the metabolism and clearance of Aβ therefore reducing aggregation and toxicity. However, others have reported that clusterin inhibits astrocytic uptake of Aβ by astrocytes (Mulder et al., 2014; Nielsen et al., 2010). Therefore, it remains unclear whether clusterin generated by astrocytes has a role in promoting or preventing Aβ induced toxicity, and the mechanisms by which clusterin may mediate the uptake of Aβ by astrocytes is unexplored.

1.2.7 Tau, AD and clusterin

One of the pathological hallmarks identified in the AD brain is the formation of intraneuronal NFTs that are formed of hyperphosphorylated and aggregated tau protein (Braak & Braak, 1991, 1996). The development of NFT pathology follows a distinct and well characterised pattern (Braak et al., 2006); first the tangles appear in the transentorhinal

area, then moving to the limbic areas and the hippocampus and finally into the neocortex (Braak & Braak, 1991, 1996). Tau pathology is closely associated with both AD severity (Nelson et al., 2012) and cognitive decline (Braak & Braak, 1991) highlighting a crucial role of tau in AD. Tau is encoded by the *MAPT* gene and mutations in *MAPT* do not directly cause AD, therefore the use of tau animal models expressing tauopathy related mutations to study AD is questionable (Götz et al., 2018). However, much can still be learnt from these animal models. Several tau KO mice have now been generated all of which show no behavioural abnormalities and are viable (Dawson et al., 2001; Fujio et al., 2007; Harada et al., 1994), although behavioural and motor deficits are observed in aged tau KO mice (Ikegami et al., 2000; Lei et al., 2012). The Amyloid Cascade Hypothesis postulates Aβ is the triggering factor for AD pathogenesis and therefore development of NFTs is downstream of Aβ deposition, Lewis et al., crossed transgenic mice expressing tau mutations with transgenic APP mice and demonstrated an interaction between APP/Aβ and tau that results in the formation of NFTs (Lewis et al., 2001). Rapoport et al., demonstrated tau is required for Aβ toxicity in *vitro*; neurons obtained from tau KO mice are protected against Aβ when cultured *in vitro* (Rapoport et al., 2002). The requirement of tau for Aβ toxicity was later replicated *in vivo,* Roberson et al., crossed APP transgenic mice, which exhibit memory deficits with tau KO mice (Roberson et al., 2007). Heterozygous and homozygous tau KO protected APP transgenic mice from Aβ induced memory deficits and exhibited reduced susceptibility to excitotoxicity. Protection from excitotoxicity was later confirmed in tau KO mice in the absence of an APP transgenic background (Ittner et al., 2010). Although these studies appear to indicate tau facilitates Aβ toxicity both *in vitro* and *in vivo*, other studies have demonstrated the loss of tau augments Aβ pathology in aged mice (Dawson et al., 2010) and reduces outgrowth of

neurons generated from tau KO mice (Dawson et al., 2001). Therefore, it is not clear if tau deficits play differing roles in mice dependent on age and genetic background of the mice.

Many studies examining clusterin's relationship with AD pathology have focused on clusterin's relationship to Aβ, while few studies have examined how clusterin may contribute to tau pathology. Clusterin colocalization has been demonstrated with phosphorylated tau depositions in neurites (Martin-Rehrmann et al., 2005) and with NFTs in the AD brain (Dunckley et al., 2006). Treatment of primary mouse cortical neurons and injection of rats with clusterin demonstrated increased levels of total tau and phosphorylated tau (Martin-Rehrmann et al., 2005). A recent study demonstrated clusterin KO in tau Tg301L mice promotes anxiety and increases tau phosphorylation but does not alter learning and memory demonstrating clusterin KO facilitates tau pathology (Wojtas et al., 2020b).

Clusterin's binding to Aβ has long been known (Ghiso et al., 1993) but more recently, clusterin's direct binding and interaction with tau was also demonstrated (Zhou et al., 2014). This interaction was demonstrated in AD brains, between clusterin, tau and GWAS AD risk factor *BIN1* (bridging integrator protein 1) identifying a direct link between clusterin and tau. However, it is not clear how this interaction is related to AD pathogenesis nor is it clear what the biological function of this interaction is. The same group identified a relationship between *CLU* SNP rs11136000, increased CSF tau and increased CSF clusterin in AD patients, demonstrating a link between *CLU* variants and tau expression. In support, the overexpression of tau in transgenic mice Tg4510 also demonstrated increased clusterin expression in the cortex and hippocampus of these mice (Zhou et al., 2014). These studies therefore demonstrate that the expression of these proteins may be linked, although it is not clear what the mechanism of this link is, or

whether this contributes to AD development or is generated because of AD pathogenesis. Finally, a recent *post-mortem* brain study identified a link between clusterin expression, Aβ and tau pathology (Shepherd et al., 2020). AD brain samples contained higher amounts of insoluble Aβ, increased insoluble tau, increased insoluble and soluble hyperphosphorylated tau. Furthermore, the same samples also contained higher levels of clusterin proteins, which were associated with increased tau pathology. This study provides evidence of direct associations between clusterin expression and both Aβ and tau pathology.

It is clear from studies using animal models, *post-mortem* brain tissue and *in vitro* cell models that clusterin plays a role in mediating AD pathology and toxicity. Although most research focuses on clusterin's relationship to Aβ, there is nevertheless evidence that clusterin also regulates tau pathology. Therefore, clusterin may represent a potential target for therapeutics to ameliorate many features of AD.

1.3 CRISPR/Cas9

1.3.1 Overview

There are a number of methods in which gene function can be interrogated including RNA interference (RNAi) (Elbashir, 2002), Zinc- finger nucleases (ZFNs) (Miller et al., 2007; Urnov et al., 2010), transcription activator-like effector nucleases (TALENS) (Joung & Sander, 2013; Miller et al., 2011), and the **C**lustered **R**egularly **I**nterspaced **S**hort **P**alindromic **R**epeats/**C**RISPR-**as**sociated proteins (**CRISPR/Cas**) system (Jinek et al., 2012, 2013). An increasing number of studies are incorporating the use of CRISPR/Cas9 gene editing to interrogate the function of genes and proteins in cells and in disease. This thesis aims to explore clusterin's relationship with Aβ using human iPSC-derived neurons and

CRISPR/Cas9 gene editing technology. Here, the focus will be placed on the use of the CRISPR/Cas9 system for gene editing, given its use in this thesis.

1.3.2 CRISPR/Cas adaptive immune system in bacteria

The **C**lustered **R**egularly **I**nterspaced **S**hort **P**alindromic **R**epeats (**CRISPR**) system is an adaptive immune system that was first identified in *Escherichia coli (E.coli)* (Barrangou et al., 2007; Ishino et al., 1987). This system provides protection in bacteria and archaea against the insertion of exogenous, foreign material from plasmids and viruses (Grissa et al., 2007; Horvath & Barrangou, 2010). There are two main components of the CRISPR system, DNA repeats and the spacer DNA. Firstly, the repeats are short segments of DNA (around 20bp in length each) that are palindromic (Ishino et al., 1987; Jansen et al., 2002; van Belkum et al., 1998). These are identical to each other and are regularly interspaced and separated by the spacer DNA known as the protospacer (Mojica et al., 1995, 2000). Each protospacer sequence is unique and is identical to viral and bacteriophage DNA (Bolotin et al., 2005; Mojica et al., 2005, 2009; Pourcel et al., 2005). Together the protospacer and the repeat sequences form the CRISPR locus (Mojica et al., 1993). Associated with the CRISPR locus are cas genes that make helicases and nucleases known as cas proteins, which unwind and cut DNA (Jansen et al., 2002).

In the absence of an immune system, when a bacteriophage injects its DNA into bacteria DNA would become integrated and result in the replication of bacteriophages and would ultimately lead to the death of the bacteria. In the presence of the CRISPR system, cas genes are transcribed and translated into the cas complex and the DNA spacers in the CRISPR locus generate CRISPR RNA also known as crRNA (Brouns et al., 2008). Cas proteins and crRNA form a complex and protect the bacteria by binding and cutting foreign DNA to generate a double strand break (DSB) preventing replication (Garneau et al., 2010). At

each instance when the bacteria encounter a novel virus or plasmid, a different subclass of cas protein is activated to insert the foreign DNA sequence into the CRISPR locus forming a new protospacer (Barrangou et al., 2007). Therefore, each protospacer represents a previous invasion of the bacterial cell by foreign DNA and protects bacteria against future interactions with this same DNA sequence. The discovery of the CRISPR system led scientists to identify methods in which the CRISPR/Cas system can be modified and utilised in research to study the function of genes and understand the functional consequences of disease linked gene mutations.

1.3.3 The CRISPR/Cas9 system

The most utilised CRISPR/Cas system used in research is the Cas9 system (Jinek et al., 2012; Sander & Joung, 2014), originally identified in *Streptococcus thermophilus* (Bolotin et al., 2005) and *Streptococcus pyogenes (S. pyogenes)* (Brouns et al., 2008; Nozawa et al., 2011). *S. pyogenes* contains two distinct types of RNA, known as CRISPR RNA (crRNA) and trans-activating CRISPR RNA (tracrRNA) (Deltcheva et al., 2011). The crRNA and tracrRNA complex to form a functional guide RNA (gRNA) that binds and activates Cas9 (Jinek et al., 2012). An additional component of the CRISPR/Cas9 system is the protospacer adjacent motif (PAM). PAMs are short sequences of DNA (typically 2-6bp) that are found immediately after the sequence that is targeted by Cas9 (Bolotin et al., 2005; Mojica et al., 2009). The gRNA screens foreign genetic material for the correct PAM sequence and once identified, Cas9 cleaves the DNA producing a DSB (***Figure 1.4***). Therefore, recognition of the correct PAM sequence is essential for cleavage of DNA by Cas9 (Gasiunas et al., 2012; Jinek et al., 2012). PAMs represent sequences found in the invading virus or plasmid DNA sequence and are not found in the bacterial genome or CRISPR locus. Therefore, this

protects the bacteria and enables the recognition of self and foreign DNA and prevents the cutting of the bacterial CRISPR locus by Cas9 (Westra et al., 2013).

The CRISPR/Cas9 system was demonstrated to be modifiable and therefore can be used to target, cut, and modify any gene locus providing a unique opportunity to study the functional importance of genes and their contribution to disease. It was demonstrated that the crRNA and tracrRNA elements of the Cas9 system can be replaced with a synthetic gRNA to enable recruit of Cas9 to any target gene locus (Jinek et al., 2012). The crRNA component of this synthetic gRNA is modifiable and can be designed for each new target making them specific to a single gene locus. The tracrRNA element remains the same between each gRNA used.

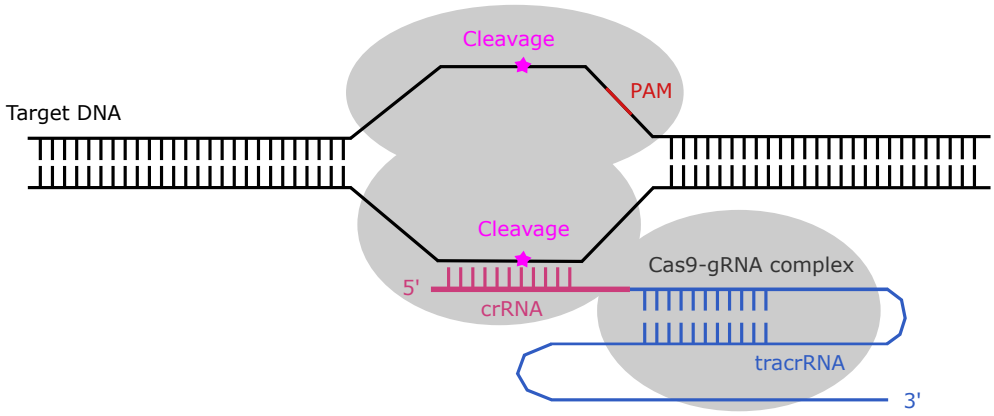


Figure 1.4. Schematic diagram of the CRISPR/Cas9 system.

A guide RNA (gRNA) molecule is generated by the complexing of the crRNA and tracrRNA molecules. This complex binds to Cas9 protein forming the Cas9-gRNA complex in which Cas9 is active. gRNAs screen the target DNA sequence for the correct PAM sequence, after this is identified gRNAs recruit Cas9 to the gene locus. Cas9 binds to the target locus and cuts DNA to generate a DSB. This stimulates the repair of DNA by cellular repair mechanisms. This system can be modified by changing the sequence of the crRNA component of the synthetic gRNA molecule, to target any gene locus for editing.

1.3.4 DNA repair mechanisms

Each Cas9 nuclease contains two active domains, RuvC and HNH, which cleave the complementary and non-complementary DNA strands respectively (Gasiunas et al., 2012; Jinek et al., 2012; Nishimasu et al., 2014). Following the introduction of a DSB, endogenous cellular repair mechanisms are activated to repair the DNA. There are two main pathways identified in cells that perform this function, these are the non-homologous end joining (NHEJ) and the homology directed repair (HDR) pathways (***Figure 1.5***) (Symington & Gautier, 2011). NHEJ is the most active pathway, while HDR plays a primary role in replicating cells (Jackson & Jeggo, 1995; Lee et al., 1997; Takata et al., 1998). NHEJ repairs DNA by ligating of the cut DNA strands together and is therefore likely to introduce random indels, premature stop codons and frameshift mutations. NHEJ is more error prone and is typically used to generate gene knockouts. HDR utilises a sequence of DNA known as the DNA repair template or DNA donor template. This template contains a sequence homologous to that of the DNA sequence that has been cut to provide a template to be used during the repair of the DNA strands. Exogenous repair templates can be delivered into cells, typically as a single stranded or double stranded oligonucleotide sequence or plasmid, to introduce a precise change in the genome and can be used to introduce SNPs or specific gene mutations or revert gene mutations back to WT. In this thesis, the NHEJ pathway will be utilised following the excision of exon 2 to generate *CLU* exon 2 KO models.

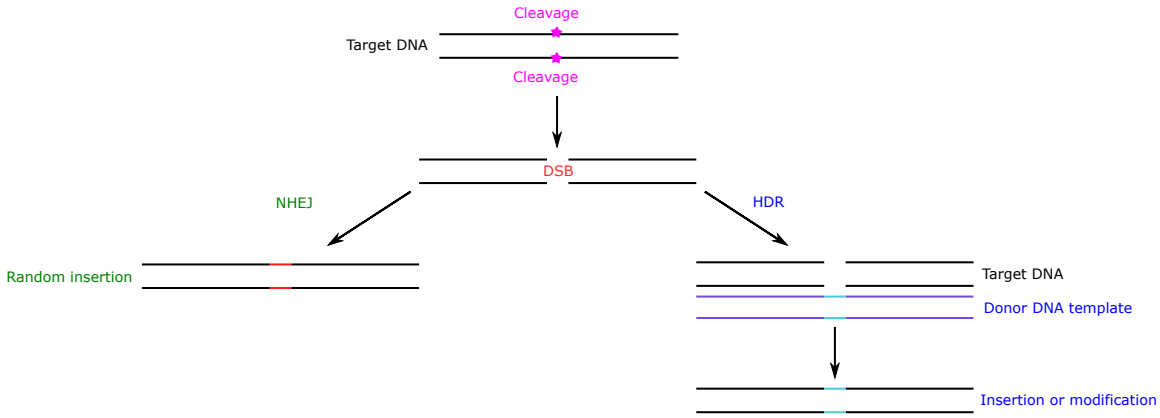


Figure 1.5. Cellular DNA repair mechanisms.

Cas9 binds and cuts DNA to introduce a DSB. This activates cellular repair mechanisms in cells to repair the DNA. Two major pathways are found endogenously in cells: the non-homologous end joining (NHEJ), and the homology directed repair (HDR) pathway. NEHJ is more error prone but is also more active in cells, in this system DNA ends are ligated resulting in the generation of random indels and gene knockouts. The second pathway, HDR, is more precise, but less active and uses DNA templates to repair the DNA. This results in specific insertions or modification at the site of the DSB. Both pathways can be utilised by scientists to edit a desired gene locus.

1.3.5 Off-target editing

The potential to study genes and gene mutations in disease has advanced greatly following the demonstration that the CRISPR/Cas9 system is modifiable. Although this system is considered specific and highly precise, a major concern regarding the use of CRISPR/Cas9 gene editing is the generation of off-target editing. Specificity of the Cas9 system is dependent on the use of an appropriate gRNA and the presence of the correct PAM sequence near to the target gene locus. Despite this, several studies have demonstrated off-target editing still occurs and has been demonstrated to be higher in human iPSCs too (Cong et al., 2013; Fortin et al., 2019; Fu et al., 2013; Hsu et al., 2013; Jinek et al., 2012).

Increased off-target events is associated with reduced cell viability and increased cell toxicity, which has an overall negative influence on cell cultures (Fortin et al., 2019). Several strategies exist for reducing off-target editing.

Several Cas9 variants have been generated to reduce off-target editing generated by Cas9 nucleases. One example is the Cas9 nickase variant. In this variant, either the RuvC or the HNH domain are mutated, and therefore inactivated and Cas9 nickcase will bind to DNA but will not cut it (Cong et al., 2013; Gasiunas et al., 2012; Jinek et al., 2012). Therefore, each single Cas9 nickase can bind to DNA and cut one single strand of DNA generating a single strand break (SSB) depending on which domain was mutated. Paired Cas9 nickases can then be used together, with different gRNA to target the complementary and non-complementary DNA strands independently to generate a DSB. This has been demonstrated to reduce off-target cutting but requires the use of two gRNA to achieve the desired gene editing (Ran et al., 2013).

Other factors influencing Cas9 off-target editing have also been identified, including the delivery method used to introduce Cas9 and gRNA into cells. Delivery of purified Cas9 protein and gRNA as a ribonucleotide (RNP) generates fewer off-target events than plasmids but may negatively impact on editing efficiency (Kim et al., 2014; Ramakrishna et al., 2014). The PAM sequence varies between different Cas9 variants but 5'-NGG-3' is the most used (Jinek et al., 2012) and the requirement of the PAM therefore restricts where Cas9 can bind and where cutting can take place. Studies have attempted to determine how the gRNA sequence may influence the probability of off-target events and have demonstrated the need for careful design and testing of gRNA before use. Although, in theory, gRNA must be complementary to the target sequence, mismatches between these sequences have been demonstrated to be tolerated and still induce Cas9 cutting of

DNA. This increases the probability of off-target Cas9 cutting since mismatches in the DNA sequence can be tolerated. The location of the mismatch may influence if off-target events can occur; for example, a single mismatch located in the 5' end of a gRNA positioned away from the PAM site appear well tolerated whereas mismatches in the seeding region of gRNA are not tolerated (Anderson et al., 2015; Pattanayak et al., 2013). This highlights the need for careful design and testing of gRNA prior to use. Several online programmes can be used to predict locations of off-target editing (Bae et al., 2014; Cradick et al., 2014; Heigwer et al., 2014), however, these are based on statistical models and therefore cannot always accurately predict all off-targets (Tycko et al., 2016).

CRISPR/Cas9 gene editing gives researchers the unique opportunity to generate specific and precise gene alterations at any gene locus and in any cell type or tissue, enabling research and preclinical study of diseases. The potential for CRISPR/Cas9 in research is huge, however, this technique does not come without its limitations. Off-target editing presents not only a challenge in research settings but also presents a problem for the use of CRISPR/Cas9 for *in vivo* editing and gene therapy.

1.4 Human induced pluripotent stem cell technology

1.4.1 Overview

AD is associated with progressive atrophy of the cortex (Ray & Zhang, 2010) and cortical neurons appear selectively vulnerable to AD pathology and dysfunction, although it is not clear why (Braak et al., 2006). Aβ pathology is widespread in the neocortex, entorhinal cortex and hippocampus (Sepulcre et al., 2017; Thal et al., 2002) and NFT pathology progresses in a similar pattern as described by the pattern of neurodegeneration (Braak & Braak, 1991; Bussière et al., 2003; Lewis et al., 1987). Much AD research has utilised animal models and human *post-mortem* brain tissue, and although this has advanced our

understanding of disease mechanisms and pathologies, they have their limitations and do not recapitulate all key aspects of AD including Aβ plaques, NFT, synapse loss and neurodegeneration. Typically, animal models of AD express genes related to fAD development or overexpress *APP* to drive Aβ generation, burden and pathology (Drummond & Wisniewski, 2017) and therefore cannot fully recapitulate sAD, which represents the majority of cases of AD. Furthermore, the use of *post-mortem* brain tissue enables the study of end stage AD but does not inform us of disease progression or functionality. Therefore, better models are needed to study the neurons afflicted in AD brains *in vitro*.

In 2007, it was demonstrated that differentiated, somatic cells can be reverted back to an undifferentiated, embryonic-like state by the use of four transcription factors: *KLF4*, *c-MYC*, *OCT4* and *SOX2*, also known as the 'Yamanaka four' (Takahashi & Yamanaka, 2006). Pluripotency of these cells known as induced pluripotent stem cells (iPSCs) was confirmed and cells were demonstrated to be able to generate cells of each of the three germ layers (Takahashi & Yamanaka, 2006). It was later demonstrated that iPSCs can be generated from human adult fibroblasts (Takahashi et al., 2007). The development of human iPSC technology provides a unique *in vitro* system in which human diseases can be modelled using cells derived from both healthy individuals and disease patients. Furthermore, with the advancement of genome engineering and the development of the modifiable CRISPR/Cas9 system, iPSCs can be edited to introduce mutations, delete genes or sections of genes, and revert disease mutations back to WT. These techniques provide a human derived cell system that can model monogenic and polygenic diseases *in vitro*, and the chance to explore the functional importance of specific genes and proteins in human diseases. Although, the development of iPSC technology has provided major advances in

the ways in which we model human diseases, an important issue associated with iPSC-derived neurons is their maturity. Neurons generated from iPSCs reflect those present in early human embryonic development (Patani et al., 2012), and therefore do not reflect those neurons afflicted in the AD brain. This presents a challenge for researchers who are attempting to model age related diseases including AD *in vitro*. In this thesis, human iPSCs were used to model altered clusterin trafficking *in vitro* to explore clusterin's role in mediating Aβ toxicity in human derived neurons.

1.4.2 Differentiation of human iPSCs into cortical neurons

Protocols have been developed to mimic neural differentiation so that cortical neurons can now be generated from iPSCs *in vitro*. These have adopted two main strategies to generate neurons, the first is the forced expression of transcription factors that are expressed during cortical differentiation, and the second is mimicking developmental cues that mediate cortical development *in vivo*. In this thesis, cortical neurons were generated from iPSCs using the King's College protocol, which is based on the Shi et al., protocol (Shi, Kirwan, & Livesey, 2012; Shi, Kirwan, Smith, et al., 2012). This protocol uses the addition of components into media that stimulates neurogenesis and promotes the differentiation of iPSCs into neurons of cortical lineage and this will be the focus here.

In 2009, Chambers et al., identified that the inhibition of bone morphogenetic protein (BMP) signalling by addition of activin and nodal can be used *in vitro* to inhibit SMAD signalling to initiate neural induction (Chambers et al., 2009). To do so, human embryonic stem cells were cultured in the presence of noggin and SB-431542, which induced neural fate in these cells. This demonstrated that SMAD inhibition was sufficient to induce neural fate in stem cells while the inhibition of BMP signalling alone was not. The

approach of dual SMAD signalling inhibition has formed the basis for many cortical neuron differentiation protocols.

In 2012, Shi et al., described a protocol in which iPSCs could be differentiated into neurons of cortical lineage (Shi, Kirwan, & Livesey, 2012; Shi, Kirwan, Smith, et al., 2012). This was based on the dual SMAD inhibition approach identified by Chambers et al., combined with retinoid signalling. The development of neurons *in vitro* from human iPSCs was compared to neurons generated during cortical neurogenesis *in vivo* to determine how well cortical development was recapitulated. In humans the development of the cortex is around 100 days (Clancy et al., 2001) while *in vitro* the removal of basic fibroblast growth factor (FGF2) from culture medium resulted in cortical neurogenesis over a period of about 70 days (Shi, Kirwan, & Livesey, 2012; Shi, Kirwan, Smith, et al., 2012). During differentiation a cortical neural rosette structure was formed, reminiscent of the cortical neuroepithelium developed *in vivo.* Finally, over a 70-day neural induction period the development of different subtypes of neurons was recorded. During cortical neurogenesis, deep layer neurons (layers 5-6) are generated first followed by upper layer neurons (layers 2-4) (Bystron et al., 2008; Jiang & Nardelli, 2016; Mountcastle, 1998). In the 70 days following removal of FGF2, the first subtype of neurons identified were the TBR1 positive deeper layer neurons (layer 6) followed by layer 5/6 CTIP2 positive neurons and then after 25-30 days upper layer CUX1/BRN2 positive neurons were generated. Finally, at around days 65-80 days, SATB2 upper layer neurons were identified. Therefore, the temporally defined sequence of cortical neuron development *in vitro* resembles those generated in the cortex during development. Importantly, the neurons generated by this protocol were also demonstrated to be functionally active and generate functional excitatory synapses. Further refinement of this protocol led to the replacement of BMP signalling inhibitor

noggin with dorsomorphin to increase protocol efficiency (Shi, Kirwan, & Livesey, 2012; Shi, Kirwan, Smith, et al., 2012). The development of iPSC technology combined with the differentiation of iPSCs into cortical neurons provides a unique opportunity to study neurons afflicted in AD *in vitro* and in a large abundance, additionally, it enables research to be conducted on human derived cells relevant to human disease.

1.4.3 iPSC models of AD

Typically, studies that have used iPSC-neurons to model AD have included iPSC lines generated from fAD patients and typically carry AD causing mutations (Armijo et al., 2017; Duan et al., 2014; Israel et al., 2012; Kondo et al., 2013; Mahairaki et al., 2014; Moore et al., 2015; Muratore et al., 2014; Shi et al., 2012; Sproul et al., 2014; Yagi et al., 2011), but a few have also generated iPSC-neuron lines from sAD patients (Armijo et al., 2017; Duan et al., 2014; Hossini et al., 2015; Israel et al., 2012; Kondo et al., 2013). Various phenotypes have been demonstrated in fAD iPSC-derived neuron lines, including increased $A\beta_{42}$ (Kondo et al., 2013; Yagi et al., 2011) and increased $A\beta_{42:}$ $A\beta_{40}$ ratio (Duan et al., 2014; Muratore et al., 2014; Sproul et al., 2014; Woodruff et al., 2013; Yagi et al., 2011). This resembles phenotypes observed in fAD transgenic animals. An interesting study by Shi et al., generated iPSC lines from Down Syndrome patients and healthy controls and demonstrated the development of $A\beta_{42}$ positive aggregates in cultures of patient cells that were absent in healthy, control cell cultures (Y. Shi, Kirwan, Smith, et al., 2012). This is an interesting approach since the *APP* gene is located on chromosome 21 and overexpression of this gene in Down Syndrome has been linked to early onset AD (Doran et al., 2017), therefore again implicating the importance of Aβ in AD development.

Other studies have attempted to identify AD relevant phenotypes *in vitro* by comparing Aβ metabolism between healthy, control cells and those obtained from both

fAD and sAD patients (Israel et al., 2012). Interestingly, while phenotypes of fAD lines were similar to each other, sAD lines were distinct. Some sAD lines possessed phenotypes resembling those observed in fAD lines, while other sAD lines demonstrated phenotypes resembling those of healthy, control cells. Similarly, Kondo et al., identified phenotypes that were not consistent in all sAD lines, such as increased accumulation of intracellular Aβ oligomers (Kondo et al., 2013). Duan et al., generated various iPSC lines from healthy controls, *APOE E3/E4* with early and late onset AD and those with fAD and compared a number of phenotypes (Duan et al., 2014). This study demonstrated increased $A\beta_{42}$: $A\beta_{40}$ ratio and vulnerability to glutamate induced excitotoxicity in fAD and sAD patient lines with *E3/E4* risk genotypes. Again however, not all sAD patient lines presented similar phenotypes highlighting the heterogeneity of sAD iPSC-neurons. While these studies have demonstrated consistent phenotypes in iPSC-neurons generated from fAD patients this is not the case in studies utilising sAD derived iPSC-neuron lines. This reflects the complexity and heterogeneity of sAD as well as the varied genetic background that may contribute to sAD development in each individual patient. This can make identification of suitable control iPSC lines for projects difficult, especially since genetic backgrounds are likely to vary greatly and, in some cases, may not be explicitly known beyond an *APOE* genotype. Furthermore, it is unclear how easily iPSC lines generated from different sAD patients can be compared to each other.

Several studies have demonstrated the power of combining human iPSC technology and CRISPR/Cas9 gene editing to interrogate gene function, and in identifying consequences of specific disease mutations. Wang et al., generated iPSC neurons from *APOE E3* and *E4* homozygous non-AD individuals and demonstrated increased levels of phosphorylated tau and higher Aβ expression in *E4/E4* neurons than *E3/E3* neurons (Wang

et al., 2018). Interestingly, the same group also generated an isogenic *E3/E3* line by gene editing of an *E4/E4* line. This was demonstrated to rescue the phenotype of the neurons, reducing both tau phosphorylation and Aβ secretion (Wang et al., 2018), therefore highlighting the role of the *E4* genotype in AD pathology but also the unique opportunity that gene editing can bring to iPSC technology studies to demonstrate phenotypes directly related to sAD risk genes. Although this paper did use ZFN technology and not the CRISPR/Cas9 system, the same approach can be achieved using the CRISPR/Cas9 system. Wadhwani et al., generated neurons from patients with the *APOE E4/E3* genotype and demonstrated increased tau phosphorylation and APP processing compared to control iPSCs. CRISPR/Cas9 was then used to generate an isogenic *E3/E3* line, which resulted in the rescue of tau phosphorylation, but Aβ processing was not altered. Additionally, the conversion of *E4/E3* to *E3/E3* made the neurons more resistant to calcium deregulation demonstrating how CRISPR/Cas9 gene editing can be used to study alterations in neuronal sensitivity *in vitro* to stress (Wadhwani et al., 2019). Gene mutations can also be corrected by CRISPR/Cas9, one such study corrected a *PSEN2* point mutation, which reduced the $A\beta_{42}$: $A\beta_{40}$ ratio following gene editing (Ortiz-Virumbrales et al., 2017). These studies demonstrate how CRISPR/Cas9 can be used to alter gene sequences and correct gene mutations, enabling researchers to identify phenotypes of disease lines that are relevant to a specific gene mutation.

Gene editing can also be used to introduce disease associated mutations into control, healthy iPSC lines to directly study the consequence of mutations in non-diseased cells. Paquet et al., used CRISPR/Cas9 to generate iPSCs with both heterozygous and homozygous gene mutations identified in fAD patients (Paquet et al., 2016). The neurons generated from these lines displayed altered Aβ metabolism; an *APP* mutation increased

Aβ production while a *PSEN1* mutation increased the $A\beta_{42}$: $A\beta_{40}$ ratio, resembling phenotypes previously described by others in fAD iPSC lines. In another study, the authors used CRISPR/Cas9 to introduce the same mutations in a range of iPSC lines with an isogenic background to compare phenotypes (Kwart et al., 2019). This study highlights the potential use CRISPR/Cas9 editing to identify differences in phenotypes of iPSCs that differ by a single gene mutation.

AD is a multifactorial, complex and heterogenous disease that in most cases is not caused by a single genetic mutation. However, there are several known risk genes including *CLU* that increase the risk of developing AD. The associations, however, for most genes no functional variant or mechanism by which they increase risk is known. Therefore, better methods and models are needed for us to study the functional consequences of risk variants, and identify how variants alter AD risk, development, and pathogenesis. This will lead to a better understanding of the factors contributing to AD and will ultimately facilitate the identification of better therapeutic strategies. The development of human iPSC technology has enabled the production of large numbers of human derived cells resembling those afflicted in the AD brain that can be studied *in vitro*. This can be then combined with the advances made in recent years in gene editing technology. The combinatory use of human iPSC and CRISPR/Cas9 technology enables researchers to correct mutations in patient lines and rescue phenotypes, knockout genes to study their function and relevance to AD pathology, as well as introduce mutations where no functional consequence has been described. Surprisingly, few iPSC and CRISPR/Cas9 studies have interrogated the relevance of clusterin in AD.

1.5 Aims

As reviewed above, it is still unclear what contribution clusterin plays in neurodegeneration and AD. Although several studies have demonstrated clusterin trafficking is altered by *CLU* mutations and Aβ treatment, there is a lack of understanding if glycosylated clusterin proteins contribute to neuronal sensitivity to Aβ induced toxicity in human derived cells. Additionally, the field highlights the pro-cell death role of non-glycosylated clusterin species in cells but their role in mediating Aβ induced apoptosis in neurons remains unexplored. So far, the modelling of AD using iPSC technology and CRISPR/Cas9 gene editing has focused on identifying changes in neuronal phenotype in the presence of fAD and sAD mutations, with few studies have attempted to find mechanisms by which AD risk genes may promote AD development and pathogenesis. Therefore, the generation of an iPSC line with altered clusterin trafficking by use of CRISPR/Cas9 would enable assessment of the contribution that clusterin species play in mediating Aβ toxicity in iPSC-derived cells *in vitro*.

Research hypothesis*:* It is hypothesised that the removal of *CLU* exon 2 will result in the increased abundance of non-glycosylated clusterin proteins, which will render iPSC-neurons more vulnerable to Aβ treatment.

To this end, the aims of this thesis are:

1. To use CRISPR/Cas9 genome engineering to remove *CLU* exon 2 from iPSCs-derived from a healthy, control individual.
2. To characterise the expression of *CLU* mRNA and clusterin protein species in control, and *CLU* exon 2 lacking iPSCs.
3. To generate and compare the phenotypes of iPSC-derived cortical neurons from control and *CLU* exon 2 lacking iPSCs to Aβ treatment.

2 Materials and Methods

2.1 Materials

2.1.1 Cell culture reagents

AraC (Sigma Aldrich, C1768)

B-27 supplement (50X) serum free containing antioxidants (Life Technologies, 17504044)

B-27 supplement (50X) minus antioxidants (Life Technologies, 10889038)

Biolamina-521 LN (Biolamina, LN521)

DMEM/F12 (Life Technologies, 11320033)

DPBS (+ Ca^{2+}) (Life Technologies, 14040133)

DPBS (- Ca^{2+}) (Life Technologies, 14190094)

Essential 8, E8 (Life Technologies, A1517001)

Geltrex LDEV-Free Reduced Growth Factor Basement Membrane Matrix (Life technologies, A1413202)

GlutaMAX (Life Technologies, 35050038)

Hank's Balanced Salt Solution (Life Technologies, 14025092)

KnockOut DMEM (Life Technologies, 10829018)

Laminin (Sigma Aldrich, L2020, Engelbreth-Holm-Swarm murine sarcoma basement membrane)

LDN-193189 (Sigma, SMLO559)

N-2 supplement 100X (Life Technologies, 17502048)

Neurobasal (Life Technologies, 21103049)

Opti-MEM™ Reduced Serum Medium (ThermoFisher, 31985062)

Poly-D-Lysine Hydrobromide High Molecular Weight (Corning, 354210)

Poly-L-ornithine (Sigma Aldrich, P4957)

Rock(i)/Y-27632 dihydrochloride (ApexBio, A3008)

SB-431542 (APExBIO, A8249)

StemPro Accutase Cell Dissociation Reagent (Life Technologies, A1110501)

TryplE Express Enzyme Solution (Life Technologies, 12604013)

Versene (Life Technologies, 15040066)

2.1.2 Mammalian cells

2.1.2.1 Primary neuronal cultures

Time-mated Sprague–Dawley dams (Charles Rivers, UK Ltd) were sacrificed by cervical dislocation. E18 foetuses were collected and placed in Hank's Balanced Salt Solution (Life Technologies, 14025092). Brains were removed, and meningeal tissue dissected away, and cerebral hemispheres were isolated by dissection and transferred to a 15ml tube and washed three times. Neuronal cells were dissociated by papain dissociation according to the manufacturer's instructions (Worthington, Lakewood, NJ, USA) and then triturated with a P1000 pipette. Dissociated cells were diluted in rat neuron media (***See 2.1.3.5***) forming a solution of 300,000 cells per ml of media. Cells were plated onto poly-D-lysine coated 12 well plates at 300,000 cells/well (***See 2.1.4.5***). Primary neurons were cultured for 7-9 days in rat neuron media (***See 2.1.3.5***) prior to experimentation and treatment with Aβ (***See 2.2.3.2***).

2.1.2.2 Human iPSC cultures

The control iPSC line CTR M3 36S (CTR) was generated from the reprogramming of keratinocytes donated from a neurotypical, Caucasian male aged 36 years old (Cocks et al., 2014) and was supplied by the Price Lab (King's College London, UK). CTR iPSCs were used in all experiments including in the generation of the exon 2 +/- and exon 2 -/- iPSC lines.

All lines were confirmed as negative for mycoplasma and were karyotypically normal.

Details of all lines are found in ***table 2.1***.

Cell Line(s)	*CLU* exon 2 status	Genome engineering method
CTR M3 36S (CTR)	Homozygous (+/+)	NA, parental line
Exon 2 +/- (+/-)	Heterozygous knockout (+/-)	RNP lipofectamine
Exon 2 -/- (-/-) (A4 and D1 clones)	Homozygous knockout (-/-)	RNP electroporation

Table 2.1. iPSC lines for experimental use

2.1.3 Media formulations

All media components were purchased from ThermoFisher Scientific (including Gibco, Invitrogen and Life Technologies) unless otherwise stated (***See 2.1.1***).

2.1.3.1 Essential 8 media (E8)

100% v/v Essential 8 media supplemented with 2% E8 supplement.

2.1.3.2 Neural Induction Media (NIM)

50% v/v Neurobasal and 50% v/v DMEM/F12, 1:50 B27, 1:100 N2, 1:100 GlutaMAX, SB-431542 (10µM) and LDN-193189 (1µM).

2.1.3.3 Neural Maintenance Media (NMM)

50% v/v Neurobasal and 50% v/v DMEM/F12 containing, 1:50 B27 supplement, 1:100 N2 supplement and 1:100 GlutaMAX.

2.1.3.4 B27 media

100% Neurobasal medium v/v containing 1:50 B27 and 1:100 GlutaMAX.

2.1.3.5 Rat neuron media

100% Neurobasal medium without phenol red v/v containing 0.2mM L-Glutamine, B27 supplement (minus antioxidants and serum) and 1% penicillin-streptomycin (P/S).

2.1.4 Coating reagents and conditions

2.1.4.1 Geltrex

100% v/v cold KnockOut DMEM supplemented with 1% Geltrex LDEV-Free Reduced Growth Factor Basement Membrane Matrix. Plates were coated in diluted Geltrex and incubated at 37°C for at least 1 hour prior to plating cells.

2.1.4.2 Biolamina

100% v/v DPBS ($+Ca^{2+}$) containing 10% Biolamina-521 LN. Dishes were coated and incubated at 37°C for 1 hour prior to plating cells.

2.1.4.3 Poly-L-ornithine

100% v/v DPBS ($+Ca^{2+}$) containing 1% Poly-L-ornithine. Plates were coated in Poly-L-ornithine and incubated at 37°C for at least 3 hours prior to plating cells.

2.1.4.4 Laminin

100% v/v DPBS ($+Ca^{2+}$) supplemented with 1µg/cm^2 laminin. Poly-L-ornithine was removed from wells, and laminin added. Plates were coated in laminin overnight at 37°C.

2.1.4.5 Pre-coating of plates with Poly-D-Lysine

Poly-D-Lysine was resuspended in DNA/RNase free water to make a 1mg/ml solution. This was further diluted in nuclease free water to 0.1mg/ml. Plates were incubated in Poly-D-Lysine for 4 hours at room temperature (R.T). Poly-D-Lysine was then removed, and plates washed twice with nuclease free water before plating cells.

2.2 Methods

2.2.1 Human iPSC culture

2.2.1.1 Maintenance of human iPSCs

Human iPSCs were maintained in E8 media on Geltrex coated plates (Nunc) (***See 2.1.4.1***). 100% media changes were carried out daily with warmed E8. Cells were passaged at approximately 70% confluency: cells were washed with DPBS (-Ca^{2+}), incubated in Versene at 37°C for 2-5 minutes and washed off plates with warmed E8. Cells were plated at a density of 200,000 cells per well in a 6-well plate. iPSC morphology was regularly checked using an Evos™ XL Core Imaging System (Invitrogen) to ensure no evidence of spontaneous differentiations in cell cultures (***Figure 2.1***).

CTR Exon 2 +/-

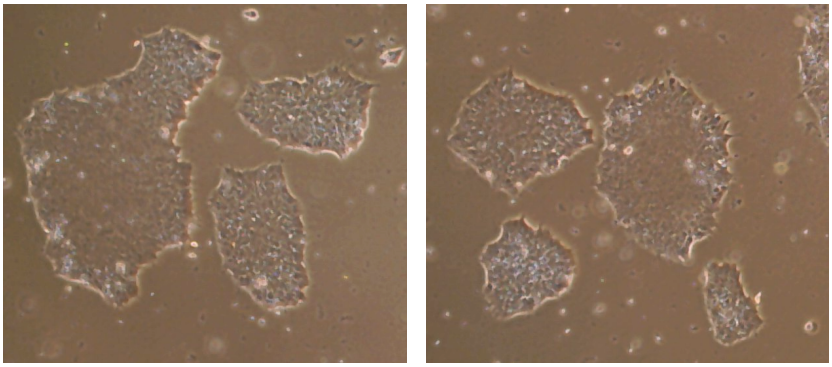


Figure 2.1. CTR and exon 2 +/- iPSC cultures following thawing.

iPSC cell cultures are regularly checked using an Evos light microscope (20x magnification) to confirm similarities in cultures and to check for signs of spontaneous differentiations. CTR and exon 2 +/- iPSCs were regularly checked 24 hours following thawing and passaging to confirm morphology and cell survival. Representative images are included here of CTR and exon 2 +/- iPSCs 2 days post thawing.

2.2.1.2 King's College protocol for differentiation of iPSCs into cortical neurons

iPSCs were differentiated into cortical neurons using the King's College protocol, a modified version of the Shi et al., protocols (Shi, Kirwan, & Livesey, 2012; Shi, Kirwan, Smith, et al., 2012). iPSCs were maintained in E8 (***See 2.2.1.1***) until reaching 100%

confluency. E8 was aspirated and neural induction media (NIM, ***see 2.1.3.2***) containing SB-431542 and LDN-193189 to induce dual SMAD inhibition was added. This represented day 0 of neural induction. Full media changes were carried out daily until day 7 when cells were passaged as follows: NIM was aspirated, cells washed with DPBS (- Ca^{2+}) and incubated in Accutase at 37°C for 2-5 minutes. Cells were washed off wells in Accutase and warmed NIM and transferred to a 50ml tube. Cells were then gently resuspended in NIM and centrifuged at 177g for 2 minutes. Supernatant was aspirated and cells resuspended in NIM supplemented with 10µM Ri. Cells were then plated on Geltrex coated 6-well plates at a ratio of 1:1 (number of wells passaged: number of wells plated). The following day (day 8) NIM was removed and replaced with neural maintenance media (NMM, ***see 2.1.3.3***).

NMM was replaced daily until day 12 when cells were passaged as described above. Cells were maintained until day 15 when they were passaged again. On day 15 cells were centrifuged at 315g for 2 minutes and plated at a well ratio of 2:3. Cells again were maintained in NMM and passaged at day 18, as described at day 15 but at a well ratio of 1:2. NMM was replaced daily until day 21 when cells were passaged for a final time. On day 21, cells were centrifuged at 177g for 5 minutes, supernatant aspirated and cells were resuspended in B27 media (***See 2.1.3.4***) supplemented with 10µM Ri. Cells were plated on Poly-L-ornithine and laminin coated plates (***See 2.1.4.3 and 2.1.4.4***) at a density of 10,000 cells per well in a 96-well plate (Grenier Bio-One) and 200,000 cells per well in a 12-well plate. A full media change was carried out the following day (day 22) to remove cell debris and cells were maintained at 37°C until day 25 when cells were treated with 0.1µM AraC. On day 28 a full media change was carried out to remove AraC and cell debris. Finally, a

half media change was carried out on day 31. Cells were then incubated at 37°C until day 35 for experimentation.

2.2.2 CRISPR/Cas9 genome engineering

2.2.2.1 Design of sgRNA

A dual, single guide RNA (sgRNA) approach was chosen to excise *CLU* exon 2. One sgRNA recruited Cas9 to the 5' region of exon 2 (intron 1) and another recruited Cas9 to 3' region of exon 2 (intron 2). sgRNA were designed by Dr. Hublitz (Weatherall Institute of Molecular Medicine, University of Oxford). DNA sequences of the regions flanking exon 2 were obtained from NCBI and submitted to CRISPOR software (http://crispor.tefor.net/) to predict off-targets and editing efficiency of each sgRNA. Three 5'sgRNA (#1, #2, #3) and three 3'sgRNA (#1, #2, #3) were chosen as they contained more than 2 mismatches in their seeding region, and no exonic off targets with less than 3-4 mismatches. Sequences of these sgRNA can be found in ***table 2.2***.

sgRNA name	Sequence (5'-3')
5' sgRNA # 1	GACGGAAGCGAAGTAAGC
5' sgRNA # 2	CGGAAGCGAAAGTAAGCTC
5' sgRNA # 3	CTCCACAGGTACCGTTCAG
3' sgRNA # 1	GAGATAGTCCGGGGTCACA
3' sgRNA # 2	TCGTACTACAAGGAGACCGG
3' sgRNA # 3	TACTACAAGGAGACCGGTGT

Table 2.2. sgRNA sequences generated by Dr. Hublitz for editing CLU exon 2.

2.2.2.2 Surveyor Nuclease Assay

2.2.2.2.1 sgRNA cloning

Oligonucleotides for sgRNA cloning were ordered from MERCK (USA) by Dr. Hublitz and cloned into either opX458 or pX458-Ruby plasmid backbones (Addgene entries 48138 and

110164 respectively). Oligonucleotides were reconstituted to 100µM in nuclease free water. 10µl of each was added with 10µl NEB buffer 2.1 (New England BioLabs, B7202S) and made to a final volume of 100µl by the addition of nuclease free water. These were incubated at 99°C for 5 minutes and cooled slowly to promote sgRNA annealing. Double stranded oligonucleotides (dsODNs) were precipitated by addition of 30µl 3M sodium acetate (pH 5.6) and 300µl 100% ethanol (EtOH). This was centrifuged at 18,000g for 30 minutes at 2°C. Supernatant was removed and dsODN washed with 70% EtOH. dsODN were centrifuged again at 18,000g for 10 minutes at R.T. Again, supernatant was removed and dsODNs left to air dry. dsODN were resuspended in 100µl nuclease free water and OD_{260} was determined by Nanodrop (ThermoFisher). 1µg of dsODNs was added to 2µl of 10X ligase buffer and 1µl of NEB T4 PNK (New England BioLabs, M0201S). Total volume was made up to 20µl with nuclease free water and incubated for 1 hour at 37°C. A 10µl final volume of NEB T4 ligase and 10X T4 ligase buffer containing 20ng backbone and 0.5µl dsODNs were assembled and incubated at R.T for 1 hour. To transform cells, 5µl of the ligation reaction was added to competent DH5a bacteria and incubated on ice for 20 minutes. Cells were heat-shocked at 42°C for 2 minutes and immediately placed on ice for 5 minutes. Standard S.O.C medium (ThermoFisher, 15544034) without antibiotics was added to cells and cells were incubated at 37°C for 1 hour to enable recovery of cells. Cells were collected by spinning at 8,000g for 1 minute and plated on agar plates containing 100µg/ml ampicillin (Sigma, A9518). Cells were incubated overnight at 37°C.

2.2.2.2.2 Miniprep of plasmid DNA

The next day single cell colonies were inoculated into 1.4ml luria broth containing 100µg/ml ampicillin in a 2ml microtube with a punctured lid to enable aerobic growth and incubated overnight shaking at 90g at 37°C. Eppendorfs were centrifuged at 13,000g for 1

minute and cell pellets were resuspended in 200µl of Qiagen Buffer P1 (Qiagen, 19051). Pellets were vortexed briefly at full speed in an Eppendorf MixMate. 200µl of Qiagen Buffer P2 (Qiagen, 19052) was added and tubes inverted carefully and incubated at R.T for 5 minutes. 200µl of cold Qiagen Buffer P3 (Qiagen, 19053) was added and tubes inverted 5 times vigorously to precipitate bacterial proteins. Tubes were centrifuged at 14,000g for 10 minutes at 4°C. Supernatant from each tube was transferred to a new tube and 500µl 100% isopropanol was added to the supernatant and mixed vigorously by inversion. DNA was pelleted by spinning at 14,000g for 10 minutes at 4°C. Supernatant was discarded, 500µl of 70% EtOH was added briefly and then discarded. Residual EtOH was removed, and the pellet left to air dry. 50µl of nuclease free water was added and DNA dissolved by shaking at 3,00g for 5 minutes at R.T.

2.2.2.2.3 HEK293T transfection

HEK293T cells were maintained in serum-free DMEM (Life Technologies, 11965092) supplemented with 10% fetal bovine serum (FBS) (Life Technologies, 10270-106), 0.5% P/S (Life Technologies,15140122) and glutamine (2mM, Life Technologies, 25030081). Cells were plated at a density of 150,000 cells per well in a 12-well plate. 500ng of DNA was mixed into 50µl DMEM. 3µl of Lipofectamine 2000 Transfection Reagent (ThermoFisher, 11668030) was added into 50µl DMEM in a different tube. Tubes were inverted, combined, and incubated for 5 minutes at R.T to enable formation of liposomes. 100µl total volume was added to cells. Plates were then incubated overnight at 37°C until cells reached 50-70% confluency. Media was aspirated and replaced with fresh DMEM. 100% media changes were carried out every other evening until cells were harvested.

2.2.2.2.4 Harvesting cells

Media was aspirated, cells washed with PBS, and incubated with 100µl 0.25% Trypsin-EDTA solution (Life Technologies, 15400054) for 5 minutes at 37°C. Cells were then transferred into a 1.5ml tube.

2.2.2.2.5 gDNA extraction

After cells were collected as described in ***2.2.2.2.4***, cell pellets were resuspended in 500µl of Cell Lysis buffer and 5µl of proteinase K. This was incubated overnight shaking at 20g at 56°C. This was then cooled to R.T and 600µl 100% isopropanol added to precipitate genomic DNA (gDNA). This was centrifuged at 16,000g for 30 minutes (Eppendorf, 5424R), supernatant was discarded and 500µl of 70% EtOH added. Tubes were centrifuged again at 18,000g for 5 minutes at R.T. EtOH was discarded, and pellets left to air dry. 500µl of sterile nuclease free water was added and incubated at 56°C for 4 hours, shaking at 90g. Samples were then vortexed and shaken at 300g for 5 minutes. Samples were vortexed again and OD_{260} was determined by Nanodrop.

2.2.2.2.6 PCR amplification of surveyor template

A Surveyor Nuclease Assay (IDT, Integrated DNA Technologies, 706025) was performed according to manufacturer's instructions to determine the efficiency of each sgRNA to recruit Cas9: (https://sfvideo.blob.core.windows.net/sitefinity/docs/default-source/user-guide-manual/surveyor-kit-for-gel-electrophoresis-user-guide.pdf?sfvrsn=a9123407_6), see also ***2.2.2.2.6*** - ***2.2.2.2.8***. Firstly, primers to amplify *CLU* exon 2 were designed by Dr. Hublitz. Primer sequences can be found in ***table 2.3***.

Primer name	Sequence (5'-3')
47 FW	GATACCACTCTGGACAAGGAGGC
56 RV	CACAGGAGGGATAAGCTCTGGGC

Table 2.3. Primers used to amplify CLU exon 2 locus.

PCR reactions consisted of: 25µl Platinum HiFi Master Mix (Life Technologies, 12532016), 3% Dimethyl sulfoxide (DMSO, Sigma Aldrich, D2650), 100ng template gDNA and 1µl 10µM primer mix. Nuclease free water was added to make a total volume of 50µl. These were amplified using the following programme:

Stage	Temperature	Time	Cycles
Enzyme activation	94°C	2 minutes	1X
Denature	94°C	30 seconds	45X
Anneal	Tm = 62°C	30 seconds	
Extend	68°C	45 seconds	
Final extension	68°C	5 minutes	1X
Hold	12°C	Hold	1X

3µl of PCR products were run on a 0.8% agarose gel and stained with ethidium bromide (20µl of 20µg/ml solution, Gerlinde Kisker Inc). TAE gel running buffer was added to the DNA sample and the reaction was run alongside a 100-bp DNA ladder (NEB 100bp marker, N3231). Gels were photographed using a BioRad gel documentation station.

2.2.2.2.7 Heteroduplex formation

Single fragment PCR products were added to a 0.2ml tube giving a total volume of 10µl diluted with the Platinum HiFi PCR buffer (ThermoFisher, 11304011). Tubes were then heated to randomly form re-annealed amplicons of heteroduplexes or homoduplexes according to the following protocol:

Temperature	Time	Temperature ramp
95°C	10 minutes	
95°C to 85°C		(-2.0°C/s)
85°C	1 minute	
85°C to 75°C		(-0.3°C/s)
75°C	1 minute	
75°C to 65°C		(-0.3°C/s)
65°C	1 minute	
65°C to 55°C		(-0.3°C/s)
55°C	1 minute	
55°C to 45°C		(-0.3°C/s)
45°C	1 minute	
45°C to 35°C		(-0.3°C/s)
35°C	1 minute	
35°C to 25°C		(-0.3°C/s)
25°C	1 minute	
4°C	Hold	

2.2.2.2.8 Treatment with Surveyor Nuclease

A premix of 1.4µl $MgCl_2$, 1µl Enhancer and 1µl Surveyor Nuclease (IDT, 706025) was prepared and 3.4µl total volume was added to each of the 10µl re-annealed amplicons generated above. These were incubated for 50 minutes at 42°C. 1.5µl of STOP solution (IDT, 706025) was added immediately and samples run immediately on an agarose gel.

2.2.2.2.9 Analysis of DNA fragments

Samples were loaded with 10% glycerol and 50% sucrose and separated on a 2.5% agarose gel, later stained with ethidium bromide. Gels were run at 80V for 45 minutes and imaged on a BioRad gel documentation unit. Images were exported in a TIFF format and efficiency of Cas9 cutting was assessed based on the extent to which cleaved bands were observed in each transfection condition.

2.2.2.3 Preparation of cells for GeneArt Cleavage Detection Kit

CTR iPSCs were maintained as described in ***2.2.1.1***. Media was aspirated, cells washed with DPBS (- Ca^{2+}) and incubated with TryplE Express Enzyme Solution at 37°C for 2-3 minutes.

Cells were then removed from wells in TryplE and E8 and transferred to a 50ml tube. Cells were centrifuged at 300g for 5 minutes. Supernatant was aspirated and cells plated in 500µl E8 supplemented with 10µM Ri per well in a 24-well plate. Cells to be transfected according to the Yu et al., protocol were plated at a density of 40,000 cells per well (***See 2.2.2.6***) (Yu et al., 2016), while cells to be transfected according to the Jacobi et al., protocol were plated at 40,000, 100,000, 150,000 and 200,000 cells per well (***See 2.2.2.7***) (Jacobi et al., 2017). 24 hours later, media was aspirated and replaced with fresh 500µl of E8 media supplemented with 10µM Ri. Cells were transfected 3 hours later.

2.2.2.4 Preparation of Cas9 nuclease

Prior to transfections, Cas9 (IDT, USA, Alt-R® S.p. HiFi Cas9 Nuclease 3NLS, 100µg, 61µM) was diluted as required in Opti-MEM (***See 2.2.2.6 and 2.2.2.7***). Preparation of Cas9 to the required concentrations can be found in ***table 2.4***.

Concentration of Cas9 (µM)	Volume of 61µM Cas9 (µl)	Volume of Opti-MEM (µl)
1.0	0.3	19.7
1.7	0.6	19.4
2.5	0.8	19.2
3.3	1.1	18.9

Table 2.4. Dilution preparations of Cas9 nuclease for transfection (volumes given per well of cells).

2.2.2.5 Preparation of sgRNA

Individual synthetic oligonucleotides crRNA (IDT, Alt-R® CRISPR-Cas9 crRNA, 10nmol) and tracrRNA (Alt-R® CRISPR-Cas9 tracrRNA, 20nmol) were diluted to 100µM by the addition of IDTE Buffer (IDT, 11-01-02-05). sgRNA were formed by combining 5' crRNA, 3' crRNA and

tracrRNA in a proportion 1:1:2 in a sterile 0.2ml microtube. This was then diluted to the desired concentrations by the addition of nuclease free duplex buffer (IDT, 11-01-03-01, ***see table 2.5***). 1µM of sgRNA was required for the Jacobi et al., protocol (***See 2.2.2.7***). For the Yu et al., protocol, 1.0µM, 1.7µM, 2.5µM and 3.3µM sgRNA was required (***See 2.2.2.6***). Once combined, solutions were mixed by pipetting, heated at 95°C for 5 minutes and cooled to R.T prior to the addition to cells.

Concentration of sgRNA (µM)	Volume of 5' crRNA vol (µl)	Volume of 3' crRNA vol (µl)	Volume of tracrRNA (µl)	Volume of nuclease free duplex buffer (µl)
1	1.0	1.0	2.0	96.0
1.7	1.7	1.7	3.4	93.2
2.5	2.5	2.5	5.0	90.0
3.3	3.3	3.3	6.6	86.8

Table 2.5. Volumes required for sgRNA preparation (volumes given per well of cells).

2.2.2.6 Preparation of Cas9 RNPs and lipofectamine solutions: Yu et al., protocol

To transfect a single well of a 24-well plate, the following reagents were combined in a sterile 2.0ml tube:

- 25µl Opti-MEM
- 6µl Cas9 (various concentrations, ***see table 2.4***)
- 6µl sgRNA (various concentrations, ***see table 2.5***)
- 6µl Cas9 PLUS™ reagent (Lipofectamine™ CRISPRMAX™ Cas9 Transfection Reagent Kit, Thermo Fisher, CMAX00001).

Reagents were mixed thoroughly and incubated at R.T for 5 minutes to promote the formation of Cas9 RNPs complexes. Lipofectamine reagents were then prepared by the addition of:

- 25µl Opti-MEM
- 1.5µl CRISPRMAX Reagent (Lipofectamine™ CRISPRMAX™ Cas9 Transfection Reagent Kit, Thermo Fisher, CMAX00001).

This was then incubated at R.T for 5 minutes.

2.2.2.7 Preparation of Cas9 RNPs and lipofectamine solutions: Jacobi et al., protocol

To transfect a single well of a 24-well plate, the following reagents were combined in a sterile 2.0ml tube:

- 85.6µl Opti-MEM
- 6µl Cas9 (1µM)
- 6µl sgRNA (1µM)
- 2.4µl Cas9 PLUS™ reagent (Lipofectamine™ CRISPRMAX™ Cas9 Transfection Reagent Kit, Thermo Fisher, CMAX00001).

Reagents were mixed thoroughly and incubated at R.T for 5 minutes to promote the formation of Cas9 RNPs complexes. Lipofectamine reagents were then prepared by the addition of:

- 94.2µl Opti-MEM
- 4.8µl CRISPRMAX Reagent (Lipofectamine™ CRISPRMAX™ Cas9 Transfection Reagent Kit, Thermo Fisher, CMAX00001).

This was incubated at R.T for 5 minutes.

2.2.2.8 Transfection of cells for GeneArt Cleavage Detection Kit

Total volumes of Cas9-RNP complexes were combined with the total volumes of Lipofectamine CRISPRMAX™ reagents (*See 2.2.2.6 and 2.2.2.7*). These were mixed thoroughly by pipetting and incubated for 10 minutes at R.T. Total volumes were added dropwise to the corresponding well of cells and incubated on cells for 6 hours at 37°C. After 6 hours media was replaced, and cells incubated overnight at 37°C. A full media change was carried out the following day.

2.2.2.9 GeneArt Cleavage Detection Kit

48 hours after transfections, cells were passaged as described in *2.2.1.1*. Cells were centrifuged at 200g for 5 minutes at 4°C and resuspended in 50µl Cell Lysis Buffer supplemented with 2µl Protein Degrader (GeneArt Cleavage Detection Assay, ThermoFisher, A24372). This was then heated according to the following protocol in a Veriti 96-well thermal cycler (Applied Biosystems, 4375786):

Temperature	Time
68°C	15 minutes
95°C	10 minutes
4°C	hold

This was then vortexed, and 2µl of each sample was combined with the following:

- 1µl (10µM) primer mix (*See table 2.3*)
- 25µl AmpliTaq Gold® 360 Master Mix
- 22µl nuclease free water

PCR products were then amplified:

Stage	Temperature	Time	Cycles
Enzyme activation	95°C	10 minutes	1X
Denature	95°C	30 seconds	40X
Anneal	*T_m = 68°C	30 seconds	
Extend	72°C	30 seconds	
Final extension	72°C	7 minutes	1X
Hold	4°C	Hold	1X

*Annealing temperature was calculated according to the Tm calculator provided by Thermo Fisher Scientific.

Random annealing of PCR fragments with and without indels was set up by the addition of 1µl of PCR product, 1µl 10X Detection Reaction Buffer and 7µl nuclease free water and heated at the following protocol:

Temperature	Time	Temp/time	RAMP setting (%)
95°C	5 minutes	/	/
95°C - 85°C	/	-2°C per second	47.1%
85°C - 25°C	/	-0.1°C per second	2.35%
4°C	/	Hold	/

1µl of Detection enzyme and 1µl water was added to all samples and incubated at 37°C for 1 hour. 10µl of the sample was loaded with 10µl water per well in a 2% agarose gel (Sigma, A9539) made in 1 X TAE (Alfa Aesar, J63677). Samples were run alongside 6µl of 100bp DNA loading dye (BenchTop 100bp DNA Ladder, Promega, G8291) at 100 V for 1 hour. To visualise, gels were incubated at R.T for 40 minutes in SYBR™ Gold Nucleic Acid Gel Stain

(Thermo Fisher Scientific, S11494) and then imaged on a ChemiDoc™ Touch Imaging System (BioRad). Images were imported into Image Lab 6.0 software (BioRad).

Cleavage efficiency was then calculated using the following equations:

$$\text{Fraction Cleaved} = \frac{\text{Sum of cleaved band intensities}}{\text{Sum of cleaved and uncleaved band intensities}}$$

$$\text{Cleavage Efficiency} = 1 - (1 - \text{Fraction Cleaved})^{1/2}$$

Uncleaved bands were defined as PCR products that did not contain indels and therefore were not cleaved by the T7 endonuclease I detection enzyme. Cleaved bands were defined as PCR products that contained indels and were cut by the detection enzyme.

2.2.2.10 Generation of the exon 2 +/- line

CTR iPSCs were transfected according to the protocol outlined (***See 2.2.2.6 and 2.2.2.8***). 1.7µM RNP complexes were delivered to 40,000 CTR iPSC plated per well in a 24-well plate cultured in 500µl of E8 media.

2.2.2.11 Generation and expansion of single cell clones

48 hours after transfection, cells were passaged as described with TryplE solution (***2.2.2.3***). 100 cells were plated per 90mm dish (Nunc) coated in Biolamina (***See 2.1.4.2***) in 10ml E8 supplemented with 10µM Ri. Half media changes were carried out daily with warmed E8 for 2 weeks. After 12-14 days, when single cell clones were visible on the dishes by eye, individual clones were isolated using 8mm x 8mm Cloning Cylinders (Millipore, Cat. # TR-1004). Media was removed from each dish and a Cloning Cylinder was placed around each clone. Cells were incubated at R.T for 5 minutes in 100µl Versene. Cells were resuspended

in E8 and plated into a single well of a 24-well plate. Cells were maintained in E8 until reaching 70% confluency when gDNA was extracted.

2.2.2.12 Generation of the exon 2 -/- line

2 vials, each containing 1 million CTR iPSCs, were supplied to Synthego Corporation (USA) for gene editing to generate two homozygous exon 2 knockout (exon 2 -/-) iPSC lines (***See table 2.1***). Several sgRNAs were designed in regions flanking *CLU* exon 2 using Synthego's internal Synthego Design Tool. Two sgRNAs were produced and chemically modified by the addition of 2'O methyl analogues and 3' phosphorothioate internucleotide linkages at the first three 5' and 3' terminal RNA residues and synthesised by Synthego as synthetic sgRNAs. The sequences of these sgRNA are found in ***table 2.6***.

sgRNA name	Sequence (5'-3')
5' sgRNA	ACTACCAGAGGACAAGAGAC
3' sgRNA	GTACTACAAGGAGACCGGTG

Table 2.6. sgRNA sequences used to generate the exon 2 -/- iPSC line.

Cells were transfected by Synthego according to their optimised nucleofection protocol (https://app.hubspot.com/documents/2418554/view/22928038?accessId=341700) and gDNA was extracted from single cell clones and amplified (***See table 2.7***). PCR products were visualised on a 2% agarose gel.

Primer	Sequence (5'-3')
SYN PCR FW	CAAATGCCGGCAGTCTGATG
SYN PCR RV	GACAGCTGAGGGCAGTGAG

Table 2.7. Primer sequences used to identify exon 2 -/- iPSCs following transfection.

Internal primers located within *CLU* exon 2 were used to amplify a 92bp region of exon 2, PCR products were submitted alongside a Sequencing Primer for Sanger Sequencing (***See table 2.8***).

Primer	Sequence (5'-3')
INTERNAL PRIMER FW	GTCTGGTCCCCCAGGACC
INTERNAL PRIMER RV	GACTCCAGAATTGGAGGCATGATG
SEQUENCING PRIMER	CACAAGATAAAAACGGTCTGTAACACTG

Table 2.8. Primer sequences used to confirm excision of exon 2 by Sanger Sequencing.

Synthego confirmed A4 and D1 iPSCs expressed pluripotency markers *OCT4* and *SSEA4* and identified no chromosomal abnormalities.

2.2.3 Aβ treatments

2.2.3.1 Preparation of $A\beta_{25-35}$ and $A\beta_{1-42}$

$A\beta_{25-35}$ trifluoroacetate salt (BACHEM AG, Bubendorf, Switzerland, #4030205) was supplied at 5mg with a purity of 97% giving 4.85mg of Aβ (molecular weight 1060.28). 2.43ml of nuclease free water was added giving a solution of 2mg/ml (1.88mM). $A\beta_{25-35}$ was stored at -20°C until required. $A\beta_{1-42}$ (TEPLOW) was resuspended in 100% 1,1,1,3,3,3-hexafluoropropanol-2-ol (HFIP) at a concentration of 1mM, this was homogenised using a syringe and HFIP was evaporated in a SpeedVac. 48 hours before treatment, $A\beta_{1-42}$ was resuspended in DMSO at 5µM and sonicated for 10 minutes. Oligomers were then prepared by dilution in DPBS (- Ca^{2+}) to 400µM and 2% SDS in H_20 was added 1:10. This was incubated at 37°C for 18 hours. Finally, oligomers were resuspended in DPBS (-Ca^{2+}) to give a solution of 100µM and was incubated at 37°C overnight.

2.2.3.2 Treatment of neurons with $A\beta_{25-35}$ and $A\beta_{1-42}$

Prior to treatment tubes containing $A\beta_{25-35}$ and $A\beta_{1-42}$ were spun and mixed by pipetting. 50% of media was removed from each well to be treated and transferred to a sterile 2ml Protein LoBind Tube (Ependorf, 0030108132). The required volume of each Aβ was added to the tubes containing media. Tubes were tapped and mixed thoroughly to ensure equal distribution of the Aβ in the media. Media was then returned to the corresponding wells for treatment. Plates were then swirled gently to ensure equal distribution of Aβ. Cells were incubated in Aβ for 24 hours at 37°C.

2.2.4 Extraction of gDNA for sequencing

gDNA was extracted using the DNeasy Blood and Tissue Kit (Qiagen, 69504). Total media was removed from wells and cells passaged (***See 2.2.1.1***). Cells were resuspended in E8 media and centrifuged at 300g for 5 minutes at R.T. Supernatant was aspirated and cell pellets resuspended in 200µl of DPBS (+ Ca^{2+}) and 20µl of proteinase K. 4µl of RNAse A (Qiagen, 19101) was added and incubated for 2 minutes at R.T. 200µl Buffer AL was added, samples inverted and 200µl of 100% EtOH was added. Total volumes were added to Mini Columns placed in Collection Tubes and centrifuged at 5,000g for 1 minute at R.T. 500µl of Buffer AWI was added and samples were centrifuged at 5,000g for 1 minute at R.T. 500µl of Buffer AW2 was added and samples centrifuged at 16,000g for 3 minutes at R.T. Columns were then placed into a 2ml tube and 200µl of nuclease free water was added, incubated for 1 minute and centrifuged at 5,000g for 1 minute. This elution step was repeated to increase DNA yield.

2.2.5 PCR and sequencing

2.2.5.1 Sanger sequencing of exon 2 +/- iPSCs

1.25µl gDNA, 0.25µl 10µM forward primer, 0.25µl 10µM reverse primer, 23.25µl nuclease free water and 25µl Phusion Flash High Fidelity Master Mix (ThermoFisher, F548S) were combined. Primer sequences are found in ***table 2.3***. Reactions were run on a thermal cycler according to the following protocol:

Stage	Temperature	Time	Cycles
Initial Denaturation	98°C	30 seconds	1X
Denature	98°C	5 seconds	40X
Anneal	68°C	30 seconds	
Extend	72°C	15 seconds	
Final extension	72°C	7 seconds	1X
Hold	4°C	Hold	1X

5µl of PCR product (10ng/µl) and primers (3.2pmol/µl) were supplied to Source Bioscience plc for Sanger sequencing. Sequences were imported as .ab1 files into Geneious Software (https://www.geneious.com/, version 11) and aligned to reference sequences downloaded from the NCBI database (https://www.ncbi.nlm.nih.gov/).

2.2.5.2 PCR and gel electrophoresis of exon 2 +/- iPSCs

80ng gDNA, 0.25µl 10µM forward primer, 0.25µl 10µM reverse primer and 25µl Phusion Flash High Fidelity Master Mix were combined. Volumes were made to 50µl by addition of nuclease free water. Primers were positioned in introns 1 and 2 and sequences are found in ***table 2.9***.

Primer name	Sequence (5'-3')
E1 FW	GAACCCCATCGTCCTGTTGG
E3 RV	GACGTACTTACTTCCCTGATTGG

Table 2.9. Primer sequences used to amplify gDNA for separation of CLU alleles by agarose gel electrophoresis.

Reactions were run on a thermal cycler according to the following protocol:

Stage	Temperature	Time	Cycles
Initial Denaturation	98°C	10 seconds	1X
Denature	98°C	1 seconds	40X
Anneal	68°C	5 seconds	
Extend	72°C	15 seconds	
Final extension	72°C	1 minutes	1X
Hold	4°C	Hold	1X

PCR products were diluted 1:5 in Nucleic Acid Sample Loading Buffer (BioRad, 161-0767), of which 20µl was loaded per well alongside 6µl of 100bp DNA ladder (Promega, G2101). 1% agarose gels were prepared, run, and imaged as described in ***2.2.2.9***.

2.2.5.3 Validation of allelic edits by cloning and Sanger sequencing of exon 2 +/- iPSCs

2.2.5.3.1 Generating PCR products.

gDNA was extracted from CTR and exon 2 +/- iPSCs as described in ***2.2.4***. 10-100ng of gDNA, 5µl of 10X PCR buffer, 0.5µl 50mM dNTPs, 1µl of Qiagen Taq polymerase with buffer Q (Cat No. 201203), 1µM of forward and 1µM of reverse primer (***See table 2.9***)

were combined and total volume made to 50µl with nuclease free water. This was amplified using the combinations outlined in *2.2.2.2.6*, except annealing was performed at 64°C and elongation at 72°C.

2.2.5.3.2 TOPO® cloning reaction

PCR products were TOPO® cloned into a pCR2.1-TOPO® vector to transform competent *E.coli* cells. Between 0.5µl and 4µl of PCR products was combined with 1µl of TOPO® salt solution (THERMO, proprietary solution), 1µl of TOPO® vector and the final volume was made up to 6µl by the addition of nuclease free water. These were mixed gently and incubated at R.T for 5 minutes. Reactions were placed on ice while performing the One Shot® chemical transformation protocol. S.O.C. medium was warmed to R.T, and luria broth plates warmed to 37°C for 30 minutes. 40µl of 40mg/mL X-gal was spread on each luria broth plate and plates incubated at 37°C. 2µl of TOPO® cloning reaction was added to a vial of One Shot® chemically competent *E.coli* cells (ThermoFisher, 18265017), mixed gently and incubated on ice for 30 minutes. Cells were then heat shocked for 30 seconds at 42°C. Tubes were transferred to ice and 250µl of S.O.C medium added to each tube. Tubes were shaken horizontally at 3g for 1 hour at 37°C. 10-50µl of each transformation was spread on prewarmed plates with 20µl of S.O.C medium. Plates were incubated at 37°C and 10-20 colonies were picked with the aim of isolating and sequencing 5-10 copies of each allele, representing the allelic status of gene editing in a diploid cell line. DNA was isolated as described in *2.2.2.2.2*.

2.2.5.3.3 Sanger Sequencing

Isolated plasmid DNA was submitted to commercial Sanger sequencing as detailed by the Weatherall Institute of Molecular Medicine, Sanger sequencing facility. Sequencing traces (.ab1 format) were imported into SnapGene (https://www.snapgene.com/) and aligned to

the respective WT and edited allele variants. Sequences were compared to reference sequences obtained from NCBI.

2.2.6 RNA analysis

2.2.6.1 RNA extraction for RT-qPCR

Media was aspirated and 1ml TRIzol (Life Technologies, 15596018) added per well. This was transferred to a 2ml tube and placed on ice. 200µl chloroform was added to each sample, shaken vigorously, and incubated at R.T for 3 minutes. Samples were centrifuged at 12,000g for 15 minutes at 4°C. The upper, clear supernatant layer containing RNA was transferred to a 2ml tube. 10µg of RNase-free glycogen (Merck, 10901393001) and 500µl isopropanol were added and incubated for 10 minutes at R.T. Samples were centrifuged at 12,000g for 10 minutes at 4°C and supernatant was removed carefully so not to disturb the white pellet of RNA formed at the bottom of the tube. RNA pellets were washed with 1ml 75% EtOH and centrifuged at 7,500g for 5 minutes at 4°C. EtOH was removed, and pellets were air dried at R.T for 10 minutes. Pellets were resuspended in 15µl DNase nuclease free water and incubated at 55°C for 15 minutes. Samples were then vortexed and placed on ice. RNA concentrations were determined using a Nanodrop Spectrophotometer (DeNOVIX, DS-11 Series Spectrophotometer).

2.2.6.2 cDNA synthesis

150ng-1000ng RNA was reverse transcribed using the Taqman Reverse Transcription kit (ThermoFisher, 4304134). Per reaction, RNA and nuclease free water was added in a total combined volume of 3.85µl, followed by 1µl of 10X buffer, 2µl of dNTPs, 2.2µl of $MgCl_2$, 0.5µl of random hexamers, 0.25µl of reverse transcriptase and 0.2µl of RNase inhibitor. Reactions were run on a thermal cycler according to the following protocol:

Stage	Temperature	Time
1	25°C	10 minutes
2	37°C	30 minutes
3	95°C	5 minutes
4	4°C	Hold

2.2.6.3 RT-qPCR

FastStart Universal SYBR Green Master Mix (Sigma Aldrich)-based PCR reactions were performed on a StepOne Plus™ Real-Time PCR System (Applied Biosystems, 4376600). 2µl of diluted cDNA (1:5 dilution in nuclease free water) was added per well of a 96 well plate (ThermoFisher Scientific Applied Biosystems™, 4326659). cDNA samples were run in triplicate for each target gene. 8µl of RT-qPCR master mix containing 5µl of FastStart Universal SYBR Green Master Mix, 2µl of nuclease free water, 0.5µl of forward primer (10µM) and 0.5µl of reverse primer (10µM) was added to each well. Primer sequences can be found in ***table 2.10***. All *CLU* primers were obtained from publication (Prochnow et al., 2013). *NANOG* and *GAPDH* primer sequences were obtained from the Hooper Lab (University of Manchester). *OCT4* primers were obtained from the Ackerman Lab (University of Oxford).

Plates were sealed and centrifuged at 2,000g for 2 minutes to ensure mixing of reagents at the bottom of each well. Samples were then run using the following protocol:

- Hold at 95°C for 3 minutes.
- Cycle between 95°C for 20s and 60°C for 30 seconds for 40 cycles.
- Heat from 60°C to 95°C for 15 seconds.

- Cool to 60°C for 1 minute.
- Heat to 95°C for 10 seconds at increments of 0.5°C.

Primer	Forward (5'-3')	Reverse (5'-3')
CLU variant 1	ACAGGGTGCCGCTGACC	CAGCAGAGTCTTCATCATGCC
CLU variant 1 Δ exon 2	GGGTGCCGCTGACCGAAAT	GAGTCTTTATCTGTTTCACCCCG
CLU variant 2	ATGCAGATGGATTCGGTGT	AGTCTTTGCACGCCTCTGA
CLU variant 3	TCGTCCTGTTGGTTCTGTGATG	CAGCAGAGTCTTCATCATGCC
GAPDH	CCTGTTCGACAGTCAGCCG	CGACCAAATCCGTTGACTCC
NANOG	ATGGAGGAGGGAAGAGGAGA	GATTTGTGGGGCCTGAAGAAA
OCT4	ACATGTGTAAGCTGCGGCC	GTTGTGCATAGTCGCTGCTTG
Total CLU	CTATCTGCGGGTCACCAC	CTCAGTGACACCGGAAGGAAC

Table 2.10. List of RT-qPCR primers.

2.2.6.4 Analysis

Relative quantification of gene expression was achieved using the Pfaffl method (Pfaffl, 2001). Average C_t values were calculated for the gene of interest (GOI) and housekeeper gene (HKG) for control samples giving the average C_t GOI and average C_t HKG respectively. This was done to normalise for RNA input. Average C_t values for each sample was then compared to the average C_t GOI and average C_t HKG, giving the ΔC_t GOI and ΔC_t HKG for each sample. The Pfaffl equation (Gene Expression Ratio) for each sample was then calculated using the following equation:

$$\text{Gene Expression Ratio} = \frac{2^{\Delta \text{CtGOI}}}{2^{\Delta \text{CtHKG}}}$$

The average of the Gene Expression Ratio values for control samples was then calculated and to normalise to 1, each sample Pfaffl equation was divided by the average Gene Expression Ratio of the control samples. The mean and standard error of the mean (SEM) between of each biological group were then calculated.

2.2.6.5 RNA extraction for RNA-Seq

RNA was collected and prepared for RNA-Seq analysis using the Qiagen RNeasy Mini PLUS Kit (Qiagen, 74134). Media was aspirated and cells collected directly in 350µl of Buffer RLT. This was briefly vortexed to ensure homogenisation and transferred to a gDNA eliminator spin column. Columns were centrifuged at 8,000g for 30 seconds and 350µl of 70% EtOH was added to the flow through and mixed by pipetting. Flow through was transferred to a new spin column and centrifuged at 8,000g for 15 seconds. 700µl of Buffer RW1 was added to the collection tube, which was then centrifuged at 8,000g for 15 seconds. 500µl of Buffer RPE was added to each spin column and centrifuged at 8,000g for 10 seconds to wash the membrane. Flow through again was discarded. 500µl of Buffer RPE was added to each column and centrifuged at 8,000g for 2 minutes. The spin column was placed into a new collection tube and columns centrifuged at 16,000g for 1 minute. Spin columns were then placed in a 1.5ml tube and 50µl of RNase free water added to each membrane to elute the RNA. Columns were centrifuged at 8,000g for 1 minute and elute reapplied. Columns were spun for a final time at 8,000g for 1 minute to increase RNA yield. RNA concentrations, 260/280 and 260/230 ratios were determined using a Nanodrop Spectrophotometer.

2.2.6.6 Ethanol precipitation of RNA samples

EtOH precipitation was carried out to improve quality of RNA and remove contaminants from RNA. 100µl of 100% ice cold EtOH and 4µl 3M sodium acetate (pH 5.2) were added

to each sample. Samples were vortexed and stored overnight at -20°C. Samples were thawed at R.T and centrifuged at 13,000g for 30 minutes at 4°C. Supernatant was removed and pellets washed twice with 500µl ice cold 75% EtOH, after each wash samples were centrifuged at 13,000g for 10 minutes at 4°C. EtOH was removed, and samples centrifuged at 13,000 for 10 seconds to remove traces of EtOH. Pellets were air dried and resuspended in 10µl RNase free water. RNA properties were determined again using a Nanodrop spectrophotometer ensuring 260/230 and 260/280 values were ~2.

2.2.6.7 RNA-Seq and analysis

100ng of RNA was diluted in nuclease free water to give a total volume of 40µl and submitted to the Wellcome Trust Centre for Human Genetics (University of Oxford). RNA integrity numbers were confirmed to be >8 for all samples. Library preparation and RNA-Seq was performed by the Wellcome Centre for Human Genetics. TruSeq RNA Library Preparation Kit (Illumina) was used, and mRNA was enriched by polyA selection. The mRNA fraction was selected from total RNA and converted to cDNA. cDNA was then end-repaired, A-tailed and adaptor ligated. Samples were sequenced at 150 paired ends (PE) on a NovaSeq6000 for PolyA- RNA-Seq. Data was provided in both fastq and bam files for analysis by Dr Marco Fernandes (Translational Neuroscience and Dementia Research Group, University of Oxford). All analysis was conducted using the Ensembl transcript annotations for the Human Build 37 (GRCh37), release-87 in the 'gtf format (avail@ftp://ftp.ensembl.org/pub/grch37/release-87). Reads that overlap multiple features were resolved by the `summarizeOverlaps` function of the (GenomicAlignments R package) (Lawrence et al., 2013), with the follow settings:

i) mode=Union, ii) singleEnd=F, iii) ignore.strand=T, iv) fragments=T and features were summarised to the gene-level. This yielded an Ensembl gene ID by sample counting matrix

of the class S4 (R-object). The latter counting matrix was modelled using the DESeq2 pipeline which performs i) size factors estimation, ii) dispersion estimation and iii) Gamma-Poisson Generalized Linear Model (GLM) fitting (Love et al., 2014). The following comparisons were tested for differential gene expression analysis:

1. $A\beta_{25-35}$ treated CTR vs untreated CTR
2. $A\beta_{25-35}$ treated exon 2 +/- vs untreated exon 2 +/-
3. Untreated exon 2 +/- vs untreated CTR
4. $A\beta_{25-35}$ treated exon 2 +/- vs $A\beta_{25-35}$ treated CTR

Functional Enrichment Analysis (ORA) was performed using KEGG pathway annotations with the minimal gene set to 10, p-value adjustment with the Benjamini-Hochberg (BH) procedure and cut-off set to 0.05 (Kanehisa et al., 2021).

2.2.7 Protein analysis

2.2.7.1 Media preparation

Media was collected from wells and transferred to a 1ml tube. Media was centrifuged at 10,000g for 2 minutes to pellet cellular debris. To concentrate media, 900µl each sample was added to a Amicon Ultra-2ml 10K Centrifugal Filter Unit (Sigma, Aldrich, UFC201024). Units were centrifuged for 40 minutes at 4,000g at 4°C. Filtrates were removed and stored at 20°C. Filter Units were inverted and centrifuged at 1,000g for 2 minutes at 4°C to collect the media concentrate. Media samples were concentrated 45X times generating ~44µl of concentrated media per sample.

2.2.7.2 Protein quantification

Concentrated media samples were quantified using a standard curve generated from Bovine Serum Albumin (BSA) samples of known protein concentrations. BSA was diluted in Neuronal Protein Extraction Reagent (N-PER, ThermoFisher 87792) containing 1:100

HALT™ protease inhibitor cocktail (ThermoFisher, 78429) to form standards of 2mg/ml, 1.5mg/ml, 1mg/ml, 0.75mg/ml, 0.5mg/ml, 0.25mg/ml and 0mg/ml. 10µl of each standard and concentrated media sample were added in duplicate wells of a clear 96-well plate. 150µl of Pierce™ 660nM Protein Reagent (ThermoFisher, 22662) was added to each well. And plates were shaken gently at R.T for 5 minutes. Plates were run in a CLARIOstar Plus plate reader (BMG LABTECH) and absorbance was measured at 660nM. Standard curves of absorbance for BSA standards were plotted and used to calculate the protein concentration of concentrated media samples.

2.2.7.3 Preparation of human recombinant proteins

Human clusterin recombinant protein (Recombinant Human Clusterin Protein, CF #2937-HS-050, R & D) was reconstituted at 250µg/ml in DPBS (- Ca^{2+}). For testing antibody specificity, 2µg, 0.2µg and 0.02µg samples were prepared by dilution in DPBS (- Ca^{2+}).

2.2.7.4 Extraction of total cell lysates

Following removal of media (***See 2.2.7.1***), total cell lysates were collected by the addition of 200µl 2x Laemmli Sample Buffer (LB, BioRad, #1610737) supplemented with 1:100 HALT™ protease inhibitor per well. Cells were scraped and total volumes transferred to 2ml tubes. Samples were vortexed, boiled at 95°C for 5 minutes and centrifuged at 10,000g for 1 minute. Supernatants were transferred to a new tube and stored at -20°C.

2.2.7.5 Subcellular fractionation

Cells were washed with ice cold DPBS (+ Ca^{2+}) and 150µl homogenate hypotonic buffer (10mM KCl, 1.5mM $MgCl_2$, 1mM Na-EDTA, 1mM Na-EGTA, 1mM dithiothreitol, 10mM TRIS-HCl, 0.1mM HALT, pH= 7.4) was added to each well and cells scraped. Homogenates were transferred to a 2ml tube and placed on ice for 30 minutes. 0.1% Non-Ionic Detergent (NP-40, Thermo Scientific, 9016-45-9) was added to each homogenate and

vortexed for 30 seconds. Samples were homogenised 40X times with 1ml syringes and 23-gauge needles. Samples were stored overnight at -20°C to maximise membrane disruption. Samples were thawed at R.T and centrifuged at 720g for 5 minutes at R.T. This generated a pellet (the nuclear fraction) and supernatant (mitochondrial and cytoplasmic fractions). The supernatant was transferred to a new tube and centrifuged at 10,000g for 10 minutes. Following this the supernatant (cytoplasmic fraction) was stored at -20°C. The pellet (mitochondrial fraction) was resuspended in 40µl of 2x LB supplemented with 5% β-mercaptoethanol (BME) (Sigma Aldrich, M3148). The nuclear fraction pellet was washed 3 times with 100µl of 0.25M sucrose solution (made in homogenate hypotonic buffer) and centrifuged at 720g for 5 minutes at R.T following each wash. The nuclear pellet was then resuspended in 50µl of 2x LB supplemented with 5% BME.

2.2.7.6 Deglycosylation of proteins

Proteins were N-deglycosylated using recombinant PNGase F (NEB, P0708). 2.5µl of each sample was combined with 6.5µl of water and 1µl of Glycoprotein Denaturing Buffer. This was heated at 100°C for 10 minutes, placed on ice for 5 minutes and centrifuged at 12,000g for 10 seconds. 2µl of 10X Glycoprotein Buffer 2, 2µl of NP-40 and 6µl of water was added to each sample. 1.55µl of recombinant PNGase F was added to each sample and gently mixed by pipetting. Samples were then incubated for 24 hours at 37°C and stored at -20°C.

2.2.7.7 Western blotting

All samples for western blotting were run on 10% gels. Samples were prepared as described in ***table 2.11***. Samples were heated to 95°C for 10 minutes to denature proteins and centrifuged at 10,000g for 10 seconds at R.T. Samples were resolved in running buffer (Pierce™ TRIS-glycine SDS buffer, ThermoFisher, 28362) at 150 V for 1 hour alongside 5µl

of Precision Plus Protein™ Dual Color Standards Ladder (BioRad, #1610374) using the Mini Trans-blot Cell System (BioRad). Resolved bands were transferred onto 0.45µm nitrocellulose membranes (BioRad, 1620115) in 4°C transfer buffer (Pierce™ TRIS-glycine SDS buffer, ThermoFisher, 28363) with 20% v/v methanol at 100 V for 1 hour at 4°C. Membranes were stained with Ponceau Staining Solution (0.1% (w/v) Ponceau S in 5% (v/v) acetic acid) to confirm the presence of proteins. Ponceau was removed from membranes by washing with MilliQ water before proceeding to blocking. Membranes were blocked in 5% w/v BSA in TBST for at least 1 hour on a shaker at R.T. Primary antibodies (*See table 2.12*), were incubated overnight at 4°C in 5% w/v BSA in TBST except in the case of β-actin, which was incubated for 2 hours at R.T. Membranes were washed 3 times for 5 minutes with TBST following primary antibody incubation. Species specific IRDYE® secondaries (LI-COR Biosciences, UK) were diluted at 1:10,000 in 5% w/v BSA in TBST. Secondary antibodies (*See table 2.13*) were incubated on membranes for 2 hours at R.T. Membranes were washed 3 threes for 5 minutes with TBST before imaging on an Odyssey Imager (LI-COR Biosciences, UK).

Sample type	Volume of sample (µl)	Volume of LB/BME (µl)	Total volume loaded (µl)
Total cell lysate	17.5	17.5	33.0
Cytoplasmic fraction	20.0	20.0	35.0
Nuclear fraction	10.0	10.0	18.0
Concentrated media	4µg (volume dependent on concentration)	17.5 (volume made up by addition of DPBS)	33.0
Recombinant human clusterin protein	20.0 (at each concentration)	20.0	35.0
PNGase F treated samples	20.0	20.0	35.0

Table 2.11. Sample preparation for western blotting.

Antibody	Raised in	Concentration	Supplier	Catalogue details
B-actin	Rabbit	1:1000	Cell Signalling Technology	D6A8
Clusterin	Goat	1:500/1000 (Neuron/iPSC samples)	Santa Cruz	SC-6420
Clusterin	Rabbit	1: 1:1000	Abcam	Ab69644
H3 Histone	Rabbit	1:1000	Cell Signalling Technology	#9715
β III Tubulin (TUJ1)	Mouse	1:1000	BioLegend	801213

Table 2.12. List of primary antibodies used in western blotting.

Antibody	Conjugate	Raised in	Concentration	Supplier	Catalogue
Anti- goat	IRDye 680/800	Donkey	1:1000	LI-COR Biosciences	926-68074 926-32214
Anti- rabbit	IRDye 680/800	Donkey	1:1000	LI-COR Biosciences	926-68073/ 926-32213
Anti- mouse	IRDye 680/800	Donkey	1:1000	LI-COR Biosciences	926-68072/ 926-32212

Table 2.13. List of secondary antibodies used in western blotting.

2.2.7.8 Analysis

Images were imported into Li-COR Image Studio™ Lite Quantification Software for densitometry analysis (https://www.licor.com/bio/image-studio-lite/). Around each protein band, a rectangle was placed inclusive of all staining to give the signal density value. The ratio of the signal density of the protein of interest to housekeeper was calculated giving the relative density. The average relative density of the control samples was then calculated, and all samples normalised to this value. The average expression of each protein was quantified. The mean and SEM between each biological group was then calculated unless otherwise stated.

2.2.8 Imaging

2.2.8.1 Live imaging

2.2.8.1.1 Live/Dead Cell Staining

Calcein AM and Ethidium Homodimer (ET/HD) (Live/Dead Cell Staining Kit II, Promokine, PK-CA707-30002) were diluted from 4mM to 500nM and from 2mM to 1µM respectively in B27 media. 50% of media in each well containing iPSC-neurons was removed and

replaced with B27 containing Calcein AM and ET/HD. Cells were incubated at 37°C for 40 minutes and then imaged live at 37°C and 5% CO_2 using an Operetta Phenix Confocal Microscope (Perkin Elmer). Images were taken at 20x magnification to obtain images of live and dead cells. A water immersion objective was used in the confocal operational mode. Images were taken with the following properties for each channel:

- Alexa 488: time 20ms, power 20% and height 0.0μm (Calcein AM).
- Alexa 555: time 40ms, power 80% and height 0.0μm (ET/HD).

For each independent differentiation, 12 wells in each 96 well-plate were imaged, including 17 fields within each well. 6 wells contained untreated cells and 6 contained treated cells. Within each well 17 fields were imaged with 1% overlap. Stack images were taken at heights of -2μm, 0μm and +2μm.

See section ***2.2.8.4.1*** for details on image analysis.

2.2.8.1.2 CytoTox-Glo™ Cytotoxicity Assay

Components of the CytoTox-Glo ™ Cytotoxicity Assay kit (Promega, G9291) were thawed at 37°C for 10 minutes prior to addition to cells. Per well of a 96-well plate 50μl of the AAF-Glo™ reagent was added and incubated at R.T for 15 minutes. AF-GlO™ is a lumogenic peptide substrate that cannot cross the membrane of live cells and was used to quantify the number of dead cells in each culture following treatment. Luminescence was read on a PHERAstar FSX after the addition of AF-Glo™. Cell death was then induced in the remaining live cells in each culture by the addition of 50μl of Lysis reagent containing digitonin and AF-GlO™. Cells were incubated in this for 15 minutes at R.T. Again, luminescence was read giving the total number of dead cells in each well. Dead/Total Dead ratios for each condition were then calculated.

2.2.8.2 Immunocytochemistry

50% of media in each well was removed from cells and replaced with the same volume of 8% paraformaldehyde (PFA, ThermoFisher, 28908). Cells were incubated in 4% PFA/media solution for 15 minutes at R.T. Total volume was removed and cells washed twice with 100µl of DPBS (- Ca^{2+}). Cells were simultaneously permeabilised and blocked in 100µl DPBS (- Ca^{2+}) containing 0.25% v/v Triton-X -10% v/v donkey serum for 1 hour at R.T. Primary antibodies (***See table 2.14***) were diluted in DPBS (- Ca^{2+}) containing 0.25% v/v Triton-X and 5% v/v donkey serum. 50µl diluted primary antibodies were added to each well and cells incubated overnight at 4°C. Primary antibodies were removed and cells were washed with 100µl DPBS (- Ca^{2+}) for 5 minutes, this was done 3 times. Secondary antibodies (***See table 2.15***) were diluted 1:500 in DPBS (- Ca^{2+}) for 1 hour at R.T. Secondary antibodies were removed and cells were incubated for 1 minute with 100µl Hoechst/DAPI nuclear stain (Thermo Fisher, 20mM, #62249) diluted 1:10,000 in DPBS (- Ca^{2+}). This was removed and cells washed a further 3 times with 100µl DPBS (- Ca^{2+}).

Antibody	Raised in	Concentration	Supplier	Catalogue details
MAP2	Chicken	1:1000	Abcam	Ab5392
CTIP2	Rat	1:500	Abcam	Ab18465

Table 2.14. List of primary antibodies used in confocal microscopy.

Antibody	Conjugate	Species raised in	Concentration	Supplier	Catalogue
Anti-chicken	AlexaFluor 647	Goat	1:500	Life Technologies	A-21449
Anti-rat	AlexaFluor 488	Donkey	1:500	Life Technologies	A-21208

Table 2.15. List of secondary antibodies used in confocal microscopy.

2.2.8.3 Imaging of fixed cells

2.2.8.3.1 Imaging of cortical marker CTIP2

Images were taken at 20x magnification using an Opera Phenix High Content Screening System (Perkin Elmer), in a water objective and confocal operational mode. Images were taken with the following properties for each channel:

- Alexa 488: time 600ms, power 80% and height 2.0µm (CTIP2)
- Alexa 647: time 600ms, power 80% and height 2.0µm (MAP2)
- DAPI: time 160ms, power 80% and height 2.0µm

For each independent differentiation 3 wells per 96-well plate were imaged, including 10 fields within each well with 0% overlap. Stack images were taken at a height of -2µm, 0µm and +2µm.

2.2.8.3.2 MAP2 imaging of neurite length

Images were taken at 20x magnification in a water objective and confocal operational mode. Images were taken with the following properties for each channel:

- Alexa 647: time 600ms, power 80% and height 2.0µm (MAP2)
- DAPI: time 160ms, power 80% and height 2.0µm

Per each treatment condition 6 wells of a 96-well plate were imaged. Each plate represented an independent differentiation of iPSC-neurons. In each well 10 fields were imaged with 0% overlap 3 stack images were taken at a height of -2μm, 0μm and +2μm

2.2.8.4 Harmony analysis

Immunofluorescent images were analysed using the Harmony High-Content Analysis Software (Perkin Elmer). Images were imported into the Harmony interface and analysed using pipelines as detailed below.

2.2.8.4.1 Live/Dead Ratio analysis

Analysis began with 'input image' command, which processed the 3 stack images by stacking with maximum projection. A flat field correction was implemented with basic correction to all images. Live nuclei were identified using the 'find nuclei' method 'A' in the Alexa 488 channel. 'Dead cells' were identified using the 'find nuclei' method 'C' in the Alexa 555 channel. Alexa 555 channel intensity was then measured using the 'calculate intensity properties'. Using the 'select population' command 'dead nuclei' were filtered out of the analysis if the intensity in the Alexa 555 channel was < 4000. The 'calculate property' command calculated properties of 'dead nuclei' including length, roundness, and area. The 'select population' command selected 'dead nuclei' with a length of <15μm, roundness > 0.75 and area >17$\mu m^{2.}$ This gave the confirmed number of 'dead cells'.

2.2.8.4.2 CTIP2 expression analysis

Analysis began with the 'input image' command, which processed the stack images by stacking with maximum projection. A flat field correction was implemented with basic correction to all images. 'Find cells' method 'B' was used in the Alexa 647 channel identifying MAP2 positive cells. The 'find nuclei' method 'B' was then used in the DAPI channel and ROI 'cells' to confirm DAPI and MAP2 expression in cells termed 'confirmed

cells'. The 'calculate morphology properties' command was applied to the 'confirmed cells' population using a standard method. The roundness of nuclei was calculated. Filtering of nuclei was achieved by using the 'select Population' command. Nuclei were selected with roundness >0.6 and area of <350μm^2. The 'calculate intensity properties' quantified the intensity of fluorescence in the 488 channel (CTIP2) of the 'confirmed cells' population. Cells were selected with 488 intensity of >3000 using the 'select population' command.

2.2.8.4.3 MAP2 neurite length analysis

Analysis began with 'input image' command, which processed the stack images by stacking with maximum projection. A flat field correction was implemented with basic correction to all images. 'Find nuclei' method 'A' identified the population of nuclei in the DAPI channel, these nuclei were termed 'nuclei'. The 'calculate morphology properties' command was applied to the 'nuclei' population using a standard method. The area and roundness of nuclei were calculated. Filtering of nuclei was achieved by using the 'select Population' command. Nuclei were selected with an area > 40μm^2 generating a population of 'confirmed nuclei'. Using the 'confirmed nuclei' population, neurites were identified using the 'find neurite' command. Neurites were identified in the Alexa 647 channel and the CSIRO neurite analysis method used for calculating neurite segment properties.

2.2.8.5 Statistics

Statistical significance was set as $p<0.05$. Statistical tests were performed in GraphPad Prism (v. 7.02). A normal distribution in cell populations was assumed and two-tailed parametric tests used. Comparisons between two groups were made using an unpaired t-test. For comparisons of more than two groups, One-way ANOVA with Tukey's multiple comparisons *post hoc* test was used. For comparisons between populations with two independent variables (i.e., genotype and treatment condition), two-way ANOVA with

Tukey's multiple comparisons *post hoc* test was used. Data are shown as mean ± SEM unless otherwise indicated.

3 Optimisation of CRISPR/Cas9 protocols and generation of the exon 2 +/- iPSC line

3.1 Introduction

The combined use of human iPSC technology and CRISPR/Cas9 gene editing has revolutionised the way researchers study human diseases *in vitro*. CRISPR/Cas9 can be used to introduce specific and precise changes to DNA sequences enabling the study of genes, and gene variants and their contributions to human diseases. Increasing numbers of papers incorporate CRISPR/Cas9 to study neurodegenerative diseases (Y.-C. Chen et al., 2017; Paquet et al., 2016; S. Yang et al., 2017). However, editing efficiency is lower in human iPSCs compared to other cell types (Cong et al., 2013; Le et al., 2019; Mali et al., 2013; L. Yang et al., 2013). Therefore, the testing and optimisation of CRISPR/Cas9 protocols is essential to increase the success of generating iPSCs with the desired edit. Several factors have previously been shown to influence editing efficiency in cells, which includes, but is not limited to, cell density/confluency at time of editing (Yu et al., 2016), the composition of RNP complexes and the concentration of Cas9 reagents delivered to cells (Liang et al., 2015; Seki & Rutz, 2018). Typically, CRISPR/Cas9 protocols require the generation of single cell suspensions to promote contact between cells and CRISPR/Cas9 reagents. This is tolerated by many cell lines but not so well by human iPSCs and a major barrier to editing human iPSCs is cell death, which subsequently reduces the efficiency of gene editing. Typically, most protocols suggest the addition of reagents such as rock inhibitor (Ri) to support growth of single cell colonies (Chen & Pruett-Miller, 2018; Watanabe et al., 2007) and others have demonstrated BCL-XL overexpression also promotes survival of human iPSCs (Li et al., 2018).

Other considerations such as the method used to deliver CRISPR/Cas9 reagents can be made. Electroporation and nucleofection techniques are shown to generate higher efficiencies of editing in cell lines (Kim et al., 2014; Yu et al., 2016), however, these induce large amounts of cell death especially when combined with the use of plasmids to introduce the CRISPR/Cas9 reagents (Li et al., 2018), which is not ideal for sensitive cell lines such as human iPSCs. The delivery of Cas9 and gRNA as RNPs provides a reduction in the probability of generating off-target editing and reduced cell toxicity (Kim et al., 2014; Liang et al., 2015; Ramakrishna et al., 2014). However, editing efficiency at the target locus may be reduced when using lipofectamine delivery methods compared to electroporation and nucleofection (Liang et al., 2015; Yu et al., 2016). Therefore, it is essential for protocols, transfection conditions and reagents to be tested prior to use. Ideally, a delivery system is chosen with a balance between good editing efficiency and low toxicity.

Exon 2 of *CLU* contains the ER signal peptide that is thought to be required for the generation of mature, glycosylated and cleaved clusterin, that is ultimately secreted from cells (Kapron et al., 1997; Rohne et al., 2016; Urban et al., 1987). However, intracellular clusterin proteins also exist that arise from *CLU* mRNA transcripts that lack exon 2 (Leskov et al., 2003; Prochnow et al., 2013; Reddy et al., 1996) and have a pro-apoptotic function in cells (Leskov et al., 2003; Yang et al., 2000). However, their role in neurodegeneration and AD is unexplored. Trafficking of glycosylated clusterin species is altered by Aβ in rodent neurons (Killick et al., 2014) but this has not yet been demonstrated in human iPSC-neurons. It is the aim of this chapter to use CRISPR/Cas9 gene editing to generate an iPSC line that lacks *CLU* exon 2 to generate a model in which altered clusterin trafficking can be studied *in vitro*.

In this chapter the following questions were addressed:

1. What factors influence the efficiency of Cas9 cleavage at the *CLU* exon 2 locus in CTR human iPSCs?
2. Can CRISPR/Cas9 gene editing be used to successfully excise exon 2 from *CLU*?
3. Can *CLU* exon 2 edited cells be used to generate a neuronal model for studying altered clusterin trafficking in AD?

3.2 Results

3.2.1 Generating an optimised CRISPR/Cas9 protocol for excision of *CLU* exon 2 in human iPSCs

To generate an iPSC line lacking *CLU* exon 2, a dual guide sgRNA approach was chosen, in which a 5' sgRNA would recruit Cas9 to cut within *CLU* intron 1 and a 3' sgRNA would recruit Cas9 to cut *CLU* intron 2 (***Figure 3.1***). sgRNAs were designed by Dr. Hublitz (Weatherall Institute of Molecular Medicine, University of Oxford). DNA sequences of *CLU* introns 1 and 2 were obtained from NCBI and submitted to CRISPOR Software to generate sgRNA sequences. The CRISPOR Software (http://crispor.tefor.net/) enables generation of sgRNA detailing their specificity and off-targets. Three 5'sgRNA (#1, #2, #3) and three 3'sgRNA (#1, #2, #3) were identified with low number of off-targets and were chosen for this project (***See Chapter 2, 2.2.2.1***).

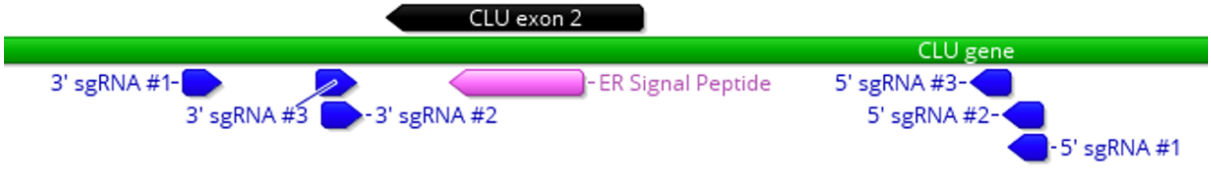


Figure 3.1. Schematic diagram of the dual sgRNA approach used to excise CLU exon 2.

Three 5' sgRNAs (#1, #2 and #3) were designed to recruit Cas9 to cut intron 1 of CLU. Three 3' sgRNAs (#1, #2 and #3) were designed to recruit Cas9 to cut in intron 2 of CLU. sgRNA were designed by Dr. Hublitz.

A Surveyor Nuclease Assay was used to test the efficiency of each 5' sgRNA and 3' sgRNA to recruit Cas9 to the target DNA sequence and produce a cut (***See Chapter 2, 2.2.2.2***). HEK293T cells were transfected with one of the six sgRNA outlined in ***Figure 3.1***. A negative control condition was included in which HEK293T cells were transfected with Cas9 but no sgRNA therefore Cas9 should not be recruited to the target locus to induce

any cutting in these cells. Following transfections, gDNA was extracted from cells and run in a Surveyor Nuclease Assay performed by Dr. Hublitz. WT and mutant double stranded DNA were subjected to a series of PCR annealing and denaturing steps to produce homoduplexes and heteroduplexes. Duplexes were then combined with a Surveyor Nuclease enzyme that detects mismatches in the sequence of the two DNA strands. These mismatches are indicative of a Cas9 cutting event that has resulted in the introduction of an indel. Once a mismatch is detected, the Surveyor Nuclease enzyme cuts the DNA into fragments that were run on an agarose gel to compare the extent to which each sgRNA recruited Cas9 to cut DNA (***Figure 3.2A***).

All three 5' sgRNAs were shown to efficiently recruit Cas9 to *CLU* intron 1 and DNA cleavage was observed, indicated by the presence of two high intensity bands on the agarose gel (***Figure 3.2B***). In the negative control condition, no mismatches were identified, and DNA was not cut. This confirms that both sgRNA and Cas9 are required to generate a cut at the target locus within *CLU* intron 1 (***Lane 2, Figure 3.2B***). In comparison, when cells were transfected with Cas9 but no 3' sgRNA two cleaved DNA bands were observed at ~200bp and ~300bp (***Lane 2, Figure 3.2C***). These bands observed in the negative control condition were also seen in each transfection condition in which sgRNA was delivered to cells. This indicates the presence of a mismatch in the sequence of the DNA strands within *CLU* intron 2; there is a heterozygous natural variant present within the sequence in HEK293T cells. Overlap between the bands generated from the presence of the natural variant and those generated from Cas9 induced cutting was observed in cells transfected with 3' sgRNA #1 generating thicker DNA bands on the agarose gel (***Lane 3, Figure 3.2C***). Based on these results, all six sgRNAs tested were suitable for use in CRISPR/Cas9 editing of *CLU* exon 2.

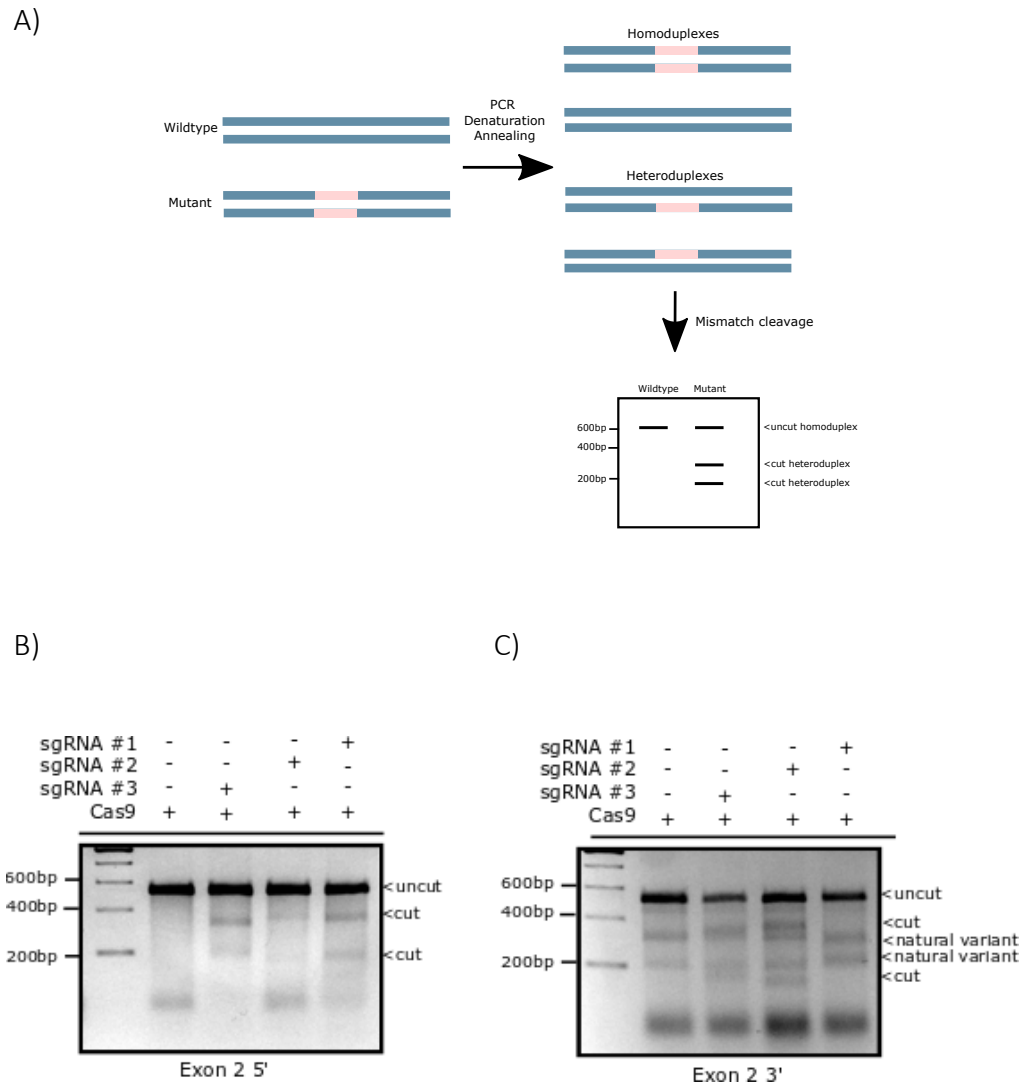
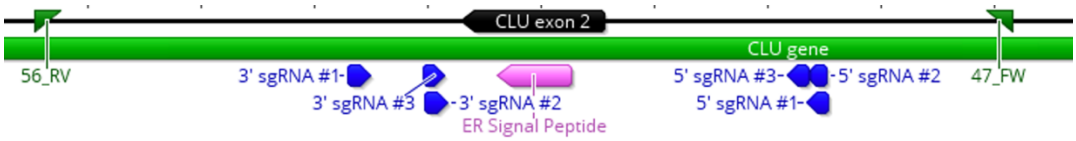


Figure 3.2. Surveyor Nuclease Assay confirms 5' and 3' sgRNA efficiently recruit Cas9 in HEK293T cells. ***A****) A schematic diagram outlining a Surveyor Nuclease Assay performed by Dr. Hublitz. Briefly, HEK293T cells were transfected with Cas9 and each of the 6 sgRNA individually. Following transfection, gDNA was extracted and a Surveyor Nuclease Assay performed. DNA fragments were run on a 2.5% agarose gel to compare efficiency of each sgRNA to recruit Cas9 to cut DNA.* ***B****) HEK293T cells were transfected with one of the three 5'sgRNA. All three 5' sgRNA efficiently recruited Cas9 to cut DNA and no bands were seen in the negative control condition (lane 2).* ***C****) HEK293T cells were transfected with one of the three 3' sgRNA. All three 3' sgRNA were shown to efficiently recruit Cas9 to cut DNA. Bands at ~200bp and ~300bp in the negative control condition (lane 2) indicate the presence of a naturally occurring variant.*

The observation of a cut DNA fragment in the 3' sgRNA negative control condition indicates the presence of a heterozygous variant within *CLU* intron 2. gDNA was extracted from CTR iPSCs and the *CLU* exon 2 locus amplified by PCR using primers located in *CLU* introns 1 and 2. PCR products were then submitted for Sanger Sequencing (***Figure 3.3A, see Chapter 2, 2.2.4-2.2.5.1***). Forward (FW) and reverse (RV) sequence traces were aligned with each other and with the genomic *CLU* sequence obtained from NCBI (***Figure 3.3B***). After alignment, a reduction in sequence quality was identified at the same position in the forward and reverse sequences (***Figure 3.3B, position indicated by the blue arrow***). Analysis of the sequence traces identified a heterozygous insertion of a 'T' nucleotide in *CLU* intron 2 (***Figure 3.3B, position indicated by the red block***). The position of this variant was located within the sequence complementary to 3' sgRNA #2 and #3 and would therefore interfere with the complementary binding of these sgRNA to the *CLU* DNA sequence at this position.

A)



B)

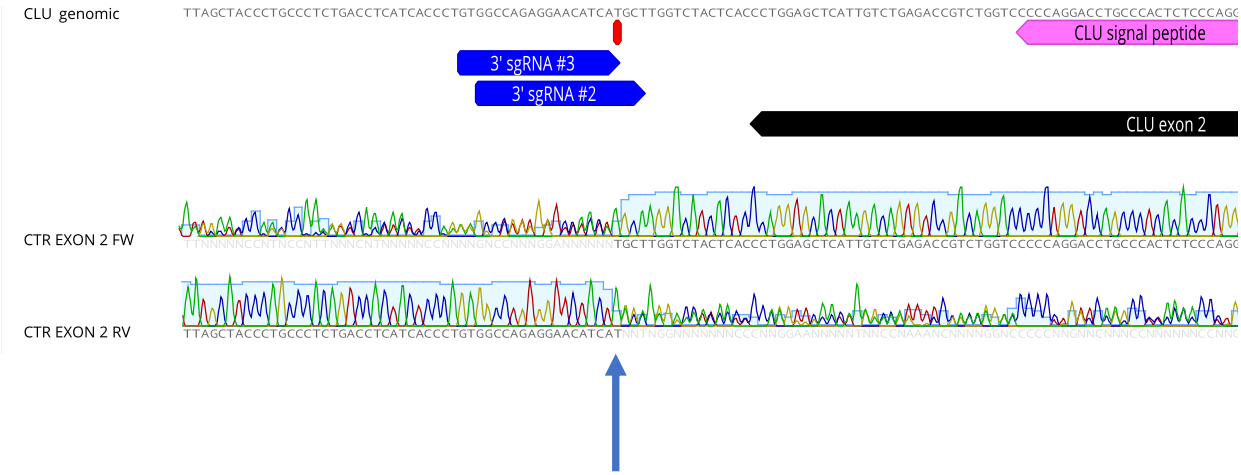


Figure 3.3. A heterozygous natural variant was identified in CLU intron 2 in CTR iPSCs.

***A**) gDNA was extracted from CTR iPSCs and CLU* exon 2 *amplified using primers located in introns 1 and 2. PCR products were then sequenced by Sanger sequencing. **B**) Forward (FW) and reverse (RV) sequences were aligned with each other and with the CLU genomic sequence obtained from NCBI. A reduction in sequence quality (at the position of the blue arrow) was observed at the same position in both FW and RV sequences indicating the position of a natural variant. A heterozygous insertion of a 'T' nucleotide was identified within the sequence complementary to 3' sgRNA #2 and #3 as shown on the schematic.*

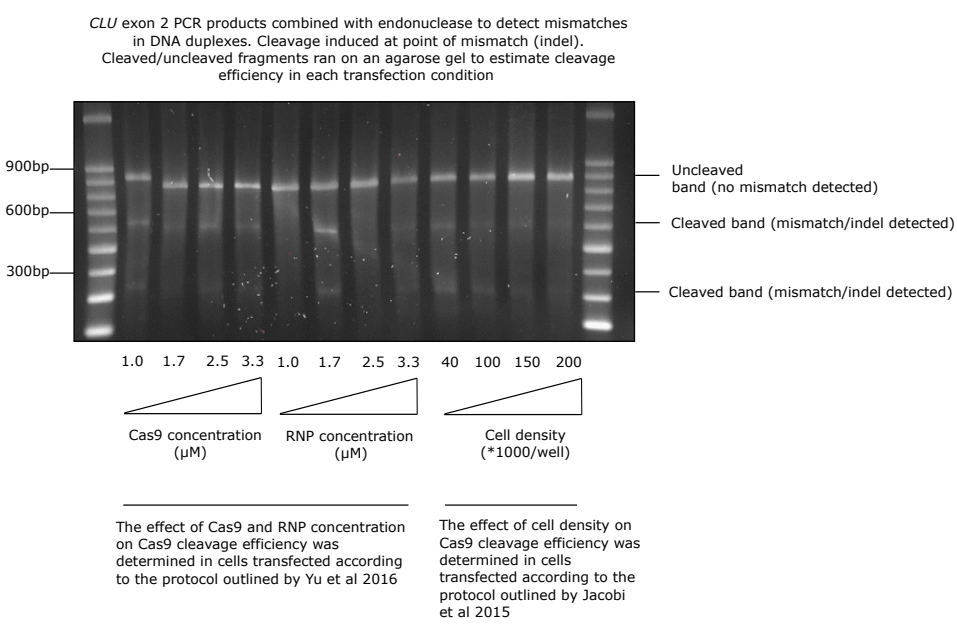
With the aim of using CRISPR/Cas9 to excise *CLU* exon 2 from human iPSCs, two protocols were identified, and their editing efficiency tested. Yu et al., previously tested 60 transfection reagents to determine which reagent had the highest efficiency when delivering Cas9 RNPs into mammalian cells, including human iPSCs (Yu et al., 2016). Jacobi et al., incorporated individual tracrRNA and crRNA elements complexed together to form

sgRNA (Jacobi et al., 2017). Using the protocol outlined by Yu et al., the concentration of Cas9 added during the formation of RNPs was altered, in addition, the concentration of RNPs delivered to cells was also altered to determine the effects on Cas9 cleavage efficiency (***See Chapter 2, 2.2.2.6***). To determine the influence of cell density on Cas9 cleavage efficiency, the density of iPSCs at plating was varied when transfecting cells according to the Jacobi et al., protocol (***See Chapter 2, 2.2.2.7***). In each condition, a single well of a 24-well plate containing CTR iPSCs was cultured and transfected with 3' sgRNA #1 and 5' sgRNA #3. Cas9 cleavage efficiency was estimated in each transfection condition using a GeneArt Cleavage Detection Kit (***See Chapter 2, 2.2.2.9***). PCR products were incubated with T7 endonucleases that identify and cut mismatches in DNA. DNA fragments generated were run on an agarose gel (***Figure 3.4A***) and efficiency was quantified by comparing the relative intensity of uncleaved and cleaved DNA fragments representing WT and edited DNA respectively (***Figure 3.4B-D***, ***see Chapter 2, 2.2.2.9***).

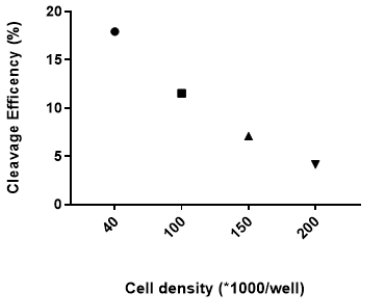
Cas9 cleavage efficiency was reduced as cell density increased (***Figure 3.4B***). The highest efficiency (~18%) was observed at 40,000 cells per well in a 24-well plate, this dropped to ~12% when 100,000 cells were plated per well, ~7% when 150,000 cells per plated and ~4% when 200,000 cells per plated per well. The highest efficiency was demonstrated when 1.7µM Cas9 and 1.0µM sgRNA (~22%) was added during RNP formation (***Figure 3.4C***). However, further increases in Cas9 concentration reduced the efficiency of Cas9 cleavage. Finally, increasing the concentration of RNPs delivered to cells to 1.7µM achieved the highest efficiency of cleavage of Cas9 (~29%) (***Figure 3.4D***). Increasing RNP concentration to 3.3µM reduced efficiency to ~6%. No cleavage of DNA was observed when either 1.0µM and 2.5µM of RNP complexes were delivered to cells (***Figure 3.4D).*** This was likely due to an error in the preparation of transfection reagents or

during the performance of the GeneArt Cleavage Detection Kit protocol. Based on these results from these results, the highest cleavage efficiency was observed when 40,000 cells per well were plated and transfected using 1.7μM of RNP complex using CRISPRMAX™ lipofectamine reagent according to a protocol outlined previously (Yu et al., 2016).

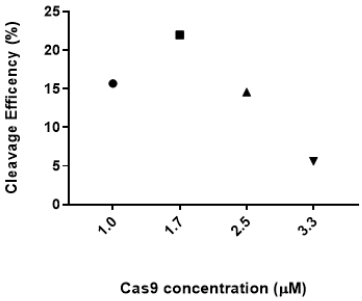
A)


CLU exon 2 PCR products combined with endonuclease to detect mismatches in DNA duplexes. Cleavage induced at point of mismatch (indel). Cleaved/uncleaved fragments ran on an agarose gel to estimate cleavage efficiency in each transfection condition
900bp
600bp
300bp
Uncleaved band (no mismatch detected)
Cleaved band (mismatch/indel detected)
Cleaved band (mismatch/indel detected)
1.0 1.7 2.5 3.3 1.0 1.7 2.5 3.3 40 100 150 200
Cas9 concentration (μM)
RNP concentration (μM)
Cell density (*1000/well)
The effect of Cas9 and RNP concentration on Cas9 cleavage efficiency was determined in cells transfected according to the protocol outlined by Yu et al 2016
The effect of cell density on Cas9 cleavage efficiency was determined in cells transfected according to the protocol outlined by Jacobi et al 2015

B)


Cleavage Efficency (%)
20
15
10
5
0
40
100
150
200
Cell density (*1000/well)

C)


Cleavage Efficency (%)
25
20
15
10
5
0
1.0
1.7
2.5
3.3
Cas9 concentration (μM)

D)

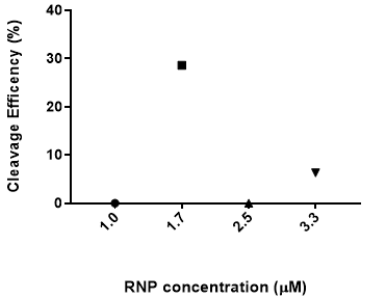

Cleavage Efficency (%)
40
30
20
10
0
1.0
1.7
2.5
3.3
RNP concentration (μM)

Figure 3.4. Cell density, Cas9 concentration and RNP concentration influence the efficiency of Cas9 cleavage at the CLU exon 2 locus.

The efficiency of two protocols to edit the CLU exon 2 locus was tested. CTR iPSCs were transfected with Cas9, 5' sgRNA #3 and 3' sgRNA #1 according to one of two protocols (Yu et al 2016 and Jacobi et al 2015, ***2.2.2.6*** *and* ***2.2.2.7*** *respectively). The influence of cell density, RNP concentration and Cas9 concentration in RNP formation on Cas9 cleavage efficiency was tested.* ***A****) 24 hours following transfection, a GeneArt Cleavage Detection Kit was used to estimate Cas9 cleavage efficiency. Lysates were collected from wells containing transfected cells and the CLU exon 2 locus was amplified. Mismatches In DNA duplexes were detected following incubation with a detection enzyme, which detects mismatches between DNA strands and cleaves DNA to produce DNA fragments. PCR products were run on a 2% agarose gel to visualise uncleaved and cleaved DNA fragments to estimate cleavage efficiency in each transfection condition. Cleaved fragments represented DNA sequences that were cut by the detection enzyme following detection of an indel. Cleavage efficiency was then calculated for each transfection condition by comparison of the uncleaved and cleaved band intensities.* ***B****) Cell density negatively influenced the efficiency of Cas9 cleavage, the highest efficiency (18%) was observed when 40,000 cells per well were plated. The lowest efficiency (4%) was observed when 200,000 cells per well were plated.* ***C****) Increasing the concentration of Cas9 added during the formation of RNP complexes resulted in the highest efficiency at 1.7µM Cas9 (22%), increasing Cas9 concentration further reduced cleavage efficiency.* ***D****) Increasing the concentration of RNP complexes delivered to cells resulted in the highest efficiency at the addition of 1.7µM RNP complexes (29%). Increasing RNP concentration to 3.3µM reduced efficiency to 6%. No cleaved bands were observed after delivery of 1.0µM or 2.5µM of RNP complexes, this is likely attributed to errors in the preparation of transfection reagents. Each data point represents a single well of CTR iPSCs transfected with CRISPR/Cas9 reagents.*

3.2.2 Generation and confirmation of a heterozygous exon 2 knockout human iPSC line

Following confirmation of the transfection conditions that provided the highest Cas9 cleavage efficiency, CTR iPSCs were plated at 40,000 cells per well in a 24-well plate and transfected with 1.7µM of RNP complexes according to the Yu et al., protocol (Yu et al., 2016). Following transfections and single cell clone expansions (*See Chapter 2, 2.2.2.10-*

11), gDNA was extracted from 80 single cell clones, the *CLU* exon 2 locus PCR amplified and submitted for Sanger sequencing (***See Chapter 2.2.4 and 2.2.5.1***). FW sequences of each iPSC clone was aligned with the FW sequence obtained from CTR iPSCs and the *CLU* genomic sequence obtained from NCBI. Sequence alignment identified Clone 30 to be edited at the *CLU* exon 2 locus (***Figure 3.5A***). A reduction of sequence quality was observed at both the 5' and 3' loci of *CLU* exon 2 in the Clone 30 FW trace (***Figure 3.5A, indicated by the position of the blue arrows***). This is absent in the CTR FW sequence, indicating the reduction of sequence quality had arisen from Cas9 cutting the *CLU* sequence in Clone 30 iPSCs. Further interrogation revealed two nucleotides present at each position in the Clone 30 sequence following the reduction in sequence quality, therefore the two *CLU* alleles at this locus contain different sequences to each other (***Figure 3.5B***). This again, was absent in the CTR FW sequence trace.

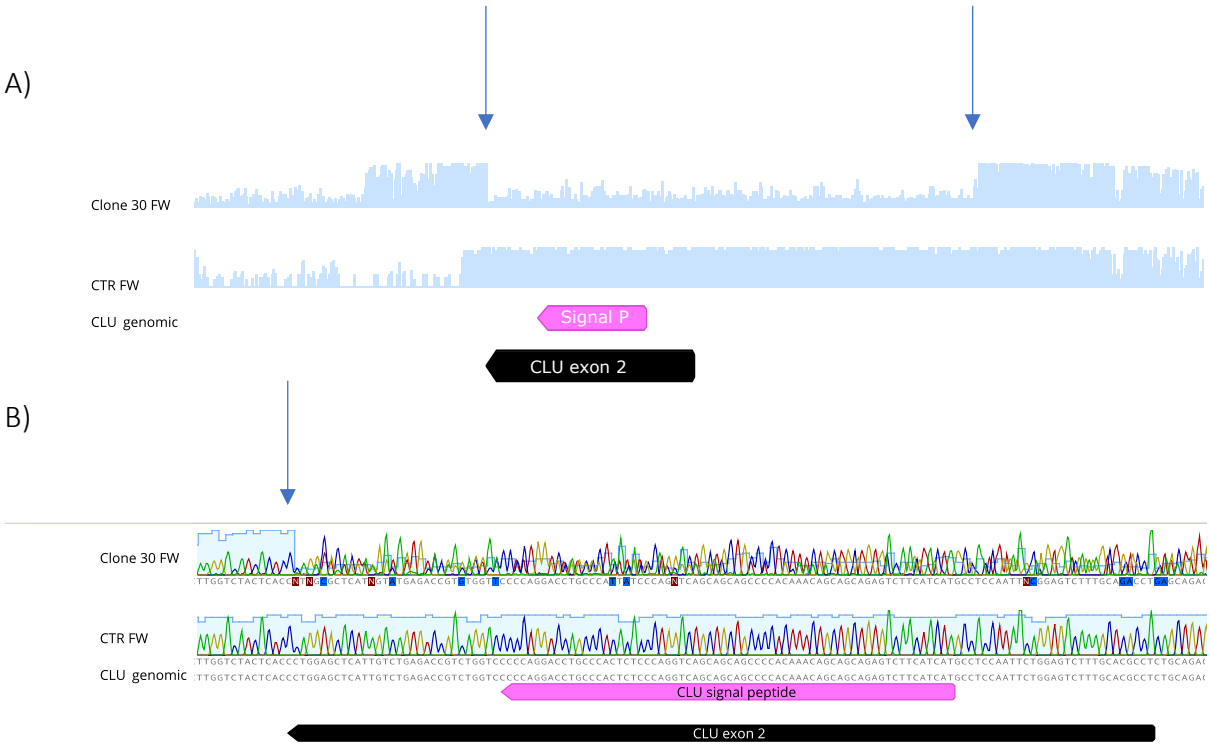


Figure 3.5. Clone 30 iPSCs are edited at the CLU exon 2 locus.

Following transfection, gDNA was extracted from all clones and amplified using primer set 47 and 56 positioned in CLU introns 1 and 2 respectively. PCR products were then submitted for Sanger sequencing to identify clones in which exon 2 had been excised. Sequencing traces were then aligned with the sequence trace from CTR iPSCs (CTR FW) and the CLU genomic sequence obtained from NCBI. ***A****) Alignment of Clone 30 sequence (Clone 30 FW) with the CTR FW and CLU genomic sequence reveal Clone 30 cells as edited. The blue arrows indicate the position of reduced sequence quality.* ***B****) Following the reduction in sequencing quality (indicated by the presence of the blue arrow) dual peaks are observed in the Clone 30 FW sequence trace indicating the two CLU alleles of Clone 30 iPSCs express differing nucleotide sequences to each other suggesting a heterozygous edit.*

The data indicate that Clone 30 iPSCs were edited at the *CLU* exon 2 locus. To confirm exon 2 had been excised from Clone 30 iPSCs, gDNA was amplified using primers located in introns 1 and 2, but further away from the sites at which Cas9 cut the DNA (***See Chapter 2, 2.2.5.2***). Products were then run on an agarose gel to visualise *CLU* alleles in CTR and

Clone 30 iPSCs (***Figure 3.6***). A single PCR band of ~2581bp was observed after amplification of CTR (+/+) gDNA indicating both *CLU* alleles are identical to each other and contain *CLU* exon 2. In comparison, two distinct PCR bands were observed after amplification of Clone 30 (+/-) gDNA. One band represented the WT allele in Clone 30 cells, this was identical to the PCR band generated in CTR gDNA. The additional, smaller PCR band represents the edited allele from which exon 2 had been excised. Based on these results, Clone 30 iPSCs are a heterozygous exon 2 knockout iPSC line.

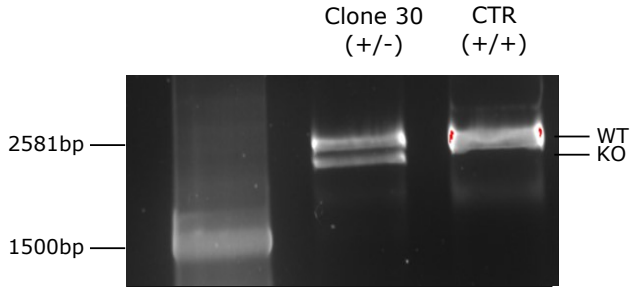


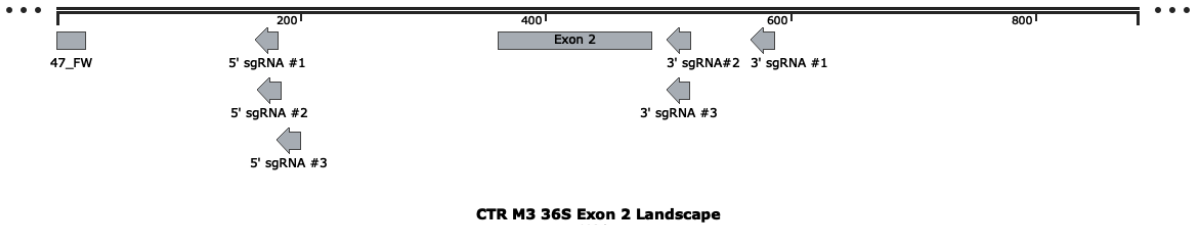
Figure 3.6. Clone 30 cells are heterozygously edited at the CLU exon 2 locus.
gDNA was extracted from CTR (+/+) and Clone 30 (+/-), amplified at the CLU exon 2 locus and PCR products separated on a 1% agarose gel. Both CLU alleles were confirmed to be of equal size in CTR (+/+) as a single PCR band (~2581bp) was observed. Two PCR bands were observed in the Clone 30 (+/-) lane. One band represents the WT, non-edited CLU allele, and the smaller PCR band represents the CLU allele from which exon 2 has been excised. Clone 30 is a heterozygous exon 2 knockout iPSC line.

Bacterial transformation was next performed by Dr. Hublitz to obtain the exact sequence of both *CLU* alleles in Clone 30 iPSCs. CTR and Clone 30 gDNA was extracted and provided to Dr. Hublitz for amplification and subcloning into *E. coli* (***See Chapter 2, 2.2.5.3***). Sequence traces of each PCR product was obtained and analysed using SnapGene software (***See Chapter 2, 2.2.5.3.3***). 17 CTR PCR products were sequenced and confirmed

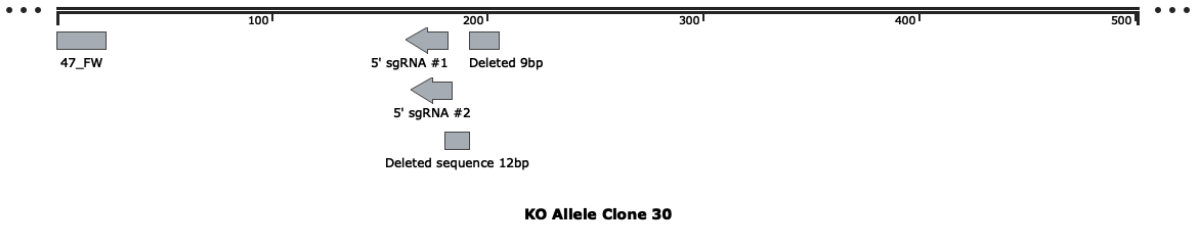
to be identical to each other (***Figure 3.7A***). This was used as the representative WT *CLU* exon 2 locus for analysis of Clone 30 PCR products (***Figure 3.7B and C***). 17 PCR products were obtained from Clone 30 gDNA, 12 of which were confirmed to be KO and 5 were confirmed to be WT. Each KO PCR product was confirmed to be identical to each other, similarly, each WT PCR product was confirmed to be identical to each other. This confirms Clone 30 iPSCs are clonal and not a mixed population of cells.

A deletion was identified between 5' sgRNA #3 and 3' sgRNA #1 sites, giving rise to a 394bp deletion in the KO allele. An additional 12 nucleotides were deleted from the 3' side of the 5' sgRNA #3 locus and 9 nucleotides were deleted from the 5' end of the 3' sgRNA #1 locus (***Figure 3.7B***). A 17bp deletion was identified in the WT allele at the 3' sgRNA #1 locus destroying the sequence complementary to 3' sgRNA #1. This was observed within the intronic region of *CLU* and therefore will not impact on the coding sequence. No deletion was observed at the 5' sgRNA #3 locus in the WT allele (***Figure 3.7C***). The previously identified heterozygous natural variant (insertion of a single 'T' nucleotide) was absent from the WT allele in exon 2 +/- iPSCs and therefore was present on the *CLU* allele from which exon 2 had been excised. Taken together these results demonstrate Clone 30 iPSCs are a clonal heterozygous exon 2 knockout cell line, which is now referred to as exon 2 +/-.

A)



B)



C)

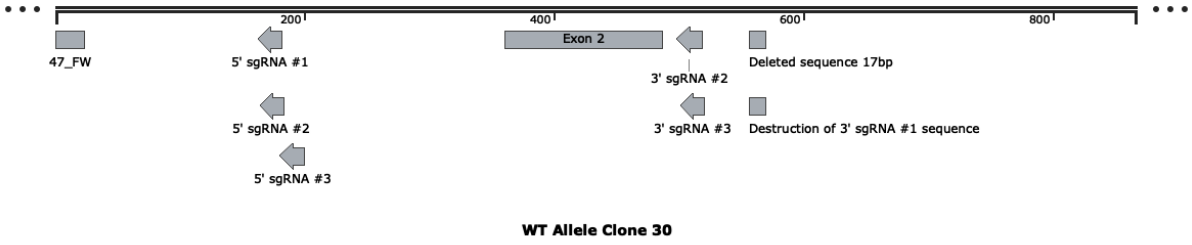


Figure 3.7. Sequencing following bacterial transformation confirms Clone 30 iPSCs are a heterozygous exon 2 knockout iPSC line (exon 2 +/-).

CTR and Clone 30 gDNA was amplified and subcloned into E.Coli for sequencing. This was performed by Dr. Hublitz. Traces were analysed and compared using SnapGene software. ***A****) Sequence traces obtained from CTR PCR products (CTR M3 36S Exon 2 landscape) were used as the reference sequence.* ***B****) Alignment of the CTR trace (CTR M3 36S Exon 2 landscape) with the PCR products defined as Clone 30 KO demonstrate a 394bp deletion in the KO allele of Clone 30 iPSCs. The deletion was between the positions of 5' sgRNA #3 and 3' sgRNA #1. Additionally, a 12bp deletion was observed at the 3' side of 5' sgRNA #3 and 9bp from the 5' of the 3' sgRNA #1.* ***C****) The WT allele of Clone 30 iPSCs retained CLU exon 2 although a 17bp deletion was observed in intron 2 at the 3' side of CLU exon 2. This destroyed the sequence complementary to 3' sgRNA # 1. No cutting or deletion was observed at the 5' end of exon 2.*

3.2.3 Confirmation of exon 2 +/- pluripotency and the generation of cortical neurons

Ultimately, the goal of this thesis was to generate a neuronal model in which clusterin trafficking is altered. With this goal in mind, CTR and exon 2 +/- iPSCs were differentiated into neurons according to the King's College protocol (***See Chapter 2, 2.2.1.2***). Cells were cultured and matured until day 35, at which point they were fixed for immunostaining (***See Chapter 2, 2.2.8.2***) and RNA was extracted for gene expression analysis (***See Chapter 2, 2.2.6.1-2.2.6.4***).

To confirm pluripotency, the expression of pluripotency markers *NANOG* and *OCT4* (*POU5F1*) was measured in CTR and exon 2 +/- iPSCs and iPSC-derived neurons and normalised to *GAPDH* (Pfaffl, 2001). *NANOG* expression was confirmed in both CTR and exon 2 +/- iPSCs and was significantly higher in iPSCs than in iPSC-neurons for both genotypes (***Figure 3.8C***). In agreement, *OCT4* expression was significantly higher in both CTR and exon 2 +/- iPSCs compared to their differentiated counterparts (***Figure 3.8D***). This is not surprising since pluripotency is lost during differentiation and therefore expression of pluripotency markers is reduced during the differentiation of iPSCs into iPSC-neurons. Interestingly, *NANOG* expression was significantly lower in exon 2 +/- iPSCs than in CTR iPSCs, whereas *OCT4* expression was similar between the two. The data confirm *CLU* exon 2 gene editing has not altered the pluripotency of exon 2 +/- iPSCs, which express two pluripotency markers. As expected, differentiation of both CTR and exon 2 +/- iPSCs into neurons resulted in a downregulation of both *NANOG* and *OCT4* expression. However, it must be noted that further investigation into the pluripotency of exon 2 +/- iPSCs may be necessary. The above data arises from a single experiment and therefore analysis may be underpowered due to the small sample size and should be repeated in future work.

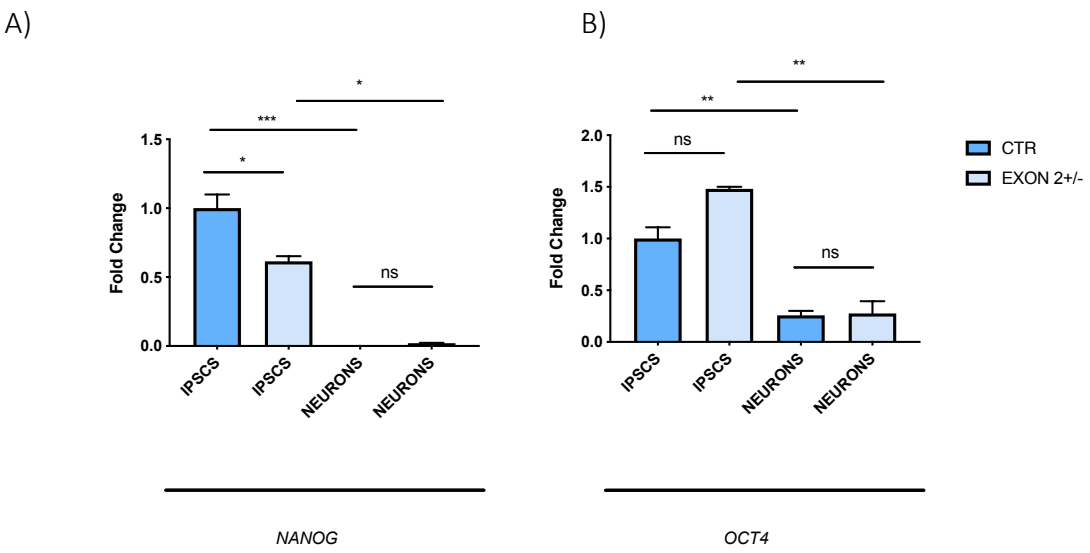


Figure 3.8. CTR and exon 2 +/- iPSCs express pluripotency markers OCT4 and NANOG.

iPSCs were then differentiated into neurons and RNA extracted from both iPSCs and day 35 differentiated neurons. Pfaffl analysis was used to quantify differences in NANOG and OCT4 expression relative to the housekeeper GAPDH. ***A****) Two-way ANOVA was used to determine the effect of cell type (iPSC or iPSC-neuron) and genotype (CTR or exon 2 +/-) on the expression of NANOG. A significant influence of cell type (p=0.0001***) and genotype (p=0.0420*) was identified. No interaction was identified between cell type and genotype (p=0.0531). Tukey's multiple comparison analysis was used to determined differences between groups. NANOG expression was significantly lower in exon 2 +/- iPSCs than in CTR iPSCs (p=0.0414*) but no significant difference was identified between exon 2 +/- and CTR iPSC-neurons (p=0.9991). NANOG expression was significantly higher in iPSCs than in iPSC-neurons for both genotypes (CTR: p=0.0070** and exon 2 +/-: p=0.0012**).* ***B****) Two-way ANOVA was used to determine the effect of cell type (iPSC or iPSC-neuron) and genotype (CTR or exon 2 +/-) on the expression of OCT4. A significant influence of cell type (p=0.0002***) but not genotype (p=0.0523) was identified. Additionally, no interaction was identified between cell type and genotype (p=0.0654). Tukey's multiple comparison analysis was used to determined differences between groups. No significant difference in OCT4 expression was identified between exon 2 +/- and CTR iPSCs (p=0.0534) or iPSC-neurons (p=0.9992). OCT4 expression was significantly higher in iPSC-neurons than in iPSCs, for both genotypes (CTR: p=0.0094** and exon 2 +/-: p=0.0016**). Data are as mean ± SEM, where n =1 (n= independent differentiation/iPSC passage set each with 3 replicate wells). Significance was tested using two-way ANOVA with Tukey's multiple comparison analysis. P<0.05*.*

Having confirmed the pluripotency of CTR and exon 2 +/- iPSCs, neuronal identity of CTR and exon 2 +/- iPSC-neurons was next confirmed. iPSC-neurons were immunostained for neuronal marker MAP2 and deeper layer cortical marker CTIP2 to confirm editing of *CLU* exon 2 in iPSCs had not impacted on the differentiation of exon 2 +/- iPSCs into neurons. Cells were imaged using an Operetta High-Content Imaging System (***Figure 3.9, see Chapter 2, 2.2.8.3.1***). CTR and exon 2 +/- iPSC-neurons were confirmed to be positive for both MAP2 and CTIP2 (***Figure 3.9A***). The percentage of MAP iPSC-neurons that were positive for CTIP2 was calculated in each condition using Harmony High-Content Imaging and Analysis Software (***See Chapter 2, 2.2.8.4.2***). 49.6 ± 10.6% of MAP2 positive CTR iPSC-neurons and 36.5 ± 3.6% of MAP2 exon 2 +/- iPSC-neurons were also CTIP2 positive. The percentage of MAP2 positive iPSC-neurons that expressed CTIP2 was comparable between CTR and exon 2 +/- cultures (***Figure 3.9B***). Therefore, the data demonstrates the suitability of using the King's College protocol for differentiating iPSCs to generate MAP2 positive neurons, of which a subpopulation are positive for cortical lineage marker CTIP2. Furthermore, the data confirm similarities in populations of CTR and exon 2 +/- iPSC-neurons.

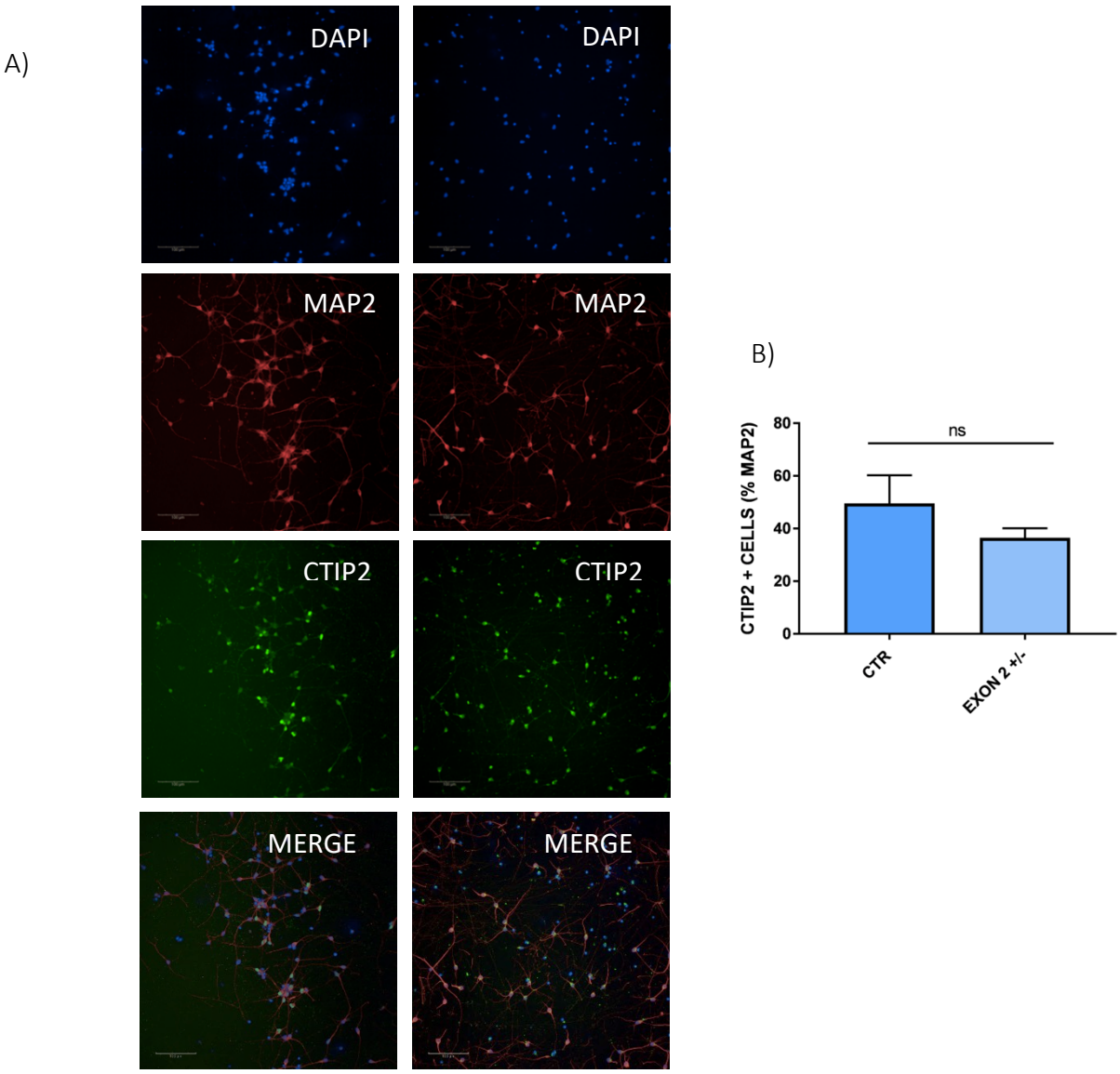


Figure 3.9. CTR and exon 2 +/- iPSCs can be differentiated into neurons positive for neuronal marker MAP2 and cortical marker CTIP2.

iPSCs were differentiated into neurons according to the King's College protocol. Cells were fixed and stained at day 35. ***A****) Images were taken at 20x magnification on an Opera Phenix Confocal Microscope and analysed using Phenix Harmony Software. Representative images of day 35 CTR and exon 2 +/- iPSC-neurons. Stains are DAPI (blue), MAP2 (red) and CTIP2 (green) positive.* ***B****) The percentage of MAP2 positive iPSC-neurons expressing CTIP2 was quantified. 49.6 ± 10.6% of MAP2 positive CTR iPSC-neurons and 36.5 ± 3.6% of MAP2 positive exon 2 +/- iPSC-neurons were CTIP2 positive. No significant differences (ns) were observed between CTR and exon 2 +/- iPSCs in the percentage of the population that expressed CTIP2 (p=0.3077). Data are shown as mean ± SEM, n= 3 (n = independent differentiations, each with 3 replicate wells). Significance p<0.05* ns = p> 0.05 using unpaired parametric t-test.*

3.3 Discussion

3.3.1 All factors tested influence Cas9 cleavage efficiency

The editing of human iPSCs is considered to be more challenging than editing of other cell types due to lower editing efficiency (Cong et al., 2013; Le et al., 2019; Mali et al., 2013; L. Yang et al., 2013). Several factors were shown to influence editing efficiency when two CRISPR/Cas9 protocols were tested and compared. Both protocols were well tolerated by iPSCs indicating their suitability for gene editing. However, a large amount of variability in editing efficiency was observed between different transfection conditions highlighting the need for careful testing and optimisation of protocols prior to their use. All three factors tested here were shown to influence editing efficiency to some degree, but Cas9 concentration and iPSC plating density were shown to be the most influential.

The optimal cell density for achieving high editing efficiency varies greatly between cell types (Yu et al., 2016). However, previous studies have indicated that iPSCs should be plated at a low density prior to transfection except when nucleofection was the transfection method of choice (Byrne & Church, 2015; Carlson-Stevermer & Saha, 2017; Yu et al., 2016). In agreement with previous findings, increasing cell density negatively impacted Cas9 editing efficiency; increasing iPSC cell density at the time of transfection is likely to result in a reduction of availability of Cas9 reagents available per cell, therefore reducing the probability of a successful editing event occurring in each cell. Although this may be circumvented by increasing the concentration of CRISPR reagents provided to cells when plated at a higher density, this was not tested here. The addition of CRISPR reagents as RNP complexes reduces toxicity but may also reduce editing efficiency, indeed, higher concentrations of RNPs are required to edit human iPSCs (Kim et al., 2014). Two concentrations of RNPs were tested and compared and the data indicates that, although

higher RNP concentration improves efficiency, this is reduced when the concentration is too high.

RNPs are generated by the mixing and heating of Cas9 and sgRNA prior to addition to cells. Typically, these are mixed at an equimolar concentration with each other (1:1) to ensure efficient RNP formation and promote higher editing efficiency. Indeed, cleavage efficiency has been shown to plateau at this 1:1 ratio (Liang et al., 2015). However, the relationship between editing efficiency and RNP composition appears not to be straight forward. Divergence from the 1:1 ratio of Cas9: sgRNA has been shown to both reduce (Yu et al., 2016), and increase Cas9 cutting efficiency (Seki & Rutz, 2018). Increasing the amount of sgRNA relative to Cas9 increases efficiency (Kim et al., 2014), but also increases the probability of off-target editing (Fu et al., 2013). In this study, editing efficiency did not plateau at 1:1 ratio, in fact it was highest at a 1.7:1 ratio of Cas9: sgRNA. Further increases of Cas9 concentration, however, reduced editing efficiency. This is likely attributed to the imbalance between Cas9 and sgRNA during RNP formation, where it is essential that Cas9 and sgRNA interact and form a complex. In agreement, previous studies have demonstrated that the addition of sgRNA but not Cas9 in excess increases the efficiency of editing (Jinek et al., 2013; Seki & Rutz, 2018), thus suggesting it is the concentration of sgRNA and not Cas9 that is the limiting factor.

An optimised protocol was generated following quantification of estimated editing efficiencies and was used to transfect CTR iPSCs to remove *CLU* exon 2. This resulted in the generation of the heterozygous exon 2 knockout line. However, generation of a homozygous exon 2 knockout line was not achieved. The GeneArt Cleavage Detection Kit enables researchers to estimate factors influencing Cas9 cleavage but only gives an overall indication of the percentage of cells in which Cas9 had cut at the target locus. This does

not give an indication of the percentage of cells where Cas9 has cut both the 5' and 3' regions of *CLU* resulting in the successful excision of exon 2. Therefore, the efficiencies calculated in this chapter are likely to be an overestimation. Further considerations for optimisation are required since only a heterozygous exon 2 KO iPSC line was generated. Although typically considered the less stressful and toxic method for delivery of Cas9 reagents, the combined use of RNPs and lipofection may not be as efficient as the use of electroporation to edit human iPSCs (Yu et al., 2016). Although requiring significantly higher number of cells and more expensive equipment, achieving high levels of editing and generation of multiple edited clones may make electroporation a more desirable approach.

3.3.2 A single heterozygous exon 2 knockout iPSC line was generated from CTR iPSCs

The combinatory use of sequencing and agarose gel electrophoresis enabled quick screening of clones, requiring a small number of cells for gDNA extraction therefore minimising culturing time. The methods chosen here for screening edited clones following transfection are optimal over other methods including the use of antibiotic selection and sorting by fluorescence (FACS). Protocols utilising FACS for selecting cells that have been edited requires many cells since FACs is stressful on iPSCs and results in a high amount of cell death. Additionally, FACS increases the risk of introducing a contamination into cells and may require the use of antibiotics as a preventative strategy. FACs is also associated with increased risk of contamination of edited cells with WT cells resulting in a loss of a clonal cell line (Jin et al., 2019). A single clone was identified as edited and confirmed to be a heterozygous exon 2 knockout iPSC line, which is referred to as exon 2 +/-. Bacteria were transformed with PCR products generated from CTR and exon 2 +/- iPSCs, enabling the sequencing of each allele of both cell lines individually. A monoallelic 394bp deletion in

exon 2 was confirmed indicating the entirety of exon 2 had been excised from one *CLU* allele. A 17bp deletion was observed in intron 2 of *CLU* in the other allele, no deletion was observed in intron 1 indicating no cutting by Cas9 had taken place at the 5' end of CLU exon 2. This allele remained as WT as the *CLU* sequence remained in intact. Sequencing also confirmed the exon 2 +/- iPSC line is clonal and not a mixed population of cells. This is critical, as the edit will be stable and not lost through iPSC passaging or culturing.

3.3.3 Exon 2 +/- iPSCs retain pluripotency and can be differentiated into MAP2 positive neurons

Culturing and maintenance of iPSCs prior to neural induction is critical, enabling the successful generation of neuron cultures for downstream experiments. Both CTR and exon 2 +/- iPSCs were shown to express two pluripotency markers, *NANOG* and *OCT4*. As expected, by day 35 of the differentiation protocol, iPSC-neurons showed a reduction in expression of both *NANOG* and *OCT4*. Neurons were also demonstrated to be positive for neuronal marker MAP2 and cortical marker CTIP2. The expression of CTIP2 resembles the generation of deeper layer cortical neurons that were confirmed to be TBR1 positive in the original protocol by Shi et al., (Shi, Kirwan, & Livesey, 2012; Shi, Kirwan, Smith, et al., 2012). Therefore, iPSC-neurons can be successfully generated using the King's College protocol, these neurons are positive for neuronal marker MAP2, and cortical lineage marker CTIP2. Thus, a model for exploring the contribution of altered clusterin trafficking in neurodegeneration and AD has been generated.

4 Characterising clusterin mRNA and protein expression in exon 2 +/- iPSCs

4.1 Introduction

Traditionally, clusterin is referred to as a highly glycosylated, secreted protein but several studies have identified the expression of intracellular glycosylated and non-glycosylated clusterin species (Debure et al., 2003; Gregory et al., 2017; Leskov et al., 2003; Li et al., 2013; Nizard et al., 2007; Prochnow et al., 2013). However, the biogenesis, structure and functional relevance of these proteins remains debated. Intracellular, glycosylated clusterin may arise from several mechanisms, as discussed in *Foster et al., 2019.* One suggested explanation is stress induced translocation of clusterin resulting in the existence of intracellular, glycosylated clusterin species in the cytoplasm of cells (Nizard et al., 2007)

Translation of *CLU* mRNA transcripts lacking exon 2 (*CLU* mRNA variant 1 Δ exon 2) generates non-glycosylated, intracellular clusterin (Leskov et al., 2003; Prochnow et al., 2013; Reddy et al., 1996; Yang et al., 2000). However, this *CLU* variant is present in low abundance in cells (Leskov et al., 2003; Prochnow et al., 2013) or not at all (Andersen et al., 2007). Furthermore, the expression of this variant has not been previously reported in either iPSCs or iPSC-derived neurons. Using the previously generated heterozygous exon 2 knockout line (exon 2 +/-) the functional relevance of *CLU* mRNA variant 1 Δ exon 2 transcripts in iPSCs was explored in this chapter.

In this chapter, the following questions were addressed:

1. Do human iPSCs express *CLU* mRNA variant 1 Δ exon 2 transcripts?
2. Do human iPSCs express intracellular and secreted clusterin? Is the expression of these proteins altered in exon 2 +/- iPSCs?
3. Are clusterin proteins found in the cytoplasm and nuclei of cells?
4. Is there evidence of non-glycosylated clusterin in iPSCs and is this altered in exon 2 +/- iPSCs?

4.2 Results

4.2.1 *CLU* transcript expression is altered in exon 2 +/- iPSCs

Previous studies have identified several *CLU* transcript variants, although this has not been previously explored in human iPSCs. The expression of several *CLU* variants with alternative exon 1s was measured by RT-qPCR using variant specific primers as described previously (Prochnow et al., 2013) (***Table 4.1***). All three *CLU* mRNA transcripts were identified in both CTR and exon 2 +/- iPSCs, although average C_t values varied greatly between each variant indicating variant expression is not equal. *CLU* variant 1 was the most abundant variant in both CTR and exon 2 +/- iPSCs, this is in agreement with previous studies (Prochnow et al., 2013). The expression of each variant was then normalised to *GAPDH* and compared between CTR and exon 2 iPSCs (Pfaffl, 2001) (***Figure 4.1***). Expression of variants 1 and 3 was comparable between CTR and exon 2 +/- iPSCs (***Figure 4.1***). In comparison, the expression of variant 2 was significantly reduced in exon 2 +/- iPSCs. Therefore, editing of *CLU* exon 2 has altered the expression of *CLU* mRNA.

	Average C_t values ± SEM	
Gene of interest	CTR	Exon 2 +/-
GAPDH	17.4 ± 0.1	17.8 ± 0.3
CLU variant 1 (exon 1a-3)	24.1 ± 0.1	25.2 ± 0.3
CLU variant 2 (exon 1b-3)	31.9 ± 0.2	33.3 ± 0.3
CLU variant 3 (exon 1c-3)	28.9 ± 0.1	29.5 ± 0.1

Table 4.1. RT-qPCR quantification of CLU mRNA transcript variants in CTR and exon 2 +/- iPSCs.

RT-qPCR was used to quantify the expression of several CLU variants and GAPDH in CTR and exon 2 +/- iPSCs. Variant specific primers were obtained from Prochnow et al.,2013. Data are shown as mean ± SEM, n=3 (n= independent experiments, each with 3 replicate wells).

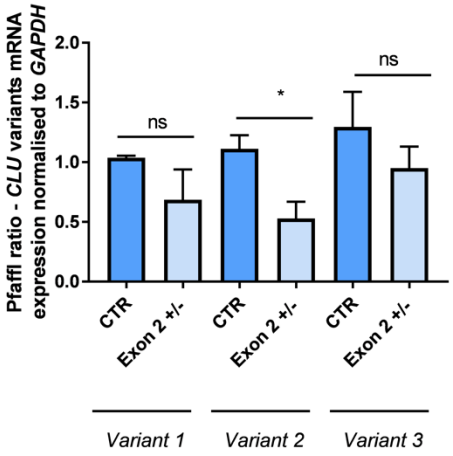


Figure 4.1. Expression of CLU variant 2 is significantly reduced in exon 2 +/- iPSCs.

The expression of CLU mRNA transcript variants 1, 2 and 3 was quantified in CTR and exon 2 +/- iPSCs and normalised to GAPDH. Pfaffl analysis was used to quantify differences in expression of CLU variants 1, 2 and 3 between CTR and exon 2 +/- iPSCs and the Pfaffl ratio quantified after normalisation to GAPDH. The expression of CLU variant 1 was similar between CTR and exon 2 +/- iPSCs (p=0.2392). The expression of CLU variant 2 was significantly reduced in exon 2 +/- iPSCs (p=0.0312). Expression of CLU variant 3 was comparable between exon 2 +/- and CTR iPSCs (p=0.3693). Heterozygous KO of CLU exon 2 has altered expression of CLU variant 2 but not 1 and 3 in exon 2 +/- iPSCs. Data are shown as mean ± SEM, n=3 (n= independent experiments, each with 3 replicate wells). Significance p<0.05* ns = p> 0.05 using unpaired parametric t-test.*

Next, the expression of the *CLU* mRNA variant 1 Δ exon 2 transcript was quantified in CTR and exon 2 +/- iPSCs. This variant was detected in CTR iPSCs and exon 2 +/- iPSCs although at different degrees. Average C_t values for *CLU* mRNA variant 1 Δ exon 2 and *GAPDH* for CTR and exon 2 +/- iPSCs were calculated and compared (***Figure 4.2***). Average C_t values for *GAPDH* were comparable between CTR and exon 2 +/- iPSCs. In comparison, average C_t values for *CLU* mRNA variant 1 Δ exon 2 transcripts were significantly higher in CTR iPSCs indicating significantly lower expression of this variant in CTR iPSCs than in exon 2 +/- iPSCs.

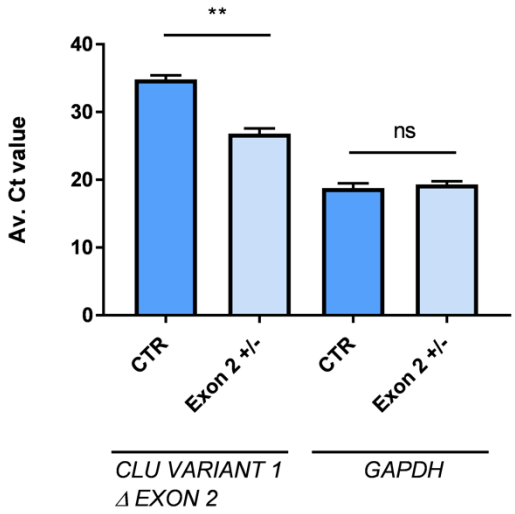


Figure 4.2. CLU mRNA transcript variant 1 Δ exon 2 expression is significantly higher in exon 2 +/- iPSCs than in CTR iPSCs.

*The expression of CLU mRNA transcript variant 1 Δ exon 2 and housekeeper gene GAPDH were measured in CTR and exon 2 +/- iPSCs by RT-qPCR. Expression of CLU mRNA transcript variant 1 Δ exon 2 was confirmed to be higher in exon 2 +/- iPSCs than in CTR iPSCs due to the significantly higher average C_t values for this variant obtained in CTR iPSCs than in exon 2 +/- iPSCs (p=0.0031**). No significant differences were identified in average C_t values for GAPDH between CTR and exon 2 +/- iPSCs (p=0.9329). Data are shown as mean ± SEM, n=3 (n= independent experiments, each with 3 replicate wells). Significance was tested using One-way ANOVA (p=0.0002***) with Tukey's multiple comparison analysis. P<0.05*. Significance p<0.05* ns = p> 0.05 using a One-way ANOVA*

4.2.2 Expression of total *CLU* mRNA is similar in exon 2 +/- and CTR iPSCs

Expression of specific *CLU* mRNA transcript variants was clearly altered in exon 2 +/- iPSCs. Next to determine if this had resulted in a change in the overall expression of *CLU*, the expression of total *CLU* mRNA transcripts was quantified by RT-qPCR (***Figure 4.3***). For this purpose, primers targeting *CLU* exons 7 and 8 were obtained from previous publication (Prochnow et al., 2013). Exons 7 and 8 were chosen since these exons are common to all *CLU* variants and are positioned at the end of the transcript so can be used to describe

'total *CLU*'. Expression was similar in CTR and exon 2 +/- iPSCs, indicating the monoallelic excision of exon 2 from *CLU* had not influenced transcription of total *CLU* mRNA.

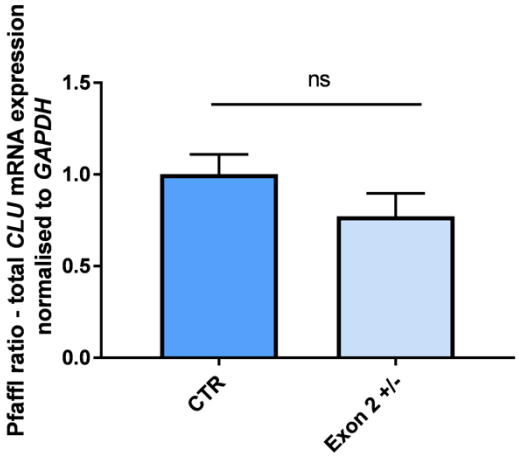


Figure 4.3. Expression of total CLU mRNA is similar between exon 2 +/- and CTR iPSCs.
The expression of total CLU mRNA transcripts and GAPDH were quantified by RT-qPCR in CTR and exon 2 +/- iPSCs. Differences in gene expression were quantified by Pfaffl analysis. No significant differences were observed in the expression of total CLU mRNA transcripts between CTR and exon 2 +/- iPSCs (p=0.2094). Data are shown as mean ± SEM, n= 4 (n = independent experiments, each with 3 replicate wells). Significance p<0.05 ns = p> 0.05 using unpaired parametric t-test.*

4.2.3 Clusterin antibodies detect human clusterin in iPSC samples

Having demonstrated alterations in *CLU* variant expression but not in overall abundance of *CLU* mRNA in exon 2 +/- iPSCs, the next goal was to determine if heterozygous exon 2 KO had impacted on clusterin protein abundance. With this goal in mind, two clusterin antibodies were tested for their ability to detect clusterin in protein samples collected from human iPSCs. Total cell lysates were extracted from the JR iPSC line and from CTR iPSCs to confirm expression of clusterin in human iPSCs (***See Chapter 2, 2.2.7.4***). The JR iPSC line is a previously generated iPSC line that was initially characterised as a *CLU* KO line

(Robbins et al., 2018). However, subsequent research demonstrated that the JR iPSC line expresses clusterin protein but at a lower abundance than CTR iPSCs. Total cell lysates were also included from rat neurons that had been previously treated with 20μM $A\beta_{25-35}$ for 0, 6 and 24 hours and collected (***See Chapter 2, 2.1.2.1 and 2.2.3.2***). These samples were included since previously it was shown that clusterin protein abundance is increased in rat neurons following treatment with 20μM $A\beta_{25-35}$ and would therefore act as a control (Killick et al., 2014). All samples were run on the same western blot and immunostained for β-actin and clusterin (***Figure 4.4, see Chapter 2, 2.2.7.7***). Two clusterin antibodies were tested for their ability to detect human clusterin. The SC-6420 antibody (C-18) is a polyclonal goat anti-α chain clusterin antibody provided by Santa Cruz. The Ab69644 antibody is a polyclonal rabbit anti-α chain clusterin antibody provided by Abcam (***See Chapter 2, table 2.12***). Low clusterin immunoreactivity was detected in rat samples prior to 20μM $A\beta_{25-35}$ treatment with both antibodies, reflecting the low expression of clusterin in these samples (***Figure 4.4A and B***). Although not quantified, clusterin immunoreactivity appeared to increase in rat samples following treatment with 20μM $A\beta_{25-35}$ for both 6 and 24 hours (***Figure 4.4A and B***). This is in agreement with previous findings (Killick et al., 2014). Clusterin of rat origin was most easily detected following incubation with the Abcam69644 antibody than the SC-6240 antibody. Both antibodies detected clusterin in human iPSC samples. B-actin staining indicated equal loading of protein in CTR and JR iPSC samples and on visual inspection, clusterin was detected in JR iPSC samples but at a lower level than in CTR iPSCs. The data demonstrates both antibodies are suitable for detecting human clusterin in iPSC samples.

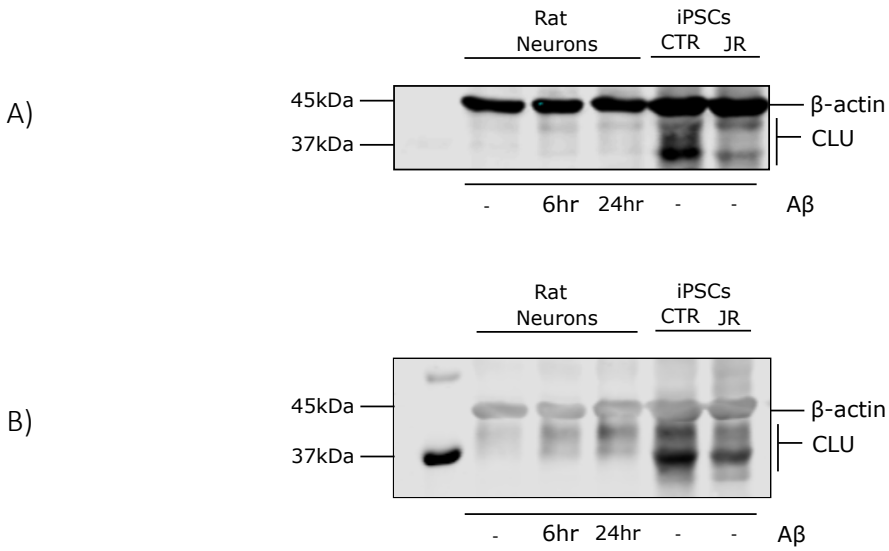


Figure 4.4. Clusterin antibodies are suitable for detecting human clusterin in iPSC samples.
Total cell lysates were extracted from rat neurons, CTR iPSCs and JR iPSCs and run on a western blot. Samples were immunostained for β-actin and clusterin with either the SC-6420 or Ab69644 antibody. ***A****) Staining with Ab69644 indicated increased clusterin immunoreactivity in rat neurons following 6 hour and 24 hours of 20μM* $A\beta_{25-35}$ *treatment. The antibody also detected clusterin in both CTR and JR iPSC protein samples.* ***B****) Staining with SC-6420 also indicated increased immunoreactivity of clusterin in rat neurons following 6 hour and 24 hours of 20μM* $A\beta_{25-35}$ *treatment. This antibody is more suitable than Ab69644 for detecting rat clusterin. SC-6420 also detected clusterin protein in human iPSC samples.*

To confirm the specificity of the Ab69644 and SC-6420 antibodies to detect human clusterin, increasingly dilute amounts of recombinant human clusterin (2μg, 0.2μg and 0.02μg) were run on a western blot (***See Chapter 2, 2.2.7.3***). Samples were then immunostained for clusterin using Ab69644 and SC-6420 antibodies (***Figure 4.5A and Figure 4.5B respectively***). Loading of 2μg of human recombinant clusterin resulted in the detection of a ~37kDa smeared band, which is consistent with other studies that detect clusterin at this weight (Killick et al., 2014; Matta et al., 2020; Moretti et al., 2007). The smeared pattern of the band may be attributed to the variable glycosylation state of

clusterin. This was observed following staining with both SC-6420 and Ab69644 antibodies. Based on these results, both antibodies detect human clusterin at the correct molecular weight when 2µg and 0.2µg of human recombinant clusterin protein is loaded on a western blot. No staining was observed when 0.02µg of recombinant human clusterin was loaded.

A)



B)

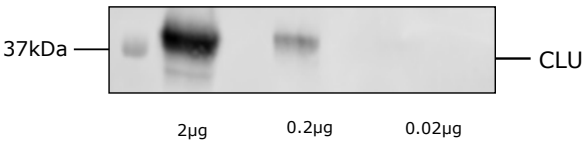


Figure 4.5. Clusterin antibodies are specific to clusterin.

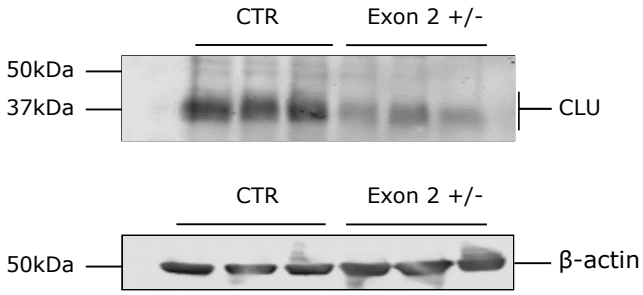
*Increasingly dilute amounts of human recombinant clusterin (2µg, 0.2µg and 0.02µg) were run on a western blot and immunostained for clusterin protein using **A**) Ab69644 and **B**) SC-6420 antibodies. A single smeared band ~37kDa was detected when both 2µg and 0.2µg of recombinant human clusterin was loaded. This was consistent with both antibodies. No staining was observed when 0.02µg was loaded.*

4.2.4 Intracellular clusterin protein immunoreactivity is reduced in exon 2 +/- iPSCs

Having established the specificity of both SC-6420 and Ab69644 antibodies for detecting human clusterin in iPSC samples, the immunoreactivity of intracellular clusterin in CTR and exon 2 +/- iPSCs was quantified using western blotting. Total cell lysates were collected from CTR and exon 2 +/- iPSCs (***See Chapter 2, 2.2.7.4***) and run on a western blot (***See Chapter 2, 2.2.7.7***). Samples were immunostained for clusterin using the SC-6420 antibody and β-actin (***Figure 4.6A***). Intracellular clusterin protein immunoreactivity was normalised

to β-actin in all samples and was significantly lower in exon 2 +/- iPSCs than CTR iPSCs (***Figure 4.6B***).

A)



B)

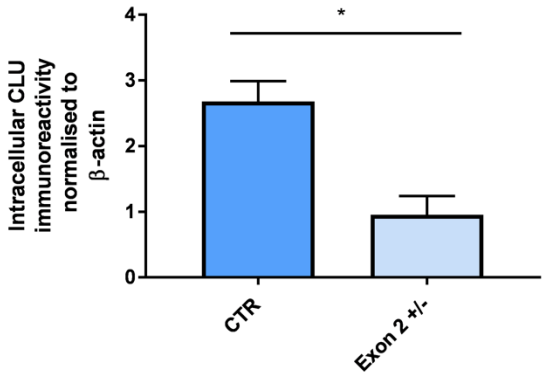


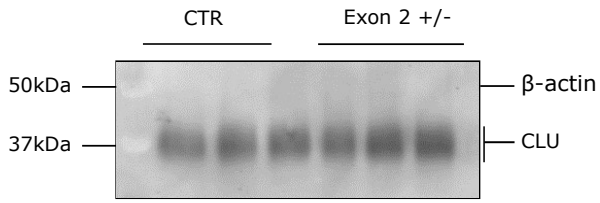
Figure 4.6. Intracellular clusterin immunoreactivity is significantly lower in exon 2 +/- iPSCs.
CTR and exon 2 +/- iPSCs were cultured and total cell lysates were collected. ***A****) Samples were run on a western blot and immunostained for clusterin and β-actin.* ***B****) Clusterin immunoreactivity was quantified relative to the immunoreactivity of β-actin in all samples. Intracellular clusterin immunoreactivity was significantly reduced (51.3 ± 6.9%) in exon 2 +/- iPSC samples compared to CTR iPSC samples (p=0.0149*). Data are shown as mean ± SEM, n= 3 (n = independent experiments, each with 3 replicate wells). Significance p<0.05* ns = p> 0.05 using unpaired parametric t-test.*

4.2.5 Secretion of clusterin is not altered in exon 2 +/- iPSCs

To measure the secretion of clusterin from human iPSCs, media was removed from wells containing CTR and exon 2 +/- iPSCs prior to the collection of total cell lysates and concentrated (***See Chapter 2, 2.2.7.1-2***). Based on the data obtained from ***figure 4.5***, at

least 2µg of concentrated media was required for loading and staining with the SC-6420 antibody. Thus, 4µg of each concentrated media sample were run on a western blot and samples were immunostained for clusterin and β-actin (***Figure 4.7A***). A clusterin positive, smeared band at ~37kDa was detected in all samples representing secreted clusterin. Samples did not demonstrate positive staining for β-actin. This confirmed the absence of cell debris in all media samples and positive clusterin staining in the media samples was attributed to secreted clusterin and not clusterin found in cell debris. Secretion of clusterin did not differ between CTR and exon 2 +/- iPSCs (***Figure 4.7B***).

A)



B)

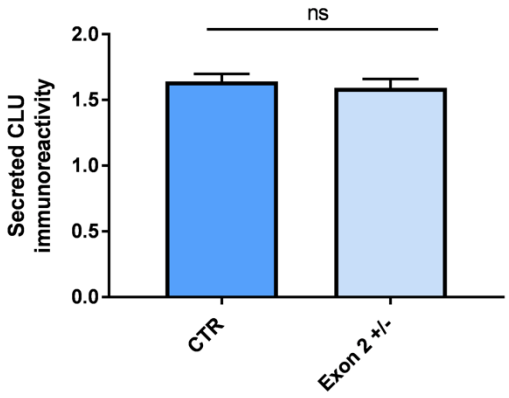


Figure 4.7. Secretion of clusterin is comparable between exon 2 +/- and CTR iPSCs.

Media was collected from wells containing CTR and exon 2 +/- iPSCs to quantify differences in clusterin secretion between the lines. Media was collected and concentrated 45X by spinning in a Amicon Ultra-2 Centrifugal Filter Unit with a 10kDa cut off. Protein content in each sample was then quantified by using a standard curve generated from BSA standards of known protein concentrations. This was done to ensure that equal loading of protein was achieved, since it is not possible to blot for a secreted, loading control protein. ***A****) 4µg concentrated samples were run and immunostained for clusterin using the SC-6420 antibody. The position of β-actin staining is indicated on the western blot but was not detected in any sample*

demonstrating the absence of cell debris in the media samples. ***B****) Secreted clusterin immunoreactivity was quantified in all samples and no significant differences (ns) were detected between CTR and exon 2 +/- iPSCs (p=0.6015). Data are shown as mean ± SEM, n= 4 (n = independent experiments, each with 3 replicate wells). Significance p<0.05* ns = p> 0.05 using unpaired parametric t-test.*

4.2.6 Intracellular and secreted clusterin proteins are glycosylated in human iPSCs

In ***figure 4.6***, intracellular clusterin was detected as a smeared band of weight ~37kDa in all samples. Similarly, secreted clusterin in all samples was detected as a smear (***Figure 4.7***). The smeared nature of these bands is likely attributed to variable glycosylation stages of clusterin proteins (Leskov et al., 2003; Prochnow et al., 2013). To confirm whether intracellular and secreted clusterin proteins generated by human iPSCs are glycosylated, total cell lysates and concentrated media samples were treated with PNGase F to remove N-linked oligosaccharides (***See Chapter 2, 2.2.7.6***). Samples were then run on a western blot and immunostained for clusterin (***Figure 4.8***). Following PNGase F treatment, intracellular and secreted clusterin proteins appeared as two distinct bands likely representing the α and β chains of clusterin. This would be in agreement with previous findings that demonstrate the appearance of two bands following deglycosylation of mature, cleaved and glycosylated clusterin proteins (Prochnow et al., 2013; Stewart et al., 2007). It is not surprising that secreted clusterin resolved to two distinct bands, since it is well known that secreted clusterin species are glycosylated and exist as a heterodimeric protein consisting of an α and β chain (Jenne & Tschopp, 1989; Kapron et al., 1997; Urban et al., 1987; Wong et al., 1993). Surprisingly, intracellular clusterin species were also confirmed to exist as an α and β chain since two bands were identified and were identical to those seen in secreted clusterin samples. PNGase F treated lysate and media samples were comparable between CTR and exon 2 +/- iPSC samples, indicating that *CLU* exon 2

editing had not altered the glycosylation or cleavage of either intracellular or secreted clusterin proteins in exon 2 +/- iPSCs.

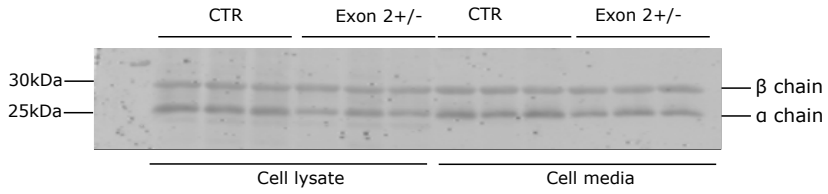


Figure 4.8. Intracellular and secreted clusterin species are glycosylated.
Total cell lysates and concentrated media samples from CTR and exon 2 +/- iPSCs were treated with PNGase F to remove N-linked glycosylation from glycoproteins. Samples were then run on a western blot and immunostained for clusterin using the SC-6420 antibody. As expected, following treatment two distinct bands were visualised in media samples representing the α and β chains of mature, cleaved, and glycosylated secreted clusterin proteins. Surprisingly, the same bands were also detected in PNGase F treated total cell lysate samples. Therefore, intracellular clusterin proteins are also glycosylated and cleaved. Clusterin maturation in the ER/Golgi apparatus appears to be unaffected in exon 2 +/- iPSCs, since bands were consistent between CTR and exon 2 +/- iPSC samples in all cases.

4.2.7 Abundance of nuclear and cytoplasmic proteins is not altered in exon 2 +/- iPSCs

It was demonstrated that both CTR and exon 2 +/- iPSCs express intracellular clusterin proteins that are glycosylated. Previously, glycosylated (Nizard et al., 2007) and non-glycosylated clusterin species have been identified in the cytoplasm of cells (Leskov et al., 2003; Prochnow et al., 2013). Furthermore, non-glycosylated clusterin has also been detected in the nucleus (Leskov et al., 2003). To interrogate the location of intracellular clusterin proteins in iPSCs, CTR and exon 2 +/- iPSCs were fractionated to yield nuclear and cytoplasmic fractions (***See Chapter 2, 2.2.7.5***). Cytoplasmic and nuclear fractions were then

run on separate western blots and immunostained. First samples were immunostained with nuclear marker H3 histone and cytoplasmic marker β III tubulin (TUJ1) to confirm the purity of each fraction. Then samples were immunostained for clusterin.

In the case of cytoplasmic samples, samples were confirmed to be negative for H3 histone indicating no contamination from the nuclear fraction (***Figure 4.9A***). Samples were then immunostained for cytoplasmic marker TUJ1 (***Figure 4.9A***) and clusterin (***Figure 4.9B***). A clusterin positive smear was detected at ~37kDa in all samples and immunoreactivity was comparable between CTR and exon 2 +/- iPSC samples (***Figure 4.9C***). Similarly, an additional clusterin protein species was detected at ~45kDa, again, immunoreactivity was comparable between CTR and exon 2 +/- iPSC samples (***Figure 4.9D***). Human iPSCs therefore express clusterin proteins in their cytoplasmic compartments, and this is not altered by the heterozygous KO of *CLU* exon 2.

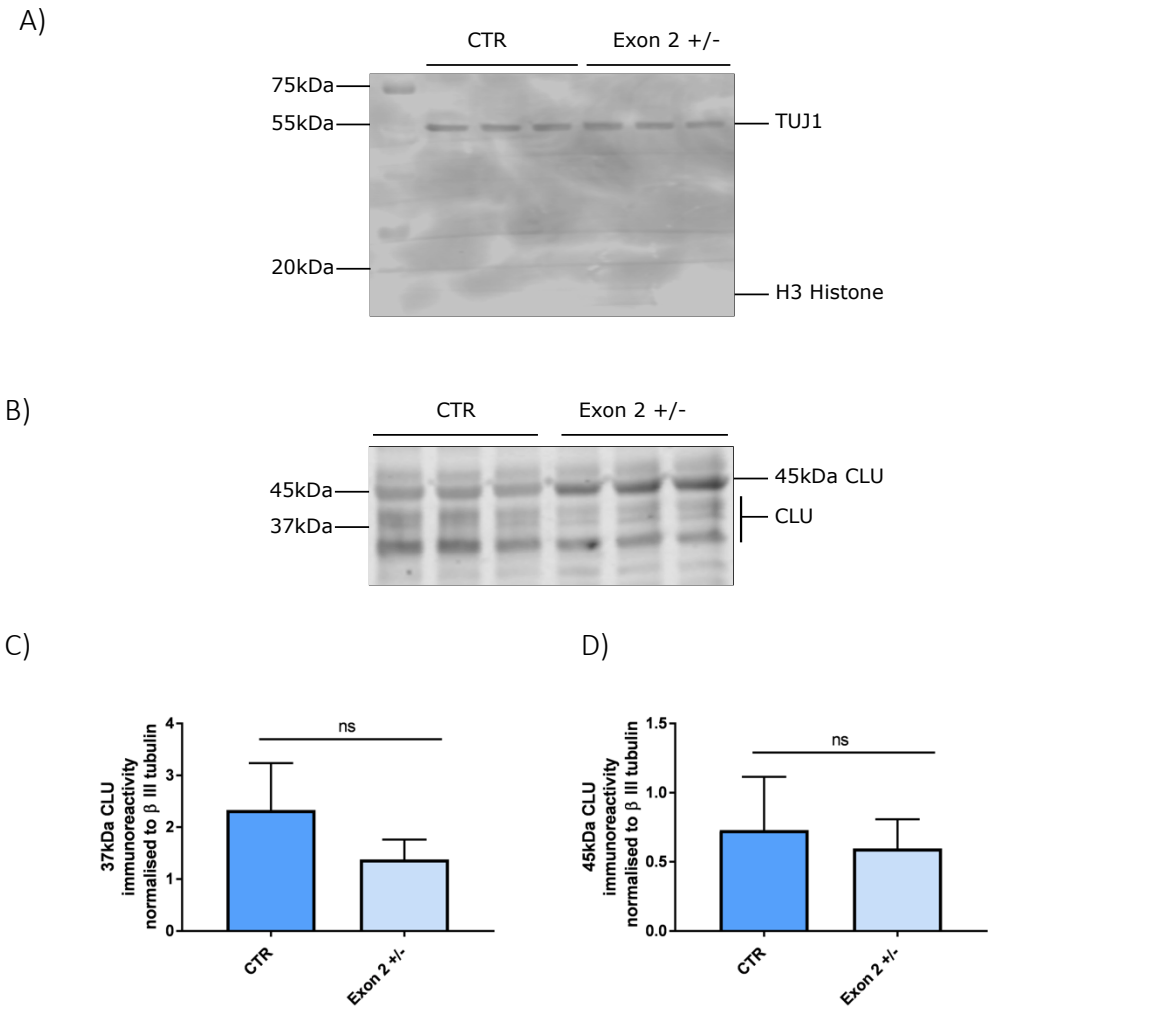


Figure 4.9. Clusterin proteins are identified in the cytoplasm of human iPSCs.

CTR and exon 2 +/- iPSCs were fractionated to yield the cytoplasmic and nuclear fractions of cells. Here the cytoplasmic fractions were run on a western blot. ***A****) Cytoplasmic samples were positive for cytoplasmic marker TUJ1. The position of H3 histone staining is indicated on the western blot but is absent in all samples. This confirms the purity of the cytoplasmic fractions.* ***B****) Cytoplasmic samples were then immunostained for clusterin. Two distinct clusterin protein species were detected in all samples. A smeared clusterin positive band was detected at ~37kDa and a distinct band at ~45kDa. Immunoreactivity of these clusterin proteins were then quantified in all samples and normalised to cytoplasmic marker TUJ1.* ***C****) Cytoplasmic immunoreactivity of ~37kDa clusterin proteins is similar in CTR and exon 2 +/- iPSC (p=0.3878).* ***D****) Cytoplasmic immunoreactivity of ~45kDa clusterin proteins is similar in CTR and exon 2 +/- iPSC (p=0.7801). Data are shown as mean ± SEM, n= 3 (n = independent experiments, each with 3 replicate wells). Significance p<0.05* ns = p> 0.05 using unpaired parametric t-test.*

Nuclear fractions were then run on a western blot and immunostained for cytoplasmic marker TUJ1 and nuclear marker H3 histone (***Figure 4.10A***). All samples were positive for H3 histone and negative for TUJ1, indicating no contamination from the cytoplasmic fractions. Immunostaining revealed clusterin protein in all samples (***Figure 4.10B***) and this was comparable between CTR and exon 2 +/- iPSC samples (***Figure 4.10C***).

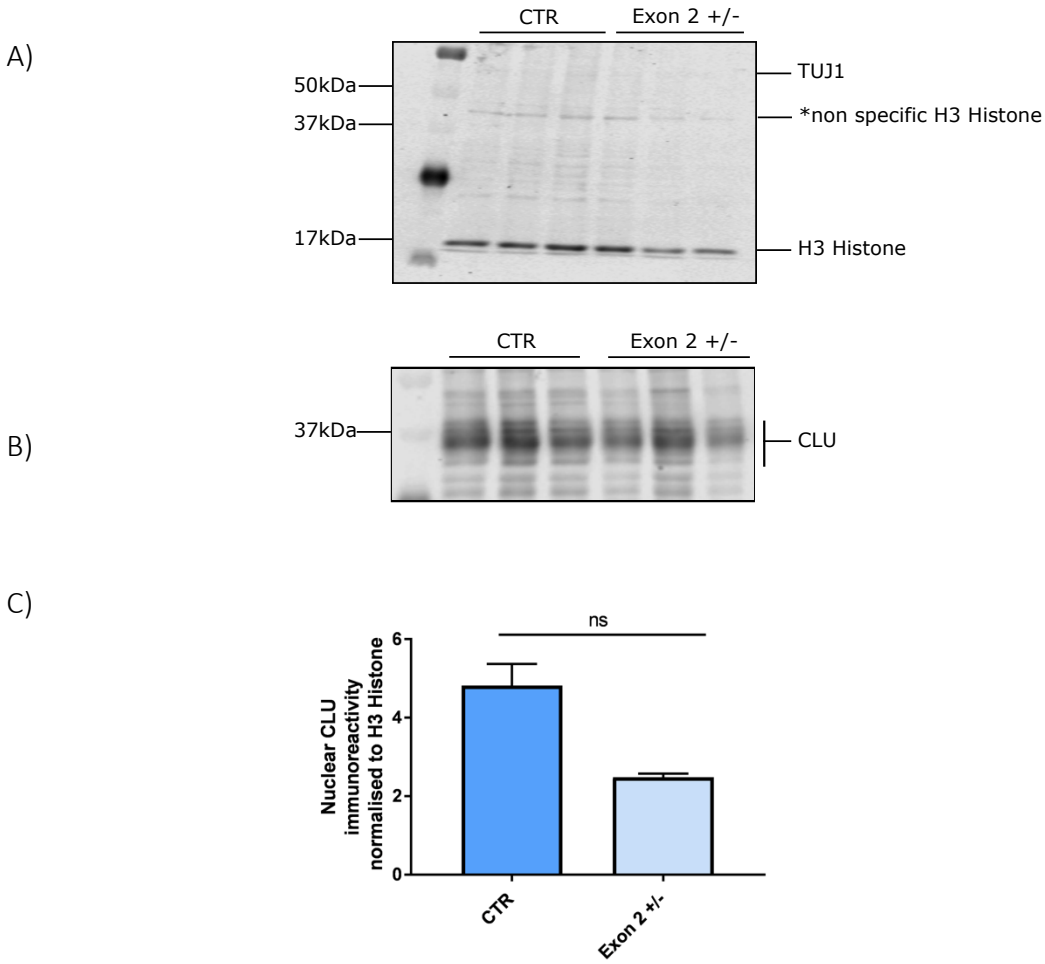


Figure 4.10. Clusterin proteins are present in the nucleus of human iPSCs.

CTR and exon 2 +/- iPSCs were fractionated to yield the nuclear fraction of each sample. ***A****) Nuclear fractions were run on a western blot and purity of the samples was confirmed by positive staining of nuclear marker H3 histone and the negative staining of cytoplasmic marker TUJ1. The position of TUJ1 staining if present, is indicated on the western blot.* ***B****) Immunoreactivity of clusterin in each nuclear fraction was confirmed after staining with the SC-6420 anti-clusterin antibody.* ***C****) Immunoreactivity of clusterin was quantified relative to H3 histone and was comparable between exon 2 +/- and CTR iPSCs (p=0.0512). Data are shown as mean ± SEM, n= 3 (n = independent experiments, each with 3 replicate wells). Significance p<0.05* ns = p> 0.05 using unpaired parametric t-test.*

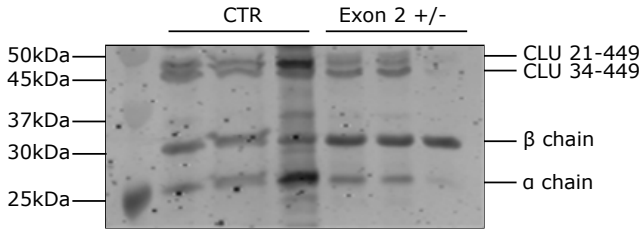
4.2.8 Non-glycosylated clusterin species exist in the cytoplasm but not the nucleus of iPSCs

Clusterin detected in both the cytoplasmic and nuclear fractions of cells were detected as expected as a ~37kDa smeared band, this suggests clusterin is glycosylated in both these compartments. To determine if cytoplasmic and nuclear clusterin species are glycosylated, fractions were treated with PNGase F to remove N-linked oligosaccharides. Samples were then run on separate western blots and immunostained for clusterin (***Figure 4.11***). Cytoplasmic fractions were demonstrated to resolve to two distinct bands of ~30kDa and ~25kDa (***Figure 4.11A***), like our observations in total cell lysates and media samples (***Figure 4.8***), indicating glycosylated clusterin species exist in the cytoplasm of human iPSCs. This was consistent in both CTR and exon 2 +/- iPSC samples. Two clusterin bands were detected at ~45kDa and ~50kDa in all samples, likely representing non-glycosylated clusterin species referred to as CLU21-449 and CLU34-449, which were previously identified (Prochnow et al 2013). CLU21-449 was previously demonstrated to be translated from the alternative translational start site CUG located in *CLU* exon 2 generating a ~50kDa clusterin protein. CLU34-449 was previously demonstrated to be translated from *CLU* variant 1 Δ exon 2 transcripts and the AUG start site positioned in *CLU* exon 2 generating a ~45kDa clusterin protein. Both proteins were previously demonstrated to be non-glycosylated (Prochnow et al 2013). Here, the immunoreactivity of either of these proteins did not differ between CTR and exon 2 +/- iPSCs.

Nuclear fractions were also treated with PNGase F to determine if nuclear clusterin proteins are glycosylated (***Figure 4.11B***). In all samples two distinct bands were detected that were positive for clusterin representing the α and β chain of cleaved and glycosylated clusterin. No other bands positive for clusterin were identified in nuclear fractions

following PNGase F treatment thus, no evidence was found to indicate the presence of non-glycosylated clusterin proteins in the nuclei of iPSCs. This was not altered by the heterozygous KO of *CLU* exon 2.

A)



B)

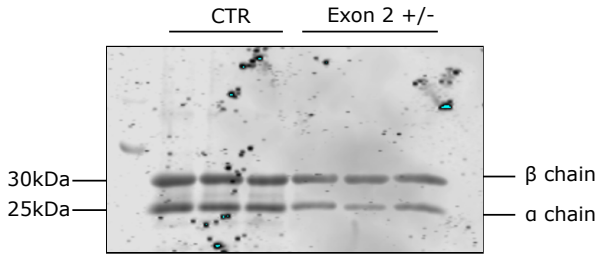


Figure 4.11. Glycosylated and non-glycosylated clusterin species are found in the cytoplasm of human iPSCs. Nuclear clusterin proteins are glycosylated.

Cytoplasmic and nuclear fractions from CTR and exon 2 +/- iPSCs were treated with PNGase to remove N-linked glycosylation. PNGase F treated samples were then run on a western blot and immunostained for clusterin. ***A****) Cytoplasmic clusterin resolved to bands at ~30kDa and ~25kDa, representing the β and α chains of clusterin respectively. Additional bands positive for clusterin were identified at ~45/50kDa. These likely arise from the ~50kDa and ~45kDa clusterin proteins identified previously by Prochnow et al., 2013 which were referred to as CLU21-449 and CLU34-449 respectively. ~50kDa clusterin proteins (CLU21-449) may arise from the translation initiated within exon 2 at the alternative CUG start site located after the ER signal peptide. The ~45kDa clusterin protein (CLU34-449) may arise from the translation of CLU variant 1 Δ exon 2 transcripts and the AUG located at the start of exon 3. These are both non-glycosylated clusterin proteins, but immunoreactivity did not differ between CTR and exon 2 +/- iPSC samples.* ***B****) PNGase F treated nuclear fractions resolved to bands at ~30kDa and ~25kDa again representing the β and α chains of clusterin respectively. Therefore, nuclear clusterin is glycosylated. There is no evidence of other clusterin positive bands indicating non-glycosylated clusterin proteins do not reside in the nucleus of iPSCs.*

4.3 Discussion

4.3.1 Expression of clusterin mRNA and protein is altered in exon 2 +/- iPSCs

Previously, Prochnow et al., quantified the expression of several *CLU* mRNA variants in a number of different cell lines (Prochnow et al., 2013). Here, this was repeated in human iPSCs as it is not known which *CLU* variants are expressed endogenously in iPSCs. In agreement with Prochnow et al., the most abundant *CLU* variant was variant 1, this was consistent in both CTR and exon 2 +/- iPSCs. Additionally, expression of variant 1 and 3 was similar between CTR and exon 2 +/- iPSCs therefore, heterozygous exon 2 removal has not altered the expression of these variants and suggests compensation from the unedited, WT allele in exon 2 +/- iPSCs. In comparison, expression of *CLU* variant 2 was significantly reduced, this did not alter the overall expression of *CLU* mRNA in cells suggesting *CLU* variant 1 is responsible for the majority of *CLU* mRNA generated by iPSCs. Finally, it was demonstrated that heterozygous exon 2 KO was sufficient to increase the expression of *CLU* variant 1 Δ exon 2 transcripts in iPSCs. This is not surprising given the removal of exon 2 would result in the splicing of exons 1 and 3 together generating *CLU* variant 1 Δ exon 2 transcripts. The low expression of *CLU* variant 1 Δ exon 2 transcripts in CTR iPSCs was consistent with other studies that demonstrated no expression (Andersen et al., 2007) or very low expression in cells (Leskov et al., 2003; Prochnow et al., 2013).

The removal of *CLU* exon 2 was predicted to prevent the trafficking of clusterin preproprotein to the ER and Golgi apparatus, therefore preventing its glycosylation, cleavage, and secretion from cells. Overall, clusterin immunoreactivity was significantly reduced in exon 2 +/- iPSCs compared to CTR iPSCs indicating reduced clusterin protein abundance in these cells. Interestingly this occurred in the absence of an alteration in *CLU* mRNA expression. This suggests that the reduction in clusterin protein abundance in exon

2 +/- iPSCs may arise from inefficient translation or increased degradation. However, this was not explored further in this chapter. Most surprisingly, secretion of clusterin was not altered in exon 2 +/- iPSCs while intracellular retention was significantly reduced. This confirms trafficking of clusterin has been altered by *CLU* exon 2 gene editing. Intracellular retention of clusterin may arise as a mechanism for storing or 'pooling' excess glycosylated clusterin that is not secreted, perhaps in the cytoplasm and nuclei of cells. This is supported by the identification that clusterin found in both the cytoplasm and nucleus of cells was glycosylated, cleaved, and composed of an α and β chain like that observed in secreted clusterin samples. Therefore, this suggests clusterin that is not secreted from cells may be trafficked to the cytoplasm and nucleus for storage. Furthermore, the retention of clusterin may be dependent on the overall abundance of glycosylated clusterin species generated by cells. Thus, if exon 2 +/- iPSCs generate less secreted clusterin, there is less clusterin left to be retained intracellularly and stored. Additionally, clusterin reuptake by iPSCs may be reduced in exon 2 +/- iPSCs contributing to the reduction in intracellular retention of clusterin.

4.3.2 Immunoreactivity and abundance of non-glycosylated clusterin species is not altered in exon 2 +/- iPSCs

Translation of *CLU* variant 1 Δ exon 2 transcripts is demonstrated to generate a non-glycosylated clusterin species of ~55kDa that resides in the cytoplasm and nucleus of cells (Leskov et al., 2003) and a ~45kDa clusterin species located in the cytoplasm of cells (Prochnow et al., 2013), Interestingly, two non-glycosylated clusterin species were identified in the cytoplasmic fraction of both CTR and exon 2 +/- iPSCs, which may resemble the CLU21-449 and CLU34-449 species previously identified (Prochnow et al., 2013). The increased expression of *CLU* variant 1 Δ exon 2 transcripts in exon 2 +/- iPSCs

did not result in an increased abundance of the ~45kDa non-glycosylated clusterin species. This is in contrast to previous studies demonstrating increased expression of *CLU* variant 1 Δ exon 2 transcripts results in increased non-glycosylated clusterin species in cancer cells (Leskov et al., 2003; Prochnow et al., 2013). It is unclear if the translation of *CLU* variant 1 Δ exon 2 transcripts is less efficient or the resulting protein species are less stable and thus, more prone to degradation. Both of which would contribute to the overall no change in immunoreactivity of these clusterin species in exon 2 +/- iPSCs. Taken together, the data question the functional importance of *CLU* variant 1 Δ exon 2 transcripts to generate non-glycosylated clusterin species in human iPSCs.

The data in this chapter demonstrate that heterozygous *CLU* exon 2 KO is sufficient to alter both *CLU* variant expression and clusterin protein abundance in human iPSCs. The loss of a single *CLU* exon 2 did not alter the secretion of clusterin but did reduce intracellular clusterin immunoreactivity. Despite the increased expression of *CLU* variant 1 Δ exon 2 transcripts in exon 2 +/- iPSCs, the abundance of non-glycosylated clusterin species was not altered in these cells. In fact, non-glycosylated clusterin species were not identified in the nucleus of exon 2 +/- iPSCs. Therefore, it is questionable whether *CLU* variant 1 Δ exon 2 transcripts have a functional relevance in human iPSCs. The data provided here adds to the growing body of evidence that mature clusterin can be trafficked intracellularly, although the mechanism regulating this has not been identified.

5 $A\beta_{25-35}$ treatment of CTR and exon 2 +/- iPSC-neurons

5.1 Introduction

The expression of *CLU* variant 1 Δ exon 2 transcripts is increased following stress and is believed to facilitate cell death (Leskov et al., 2003; Prochnow et al., 2013). However, the relationship between *CLU* variant 1 Δ exon 2 transcripts and Aβ induced toxicity has not yet been explored in human derived neurons. Given the increased expression of *CLU* variant 1 Δ exon 2 transcripts in exon 2 +/- cells, it is predicted that exon 2 +/- iPSC-neurons will be more sensitive to $A\beta_{25-35}$ induced toxicity and exhibit increased cell death. To explore this, iPSC-neurons were treated with $A\beta_{25-35}$ and responses of CTR and exon 2 +/- iPSC-neurons were compared.

In this chapter the following questions were addressed:

1. Does $A\beta_{25-35}$ treatment alter the expression of *CLU* variant 1 Δ exon 2 transcripts in iPSC-neurons?
2. Are exon 2 +/- iPSC-neurons more sensitive to $A\beta_{25-35}$ induced toxicity, as measured by cell death and neurite length?
3. Are changes in gene expression, as measured by RNA-Seq, similar between CTR and exon 2 +/- iPSC-neurons following $A\beta_{25-35}$ treatment?

5.2 Results

5.2.1 Exon 2 +/- iPSC-neurons express *CLU* variant 1 Δ exon 2 transcripts but CTR iPSC-neurons do not

In chapter 4, the expression of *CLU* variant 1 Δ exon 2 was demonstrated to be significantly higher in exon 2 +/- iPSCs than in CTR iPSCs (***See chapter 4, figure 4.2***). Here, RT-qPCR was again used to quantify the expression of *CLU* variant 1 Δ exon 2 transcripts in iPSC-neurons. CTR and exon 2 +/- iPSCs were differentiated into neurons (***See Chapter 2, 2.2.1.2***) and cultured until day 35 at which point, they were treated for 24 hours with 20μM $A\beta_{25-35}$ (***See Chapter 2, 2.2.3.2***). RNA was then extracted, and RT-qPCR used to quantify the expression of *CLU* variant 1 Δ exon 2 transcripts in cells (***Table 5.1***). *CLU* variant 1 Δ exon 2 was detected in exon 2 +/- iPSC-neurons but not in CTR iPSC-neurons (***Table 5.1***). This was confirmed after running RT-qPCR products on an agarose gel where band intensity was high in exon 2 +/- iPSC-neuron samples and very low in CTR iPSC-neuron samples (***Figure 5.1A***). Finally, $A\beta_{25-35}$ was shown to have no effect on the expression of *CLU* variant 1 Δ exon 2 in exon 2 +/- iPSC-neurons (***Figure 5.1B***).

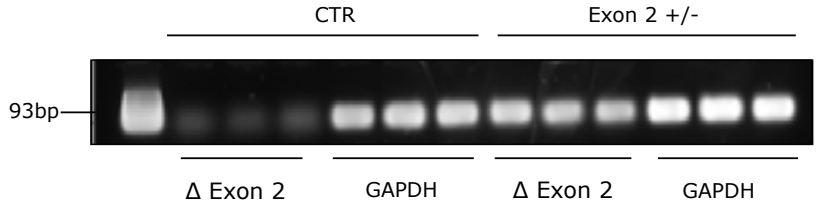
	Average C_t values ± SEM			
Gene of interest	CTR (-Aβ)	CTR (+Aβ)	Exon 2 +/- (-Aβ)	Exon 2 +/- (+Aβ)
GAPDH	22.7 ± 0.5	21.9 ± 0.1	24.4 ± 1.4	23.7 ± 1.1
CLU variant 1 Δ exon 2	'Undetermined'	'Undetermined'	30.1 ± 0.8	30.1 ± 0.4

Table 5.1. RT-qPCR quantification of CLU mRNA transcript variants in iPSC-neurons.

RT-qPCR was used to quantify the expression of the CLU variant 1 Δ exon 2 transcript in CTR and exon 2 +/- iPSC-neurons, this was done in both untreated and $A\beta_{25-35}$ treated iPSC-neurons. Variant specific primers were

obtained from Prochnow et al., 2013. Data are shown as mean ± SEM (n=3 independent differentiations, each with 3 replicate wells).

A)



B)

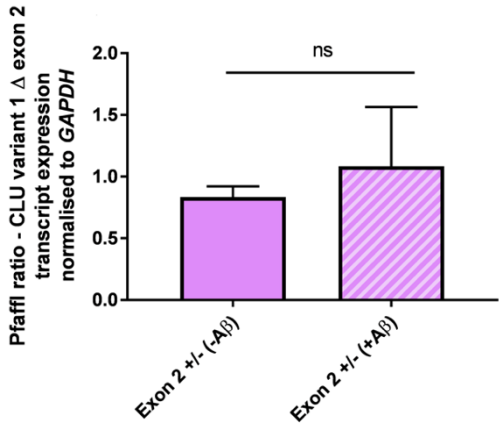


Figure 5.1. Exon 2 +/- iPSC-neurons express CLU variant 1 Δ exon 2 transcripts. Expression is not altered by $A\beta_{25\text{-}35}$.

CTR and exon 2 +/- iPSC-neurons were treated with 20μM $A\beta_{25\text{-}35}$ for 24 hours. The expression of CLU mRNA transcript variant 1 Δ exon 2 and GAPDH was then measured by RT-qPCR. ***A****) RT-qPCR products for CLU variant 1 Δ exon 2 transcripts expressed by untreated CTR and exon 2 +/- iPSC-neurons were run on a 1% agarose gel alongside GAPDH RT-qPCR products confirming higher expression of CLU variant 1 Δ exon 2 transcripts in exon 2 +/- iPSC-neurons than in CTR iPSC-neurons.* ***B****) Expression of CLU mRNA transcript variant 1 Δ exon 2 was quantified relative to GAPDH in untreated and $A\beta_{25\text{-}35}$ treated exon 2 +/- iPSC-neurons and analysed using the Pfaffl method. Transcription of CLU mRNA transcript variant 1 Δ exon 2 is not regulated by $A\beta_{25\text{-}35}$ since expression was comparable between untreated and treated exon 2 +/- iPSC-neurons (p=0.6342). Data are shown as mean ± SEM, n= 3 (n = independent differentiations, each with 3 replicate wells). Significance p<0.05* ns = p> 0.05 using unpaired parametric t-test.*

5.2.2 Expression of total *CLU* mRNA is unaltered by *CLU* exon 2 editing in iPSC-neurons

In chapter 4 (***See Chapter 4***, ***figure 4.3***), total *CLU* mRNA expression was demonstrated to be similar between CTR and exon 2 +/- iPSCs. Here, RT-qPCR was used to quantify expression of total *CLU* mRNA transcripts in untreated and $A\beta_{25-35}$ treated iPSC-neurons (***Figure 5.2***). Expression of total *CLU* mRNA transcripts was comparable in untreated CTR and untreated exon 2 +/- iPSC-neurons demonstrating that editing of *CLU* exon 2 had not impacted on the overall abundance of *CLU* mRNA generated by cells. This agrees with data obtained in chapter 4. Finally, $A\beta_{25-35}$ did not alter the expression of total *CLU* in either CTR or exon 2 +/- iPSC-neurons.

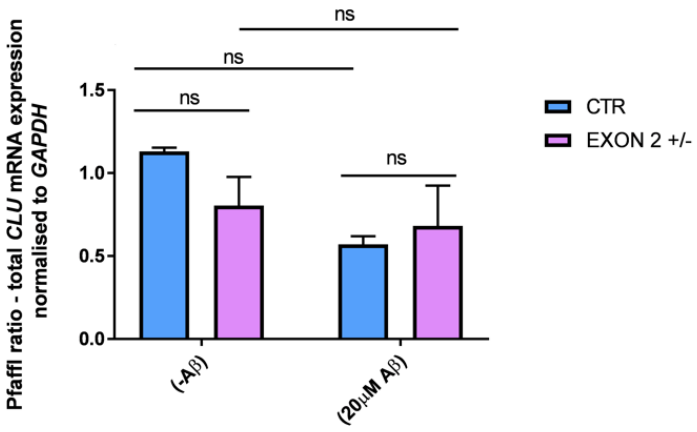


Figure 5.2. Heterozygous exon 2 KO does not alter the expression of total CLU mRNA in human iPSCs. CTR and exon 2 +/- iPSC-neurons were treated for 24 hours with 20μM Aβ$_{25-35}$. Expression of total CLU mRNA was quantified relative to GAPDH using RT-qPCR. Using two-way ANOVA analysis, it was determined that neither iPSC-neuron genotype (p=0.5157) nor treatment (p=0.0868) influenced the expression of total CLU mRNA, additionally, no significant interaction between iPSC-neuron genotype and treatment condition was identified (p=0.2222). Total CLU mRNA expression was comparable between untreated CTR and exon 2 +/- iPSC-neurons (p=0.2222). Similarly, expression was comparable between treated CTR and treated exon 2 +/- iPSC-neurons (p=0.9505). Additionally, Aβ$_{25-35}$ treatment did not influence the expression of total CLU mRNA in either CTR (p=0.1776) or exon 2 +/- iPSC-neurons (p=0.9343). Data are shown as mean ± SEM, n= 3 (n = independent differentiations, each with 3 replicate wells). Significance was tested using two-way ANOVA with Tukey's multiple comparison analysis. P<0.05.*

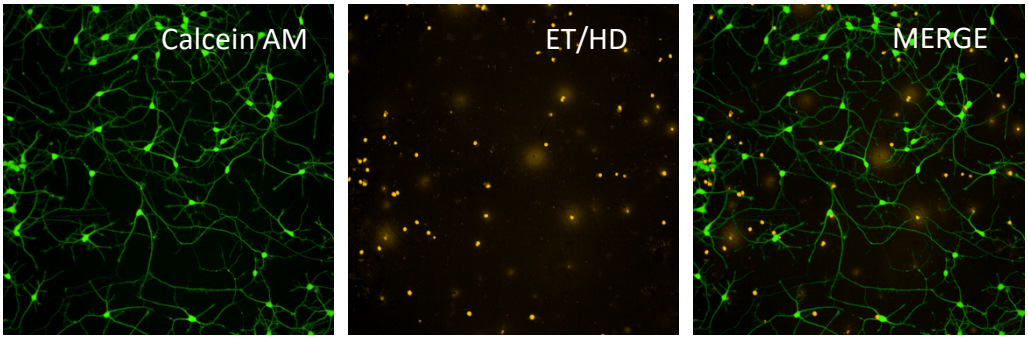
5.2.3 Aβ$_{25-35}$ induces cell death in CTR and exon 2 +/- iPSC-neurons

It is widely accepted that *in vitro* exposure to Aβ$_{25-35}$ results in toxicity and cell death (Forloni et al., 1993). As above, CTR and exon 2 +/- iPSC-neurons were treated with 20μM of Aβ$_{25-35}$ for 24 hours followed by incubation with a Dead Cell Staining Kit II to quantify cell death (***See Chapter 2, 2.2.8.1.1***). Live imaging was used to quantify the number of cells positively stained with Calcein AM and Ethidium homodimer (ET/HD) representing live and dead cells respectively (***Figures 5.3A-D, see Chapter 2, 2.2.8.4.1***).

$A\beta_{25-35}$ did not significantly alter either the number of live or dead cells in CTR or exon 2 +/- iPSC-neuron cultures (***Figure 5.3E and F respectively***), although there was a trend towards reduced cell survival in both CTR and exon 2 +/- iPSC-neurons (number of live cells: CTR: p=0.3789, exon 2 +/-: p=0.1000). The number of live and dead cells in each culture was then compared by calculation of the Live/Dead Ratio (***Figure 5.3G***). $A\beta_{25-35}$ treatment significantly reduced the Live/Dead Ratio for both CTR and exon 2 +/- iPSC-neurons indicating $A\beta_{25-35}$ treatment significantly increased the number of dead cells in both CTR and exon 2 +/- iPSC-neuron cultures. The observed reduction in the Live/Dead Ratio in both CTR and exon 2 +/- iPSC-neurons following treatment with $A\beta_{25-35}$ clearly demonstrates that 20µM of $A\beta_{25-35}$ is sufficient to induce cell death. Moreover, this response was similar between CTR and exon 2 +/- iPSC-neuron cultures therefore exon 2 +/- iPSC-neurons do not have altered sensitivity to $A\beta_{25-35}$.

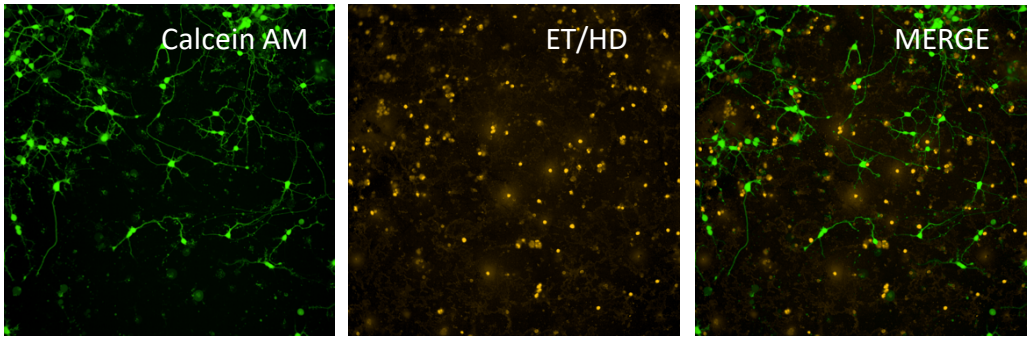
A)

CTR neurons
(-Aβ)



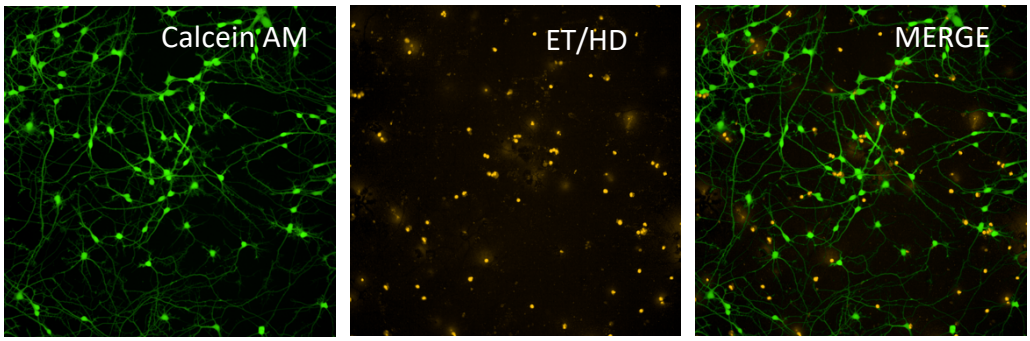
B)

CTR neurons
(+Aβ)



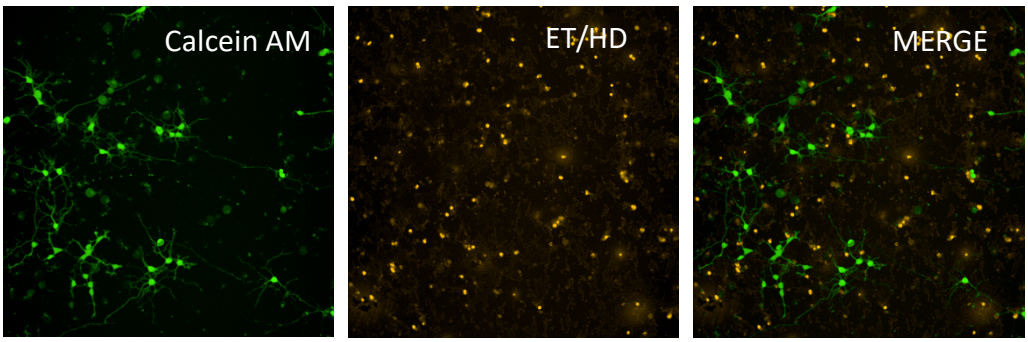
C)

Exon 2 +/-
neurons
(-Aβ)



D)

Exon 2 +/-
neurons
(+Aβ)



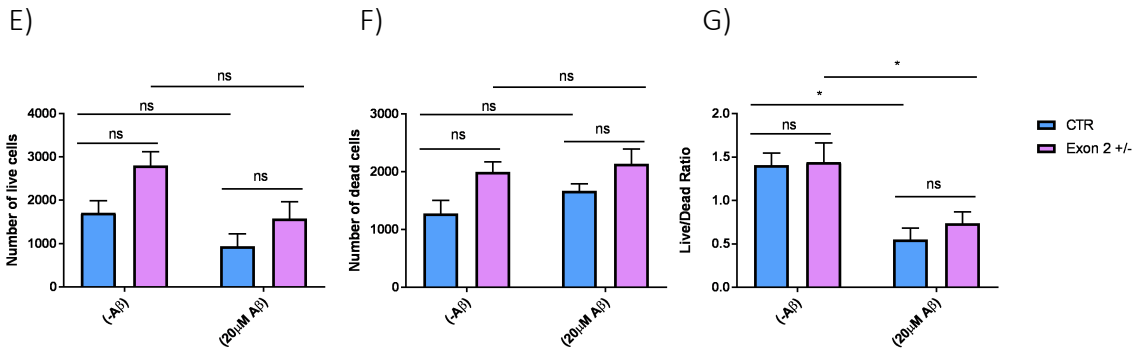


Figure 5.3. Exon 2 +/- iPSC-neurons exhibit similar amounts of death as CTR iPSC-neurons following treatment with 20μM $Aβ_{25-35}$ for 24 hours.

CTR and exon 2 +/- iPSC-neurons were treated for 24 hours with 20μM $Aβ_{25-35}$. The number of live and dead cells were then quantified by staining with Calcein AM and ET/HD respectively. The number of live and dead cells in each culture was then compared by quantifying the Live/Dead Ratio. A reduction in the Live/Dead Ratio represents increased cell death. ***A-D****) Cells were imaged live at 20x magnification on an Operetta Phenix Confocal Microscope and analysed using Phenix Harmony Software. Representative images of day 36 neurons:* ***A****) CTR (-$Aβ_{25-35}$),* ***B****) CTR (+ $Aβ_{25-35}$),* ***C****) exon 2 +/- (-$Aβ_{25-35}$) and* ***D****) exon 2 +/- (+ $Aβ_{25-35}$). Stains are Calcein AM (green) and ET/HD (orange/brown) representing the live and dead cells respectively.* ***D****) Two-way ANOVA analysis identified a significant influence of both iPSC-neuron genotype (p=0.0267*) and treatment condition (p=0.0141*) on the number of live cells. No significant interaction between genotype and treatment condition was identified (p=0.4989). No significant differences were identified following post hoc analysis; the number of live cells was comparable between untreated CTR and exon 2 +/- iPSC-neurons (p=0.1510). Treatment with $Aβ_{25-35}$ did not alter the number of live CTR (p=0.3789) or exon 2 +/- (p=0.1000) iPSC-neurons.* ***E****) Two-way ANOVA analysis identified a significant influence of iPSC-neuron genotype (p=0.0181*) but not treatment condition (p=0.2227) on the number of dead cells. No significant interaction was identified between treatment condition and iPSC-neuron genotype (p=0.5383) and no significant differences were identified following post hoc analysis. Dead cell counts were comparable between untreated CTR and exon 2 +/- iPSC-neurons (p=0.1257). Treatment did not alter the number of dead cells in either CTR (p=0.5387) nor exon 2 +/- (p=0.9614) iPSC-neuron cultures.* ***F****) Finally, the Live/Dead Ratios were calculated. Two-way ANOVA analysis identified a significant influence of treatment condition (p=0.0013**) but not iPSC-neuron genotype (p=0.5105) on the Live/Dead Ratios. Again, no significant interaction was identified between treatment condition and iPSC-neuron genotype (p=0.6508). Before treatment ratios were comparable between CTR and*

exon 2 +/- iPSC-neurons (p=0.9986). Treatment with Aβ$_{25-35}$ significantly reduced the Live/Dead Ratio of both CTR iPSC-neurons (p=0.0029) and exon 2 +/- iPSC-neurons (p=0.0477*) demonstrating increased cell death in both cultures following treatment with Aβ$_{25-35}$. Live/Dead Ratios of treated CTR and exon 2 +/- iPSC-neuron cultures were similar demonstrating comparable sensitivity to Aβ$_{25-35}$ (p=0.8438). Therefore Aβ$_{25-35}$ treatment but not iPSC-neuron genotype influenced cell death quantified in iPSC-neuron cultures. Data are shown as mean ± SEM, n = 3 (n= independent differentiations, each with 6 replicate wells). Significance was tested using two-way ANOVA with Tukey's multiple comparison analysis. P<0.05*.*

5.2.4 Aβ$_{25-35}$ induces neurite damage in CTR and exon 2 +/- iPSC-neurons

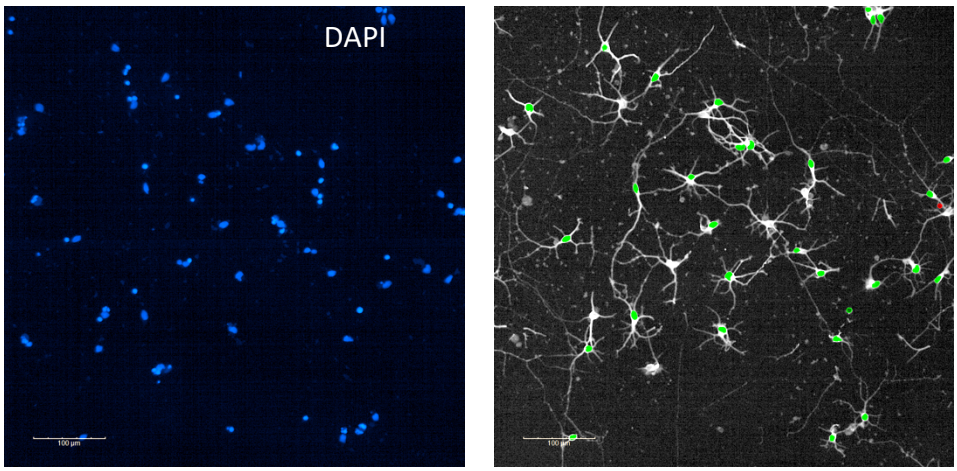
20µM Aβ$_{25-35}$ treatment for 24 hours induced significant cell death in both CTR and exon 2 +/- iPSC-neurons. Another recognised measure of downstream Aβ$_{25-35}$ toxicity is neurite damage. As in **5.2.3**, CTR and exon 2 +/- iPSC-neurons were treated with Aβ$_{25-35}$ and after 24 hours were immunostained with neuronal marker MAP2 and imaged (***See Chapter 2, 2.2.8.3.2***). Harmony software was used to identify nuclei (DAPI positive regions, ***figure 5.4A***) and neurite processes (MAP2 positive regions, ***figure 5.4B***), and to quantify changes in neurite length in CTR and exon 2 +/- iPSC-neurons (***Figures 5.4C-F, see Chapter 2, 2.2.8.4.3***).

Since neuronal response to Aβ$_{25-35}$ can be influenced by cell density, the number of nuclei were quantified and were found to be similar between CTR and exon 2 +/- iPSC-neuron cultures (***Figure 5.4G***). To determine if Aβ$_{25-35}$ induced damage to neurons, the mean segment length of neuronal processes was quantified. Aβ$_{25-35}$ treatment significantly reduced mean segment length in both CTR and exon 2 +/- iPSC-neurons (***Figure 5.4H***). Interestingly, the reduction observed was similar in CTR and exon 2 +/- iPSC-neurons.

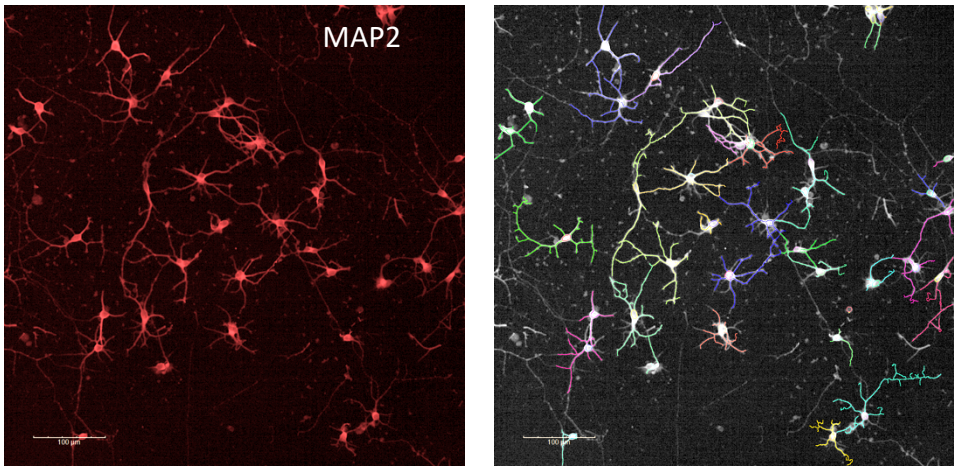
Next, neurite outgrowth was assessed by measuring the maximum length of segments generated by iPSC-neurons (***Figure 5.4I***). Aβ$_{25-35}$ treatment significantly reduced

maximum segment length in both CTR and exon 2 +/- iPSC-neuron cultures. Finally, the mean segment length to cells was quantified to give a measurement of the length of the direct pathway of each segment to the cell body of the neuron from which it originates (***Figure 5.4J***). $A\beta_{25-35}$ treatment significantly reduced mean segment length to cell in both CTR and exon 2 +/- iPSC-neurons. In all measured parameters, $A\beta_{25-35}$ induced significant reductions resulting in a retraction or shortening of neurite processes. Furthermore, the responses were in similar magnitude between CTR and exon 2 +/- iPSC-neurons demonstrating that exon 2 +/- iPSC-neurons do not have altered sensitivity to $A\beta_{25-35}$.

A)

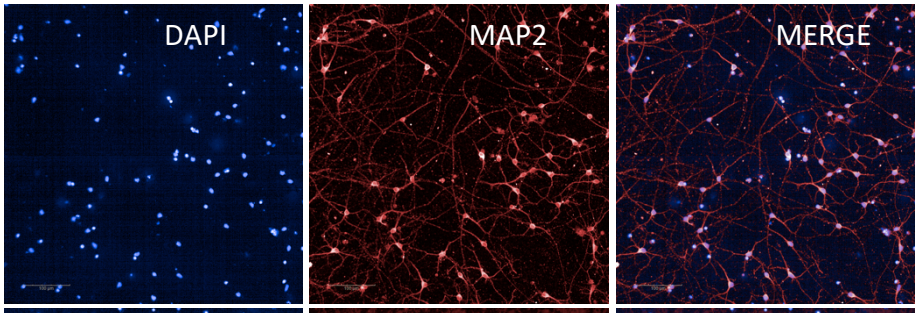


B)



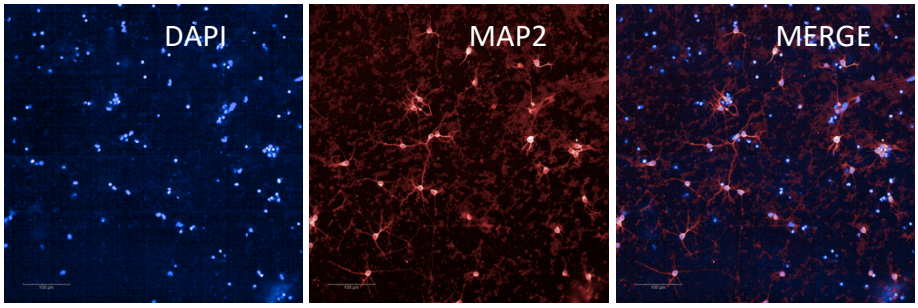
C)

CTR neurons (-Aβ)



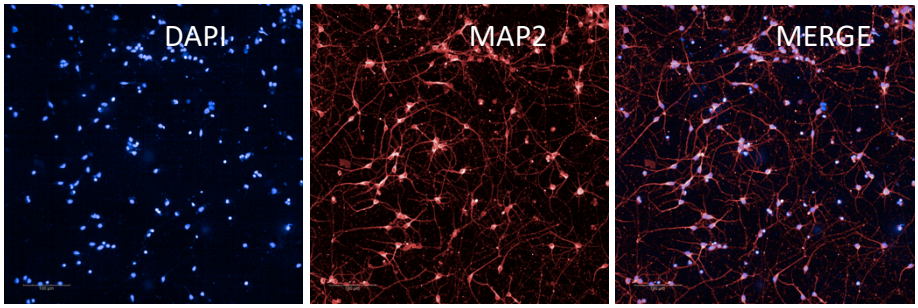
D)

CTR neurons (+Aβ)



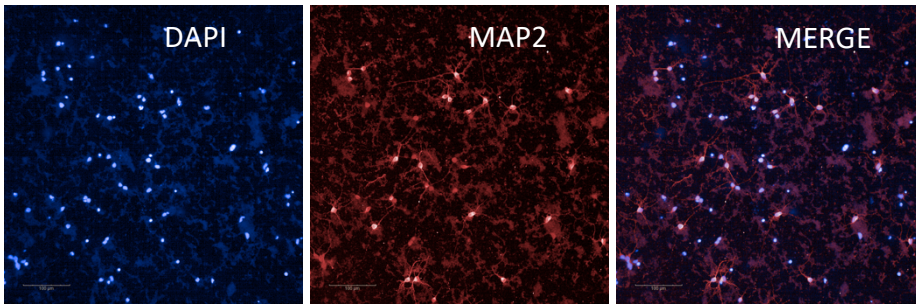
E)

Exon 2 +/- neurons (-Aβ)



F)

Exon 2 +/- neurons (+Aβ)



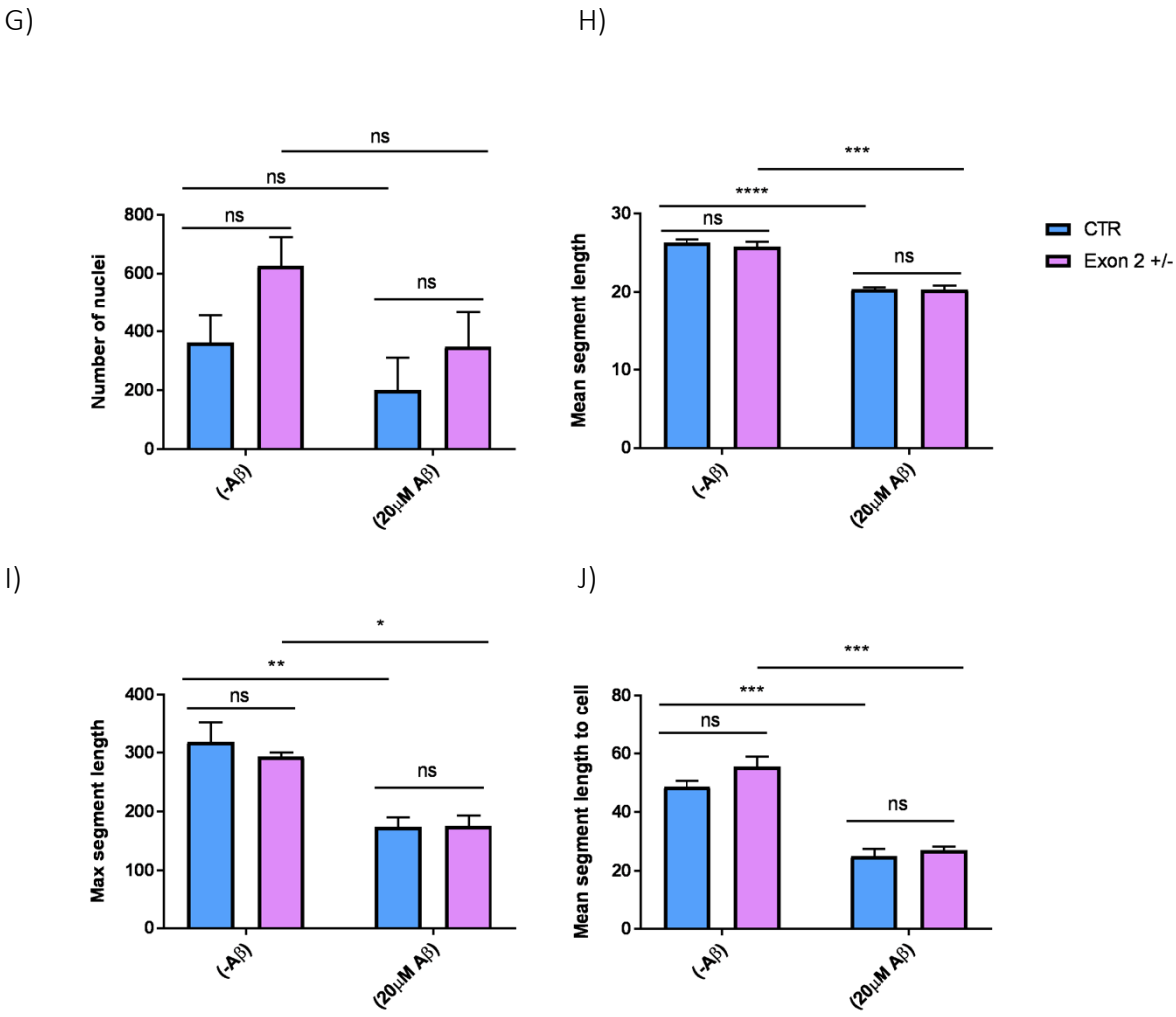


Figure 5.4. Exon 2 +/- iPSC-neurons exhibit similar retraction of neurite processes as CTR iPSC-neurons following treatment with 20μM $A\beta_{25-35}$ for 24 hours.

CTR and exon 2 +/- iPSC-neurons were treated with 20μM $A\beta_{25-35}$ for 24 hours. Cells were then fixed, immunostained and imaged. ***A-B****) Images were analysed using Phenix Harmony Software identifying* ***A****) DAPI positive nuclei and* ***B****) MAP2 positive neurite processes were identified.* ***C-D****) Images were taken at 20x magnification on an Operetta Phenix Confocal Microscope and analysed using Phenix Harmony Software. Representative images of day 36 neurons:* ***C****) CTR (-$A\beta_{25-35}$),* ***D****) CTR (+ $A\beta_{25-35}$),* ***E****) exon 2 +/- (-$A\beta_{25-35}$) and* ***F****) exon 2 +/- (+ $A\beta_{25-35}$). Stains are: DAPI (blue) and MAP2 (red).* ***G****) The number of nuclei was not altered by iPSC-neuron genotype (p=0.0854) or $A\beta_{25-35}$ treatment condition (p=0.0696), no significant interaction between iPSC-neuron genotype and treatment condition was identified (p=0.5932). The number of nuclei was comparable between all groups.* ***H****) The mean length of neurite segments was quantified in each condition. Two-way ANOVA analysis revealed significant influences from both treatment condition (p<0.0001****) but not iPSC-neuron genotype (p=0.5497). But no significant interaction was identified between treatment*

*condition and iPSC-neuron genotype (p=0.5724). Mean segment length was comparable in untreated CTR and exon 2 +/- iPSC-neurons (p=0.8259). Treatment with Aβ$_{25-35}$ significantly reduced mean segment length in both CTR (p<0.0001****) and exon 2 +/- (p=0.0005***) iPSC-neurons. Treated CTR and exon 2 +/- iPSC-neurons had comparable mean segment lengths (p>0.9999).* ***I****) Treatment condition (p=0.0002***) but not iPSC-neuron genotype (p=0.5848) had a significant influence on maximum segment length of cells. No significant interaction was identified between iPSC-neuron genotype and treatment condition (p=0.5392). Maximum segment length was comparable between untreated CTR and exon 2 +/- iPSC-neurons (p=0.8267). Treatment with 20μM Aβ$_{25-35}$ significantly reduced maximum segment length in both CTR (p=0.0049**) and exon 2 +/- (p=0.0155*). Maximum segment length did not differ between treated CTR and exon 2 +/- iPSC-neuron cultures (p>0.9999).* ***J****) Again, treatment condition was shown to influence mean segment length to cell (p<0.0001****) but iPSC-neuron genotype did not (p=0.1026). No significant interaction was identified between treatment condition and iPSC-neuron genotype (p=0.3358). Mean segment length to cell was comparable between untreated CTR and exon 2 +/- iPSC-neurons (p=0.2550) and between treated CTR and exon 2 +/- iPSC-neurons (p=0.9357). Treatment significantly reduced mean segment length to cells in both CTR (p=0.0005***) and exon 2 +/- iPSC-neurons (p=0.0001***). In all parameters, Aβ$_{25-35}$ treatment but not iPSC-neuron genotype was demonstrated to significantly decrease the length of neurite processes in iPSC-neuron cultures. Data are shown as mean ± SEM, n = 3 (n= independent differentiations, each with 6 replicate wells). Significance was tested using two-way ANOVA with Tukey's multiple comparison analysis. P<0.05*.*

A summary of the key findings from this portion of the results section in this chapter can be found in ***table 5.2***.

20μM Aβ$_{25-35}$ treated vs untreated iPSC-neurons		
Parameter	CTR	Exon 2 +/-
CLU variant 1 Δ exon 2 transcripts	No change (absent)	No change
Total *CLU* mRNA	Reduced	No change
Cell death	Increased	Increased
Neurite length	Decreased	Decreased

Table 5.2. Key changes in CTR and exon 2 +/- iPSC-neurons in response to Aβ$_{25-35}$ treatment.

5.2.5 Changes in gene expression in exon 2 +/- iPSC-neurons is similar to that of CTR iPSC-neurons after treatment with $A\beta_{25-35}$

RNA-Seq analysis was used to measure changes in gene expression following treatment of CTR and exon 2 +/- iPSC-neurons with $A\beta_{25-35.}$ As above, iPSC-neurons were treated with 20µM $A\beta_{25-35}$ for 24 hours, RNA was then collected and prepared for sequencing by the Wellcome Trust Centre for Human Genetics (University of Oxford) (*See chapter 2, 2.2.6.5-2.2.6.7*).

Gene expression profiles were obtained for the following four comparisons:

1. $A\beta_{25-35}$ treated vs untreated CTR iPSC-neurons (**Res 1**)
2. $A\beta_{25-35}$ treated vs untreated exon 2 +/- iPSC-neurons (**Res 2**)
3. Untreated exon 2 +/- iPSC-neurons vs untreated CTR iPSC-neurons (**Res 3**)
4. $A\beta_{25-35}$ treated exon 2 +/- iPSC-neurons vs $A\beta_{25-35}$ treated CTR iPSC-neurons (**Res 4**)

First, a heatmap was generated to visualise gene expression changes across all samples. The fragments per kilobase of exon per million reads mapped (FPKM) expression values were mapped for the top 20 most variable genes. Clustering was performed to group samples according to both neuronal genotype and $A\beta_{25-35}$ treatment condition (***Figure 5.5***). For the majority of differentially expressed (DE) genes, the greatest difference in gene expression was associated with $A\beta_{25-35}$ treatment condition and not iPSC-neuron genotype. Few genes were mainly influenced by neuronal genotype (*NNAT*, *SOX10*, *PCDHGA3*, *OLFML21, COL1A2* and *PCDGB4*).

Volcano plots were then generated to compare statistical significance with magnitude of changes in gene expression to enable identification of genes with large fold changes in each condition that are also statistically significant (***Figure 5.6***). Genes labelled

on the volcano plot satisfy the cut off for both p value (–log10(p value) cut off $10e^{-6}$) and fold change (log2(fold change) threshold > 1.0); those found on the right-hand side of the graph are increased in expression while those on the left are decreased. All DE genes were upregulated by $A\beta_{25-35}$ except *HES5.* This was consistent between CTR and exon 2 +/- iPSC-neurons *(**Figure 5.6A and B respectively***). Previously, a number of genes were identified whose expression is increased in rodent neurons *in vitro* treated with $A\beta_{25-35}$ (Killick et al., 2014). One of these genes was *EGR1,* which mediates $A\beta_{25-35}$ induced cell death and tau hyperphosphorylation in rodent neurons (Killick et al., 2014). Interestingly, *EGR1* expression was also upregulated in both CTR and exon 2 +/- iPSC-neurons following $A\beta_{25-35}$ treatment. Furthermore, the extent to which *EGR1* was upregulated was similar in CTR and exon 2 +/- iPSC-neurons demonstrating *EGR1* expression changes induced by $A\beta_{25-35}$ is not altered by the removal of *CLU* exon 2 (fold change = 3.12 and 2.91 respectively). In rodent neurons treatment with $A\beta_{25-35}$ induced an alteration in clusterin trafficking that resulted in induction of *DKK1* expression, which ultimately resulted in an increase in expression of several transcriptional factors including *EGR1*, and *KLF10* (Killick et al., 2014). *CLU* and *KLF10* expression were unaltered by $A\beta_{25-35}$ treatment in both CTR and exon 2 +/- iPSC-neurons. Meanwhile, *DKK1* expression was not detected in any samples, likely attributed to its low abundance in neurons (Caricasole, 2004; Mastroiacovo et al., 2009; Purro et al., 2012).

To determine the influence of *CLU* exon 2 gene editing on gene expression, DE genes were compared between untreated CTR and exon 2 +/- iPSC-neurons (***Figure 5.6C***) and treated CTR and exon 2 +/- iPSC-neurons (***Figure 5.6D***). In agreement with the data provided in the heat map in ***figure 5.5*** several DE genes were identified in exon 2 +/- iPSC-

neurons when compared to CTR iPSC-neurons and the majority of which were downregulated.

Finally, differences in gene expression data were gathered into KEGG pathways to identify enrichment of biological pathways (***Figure 5.7***). Pathways were found to be enriched in 3 of the 4 comparisons (**res 1, 2 and 4**). **Res 3**, representing untreated exon 2 +/- vs untreated CTR iPSC-neurons was excluded from KEGG analysis since no pathway enrichment was identified in this comparison. Four common pathways (MAPK signalling pathway, neuroactive ligand-receptor interaction, transcriptional misregulation in cancer and breast cancer) were identified in **res 1** and **res 2**. This again highlights the similarities in responses of CTR (**res 1**) and exon 2 +/- (**res 2**) iPSC-neurons to $A\beta_{25-35}$ treatment. In both cases, most genes differentially expressed in CTR and exon 2 +/- iPSC-neurons after treatment were found within the MAPK signalling and neuroactive ligand receptor interaction pathways. Five pathways were identified to be enriched when treated exon 2 +/- and treated CTR iPSC-neurons were compared (**Res 4**). Four of these pathways were unique to this comparison (ECM receptor interaction, protein digestion and absorption, amoebiasis and GABAergic synapse).

Overall, the RNA-Seq analysis data provided here indicates great similarities in transcriptional response of CTR and exon 2 +/- iPSC-neurons induced by treatment with $A\beta_{25-35.}$ In fact, most of the variation in gene expression arises from $A\beta_{25-35}$ treatment and not from iPSC-neuron genotype. A number of genes were identified as upregulated following treatment, one of which was *EGR1*, a transcription factor that previously was identified to be upregulated in rodent neurons treated with $A\beta_{25-35}$ (Killick et al., 2014). In combination with other data included in this chapter, it was evident that the heterozygous

removal of *CLU* exon 2 has not significantly altered the response of iPSC-neurons to $A\beta_{25-35}$. In fact, many responses are like that observed in CTR iPSC-neurons.

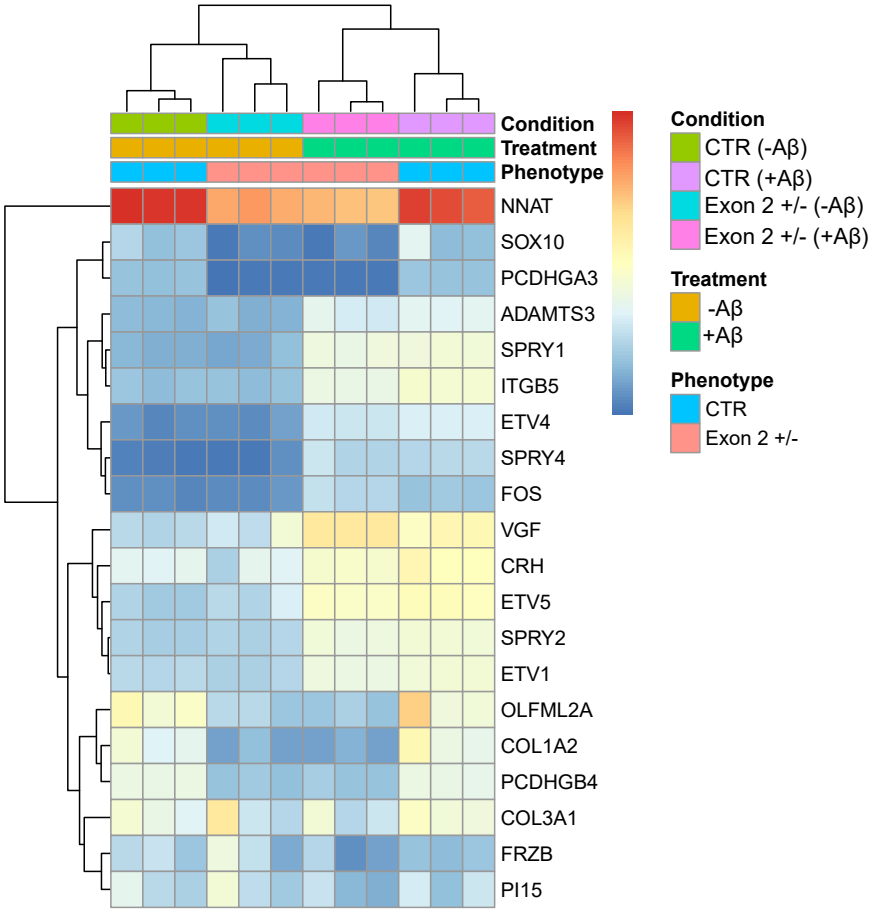


Figure 5.5. A heatmap of FPKM expression values in 4 conditions.

Heat map displays the top 20 differentially expressed genes identified across the whole genome in all four conditions; CTR and exon 2 +/- iPSC-neurons, untreated and $A\beta_{25-35}$ treated. The colour gradient represents expression of each gene in sample across the whole population: (blue = lower expression and red = higher expression).

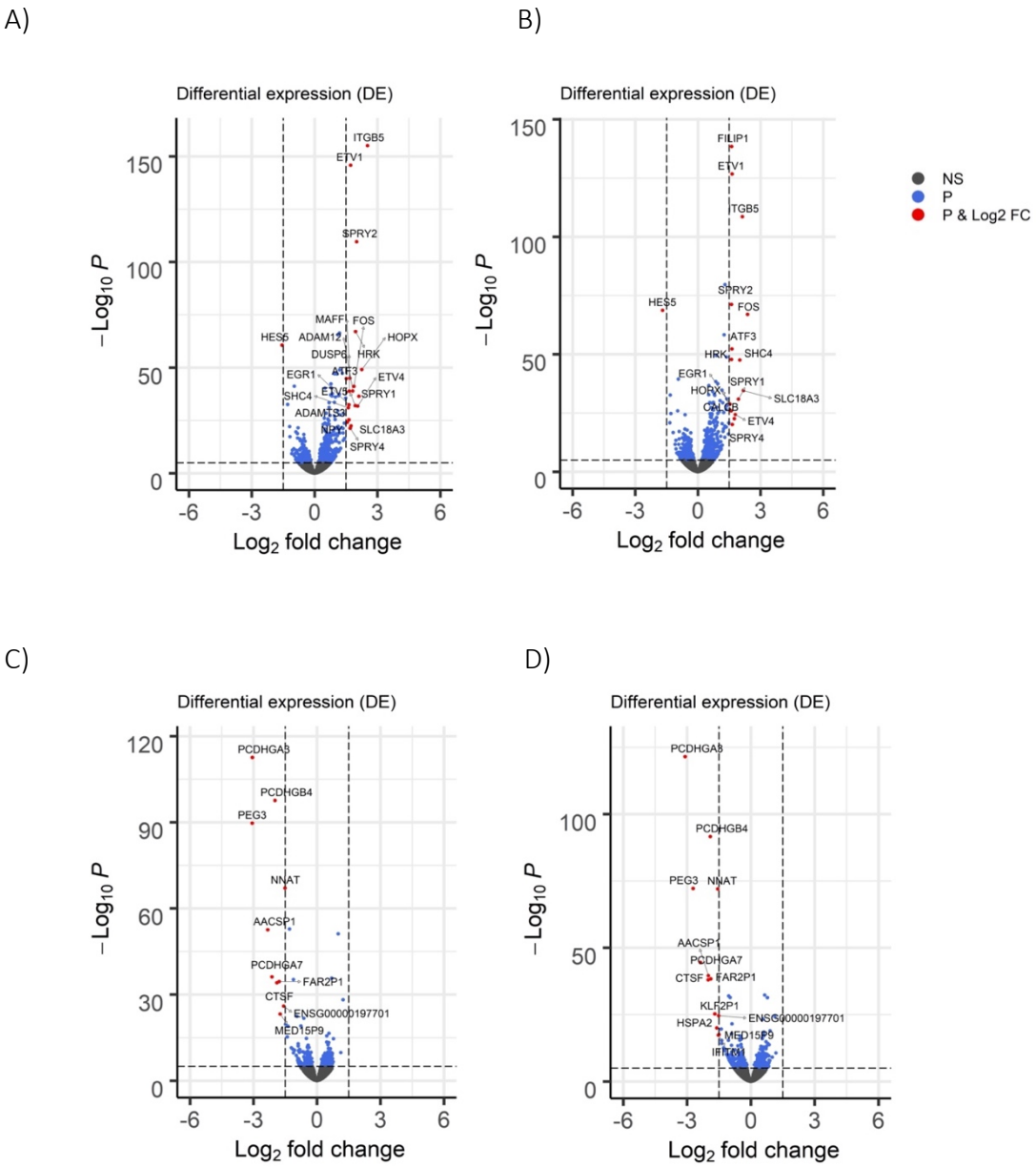


Figure 5.6. Volcano plots for comparisons between CTR and exon 2 +/- iPSC-neurons.

Each gene is plotted as a product of its fold change and statistical significance, represented on the x and y-axes respectively. ***A****) Aβ$_{25-35}$ treated vs untreated CTR iPSC-neurons.* ***B****) Aβ$_{25-35}$ treated vs untreated exon 2 +/- iPSC-neurons.* ***C****) Untreated exon 2 +/- vs untreated CTR iPSC-neuron.* ***D****) Aβ$_{25-35}$ treated exon 2 +/- iPSC-neurons vs Aβ$_{25-35}$ treated CTR iPSC-neurons. The x-axis represents the mean difference (fold change) on the log2 scale of a gene for the contrast effect between pairs of groups (either treatment or genotype). The y-axis represents transformed raw p-values (-log10 (p-value)) of an individual t-test for a gene under a given contrast. Black = non-significant, blue = satisfies -log10(p value) threshold > 1.0, red = satisfies log2(fold change) threshold > 1.0 and –log10(p value) cut off 10e^{-6}.*

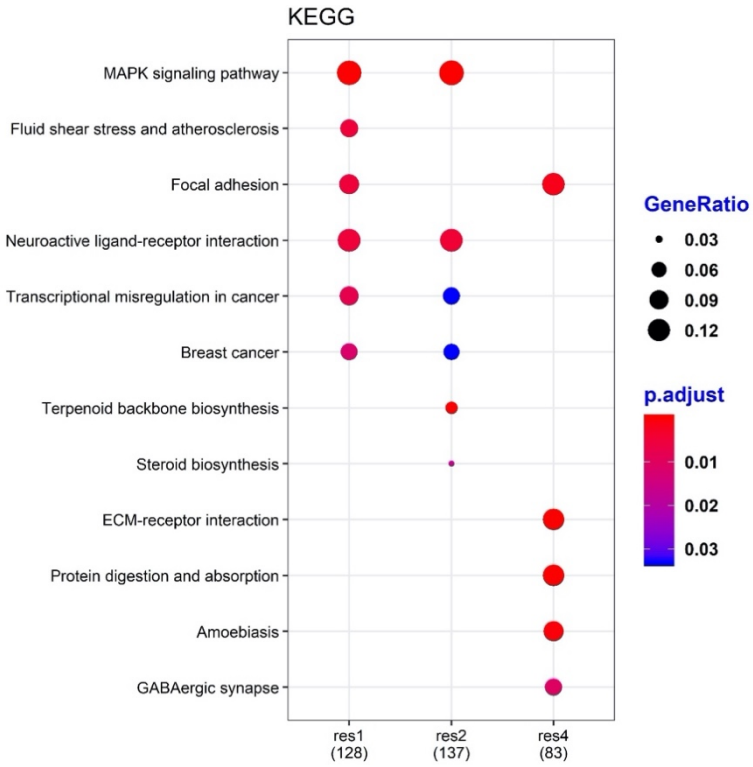


Figure 5.7. KEGG pathway analysis identifies pathway enrichment in 3 of the 4 group comparisons between CTR and exon 2 +/- iPSC-neurons.

Differential gene expression data was obtained for all four comparisons and were gathered into KEGG pathways. ***Res 1*** *describes KEGG pathway enrichment between treated and untreated CTR iPSC-neurons.* ***Res 2*** *describes KEGG pathway enrichment between treated and untreated exon 2 +/- iPSC-neurons.* ***Res 3*** *describes KEGG pathway enrichment between untreated exon 2 +/- and CTR iPSC-neurons.* ***Res4*** *describes KEGG pathway enrichment between treated exon 2 +/- and CTR iPSC-neurons. Differential gene expression data that satisfied thresholds for both fold change (>1.5) and adjusted p value (<0.05) were included in this analysis. Res 3 is not included in the analysis since no pathways were identified to be enriched when comparing untreated exon 2 iPSC-neurons and untreated CTR iPSC-neurons. Numbers represent the number of differentially expressed genes found to be in enriched in KEGG pathways for each* ***res****.*

5.3 Discussion

5.3.1 $A\beta_{25-35}$ does not alter the expression of *CLU* variant 1 Δ exon 2 transcripts

It was demonstrated that exon 2 +/- iPSC-neurons express *CLU* variant 1 Δ exon 2 transcripts while CTR iPSC-neurons do not. This is in agreement with data provided in chapter 4 (***See chapter 4, figure 4.2***) and with previous studies (Andersen et al., 2007). Others have previously demonstrated that the expression of *CLU* variant 1 Δ exon 2 transcripts is induced or increased following application of stress on cells (Leskov et al., 2003; Prochnow et al., 2013). This has been observed in a number of cell lines including MCF-7, PC-3 and HEK293T (Prochnow et al., 2013). However, the data in this chapter demonstrated that $A\beta_{25-35}$ does not alter the expression of this variant in iPSC-neurons. This is a surprising observation given previous studies have demonstrated this variant is influenced by stress and believed to mediate cell death, which was clearly demonstrated in both CTR and iPSC-neurons following treatment with $A\beta_{25-35}$. This suggests that the altered transcription of *CLU* variant 1 Δ exon 2 transcripts may vary between cell type and the type of stress, for example, Prochnow et al., demonstrated induction of this variant using heat shock and proteasomal inhibition (Prochnow et al., 2013), while Leskov et al., demonstrated similar findings following ionising radiation treatment (Leskov et al., 2003). In this thesis, $A\beta_{25-35}$ was used as the stressor and although beyond the remit of this study, it may be interesting to determine if transcription of the *CLU* variant 1 Δ exon 2 transcript is altered following shorter periods of incubation with $A\beta_{25-35}$ such as 6 hours or by other sources of stress relevant to AD such as $A\beta_{1-42}$ or hypoxia.

5.3.2 Exon 2 +/- iPSC-neurons respond similarly to CTR iPSC-neurons after treatment with $A\beta_{25-35}$

Two commonly used measures of quantifying Aβ induced toxicity, cell death and neurite length were used to compare the responses of CTR and exon 2 +/- iPSC-neurons to evaluate if the latter are more sensitive to $A\beta_{25-35}$. While $A\beta_{1-42}$ is considered to be the pathological Aβ species in AD (Näslund et al., 1994), its use in experiments is impaired due to its instability when present in an aggregated, fibrillary state (Blasko et al., 2000). Numerous studies have demonstrated similarities in activity *in vitro* between $A\beta_{25-35}$ and $A\beta_{1-42}$ (Copani et al., 1999; Li et al., 1996; Michaelis et al., 1998), making $A\beta_{25-35}$ a suitable alternative for use in this chapter. A variety of concentrations of $A\beta_{25-35}$ have been demonstrated to induce cell death previously (Killick et al., 2014; Morishima et al., 2001; Yankner et al., 1990). In this chapter, 20μM $A\beta_{25-35}$ was used, consistent to that used previously to induce cell death in rodent neurons (Killick et al., 2014).

$A\beta_{25-35}$ treatment clearly induced damage in iPSC-neurons, resulting in significant amounts of cell death and neurite damage that resulted in the shortening of neurite processes. The magnitude of neurite damage inflicted was similar between CTR and exon 2 +/- iPSC-neurons, therefore exon 2 +/- iPSC-neurons are not more sensitive to $A\beta_{25-35}$ induced toxicity. This is surprising, given the increased expression of *CLU* variant 1 Δ exon 2 transcripts it was predicted that exon 2 +/- iPSC-neurons would exhibit more damage than their CTR counterparts. The similarities in responses between exon 2 +/- iPSC-neurons and CTR iPSC-neurons was further supported by RNA-Seq data, which highlighted the similarities in changes in gene expression and pathway enrichment in both lines following $A\beta_{25-35}$. Interestingly, in agreement with previous data provided in rodent neurons (Killick et al., 2014), *EGR1* was upregulated in both CTR and exon 2 +/- iPSC-

neurons following treatment with $A\beta_{25-35}$, suggesting *EGR1* may have a role in mediating $A\beta_{25-35}$ induced toxicity in human iPSC-neurons as well as rodent neurons, which should be explored further. *EGR1* knockdown protects rodent neurons from Aβ induced cell death and tau phosphorylation (Killick et al., 2014), suggesting *EGR1* knockdown may be a potential therapeutic strategy in AD. This could further be explored in iPSC-neurons by silencing *EGR1* by use of small interfering RNA (siRNA) or CRISPR interference. Interestingly, the expression of *CLU* and *KLF10* were not altered in human iPSC-neurons following treatment. Firstly, this suggests that alterations in *CLU* expression is not mediating the response of cells to $A\beta_{25-35}$ treatment. Secondly, it suggests a divergence from gene expression changes in rodent and human iPSC-neurons, while *KLF10* is altered in rodent neurons, it is not altered by $A\beta_{25-35}$ in human iPSC-neurons.

The data provided in this chapter demonstrates that the loss of a single *CLU* exon 2 does not alter the response of iPSC-neurons to $A\beta_{25-35,}$ Despite the increased expression of *CLU* variant 1 Δ exon 2 transcripts, altered neuronal sensitivity to $A\beta_{25-35}$ treatment was absent. Furthermore, the expression of *CLU* variant 1 Δ exon 2 transcripts was demonstrated to be not altered by $A\beta_{25-35,}$ questioning the relevance of this variant in mediating $A\beta_{25-35}$ induced toxicity in iPSC-neurons. Heterozygous exon 2 KO is not sufficient to alter sensitivity of human iPSC-neurons to $A\beta_{25-35.}$

6 Characterisation of exon 2 -/- iPSCs and iPSC-neuron response to Aβ

6.1 Introduction

Clusterin's relationship with Aβ has been reported for many decades, however, it is less than straight forward. Research has identified roles for clusterin both in promoting and reducing Aβ toxicity. While glycosylated clusterin species are considered to anti-apoptotic (Trougakos et al., 2009; Zhang et al., 2005), non-glycosylated clusterin species are induced by cell stress and facilitate cell death (Leskov et al., 2003; Prochnow et al., 2013; C.-R. Yang et al., 2000). Several studies have reported altered trafficking of clusterin in cells after stress, resulting in a greater intracellular retention of clusterin (Gregory et al., 2017; Killick et al., 2014; N. Li et al., 2013a; Nizard et al., 2007; Nuutinen et al., 2007; O'Sullivan et al., 2003; Prochnow et al., 2013). However, it is unclear if this altered trafficking promotes cellular stress or is a response to protect cells. With relevance to AD, the treatment of rodent neurons with $A\beta_{25-35}$ (Killick et al., 2014) and AD-*CLU* mutations (Bettens et al., 2015; Zhou et al., 2014) increase intracellular retention of clusterin proteins while reducing clusterin secretion. These studies indicate a potential role of clusterin proteins mediating cellular response to Aβ but also give a mechanism by which *CLU* gene variants may alter an individual's risk of developing AD.

In chapter 5, heterozygous exon 2 KO iPSC-neurons were shown to be equally sensitive to $A\beta_{25-35}$ induced toxicity as CTR iPSC-neurons, indicating an increase in *CLU* variant 1 Δ exon 2 expression is not sufficient to alter neuronal sensitivity and response to $A\beta_{25-35.}$ To further explore the relationship between *CLU* variant 1 Δ exon 2 transcripts, clusterin trafficking and neuronal response to Aβ, homozygous exon 2 KO iPSCs (exon 2 -/-) were generated. First, *CLU* mRNA and clusterin protein expression were examined in exon

2 -/- iPSCs. Second, iPSCs were differentiated into neurons and treated with either $A\beta_{1-42}$ or $A\beta_{25-35}$ to compare the responses of CTR and exon 2 -/- iPSC-neurons.

In this chapter the following questions were addressed:

1. How does clusterin mRNA and protein expression compare between exon 2 -/- and CTR iPSCs?
2. Can exon 2 -/- iPSCs be differentiated into neurons?
3. What concentrations of $A\beta_{1-42}$ and $A\beta_{25-35}$ are sufficient to induce cell death and neurite length retraction in iPSC-neurons?
4. Are exon 2 -/- iPSC-neurons more sensitive to Aβ induced toxicity than CTR iPSC-neurons?

6.2 Results

6.2.1 Generation and quality control of exon 2 -/- iPSCs

CTR iPSCs were supplied to Synthego for transfection to remove *CLU* exon 2 to generate exon 2 -/- iPSCs (***See Chapter 2, 2.2.2.12***). All transfection and quality control (QC) experiments were conducted by Synthego (***Figures 6.1-6.3***). To identify successfully edited clones, gDNA was harvested and *CLU* exon 2 genotype screened by PCR amplification and agarose gel electrophoresis. PCR products were generated using primers flanking *CLU* exon 2 (***See 2.2.2.12, table 2.7***). Two clones were identified to be edited at the *CLU* exon 2 locus, referred to as clones A4 and D1. A single PCR product was generated in CTR samples, while a smaller PCR product was generated in A4 and D1 samples indicating successful excision of *CLU* exon 2 in A4 and D1 iPSCs (***Figure 6.1A***). This was confirmed by PCR amplification using primers positioned within *CLU* exon 2 (***See 2.2.2.12, table 2.8***). A single PCR product was generated in CTR samples, while no amplification was identified in A4 and D1 samples indicating the absence of *CLU* exon 2 (***Figure 6.1B***). Therefore, it can be concluded that A4 and D1 clones are homozygous exon 2 knockout cells (exon 2 -/-).

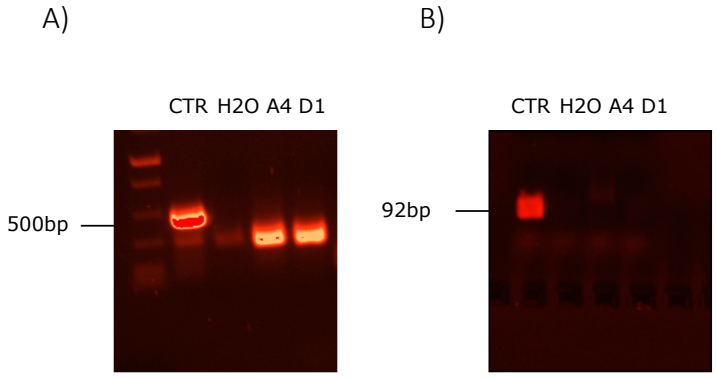
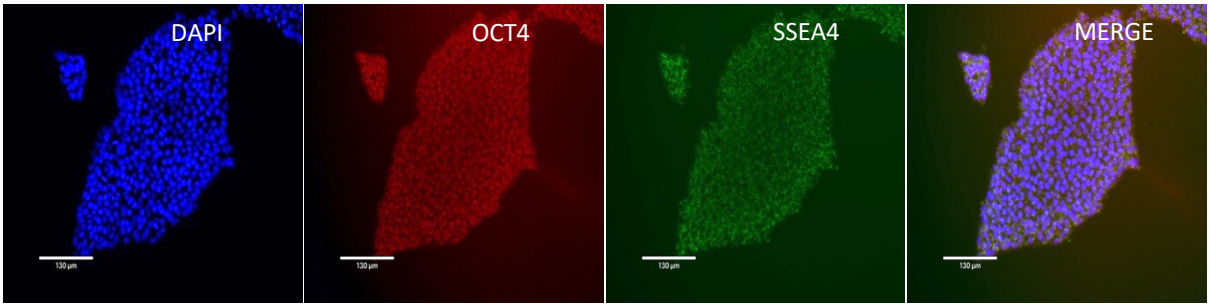


Figure 6.1. A4 and D1 iPSCs are homozygous exon 2 knockout lines.

CTR iPSCs were transfected and gDNA was collected from clones to identify cells in which CLU exon 2 had been successfully removed. gDNA was amplified to confirm the absence of exon 2 in A4 and D1 iPSCs. ***A****) A single PCR product (~500bp) was generated from CTR gDNA indicating full-length CLU exon 2 was present. Smaller PCR products were generated from A4 (~325bp) and D1 (~257bp) iPSCs indicating successful excision of exon 2.* ***B****) A single PCR product (~92bp) was generated from CTR gDNA following PCR amplification using primers positioned within CLU exon 2. No amplification was demonstrated from A4 and D1 gDNA confirming the absence of exon 2. In both PCR reactions, no amplification was seen in the negative control sample,* H_2O.

Following confirmation that A4 and D1 iPSCs were exon 2 -/- iPSC lines, further QC was carried out on the lines to ensure suitability for downstream experiments. First, cells were stained for pluripotency markers *OCT4* and *SSEA4* (***Figure 6.2***). Expression of both markers was confirmed in A4 (***Figure 6.2A***) and D1 iPSCs (***Figure 6.2B***). Secondly, a normal karyotype was identified in both A4 and D1 iPSCs (***Figure 6.3***).

A)



B)

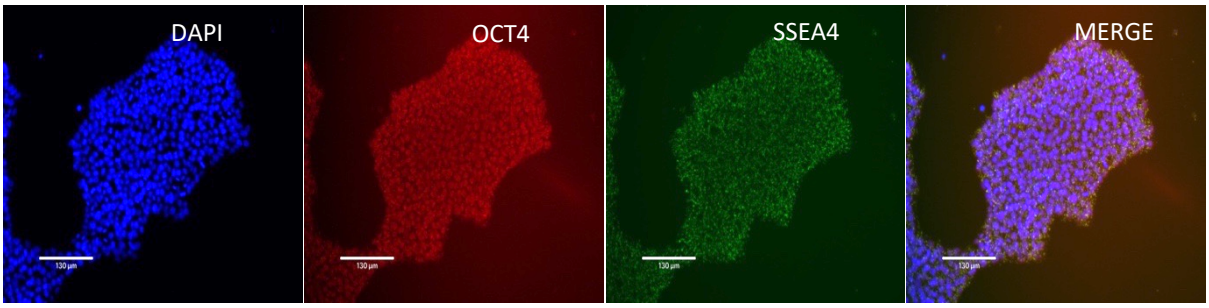


Figure 6.2. A4 and D1 iPSCs express pluripotency markers OCT4 and SSEA4.

To assess whether the removal of CLU exon 2 from iPSCs had altered pluripotency, the expression of pluripotency markers OCT4 and SSEA4 was assessed in A4 and D1 iPSCs. Stains are: DAPI (blue), OCT4 (red) and SSEA4 (green). ***A****) A4 and* ***B****) D1 iPSCs were plated for imaging and expression of OCT4 and SSEA4 pluripotency markers confirmed by immunocytochemistry in both cell lines. Co-localisation of these pluripotency markers with nuclear marker DAPI was also confirmed (final panel).*

A) B)

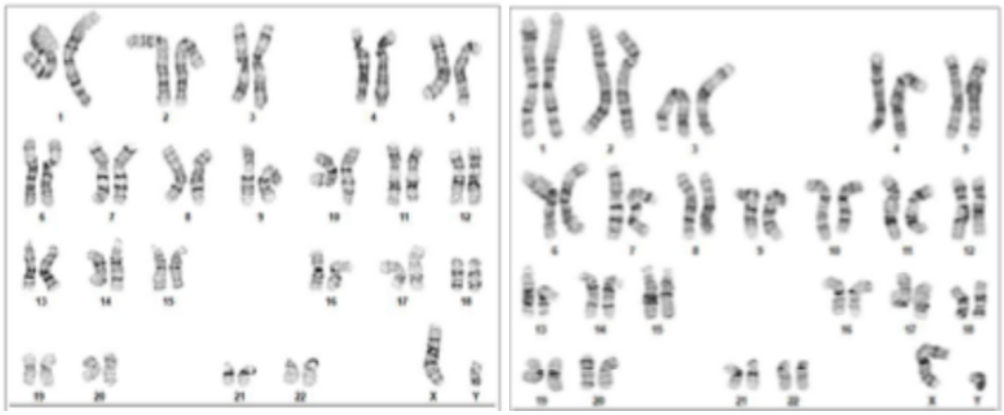


*Figure 6.3. A4 and D1 iPSCs have no chromosomal abnormalities following CRISPR/Cas9 editing. Karyotyping of **A**) A4 and **B**) D1 iPSCs confirmed no chromosomal abnormalities following removal of CLU exon 2. A4 (46, X, Y) and D1 (46, X, Y; a standard metaphase karyotype (band resolution 475-525) was performed and identified no missing or additional chromosomes in either line.*

6.2.2 Exon 2 -/- iPSCs express *CLU* variant 1 Δ exon 2 transcripts and total *CLU* transcript expression is reduced

RT-qPCR was used to measure the expression of several *CLU* mRNA variants in CTR, A4 and D1 iPSCs (***Table 6.1***). *CLU* variant specific primers were used to quantify the expression of *CLU* variants 1, 2, 3 and variant 1 Δ exon 2. Forward primers were specific to each variant and were positioned in one of three alternative *CLU* exon 1s (exon 1a, b or c). Reverse primers for variants 1, 2 and 3 were positioned in *CLU* exon 2. For the quantification of *CLU* variant 1 Δ exon 2 transcripts, primers were positioned at the boundary of exon 1a/exon 3 (forward) and exon 3 (reverse). *CLU* variant 1 Δ exon 2 transcripts were detected in both A4 and D1 iPSCs, but no other *CLU* variants were detected. This was confirmed by running RT-qPCR products for each *CLU* variant on an agarose gel (***Figure 6.4***).

	Average C_t values ± SEM		
Gene of interest	CTR	A4	D1
GAPDH	20.3 ± 0.7	20.8 ± 1.3	24.3 ± 0.9
CLU variant 1 (exon 1a-3)	26.7 ± 0.8	'Undetermined'	'Undetermined'
GAPDH	20.3 ± 0.7	20.8 ± 1.3	24.4 ± 0.9
CLU variant 2 (exon 1b-3)	'Undetermined'	'Undetermined'	'Undetermined'
GAPDH	18.6 ± 0.2	20.9 ± 1.7	22.9 ± 1.2
CLU variant 3 (exon 1c-3)	33.0 ± 1.4	'Undetermined'	'Undetermined'
GAPDH	22.5 ± 2.1	22.2 ± 1.4	22.5 ± 1.2
CLU variant 1 Δ exon 2 (exon 1a/3 boundary)	'Undetermined'	27.9 ± 1.3	28.8 ± 1.0

Table 6.1. RT-qPCR quantification of CLU mRNA transcript variants in CTR and exon 2 -/- iPSCs.

RT-qPCR was used to measure the expression of several CLU mRNA transcript variants in CTR, A4 and D1 iPSCs. Each variant was quantified with respect to GAPDH. Data are shown as mean ± SEM, n=3 (n= the number of independent plating of iPSCs and collections, each with 3 replicate wells). Each CLU variant is associated with its own GAPDH C_t due to multiple RT-qPCR plates being ran for the complete experiment.

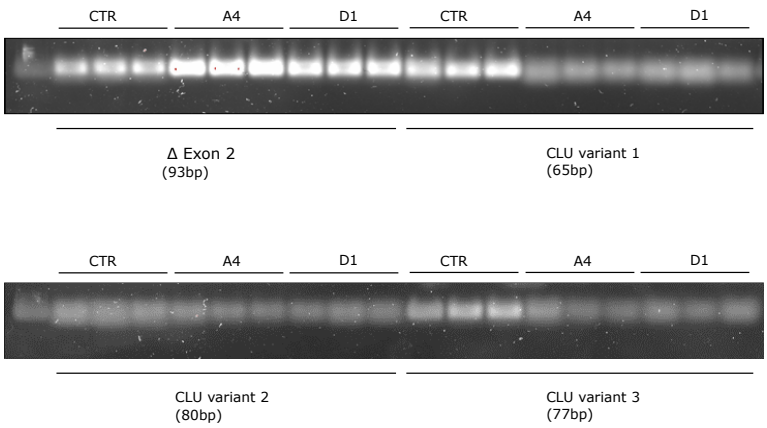


Figure 6.4. Exon 2 -/- iPSCs express CLU variant 1 Δ exon 2 transcripts but no other CLU mRNA variants. The expression of four CLU mRNA variants was measured by RT-qPCR using variant specific primers, forward primers were specific to each variant and positioned in one of the three alternative CLU exon 1s (1a, 1b or 1c). Primers quantifying variant 1 were positioned in exons 1a and 2 (amplicon size 65bp), variant 2 primers were positioned in exon 1b and exon 2 (amplicon size 80bp) and variant 3 primers were positioned in exons 1c and 2 (amplicon size 77bp). For detection of CLU variant 1 Δ exon 2, primers were positioned at the exon 1a/ exon 3 boundary and the end of exon 3 (amplicon 93bp). RT-qPCR products for all four CLU mRNA transcript variants were run on a 1% agarose gel to compare expression between CTR, A4 and D1 iPSCs. As expected, the most abundant variant in A4 and D1 iPSCs was CLU variant 1 Δ exon 2 as evidenced by the high band intensity of this variant in all samples. Band intensity of this variant was much lower in CTR samples indicating lower expression. CLU variant 1 and 3 produced band intensities in CTR samples but not in A4 or D1 iPSC samples indicating these are not expressed by exon 2 -/- iPSCs. CLU variant 2 was not detected in any sample.

The expression of total *CLU* mRNA was also measured by RT-qPCR and expression compared between CTR and exon 2 -/- iPSCs (***Figure 6.5***). A significant reduction in the expression of total *CLU* mRNA was detected in A4 and D1 iPSCs compared to CTR iPSCs. Unsurprisingly, expression was comparable between A4 and D1 iPSCs. These data indicate

that biallelic excision of *CLU* exon 2 significantly reduces the transcription and expression of total *CLU* mRNA in human iPSCs.

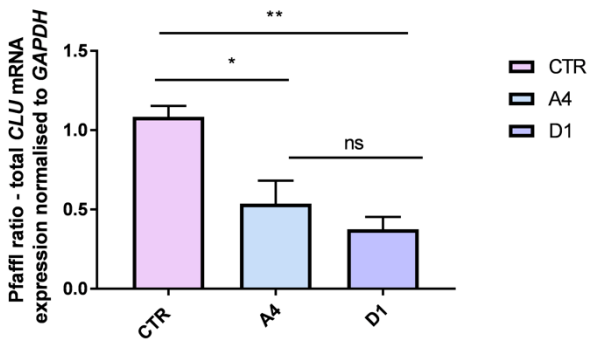


Figure 6.5. Total CLU mRNA expression is significantly reduced in exon 2 -/- iPSCs.
Using primers located in CLU exons 7 and 8 the expression of total CLU mRNA was quantified. Expression was normalised to GAPDH using the Pfaffl method. Total CLU mRNA expression was significantly reduced in exon 2 -/- iPSCs indicating biallelic KO of exon 2 significantly reduces CLU mRNA expression. This response was consistent in both A4 and D1 iPSCs and expression of total CLU was similar between the two lines. Data are shown as mean ± SEM, n = 3 (n = number of independent experiments, each with 3 replicate wells). Significance was tested using One-way ANOVA with Tukey's multiple comparison analysis. P<0.05. ANOVA p = 0.0060**, CTR vs. A4: p =0.0219* and CTR vs D1: p=0.0067**, A4 vs D1: p=0.5432.*

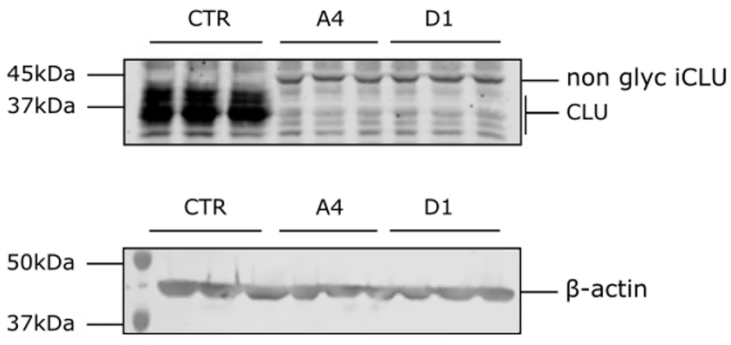
6.2.3 Exon 2 -/- iPSCs generate intracellular but not secreted clusterin proteins

Clusterin immunoreactivity was quantified in exon 2 -/- iPSCs and compared to that of CTR iPSCs. iPSCs were cultured until approximately 80% confluency at which point total cell lysate and media samples were collected. Total cell lysates were run on a western blot and immunostained for clusterin and β-actin (***Figure 6.6A***). The expected ~37kDa smeared band positive for clusterin was detected in CTR samples and was absent in A4 and D1 samples. Individual clusterin positive bands were demonstrated in both A4 and D1

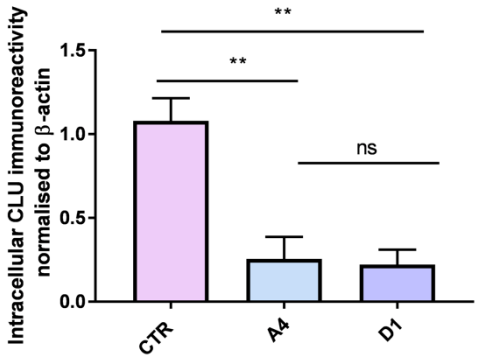
samples. An additional clusterin band was detected at ~45kDa in A4 and D1 samples that was absent in CTR samples and likely represents non-glycosylated clusterin proteins. The immunoreactivity of intracellular clusterin proteins in CTR, A4 and D1 iPSCs was quantified and normalised to β-actin (***Figure 6.6B***). Immunoreactivity of total intracellular clusterin is significantly reduced in A4 and D1 iPSCs.

Media samples were concentrated, run on a western blot and immunostained for clusterin and β-actin (***Figure 6.6C***). Secreted clusterin was detected in CTR samples but was absent in A4 and D1 samples. Overall, the data indicate intracellular clusterin abundance is significantly reduced in exon 2 -/- iPSCs than CTR iPSCs. Moreover, exon 2 -/- iPSCs do not secrete clusterin but do generate an intracellular ~45kDa clusterin species that CTR iPSCs do not.

A)



B)



C)

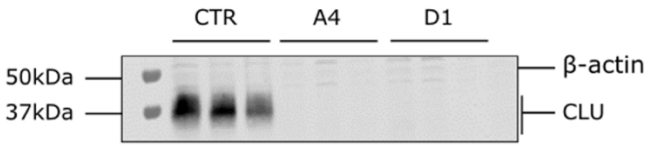


Figure 6.6. Intracellular clusterin abundance is significantly reduced in exon 2 -/- iPSCs. Exon 2 -/- iPSCs do not secrete clusterin proteins.

Total cell lysates and media samples were collected from CTR, A4 and D1 iPSCs and then run on separate western blots. ***A****) Total cell lysate samples were immunostained for intracellular clusterin and β-actin. Immunoreactivity of glycosylated, intracellular clusterin was confirmed in CTR samples (~37kDa), while immunoreactivity of a ~45kDa clusterin species was detected in exon 2 -/- iPSCs and absent in CTR iPSC samples.* ***B****) Immunoreactivity of intracellular clusterin was significantly reduced in exon 2 -/- iPSCs (average reductions: 79.0 ± 11.1% and 80.0 ± 5.8% in A4 and D1 iPSCs respectively). Immunoreactivity was comparable between A4 and D1 iPSCs (p=0.9794).* ***C****) Immunoreactivity of secreted clusterin protein was confirmed in CTR iPSCs but was absent in A4 and D1 samples. Data are shown as mean ± SEM, n = 3 (n = independent experiments, each with 3 replicate wells). Significance was tested using One-way ANOVA with Tukey's multiple comparison analysis. P<0.05*. ANOVA p = 0.0037**, CTR vs. A4: p =0.0068**, CTR vs D1: p=0.0056** and A4 vs D1: p=0.9794.*

6.2.4 Clusterin trafficking is altered in exon 2 -/- iPSCs

Intracellular clusterin was detected in samples obtained from CTR, A4 and D1 iPSCs but clusterin positive bands demonstrated in A4 and D1 samples appeared visually different to those demonstrated in CTR samples (***Figure 6.6A***). To determine if this is due to altered trafficking and glycosylation of clusterin, total cell lysates were treated with PNGase F to remove N-linked glycosylation from glycoproteins. To directly compare molecular weights of clusterin isoforms in all samples, untreated and PNGase F treated samples were run alongside each other on the same western blot and immunostained for clusterin (***Figure 6.7***).

Intracellular clusterin from PNGase F treated CTR samples resolved to two distinct bands of ~30kDa and ~25kDa weight representing the β chain and the α chain respectively, this agrees with data provided in chapter 4 (***See Chapter 4, figure 4.8***). Surprisingly, the several clusterin positive bands ~37kDa in A4 and D1 samples resolved to a single band of ~30kDa while the ~25kDa band was absent in these same samples. This indicates clusterin trafficking and translation is altered in exon 2 -/- iPSCs. The ~45kDa band was detected in untreated samples resolved to the same weight in PNGase F treated samples, indicating this clusterin species is non-glycosylates since PNGase F treatment did not alter the weight of this band/protein.

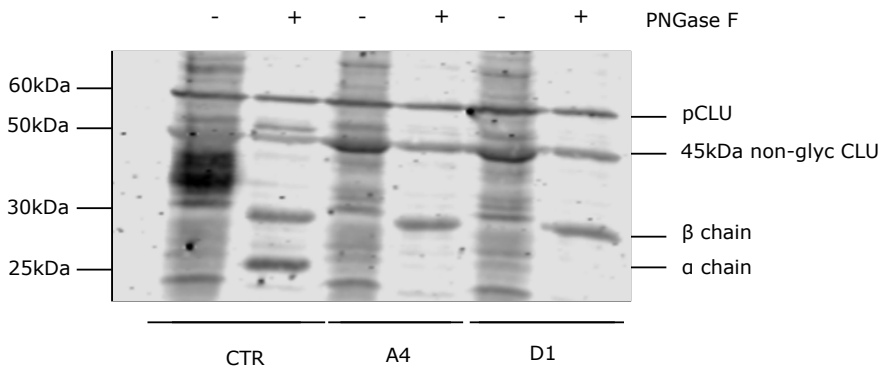


Figure 6.7. Trafficking of intracellular clusterin is altered in exon 2 -/- iPSCs.

Total cell lysate samples were collected from CTR, A4 and D1 cells and treated with PNGase F to remove glycosylation from glycoproteins. Total cell lysates and PNGase F treated samples were run alongside each other to directly compare molecular weights of clusterin proteins on a western blot. The ~37kDa intracellular clusterin in CTR samples resolved to two bands of ~30kDa and ~25kDa after PNGase F treatment. These bands represent the β chain and the α chain of mature, glycosylated, and cleaved clusterin. A single band (~30kDa) was detected in PNGase F treated samples from A4 and D1 iPSCs. The ~25kDa band was absent in samples obtained from exon 2 -/- iPSCs, indicating altered clusterin trafficking in exon 2 -/- iPSCs. In all samples a ~45kDa band was detected but was much more easily detected in exon 2 -/- samples. The weight of this clusterin species was not altered by PNGase F treatment and therefore represents non-glycosylated clusterin proteins. The position of precursor CLU (pCLU) is shown, representing the species of clusterin that has not yet undergone glycosylation or cleavage in the ER and Golgi.

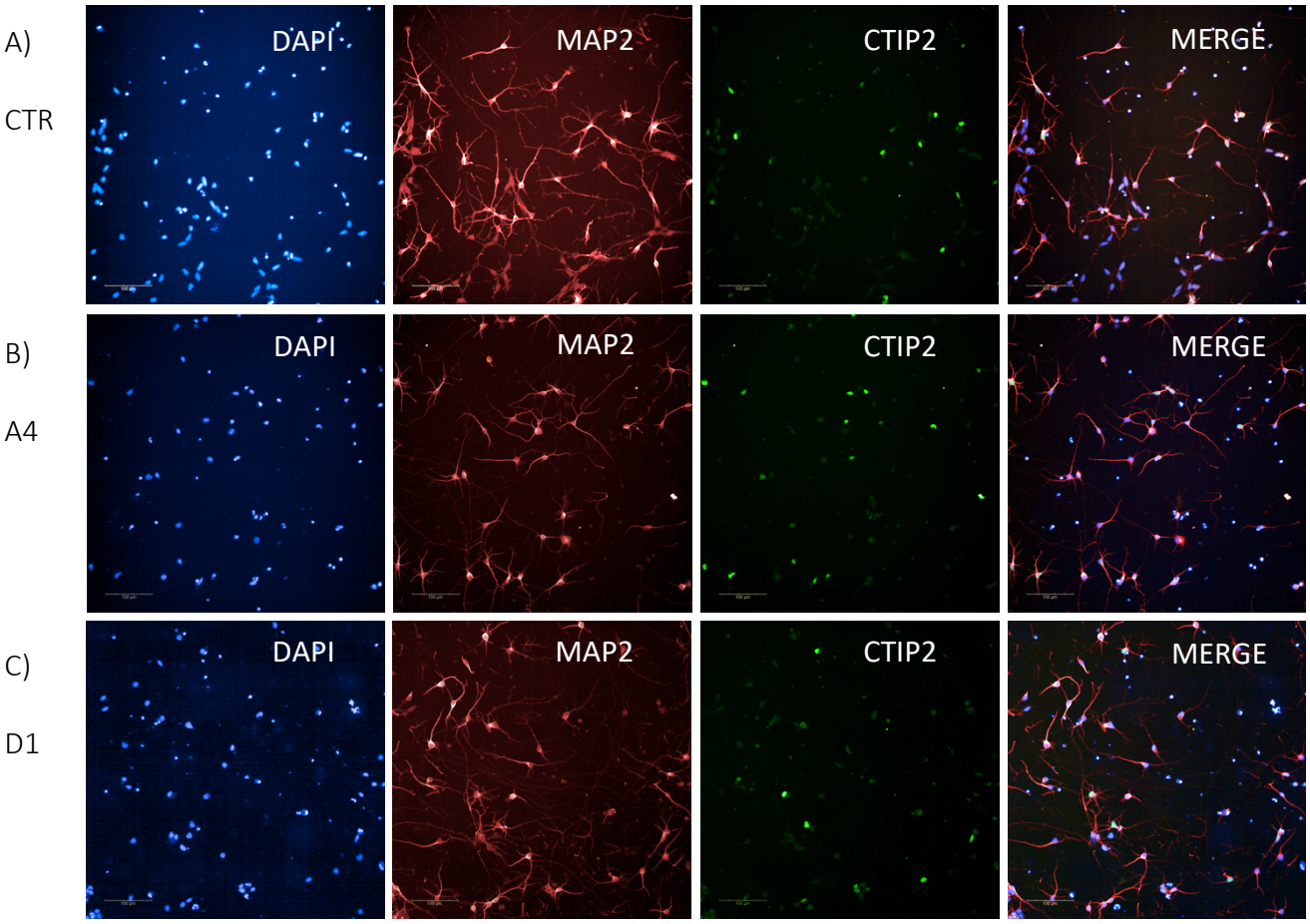
A summary of the key findings from this portion of the results section in this chapter can be found in ***table 6.2***.

Exon 2 -/- vs CTR iPSCs	
Parameter	Change
CLU variant 1	Reduced (absent)
CLU variants 2 and 3	Reduced (absent)
CLU variant 1 Δ exon 2 transcripts	Increased
Total *CLU* mRNA transcripts	Reduced
Intracellular clusterin (glycosylated)	Reduced (absent)
Intracellular clusterin (non-glycosylated)	Increased
Secreted clusterin	Reduced (absent)

Table 6.2. Key changes in exon 2 -/- iPSCs compared to CTR iPSCs.

6.2.5 Exon 2 -/- iPSC-neurons can be differentiated into neurons

The main objective of this chapter is to compare responses of CTR and exon 2 -/- iPSC-neurons to Aβ treatment. With this aim in mind, CTR, A4 and D1 iPSCs were differentiated into neurons (***See Chapter 2, 2.2.1.2***), fixed and immunostained at day 35 (***See 2.2.8.2***). Cells were imaged using an Operetta High Content Imaging System (***Figure 6.8A-C, see chapter 2, 2.2.8.3.1***). Expression of neuronal marker MAP2 was confirmed in cells and the percentage of MAP2 positive cells expressing lower layer cortical marker CTIP2 was quantified (***See 2.2.8.4.2***). Firstly, the number of MAP2 positive cells was quantified (***Figure 6.8D***). Although trends in the data indicate an increased number of MAP2 positive cells in A4 and D1 iPSC-neuron cultures, this was not significant. Next, the percentage of MAP2 positive cells that also express CTIP2 was quantified (***Figure 6.8E***). CTIP2 expression was similar between all genotypes but a negative trend of reduced CTIP2 expression was identified in exon 2 -/- iPSC-neurons, although not significant. The observed trends in the data warrant further investigation to determine if gene editing to remove *CLU* exon 2 has impacted on the differentiation of exon 2 -/- iPSCs into neurons.


A)
CTR
DAPI
MAP2
CTIP2
MERGE
B)
A4
DAPI
MAP2
CTIP2
MERGE
C)
D1
DAPI
MAP2
CTIP2
MERGE

D) E)

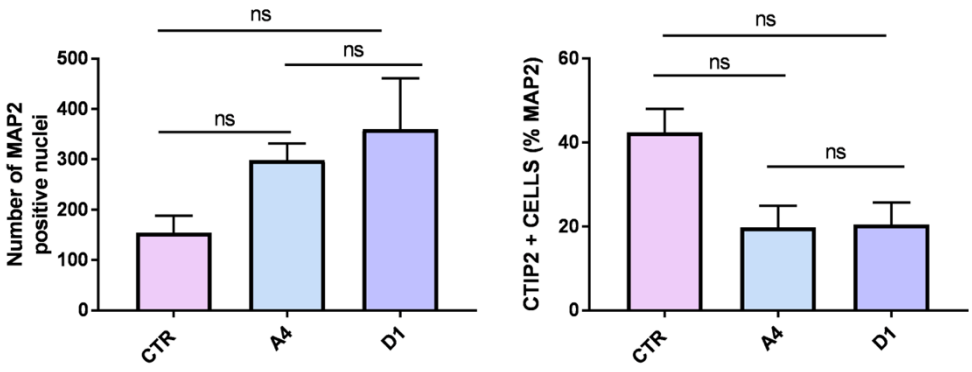


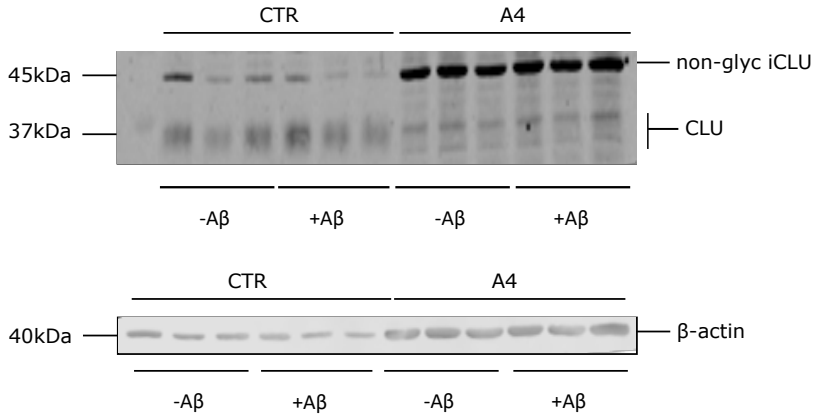
Figure 6.8. Exon 2 -/- iPSCs can be differentiated into neurons comparable to those generated from CTR iPSCs. CTR, A4 and D1 iPSCs were differentiated until day 35 when they were fixed and immunostained for DAPI, MAP2 and CTIP2. Cells were imaged at 20x magnification on an Opera Phenix Confocal Microscope and analysed using Phenix Harmony Software. ***A-C****) Representative images of day 35 cells:* ***A****) CTR,* ***B****) A4 and* ***C****) D1 iPSC-neurons; stains are DAPI (blue), MAP2 (red) and CTIP2 (green).* ***D****) The number of MAP2 positive cells was similar between all genotypes (p = 0.1474; CTR vs. A4: p = 0.3227, CTR vs D1: p=0.1396, A4 vs D1: p= 0.7873.* ***E****) The percentage of CTIP2 positive MAP2 cells was significantly influenced by iPSC-neuron genotype (p=0.0387*), however, no significant differences were identified following Tukey's multiple comparisons testing: CTR vs. A4: p =0.0699, CTR vs D1: p=0.0656 and A4 vs D1: p=0.9957. The percentage of CTIP2 positive MAP2 cells in CTR, A4 and D1 iPSC-neuron cultures was comparable (CTR: 42.5 ± 5.6%, A4: 19.8 ± 5.2% and D1: 20.5 ± 5.2%). Data are shown as mean ± SEM, n = 3 (n = independent differentiations, each with 3 replicate wells). Significance was tested using One-way ANOVA with Tukey's multiple comparison analysis. P<0.05*.*

6.2.6 $A\beta_{25-35}$ alters trafficking of glycosylated clusterin but not the expression of non-glycosylated clusterin

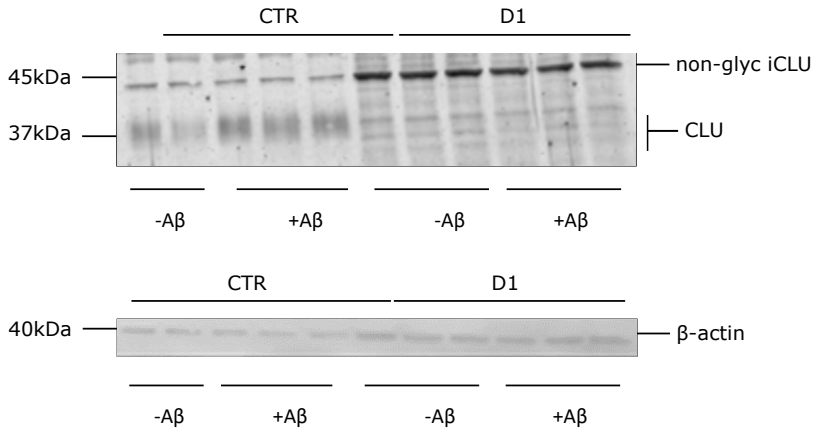
CTR, A4 and D1 iPSC-neurons were treated with 20µM $A\beta_{25-35}$ and after 24 hours, total cell lysates (***Figure 6.9***) and media (***Figure 6.10***) were collected, run on a western blot and immunostained for clusterin and β-actin. In agreement with iPSC data, intracellular clusterin (~37kDa) was detected in CTR iPSC-neuron samples but absent in A4 and D1 iPSC-neuron samples (***Figure 6.9A and B***). Expression of glycosylated clusterin species was

quantified in untreated and $A\beta_{25-35}$ treated CTR iPSC-neurons (***Figure 6.9C***) and was significantly increased following treatment. ~45kDa clusterin proteins were detected in all samples (***Figure 6.9A and B***) but expression was significantly higher in exon 2 -/- iPSC-neurons (***Figure 6.9D and E***). *S*urprisingly, $A\beta_{25-35}$ treatment did not alter the expression of this clusterin species in either CTR or exon 2 -/- iPSC-neurons (***Figure 6.9E***)

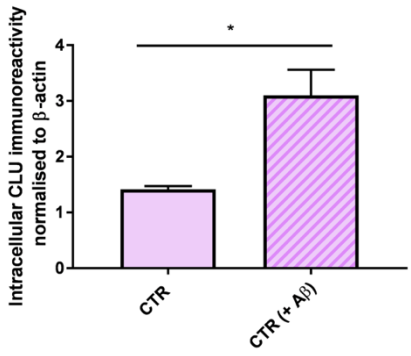
A)



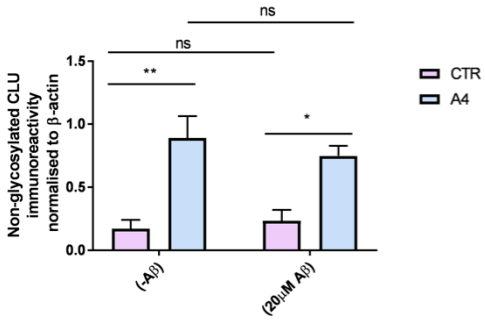
B)



C)



D)



E)

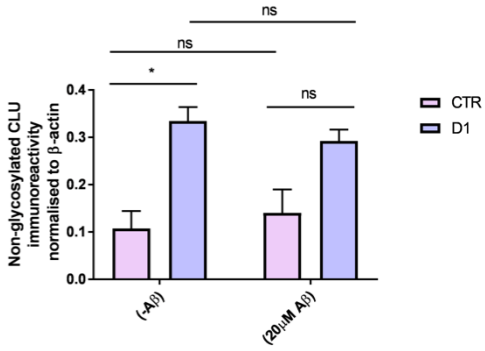


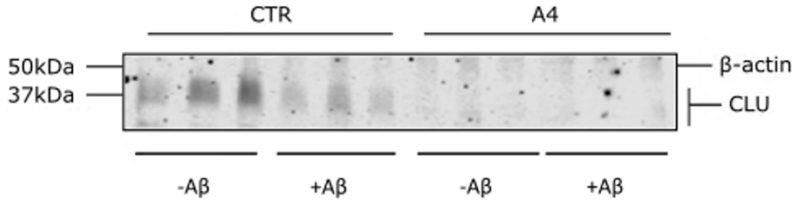
Figure 6.9. Aβ$_{25-35}$ treatment alters trafficking of glycosylated clusterin but does not alter abundance of non-glycosylated clusterin species.

CTR, A4 and D1 iPSC-neurons were treated for 24 hours with 20μM Aβ$_{25-35}$. Total cell lysates were collected, run on a western blot and immunostained for clusterin and β-actin. Western blots depict: ***A****) CTR and A4 iPSC-neuron samples and* ***B****) CTR and D1 iPSC-neuron samples. A smeared band was present at ~37kDa in all CTR samples but absent in both A4 and D1 samples. A ~45kDa clusterin species was detected in all samples.* ***C****) Immunoreactivity of glycosylated clusterin proteins was significantly increased in CTR iPSC-neurons following treatment with 20μM Aβ$_{25-35}$ (216.0 ± 36.8%, p=0.0221*).* ***D/E****) Two-way ANOVA analysis identified iPSC-neuron genotype to be significantly altering the immunoreactivity of non-glycosylated ~45kDa clusterin proteins (****D:*** *p=0.0005*** and* ***E****: p=0.0043**) but not by Aβ$_{25-35}$ treatment (****D:*** *p=0.7213 and* ***E****: p=0.9158). No significant interaction was identified between iPSC-neuron genotype and treatment condition (****D:*** *p=0.3840 and* ***E****: p=0.4122). Before treatment, non-glycosylated clusterin immunoreactivity was significantly higher in A4 (p=0.0077**) and D1 (p=0.0348*) iPSC-neurons than in CTR iPSC-neurons indicating higher abundance in*

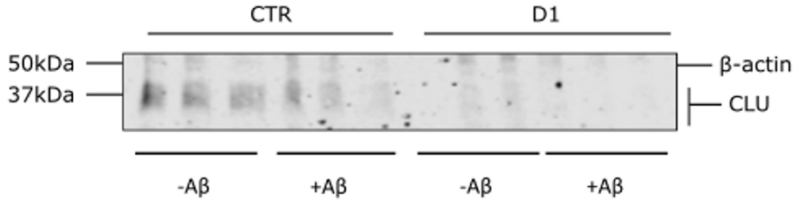
exon 2 -/- iPSC-neurons. Aβ$_{25-35}$ did not alter the immunoreactivity of non-glycosylated clusterin in iPSC-neurons of any genotype. ***D****) CTR: p=0.9785 and A4: p=0.7991.* ***E****) CTR: p=0.9255 and D1: p=0.9154. Data are shown as mean ± SEM, n= 3 (n = independent differentiations, each with 3 replicate wells). Significance p<0.05* ns = p> 0.05 using unpaired parametric t-test or two-way ANOVA analysis with Tukey's multiple comparison post hoc test.*

Next, the secretion of clusterin proteins was examined in all cells (***Figure 6.10A and B***). Secreted clusterin was detected in CTR samples and immunoreactivity was significantly decreased after 24 hours of treatment with 20µM Aβ$_{25-35}$ (***Figure 6.10C***). This agrees with previous findings in rodent neurons (Killick et al., 2014). However, secreted clusterin was not detected in samples from either A4 or D1 cells (***Figure 6.10A and B respectively***). Thus, exon 2 -/- iPSC-neurons do not secrete clusterin and this is not altered by 24-hour treatment with 20µM Aβ$_{25-35}$.

A)



B)



C)

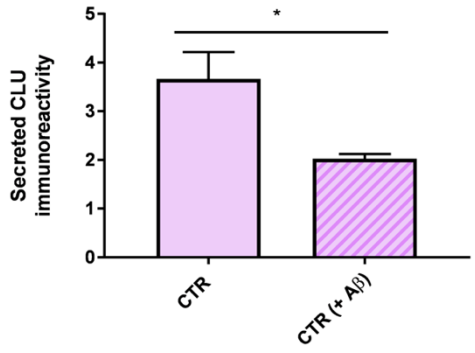


Figure 6.10. Exon 2 -/- iPSC-neurons do not secrete clusterin. Aβ$_{25-35}$ treatment reduces clusterin secretion in CTR iPSC-neurons.

CTR, A4 and D1 iPSC-neurons were treated with 20μM Aβ$_{25-35}$ for 24 hours and media samples were collected. Concentrated media were then run on a western blot and immunostained for clusterin and β-actin. ***A/B****) Secreted clusterin was detected in all CTR iPSC-neuron samples but not in samples obtained from either* ***A****) A4 or* ***B****) D1 iPSC-neurons.* ***C****) Clusterin secretion was significantly decreased in CTR iPSC-neurons following Aβ$_{25-35}$ treatment (43.1 ± 6.7%, p=0.0432*). Data are shown as mean ± SEM, n= 3 (n = independent differentiations, each with 3 replicate wells). Significance p<0.05* ns = p> 0.05 using unpaired parametric t-test.*

A summary of the key findings from this portion of the results section in this chapter can be found in ***table 6.3.***

Exon 2 -/- vs CTR iPSC-neurons	
Parameter	Change
MAP2 positive cells	No change
CTIP2 expression	No change
Intracellular clusterin (glycosylated)	Absent/altered trafficking
Intracellular clusterin (non-glycosylated)	Increased
Secreted clusterin	Reduced (absent)

Table 6.3. Key changes in exon 2 -/- iPSC-neurons compared to CTR iPSC-neurons.

6.2.7 Exon 2 -/- iPSC-neurons exhibit less cell death than CTR iPSC-neurons following treatment with $A\beta_{25-35}$

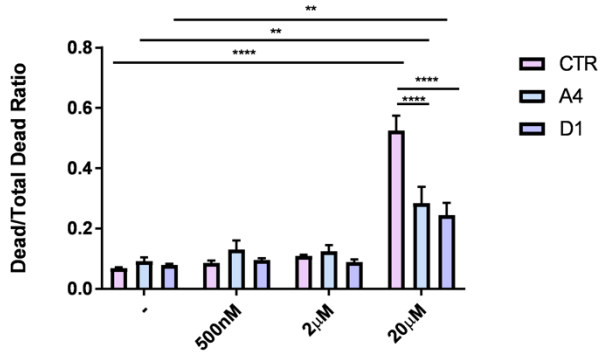
To determine if exon 2 -/- iPSC-neurons are more sensitive to Aβ induced toxicity, cell death was quantified in CTR and exon 2 -/- iPSC-neurons following treatment with either $A\beta_{25-35}$ (***Figure 6.11A***) or $A\beta_{1-42}$ (***Figure 6.11B***). iPSC-neurons were treated with one concentration of either $A\beta_{25-35}$ (500nM, 2μM or 20μM) or $A\beta_{1-42}$ (500nM or 3μM) for 24 hours, after which cell death was quantified using the CytoTox-Glo™ Cytotoxicity Assay (***See 2.2.8.1.2***). Firstly, following 24 hours of treatment, the number of dead cells in each well was quantified to give a measurement of cell death induced by $A\beta_{25-35}$ or $A\beta_{1-42}$. Following this, cell lysis and death was induced in all remaining cells and the number of total dead cells was quantified giving a measurement of the number of cells in each well. Finally, the number of dead cells and total dead cells were compared by calculating the Dead/Total Dead Ratio (***Figure 6.11***). An increase in the Dead/Total Dead Ratio reflects an increase in cell death.

Before treatment with $A\beta_{25-35}$ the Dead/Total Dead Ratios were comparable across all genotypes indicating exon 2 -/- iPSC-neurons do not display increased death before the induction of stress and cell death (***Figure 6.11A***). Next, the Dead/Total Dead Ratios were compared across all genotypes after treatment with increasing concentrations of $A\beta_{25-35}$. Treatment with either 500nM or 2μM $A\beta_{25-35}$ did not increase the Dead/Total Dead Ratios

for either CTR, A4 or D1 iPSC-neurons. Treatment with 20µM $A\beta_{25-35}$ for 24 hours increased the Dead/Total Dead Ratio in CTR, A4 and D1 iPSC-neurons confirming that 20µM $A\beta_{25-35}$ increased the number of dead cells in all iPSC-neuron cultures independent of their genotype. Interestingly, when the Dead/Total Dead Ratios of 20µM $A\beta_{25-35}$ treated CTR and 20µM $A\beta_{25-35}$ treated exon 2 -/- iPSC-neuron cultures were compared, the Dead/Total Dead Ratios were significantly higher in CTR iPSC-neuron cultures than in exon 2 -/- iPSC-neuron cultures. This indicates significantly more dead cells were present in CTR iPSC-neuron wells after treatment with 20µM $A\beta_{25-35}$ compared to the A4 and D1 iPSC-neuron wells. This suggests exon 2 -/- iPSC-neurons are less sensitive to 20µM $A\beta_{25-35}$ induced cell death.

Next, cell death was examined in the same way as above but in iPSC-neurons treated with either 500nM or 3µM $A\beta_{1-42}$ for 24 hours (***Figure 6.11B***). The Dead/Total Dead Ratios were not altered following treatment with $A\beta_{1-42}$ at any concentration tested. This was consistent in all genotypes. Therefore, 500nM or 3µM $A\beta_{1-42}$ are not sufficient to induce significant cell death in either CTR or exon 2 -/- iPSC-neurons after 24 hours.

A)



B)

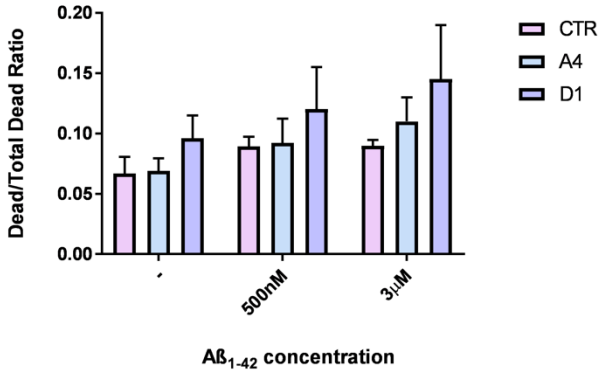


Figure 6.11. 20μM Aβ$_{25-35}$ treatment induces cell death of human iPSC-neurons. Exon 2 -/- iPSC-neurons display less death than CTR iPSC-neurons.

*CTR, A4 and D1 iPSC-neurons were treated for 24 hours with either **A**) Aβ$_{25-35}$ (500nm, 2μM or 20μM) or **B**) Aβ$_{1-42}$ (500nm or 3μM). Following treatment, the number of dead and total dead cells in each condition was quantified and the Dead/Total Dead Ratio calculated for each condition. The total dead count represents the total number of cells in each well. **A**) Two-way ANOVA analysis demonstrated that both iPSC-neuron genotype (p=0.0044**) and treatment condition (p<0.0001****) significantly influenced the Dead/Total Dead Ratios. Additionally, a significant interaction between iPSC-neuron genotype and treatment condition was identified (p<0.0001****). Cell death was not induced after treatment with 500nM and 2μM Aβ$_{25-35}$ since Dead/Total Dead Ratios were comparable to that of untreated cells, this was consistent across all iPSC-neuron genotypes. Death was induced following treatment with 20μM Aβ$_{25-35}$ given the significantly increased Dead/Total Dead Ratio. This was observed in CTR (p<0.0001****), A4 (p=0.0200*) and D1 (p=0.0254*) iPSC-neuron cultures. Prior to treatment, cell death was comparable in CTR, A4 and D1 iPSC-neuron cultures since no significant differences were identified between Dead/Total Dead Ratios in any of these conditions (p>0.9999). After treatment with 20μM Aβ$_{25-35}$, the Dead/Total Dead Ratios of CTR iPSC-neuron cultures were significantly*

*higher than the Dead/Total Dead Ratios of exon 2 -/- iPSC-neurons (p<0.0001****) indicating more cell death was induced by Aβ$_{25-35}$ in CTR iPSC-neuron cultures.* ***B****) Two-way ANOVA analysis determined that neither iPSC-neuron genotype (p=0.1256) nor treatment condition (p=0.1572) influenced cell death in iPSC-neurons following treatment with 500nM or 3μM Aβ$_{1-42}$ for 24 hours. Additionally, no interaction between genotype and treatment condition was demonstrated (p=0.9793). Aβ$_{1-42}$ did not induce significant amounts of cell death in iPSC-neuron cultures. Data are shown as mean ± SEM, n = 3 (n = independent differentiations, each with 6 replicate wells). Significance was tested using two-way ANOVA with Tukey's multiple comparison analysis. P<0.05**

6.2.8 Exon 2 -/- iPSC-neurons do not display neurite damage following Aβ$_{25-35}$ treatment

Having demonstrated that cell death was induced in both CTR and exon 2 -/- iPSC-neurons after treatment with 20μM Aβ$_{25-35}$, although to a different degree, the effect of Aβ$_{25-35}$ and Aβ$_{1-42}$ on neurite length was next examined. CTR, A4 and D1 iPSC-neurons were treated as above with Aβ$_{25-35}$ or Aβ$_{1-42}$ for 24 hours and were then fixed and immunostained for MAP2 (***See Chapter 2, 2.2.8.2***). Cells were imaged on an Operetta Phenix Confocal Microscope (***Figures 6.12A-C, See Chapter 2, 2.2.8.3.2***). MAP2 was used to confirm neuronal identity and for quantification of changes in neurite length (***See Chapter 2, 2.2.8.4.3***). To first determine if densities of the cell cultures were comparable across the different genotypes, the number of nuclei were compared (***Figure 6.12D***). Neither Aβ$_{25-35}$ nor iPSC-neuron genotype altered the number of nuclei in any condition tested.

Next, several parameters of neurite morphology were measured. Mean neurite length was significantly reduced in untreated exon 2 -/- iPSC-neurons than untreated CTR iPSC-neurons (***Figure 6.12E***)**.** Similarly, maximum neurite segment length was significantly reduced in exon 2 -/- iPSC-neurons before treatment with Aβ$_{25-35}$ compared to untreated CTR iPSC-neurons (***Figure 6.12F***). These data indicate that neurite outgrowth of exon 2 -/-

iPSC-neurons is reduced in untreated conditions, arising because of *CLU* exon 2 gene editing.

Treatment of iPSC-neurons with 20μM $A\beta_{25-35}$ generated the most consistent effects, causing a significant reduction of mean neurite length (***Figure 6.12E***), maximum length of neurite segments (***Figure 6.12F***) and mean segment length to cells (***Figure 6.12G***). These reductions in neurite length were demonstrated in CTR iPSC-neurons but not exon 2 -/- iPSC-neurons. The data indicate that exon 2 -/- iPSC-neurons are protected against neurite damage induced by $A\beta_{25-35}$. Neither 500nM nor 2μM $A\beta_{25-35}$ induced a shortening of neurite length in either CTR or exon 2 -/- iPSC-neurons, except in the case of mean segment length, which was reduced by treatment with 2μM $A\beta_{25-35}$ in CTR iPSC-neurons.

The data suggest that as well as inducing cell death, 20μM $A\beta_{25-35}$ treatment for 24 hours is sufficient to induce significant shortening of neurite processes. CTR iPSC-neurons respond to $A\beta_{25-35}$ by retracting their processes, but this response is absent in exon 2 -/- iPSC-neurons suggesting that exon 2 -/- iPSC-neurons cells are protected against $A\beta_{25-35}$ induced neurite damage.

Next, the effect of treatment with either 500nM or 3μM $A\beta_{1-42}$ on neurite length was examined (***Figures 6.13A-C***). As with $A\beta_{25-35,}$ there was no significant difference in the number of nuclei in untreated CTR, A4 or D1 iPSC-neurons (***Figure 6.13D***) but mean segment length (***Figure 6.13E***) and maximum length of segments were both significantly reduced in exon 2 -/- iPSC-neurons before treatment compared to CTR iPSC-neurons (***Figure 6.13F***). Additionally, the mean segment length to cells was significantly reduced in untreated D1 iPSC-neurons compared to untreated CTR iPSC-neurons but this did not reach significance in A4 iPSC-neurons (***Figure 6.13G***).

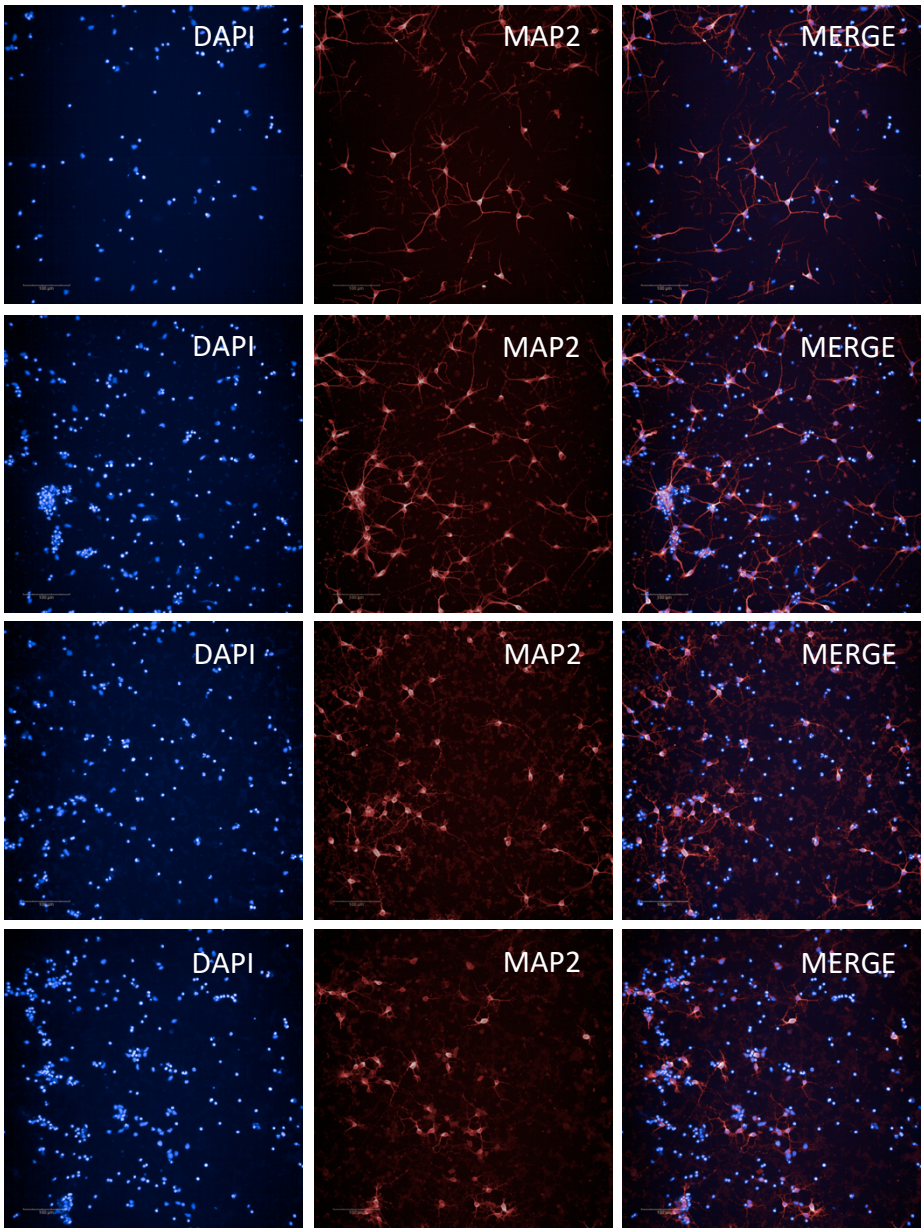
Although differences in neurite length were significantly affected by genotype, no significant effect of $A\beta_{1-42}$ treatment was seen in either CTR or exon 2 -/- iPSC-neurons for any of the parameters measured. The absence of effect may indicate that at the concentrations of $A\beta_{1-42}$ used are not sufficient to induce significant neurite damage in a 24-hour period, and thus, longer incubation times with $A\beta_{1-42}$ are required. Indeed, upon examination of the graphs several trends can be observed indicating 3µM $A\beta_{1-42}$ may reduce neurite length in iPSC-neurons, but this did not reach significance (***Figures 6.13E-G***).

A summary of the key findings from this portion of the results section in this chapter can be found in ***table 6.4***.

20µM $A\beta_{25-35}$ treated vs untreated iPSC-neurons		
Parameter	CTR	Exon 2 -/-
Intracellular clusterin (glycosylated)	Increased	No change (absent)
Intracellular clusterin (non-glycosylated)	No change	No change
Secreted clusterin	Reduced	No change (absent)
Cell death	Increased	Increased
Neurite length	Reduced	No change

Table 6.4. Key changes in CTR and exon 2 -/- iPSC-neurons in response to 20µM $A\beta_{25-35}$ treatment.

A)



-$A\beta_{25-35}$

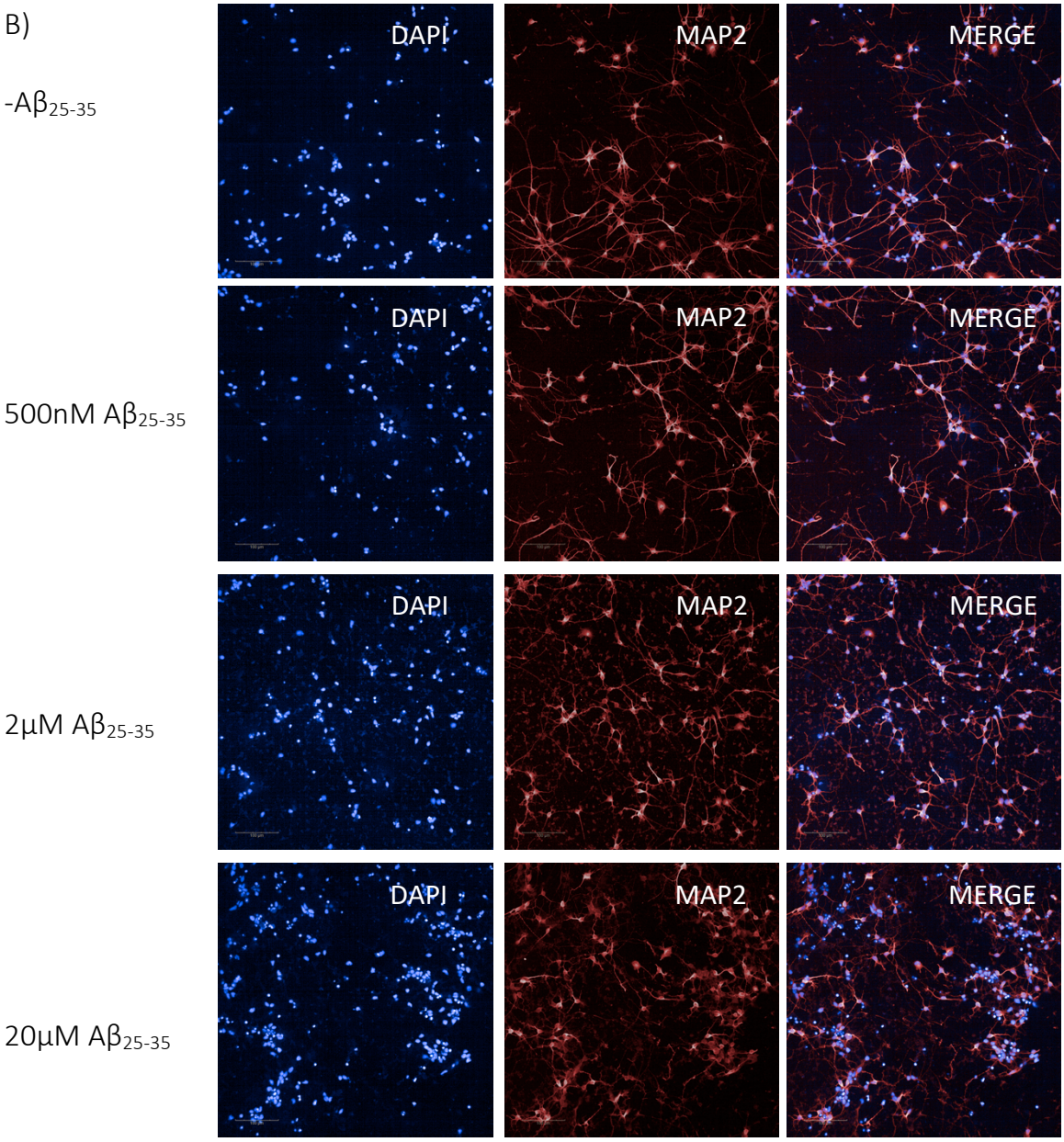
500nM $A\beta_{25-35}$

2µM $A\beta_{25-35}$

20µM $A\beta_{25-35}$

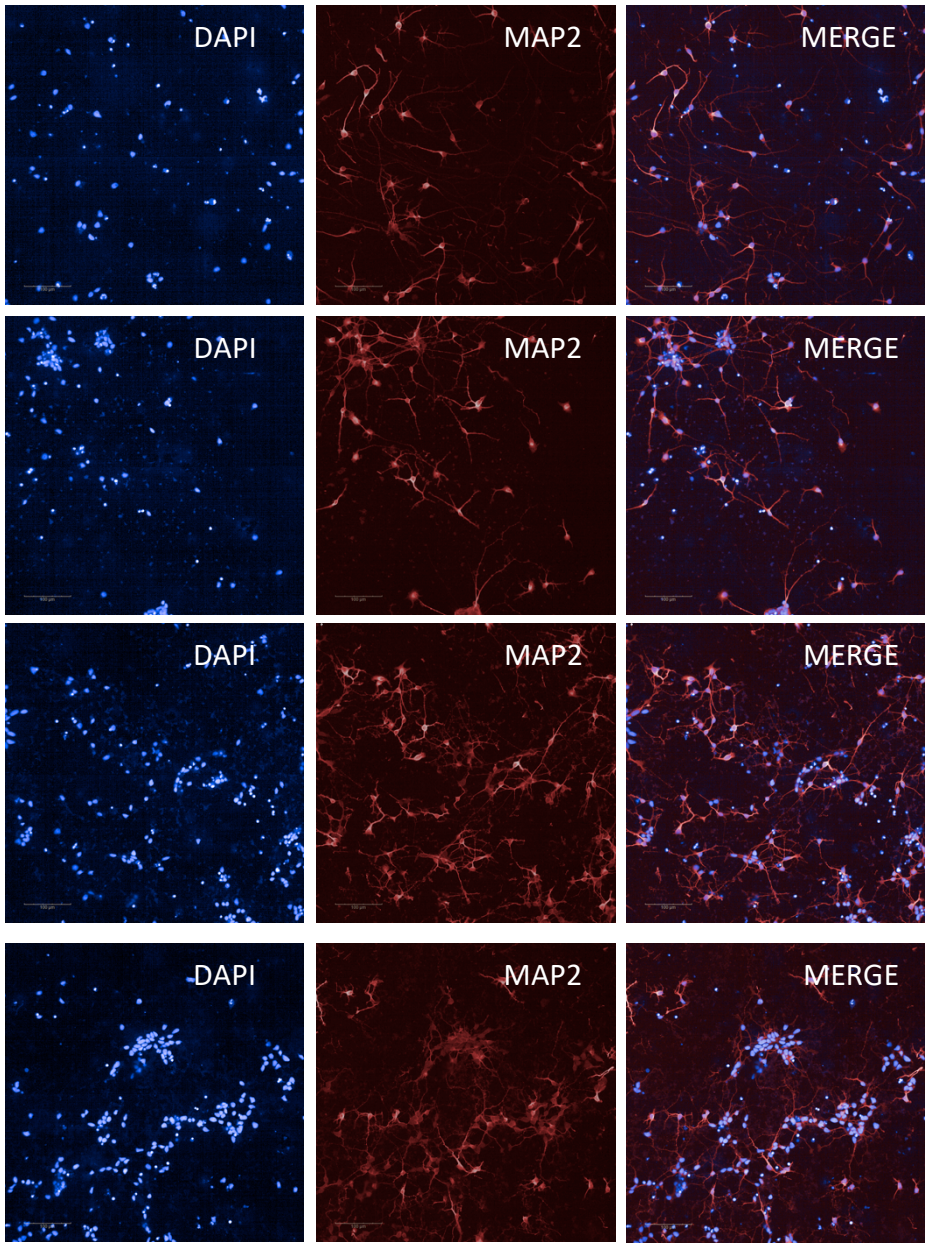
CTR iPSC-neurons

B)



A4 iPSC-neurons

C)



D1 iPSC-neurons

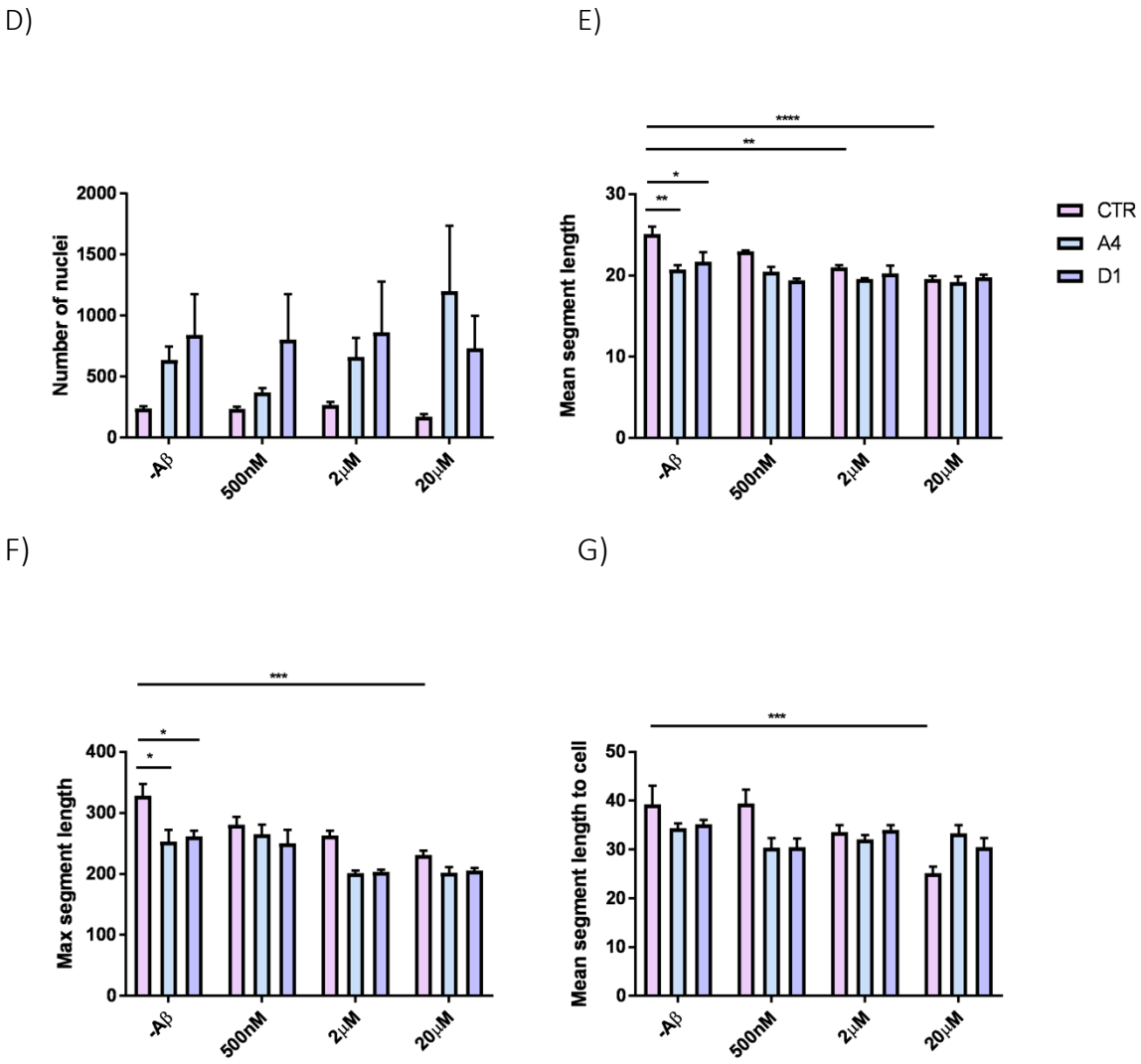
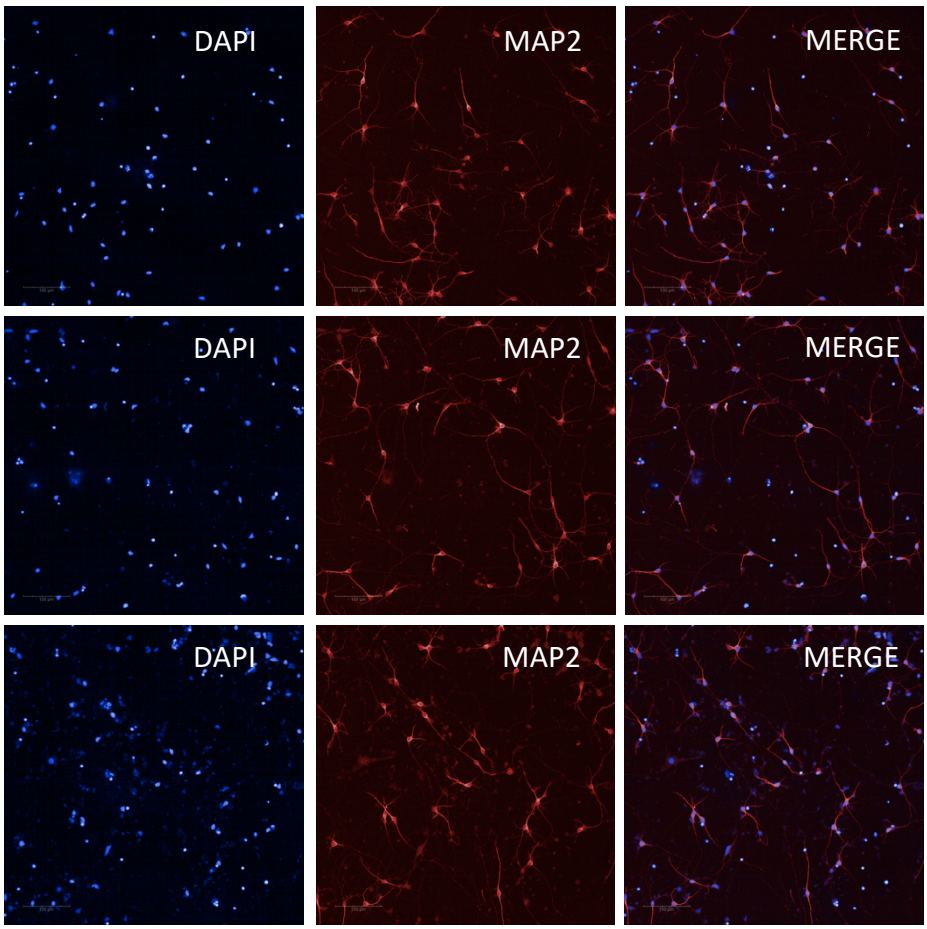


Figure 6.12. Exon 2 -/- iPSC-neurons are protected against neurite damage induced by 20μM Aβ$_{25-35}$ treatment.

*CTR, A4 and D1 iPSC-neurons were treated with 500nM, 2μM or 20μM Aβ$_{25-35}$ for 24 hours, cells were then fixed, immunostained and imaged. **A-C**) Images were taken at 20x magnification on an Opera Phenix Confocal Microscope and analysed using Phenix Harmony Software. Representative images of day 36 neurons: (**A**) CTR, (**B**) A4 and (**C**) D1 iPSC-neurons. Stains are DAPI (blue) and MAP2 (red). **D**) Two-way ANOVA analysis demonstrated iPSC-neuron genotype (p= 0.0092**) but not treatment condition (p=0.7556) influenced the number of nuclei. No significant interaction was demonstrated between treatment condition and iPSC-neuron genotype (p=0.6293). Following post hoc analysis, no significant differences in the number of nuclei was identified between any groups; number of nuclei was comparable between all groups. **E**) Two-way ANOVA analysis demonstrated both iPSC-neuron genotype (p=0.0001***) and treatment condition (p<0.0001****) significantly influenced mean segment length of iPSC-neurons. Additionally, a significant interaction between*

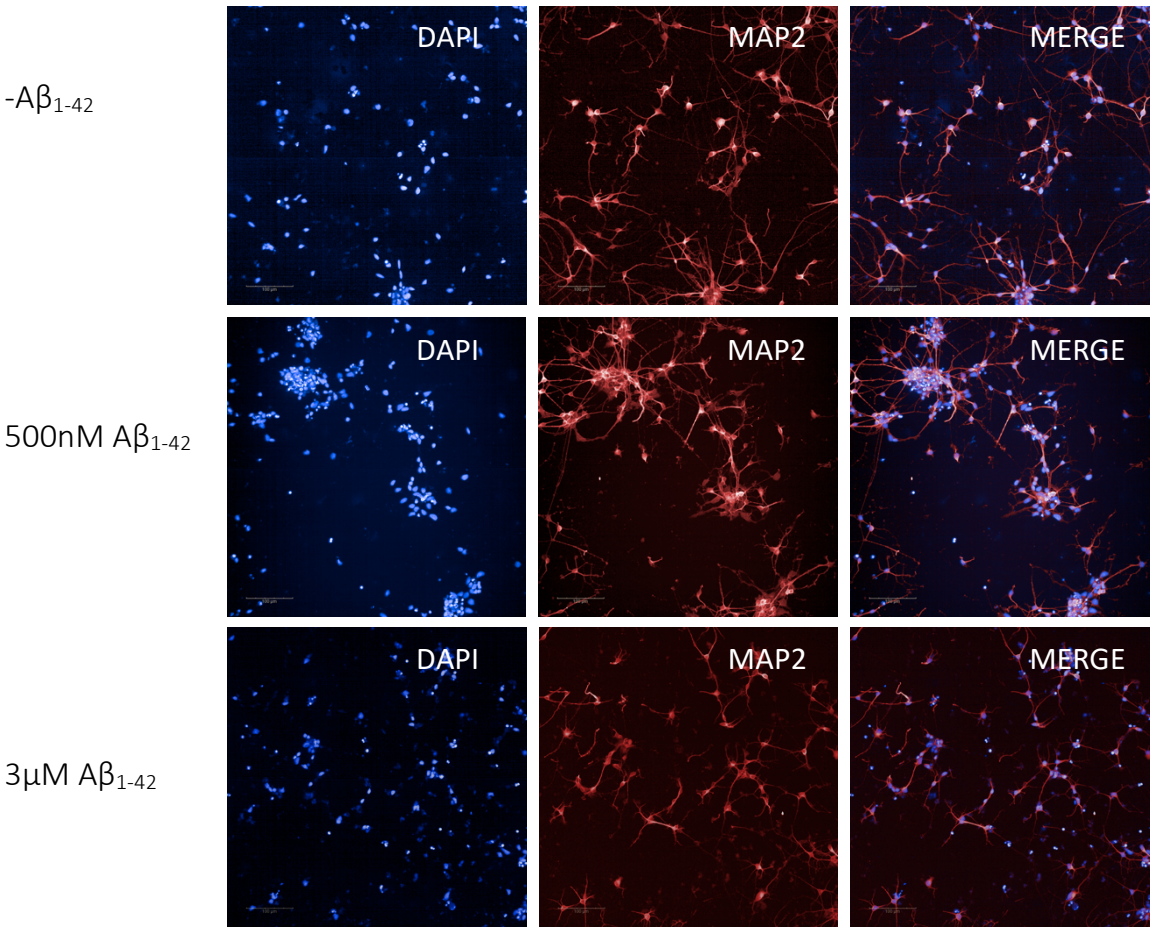
iPSC-neuron genotype and treatment condition was identified (p=0.0268). A4 and D1 iPSC-neurons have significantly reduced mean segment length compared to CTR iPSC-neurons prior to treatment with Aβ$_{25-35}$ (CTR vs A4: p=0.0310** and CTR vs D1: p=0.0379*). After treatment with 2μM (p=0.0066**) and 20μM (p<0.0001****) Aβ$_{25-35}$ mean segment length of CTR iPSC-neurons was significantly reduced. This was absent in A4 and D1 iPSC-neurons.* ***F****) Two-way ANOVA analysis demonstrated both iPSC-neuron genotype (p<0.0001***) and treatment condition (p<0.0001***) significantly influenced the maximum length of neurite segments in iPSC-neurons. However, no significant interaction between treatment condition and iPSC-neuron genotype was identified (p=0.2991). Maximum neurite length was significantly reduced in both A4 and D1 iPSC-neurons prior to treatment (CTR vs A4: p=0.0161* and CTR vs D1: p=0.0487*). Maximum length of neurite segments was significantly reduced in CTR iPSC-neurons after treatment with 20μM Aβ$_{25-35}$ (p=0.0009***), this effect was absent at lower doses and in A4 and D1 iPSC-neuron cultures at any concentration.* ***G****) Two-way ANOVA analysis demonstrated treatment condition (p=0.0029**) but not iPSC-neuron genotype (p=0.3122) significantly influenced the mean segment length to cells of iPSC-neurons. A significant interaction between iPSC-neuron genotype and treatment condition was identified (p=0.0038**). Mean segment length to cell was significantly reduced in CTR iPSC-neurons after treatment with 20μM Aβ$_{25-35}$ (p=0.0010***). This effect was absent at lower doses of Aβ$_{25-35}$ and was also absent in both A4 and D1 iPSC-neuron cultures. Data are shown as mean ± SEM, n = 3 (n = independent differentiations, each with 6 replicate wells). Significance was tested using two-way ANOVA with Tukey's multiple comparison analysis. P<0.05*.*

A)



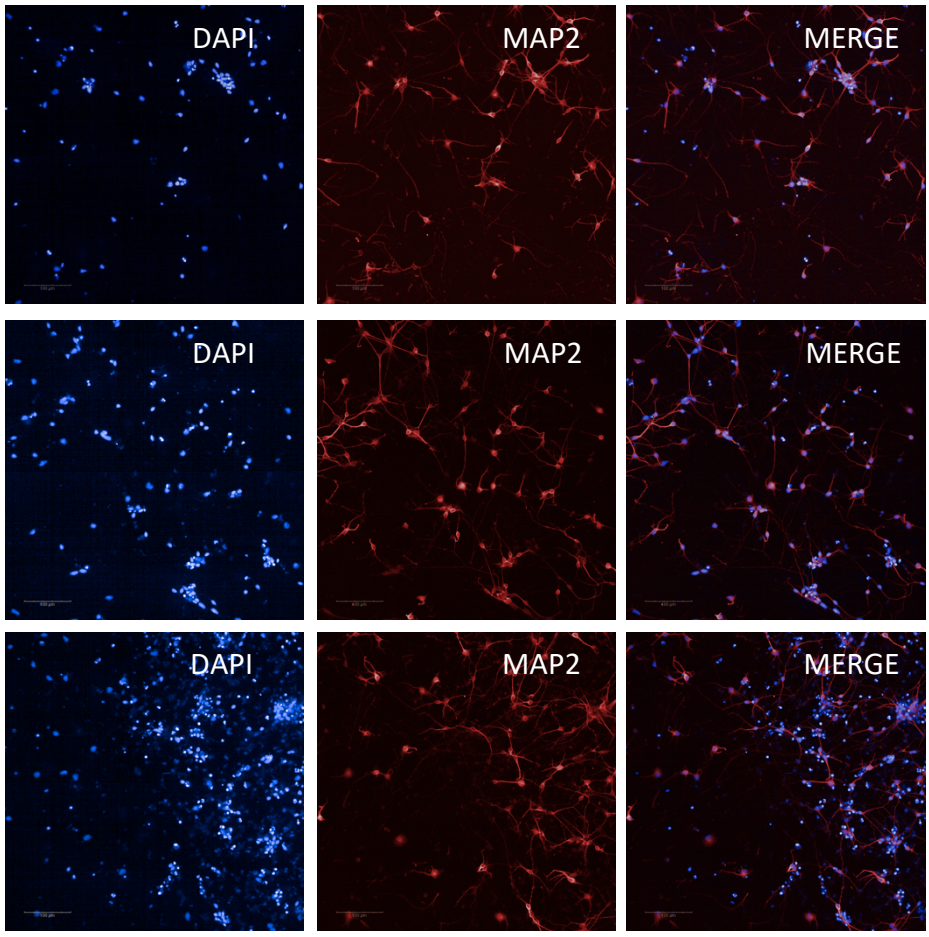
CTR iPSC-neurons

B)



A4 iPSC-neurons

C)



D1 iPSC-neurons

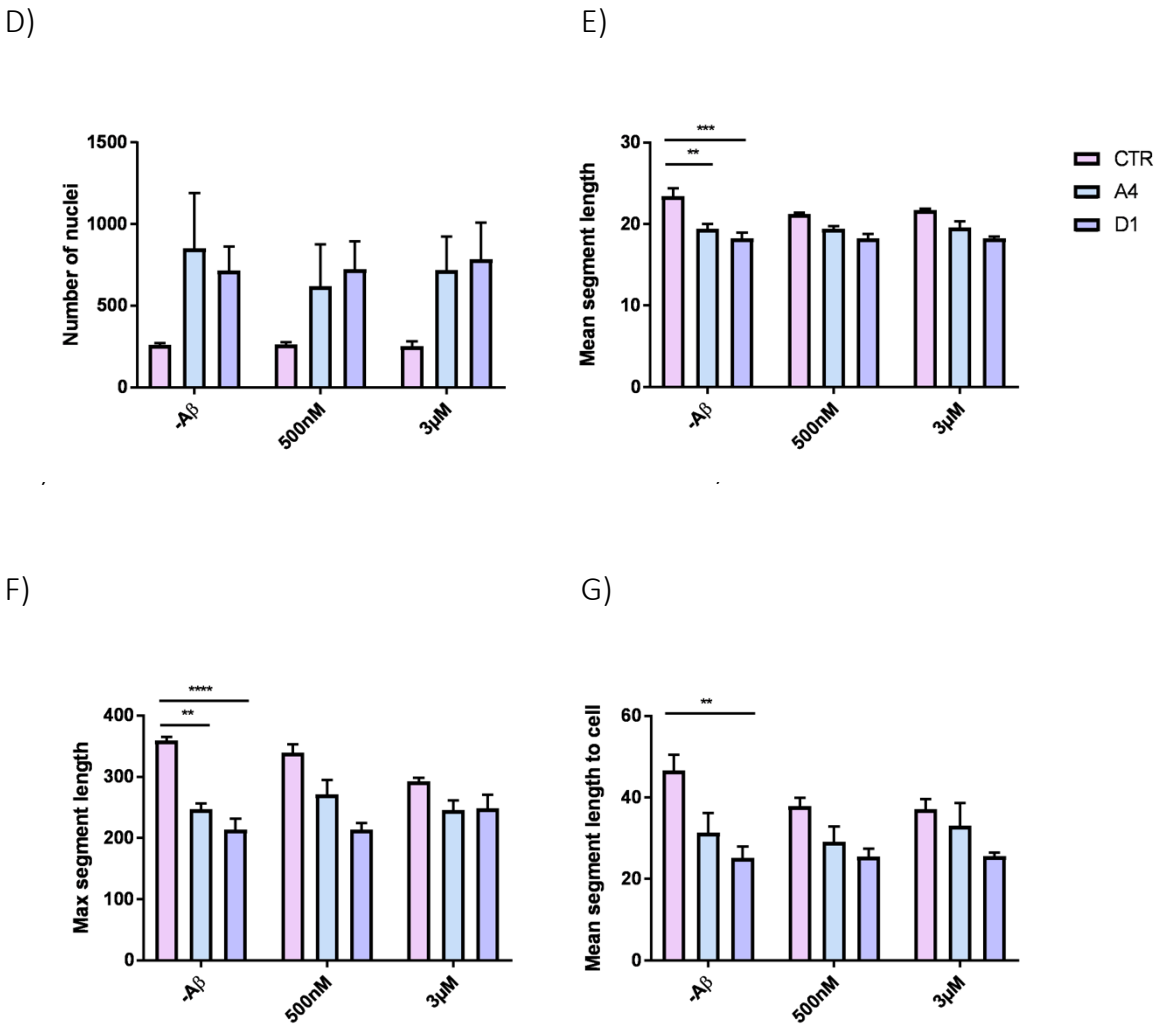


Figure 6.13. Aβ$_{1-42}$ does not induce neurite damage in human iPSC-neurons.

CTR, A4 and D1 iPSC-neurons were treated with 500nM or 3μM of Aβ$_{1-42}$ for 24 hours. Cells were then fixed, immunostained and imaged. ***A-C****) Images were taken at 20x magnification on an Opera Phenix Confocal Microscope and analysed using Phenix Harmony Software. Representative images of day 36 neurons: (****A****) CTR, (****B****) A4 and (****C****) D1 iPSC-neurons. Stains are DAPI (blue) and MAP2 (red).* ***D****) Two-way ANOVA analysis demonstrated the number of nuclei was significantly influenced by iPSC-neuron genotype (p=0.0086**) but not treatment condition (p=0.8894), no significant interaction was identified between iPSC-neuron genotype and treatment condition (p=0.9626). Following post hoc analysis, the number of nuclei was determined to be comparable across all groups.* ***E****) Two-way ANOVA analysis demonstrated iPSC-neuron genotype (p<0.0001****) but not treatment condition (p=0.3099) influenced mean segment length of iPSC-neurons. No significant interaction between treatment condition and iPSC-neuron genotype was identified (p=0.2921). Mean segment length was significantly reduced in untreated A4 and D1 iPSC-neurons compared to CTR iPSC-*

*neurons (CTR vs A4: p=0.0016** and CTR vs D1: p<0.0001****). However, $A\beta_{1\text{-}42}$ treatment did not alter mean segment length in either CTR or exon 2 -/- iPSC-neurons at any concentration tested.* ***F****) Two-way ANOVA analysis demonstrated that iPSC-neuron genotype (p<0.0001****) but not treatment condition (p=0.5686) significantly influenced maximum neurite length. A significant interaction was demonstrated between iPSC-neuron genotype and treatment condition (p=0.0280*). Maximum neurite length was significantly reduced in untreated A4 and D1 iPSC-neurons compared to untreated CTR iPSC-neurons (CTR vs A4: p=0.0031** and CTR vs D1: p=0.0001***).* ***G****) Two-way ANOVA analysis demonstrated that iPSC-neuron genotype (p=0.0002***) but not treatment condition (p=0.4441) significantly influenced mean segment length to cells. No significant interaction between iPSC-neuron genotype and treatment condition was identified (p=0.4646). Mean segment length to cells was significantly reduced in untreated D1 iPSC-neurons (p=0.0081**) but not in untreated A4 iPSC-neurons (p=0.1204). Data are shown as mean ± SEM, n = 3 (n = independent differentiations, each with 6 replicate wells). Significance was tested using two-way ANOVA with Tukey's multiple comparison analysis. P<0.05*.*

6.3 Discussion

6.3.1 Expression of *CLU* mRNA transcripts and clusterin proteins is altered in exon 2 -/- iPSCs

Exon 2 -/- iPSCs express *CLU* variant 1 Δ exon 2 transcripts, but no other *CLU* mRNA variants. This is not surprising, since A4 and D1 iPSCs do not express exon 2, and *CLU* variants 1, 2 and 3 all contain exon 2 and primers detecting these transcripts flank the exon 1/2 boundary (Prochnow et al., 2013). The increased expression of *CLU* variant 1 Δ exon 2 transcripts in exon 2 -/- iPSCs resulted in an overall reduction in both *CLU* mRNA expression and protein abundance in exon 2 -/- iPSCs. These data suggest that transcription of the *CLU* variant 1 Δ exon 2 variant is less efficient than other *CLU* variants. Alternatively, *CLU* variant 1 Δ exon 2 transcripts may be less stable and subject to increased degradation, resulting in a reduction in their expression in iPSCs.

Point mutations of the start codon in exon 2 previously did not completely prevent clusterin secretion (Prochnow et al., 2013). In comparison, secreted clusterin was absent in exon 2 -/- iPSCs following excision of exon 2 from both alleles of *CLU,* thereby demonstrating that exon 2 is required for the generation of cleaved and glycosylated clusterin proteins and for their secretion. Cells were still able to generate intracellular clusterin proteins, but these differed to those expressed by CTR iPSCs indicating altered trafficking and translation of clusterin following the loss of the ER signal peptide. This is supported by the loss of the 25kDa clusterin band, which usually represents clusterin α chain, in exon 2 -/- iPSC samples following treatment with PNGase F. The absence of the 25kDa band suggests altered translation of clusterin in exon 2 -/- cells that has resulted in the absence of a cleavage event that would normally generate the β and α chains. The identity and localisation of the 30kDa clusterin species in exon 2 -/- PNGase F treated samples warrants further investigation.

In chapter 4, non-glycosylated clusterin expression was confirmed in the cytoplasm of both CTR and exon 2 +/- iPSCs (***See chapter 4, figure 4.9***), however, abundance of this species was similar in both cell lines. Excision of exon 2 from both *CLU* alleles in exon 2 -/- iPSCs resulted in translation of non-glycosylated clusterin proteins identified in total cell lysates of both exon 2 -/- iPSCs and iPSC-neurons. Indeed, the 45kDa clusterin proteins identified in exon 2 -/- iPSCs were absent in CTR iPSCs and abundance was significantly higher in exon 2 -/- iPSC-neurons than in CTR iPSC-neurons. These data together demonstrate that the removal of *CLU* exon 2 from both alleles is required to generate increased expression of these clusterin species.

6.3.2 Generating and characterisation of exon 2 -/- iPSC-neurons

The differentiation of exon 2 -/- iPSCs according to the King's College protocol mimics the differentiation of CTR iPSCs, generating MAP2 positive neurons of which a subpopulation is CTIP2 positive. The observed trends of increased MAP2 positive cells and reduced CTIP2 expression in exon 2 -/- cultures may warrant further investigation. *CLU* exon 2 gene editing did not impact on the ability of iPSCs to generate neurons. Therefore, an iPSC-neuron model of altered clusterin trafficking was successfully generated in this chapter.

6.3.3 $A\beta_{25-35}$ treatment alters trafficking of glycosylated clusterin but does not alter abundance of non-glycosylated clusterin species

A number of factors have been shown to alter clusterin protein trafficking in cells, including *CLU* mutations (Bettens et al., 2015; Zhou et al., 2014) and $A\beta_{25-35}$ (Killick et al., 2014). $A\beta_{25-35}$ altered clusterin trafficking in CTR iPSC-neurons resulting in reduced secretion and increased retention of intracellular clusterin. This resembles the observed altered trafficking previously demonstrated in rodent neurons (Killick et al., 2014), highlighting a conserved response in rodent and human neurons in response to $A\beta_{25-35}$

induced toxicity. Previously, studies have identified an increased expression of non-glycosylated, intracellular clusterin species following stress and cell death (Prochnow et al., 2013). However, $A\beta_{25-35}$ did not alter the expression of non-glycosylated clusterin species in either CTR or exon 2 -/- iPSC-neurons. Thus, $A\beta_{25-35}$ had a specific effect on abundance of glycosylated but not non-glycosylated clusterin species. This provides further support for a role of altered clusterin trafficking in mediating $A\beta_{25-35}$ induced toxicity rather than altered *CLU* transcription.

6.3.4 Exon 2 -/- iPSC-neurons are partially protected from $A\beta_{25-35}$ induced toxicity

$A\beta_{25-35}$ induced toxicity was demonstrated in CTR iPSC-neurons resulting in reduced neurite length and increased cell death. The data demonstrated differential responses in exon 2 -/- iPSC-neurons, no retraction was demonstrated and although cell death was induced this was to a lesser degree than that induced in CTR iPSC-neurons. The diminished response of exon 2 -/- iPSC-neurons to $A\beta_{25-35}$ challenge demonstrates clearly that the removal of exon 2 from both alleles of *CLU* in iPSC-neurons offers partial protection against $A\beta_{25-35}$ induced toxicity. This contrasts with the data provided in chapter 5 where comparable responses between exon 2 +/- and CTR iPSC-neurons were identified. The protection observed in exon 2 -/- iPSC-neurons is surprising given their higher expression of both *CLU* variant 1 Δ exon 2 transcripts and non-glycosylated clusterin species, both of which are believed to promote cell death in response to stress.

Typically, Aβ peptides causes damage resulting in the retraction of neurite processes prior to cell death (Behl et al., 1994). Interestingly, although exon 2 -/- iPSC-neurons demonstrated cell death they did not demonstrate evidence of neurite damage. This suggests that although some exon 2 -/- iPSC-neurons will die because of $A\beta_{25-35}$ toxicity, cells that do not die do not exhibit neurite damage. However, it cannot be

known for certain that neurite retraction was not exhibited in cells prior to their death in exon 2 -/- iPSC-neuron cultures.

Secreted clusterin binds to Aβ peptides and may mediate the internalisation and clearance of Aβ following binding to cell surface receptors (Bartl et al., 2001; Bell et al., 2007; Ghiso et al., 1993; Nuutinen et al., 2007). This may explain the increased intracellular retention of clusterin observed after treatment of neurons with $A\beta_{25-35}$. The data provided in this chapter would suggest that uptake of clusterin-Aβ complexes may promote neurotoxicity, since the loss of secreted clusterin results in partial protection against $A\beta_{25-35}$ induced toxicity. However, the internalisation of clusterin-Aβ complexes and subsequent neurotoxicity cannot be the only mechanism leading to cell death since death is still observed in exon 2 -/- iPSC-neurons even if it is to a lesser extent.

Treatment of iPSC-neurons with $A\beta_{1-42}$ failed to induce cell death or neurite retraction in either CTR or exon 2 -/- iPSC-neurons. However, trends in the data suggest 3μM $A\beta_{1-42}$ treatment increased cell death and reduced the length of neurite processes in CTR iPSC-neurons but not in exon 2 -/- iPSC-neurons. Although it cannot be concluded and further work is required, this would suggest that exon 2 -/- iPSC-neurons may also show protection against $A\beta_{1-42}$ induced toxicity. Previously, significant cell death was induced after incubation of cells with 2.5-5μM $A\beta_{1-42}$ after 48 hours (X Xu et al., 2013). Therefore, future work should increase the incubation time of iPSC-neurons with $A\beta_{1-42}$ to 48 hours.

The data in this chapter indicate that the increased expression of *CLU* variant 1 Δ exon 2 transcripts in human iPSCs and iPSC-neurons results in the generation of non-glycosylated clusterin proteins. The expression of these clusterin species was not altered by $A\beta_{25-35}$ treatment whereas glycosylated clusterin trafficking was altered significantly. Furthermore, the loss of glycosylated clusterin in exon 2 -/- iPSC-neurons appears to

provide partial protection against $A\beta_{25-35}$ induced toxicity highlighting a toxic role of these proteins in mediating $A\beta_{25-35}$ induced neuron damage and cell death. The data also provides support for the role of altered clusterin trafficking in mediating neuronal response to $A\beta_{25-35}$ while questioning the role of non-glycosylated clusterin in mediating neuronal response to stress and damage induced by $A\beta_{25-35}$ toxicity.

7 Discussion

7.1.1 Overview

Clusterin has long been implicated in neurodegeneration and AD, however, it remains unclear whether clusterin has a protective or toxic role. Clusterin trafficking is altered by a variety of stressors (Gregory et al., 2017; Killick et al., 2014; N. Li et al., 2013b; Nizard et al., 2007), but it is not clear if glycosylated clusterin species and their altered trafficking contribute to Aβ toxicity in human neurons. Furthermore, it has long been unclear how clusterin acts as both a pro-apoptotic and anti-apoptotic protein in cells. This thesis has aimed to address these questions by generating iPSCs and iPSC-neurons expressing altered clusterin species, to identify the contribution of glycosylated and non-glycosylated clusterin proteins in neuronal response to Aβ. The data demonstrated that $A\beta_{25-35}$ induces a change in expression of glycosylated clusterin species in human iPSC-neurons, and when absent, leads to a partial protection in iPSC-neurons. Therefore, demonstrating that glycosylated clusterin species contribute to both neurite damage and cell death induced by Aβ *in vitro*. In contrast, no role was identified for non-glycosylated clusterin species. In the following discussion, the implications of this work will be outlined, set against the current understanding of clusterin's role in AD, and remaining questions will be outlined. Finally, limitations and considerations of the models generated will be discussed.

7.1.2 Exon 2 is required for the generation of glycosylated clusterin species

In this thesis, CRISPR/Cas9 gene editing was used to remove *CLU* exon 2 from iPSCs. It has long been known that exon 2 contains the ER signal peptide required for the translocation of clusterin preproprotein to the ER and Golgi apparatus, where it is cleaved and glycosylated prior to secretion. While studies have demonstrated the existence of glycosylated clusterin inside of cells, little is known of their origin or function. To address

these questions clusterin mRNA and protein expression was compared between control, exon 2 +/- and exon 2 -/- cells to determine the role of *CLU* exon 2 in generating clusterin. Overall, the abundance of glycosylated clusterin species was reduced in exon 2 +/- iPSCs and was absent following homozygous exon 2 knockout confirming that exon 2 is required to generate glycosylated clusterin in human iPSCs and iPSC-neurons.

Intracellular clusterin species were confirmed to be glycosylated and reside in both the nucleus and cytoplasm of cells, indicating that not all glycosylated clusterin is secreted. The observation of glycosylated cytoplasmic clusterin is not completely surprising, since others have reported its existence, however, these studies concluded that cytoplasmic clusterin species accumulate following the premature release of clusterin from the ER/Golgi apparatus as a consequence of cellular stress (Gregory et al., 2017; N. Li et al., 2013b; Nizard et al., 2007). However, as demonstrated in iPSCs, cytoplasmic clusterin resembled secreted clusterin, in so far as both are glycosylated and cleaved, indicating that it is mature clusterin protein. Although it is not known what mechanism contributes to the intracellular accumulation of glycosylated clusterin, the data in this thesis clearly demonstrate that it is not stress dependent.

The loss of *CLU* exon 2 was predicted to result in the absence of secreted clusterin from cells. This was confirmed in exon 2 -/- iPSCs and iPSC-neurons. Interestingly, exon 2 +/- iPSCs demonstrated similar levels of secreted clusterin to control iPSCs, meanwhile intracellular retention was halved. This suggests clusterin accumulation in cells acts as a method of 'storing' clusterin and may somewhat be dependent on the overall amount of glycosylated clusterin generated by cells. This is supported by the presence of two nuclear localisation signals in *CLU* (Leskov et al., 2003) and by the demonstration in this thesis that glycosylated clusterin proteins reside in the nucleus of iPSCs. By using iPSCs that

overexpress glycosylated clusterin it can be determined if intracellular retention is dependent on the amount of clusterin generated by cells. It is, however, unclear if intracellular retention of clusterin is simply a method of storing clusterin that is not secreted from cells, or if there is a function independent of storage.

Alternatively, the existence of intercellular, glycosylated clusterin in cells may arise following the uptake of clusterin from culture media (Killick et al., 2014). Indeed, cell surface receptors for clusterin have been identified, which may mediate clusterin's uptake (Bartl et al., 2001; Bell et al., 2007; Ghiso et al., 1993), however, little Is known of this interaction, and clusterin uptake has not been demonstrated in neurons. To confirm if clusterin is taken up into cells following secretion, exon 2 -/- iPSCs-neurons can be cultured in conditioned media obtained from control iPSC-neurons (containing clusterin) or fluorescently tagged clusterin proteins could be added to the media. Given that exon 2 -/- iPSC-neurons do not express glycosylated clusterin, the identification of glycosylated clusterin species found intracellularly would confirm clusterin uptake from the media had occurred. This could be achieved by visualising clusterin protein expression by western blot analysis, or alternatively, confocal microscopy could be used to visualise the trafficking of fluorescently labelled clusterin in cells. If uptake of clusterin is observed, an additional study could focus on determining if clusterin's uptake into cells coincides with Aβ uptake.

The expression of *CLU* variant 1 Δ exon 2 transcripts has been demonstrated previously (Leskov et al., 2003; Prochnow et al., 2013), but the existence of this variant is debated (Andersen et al., 2007). Overall, the expression of *CLU* variant 1 Δ exon 2 transcripts is low and varies among cell types. In agreement, expression of this variant could not be detected by RT-qPCR in either control iPSCs or iPSC-neurons. In comparison,

the variant was detected following both heterozygous and homozygous exon 2 knockout demonstrating that either edit is sufficient to induce the expression of this variant in both iPSCs and iPSC-neurons. Studies indicate *CLU* variant 1 Δ exon 2 transcripts are induced by stress (Leskov et al., 2003; Prochnow et al., 2013). However, Aβ treatment did not induce the expression of *CLU* variant 1 Δ exon 2 in control iPSC-neurons and did not increase the expression of this variant in heterozygous exon 2 +/- iPSC-neurons suggesting that the expression of this variant is not regulated by $A\beta_{25-35}$.

The translation of *CLU* variant 1 Δ exon 2 has previously been demonstrated to result in the generation of non-glycosylated clusterin species that reside in both the cytoplasm and nuclei of cells (Leskov et al., 2003; Prochnow et al., 2013). Although this was not explored in exon 2 -/- iPSCs, non-glycosylated clusterin species were confirmed to reside in the cytoplasm of both control and exon 2 +/- iPSCs. Given that control iPSCs do not express *CLU* variant 1 Δ exon 2 transcripts, the transcriptional origin of these cytoplasmic, non-glycosylated clusterin species is unclear. Furthermore, the abundance of non-glycosylated clusterin species was comparable between exon 2 +/- and control iPSCs. Therefore, the increased expression of *CLU* variant 1 Δ exon 2 transcripts in exon 2 +/- iPSCs, following CRISPR/Cas9 gene editing, did not result in an increased abundance of non-glycosylated clusterin proteins. Following homozygous *CLU* exon 2 knockout, an increased abundance of non-glycosylated clusterin proteins was confirmed in both exon 2 -/- iPSCs and iPSC-neurons. Thus, it appears that exon 2 must be removed from both *CLU* alleles to generate a quantifiable increase in the abundance of non-glycosylated clusterin species, highlighting the requirement for exon 2 to generate mature, cleaved, and glycosylated clusterin, the potential instability of *CLU* variant 1 Δ exon 2 transcripts and the inefficient translation of non-glycosylated clusterin proteins.

7.1.3 Clusterin trafficking facilitates Aβ induced toxicity in human neurons

Clusterin trafficking is altered by $A\beta_{25-35}$ treatment of rodent neurons (Killick et al., 2014) and by *CLU*-AD mutations *in vitro* (Bettens et al., 2015; Zhou et al., 2014); resulting in reduced secretion and increased intracellular retention of glycosylated clusterin. These studies demonstrate that altered trafficking of clusterin may mediate Aβ induced neurotoxicity and contribute to AD pathogenesis. It was confirmed in this thesis that clusterin trafficking is also altered in iPSC-neurons following treatment with $A\beta_{25-35.}$ As in rodent neurons, control iPSC-neurons demonstrated reduced secretion and increased accumulation of intracellular clusterin. This response was absent in exon 2 -/- iPSC-neurons, which do not express glycosylated clusterin. The loss of glycosylated clusterin species in exon 2 -/- iPSC-neurons resulted in less cell death than that exhibited by control iPSC-neurons. Together, these data demonstrate clusterin trafficking contributes to neuron loss induced by $A\beta_{25-35.}$

Glycosylated clusterin species are typically considered to be protective and anti-apoptotic. However, the data presented in this thesis demonstrates the opposite and provides evidence for a role of glycosylated clusterin species in promoting cell death in iPSC-neurons treated with $A\beta_{25-35}$. Previously it was suggested that the role of clusterin in cell death may be dependent on the stressor, cell type and the species/localisation of clusterin species in cells (Trougakos et al., 2005). A cytoprotective property of clusterin was previously demonstrated in prostate cancer cells; reducing *CLU* expression sensitized cells to chemotherapy and increased apoptosis indicating clusterin plays a protective role (Trougakos et al., 2004). This was later supported when *CLU* overexpression was demonstrated to reduce cell death in a fibrosarcoma cell line (H. Zhang et al., 2005). The authors overexpressed clusterin and demonstrated reduced BAX dependent apoptosis

that was mediated by an immature, cytoplasmic clusterin species (H. Zhang et al., 2005). In the same study, no role for mature, glycosylated, and secreted clusterin was identified. However, another study demonstrated a variable effect of immature, clusterin species in cells (Trougakos et al., 2005). The overexpression of full-length *CLU* cDNA resulted in an increased expression of both immature 60kDa and mature, glycosylated clusterin. This was associated with increased survival in some cells and reduced survival in others (Trougakos et al., 2005). This varying role was attributed to cytoplasmic 60kDa clusterin and not mature, secreted and glycosylated clusterin; immature clusterin proteins to Ku70-BAX complexes resulting in their stabilisation, thereby, reducing BAX dependent apoptosis (Trougakos et al., 2009). Although a cytoprotective and pro-apoptotic role of clusterin has been demonstrated, these studies suggest this is attributed to immature clusterin and there is little evidence to indicate a role of mature, glycosylated clusterin. However, it remains unclear why clusterin appears to have a pro-apoptotic role in some contexts and an anti-apoptotic role in others. Furthermore, it must be noted that cytoprotective functions of clusterin proteins were identified in cancer cell lines following treatment with chemotherapy agents, and little is known of this protective role in other cell types. It is likely that clusterin's role in apoptosis and survival in cancer lines will differ to that observed in other types of cells including neurons. Of course, it is also reasonable that clusterin may contribute to Aβ neurotoxicity in a manner that is independent of its functions in cell death pathways.

In this thesis, glycosylated clusterin species were demonstrated to contribute to Aβ neurotoxicity in human iPSC-neurons. The importance of glycosylated clusterin trafficking in mediating Aβ neurotoxicity could be explored further by utilising the exon 2 -/- iPSC-neurons generated here. Exon 2 -/- iPSC-neurons can be cultured in either their own

media (with no clusterin) or media obtained from control iPSC-neurons (with clusterin) and their response to Aβ treatment compared. Western blot analysis would confirm whether glycosylated clusterin has been trafficked into exon 2 -/- iPSC-neurons from control medium. Then, changes in cell death and neurite length can be compared between the two sets of cells. If the trafficking of glycosylated clusterin proteins into cells directly contributes to Aβ induced toxicity, exon 2 -/- iPSC-neurons cultured in media containing clusterin would exhibit more cell death and neurite retraction than exon 2 -/- iPSC-neurons cultured in media lacking clusterin. Furthermore, the neuroprotection demonstrated in exon 2 -/- iPSC-neurons would be lost. This would confirm clusterin trafficking directly contributes to Aβ induced neurotoxicity in iPSC-neurons.

Neurite retraction was absent in Aβ treated exon 2 -/- iPSC-neurons, demonstrating that glycosylated clusterin species are required for $A\beta_{25-35}$ induced neurite damage. Little is known of the role of clusterin in mediating neuronal changes induced by Aβ, but animal studies have demonstrated that clusterin facilitates the formation of dystrophic neurites found in Aβ plaques (DeMattos et al., 2002, 2004). Recently, two studies have demonstrated that clusterin may also contribute to synapse loss and synaptic dysfunction in AD induced by Aβ (Hesse et al., 2019; R. J. Jackson et al., 2019). Jackson et al., demonstrated clusterin co-localises at synapses with Aβ in *APOE E4* carriers (R. J. Jackson et al., 2019). Taken together, these studies demonstrate that clusterin may play a central role in mediating Aβ induced neurotoxicity. To determine if clusterin contributes to synapse loss in iPSC-neurons, iPSC-neurons can be cultured *in vitro* for approximately 80/90 days until synapses are generated. The number of synapses can then be quantified by quantifying co-localisation of pre-and post-synaptic markers. Following treatment with Aβ, synapse number is expected to be reduced in iPSC-neurons. If glycosylated clusterin

species contribute directly synapse loss, synapse loss should be reduced in exon 2 -/- iPSC-neurons compared to control iPSC-neurons. Furthermore, imaging can be used to identify if clusterin localises with synapses and Aβ in iPSC-neurons. If clusterin is also demonstrated to contribute to Aβ induced synapse loss, as well as cell death and neurite retraction, this would highlight a central role of clusterin in mediating AD pathogenesis and would provide evidence for further exploration of clusterin or clusterin regulated genes as a therapeutic strategy for AD. Overall, the data in this thesis demonstrate that glycosylated clusterin is essential for Aβ induced neurite retraction and facilitates cell death in human iPSC-neurons indicating a crucial role of clusterin in mediating Aβ neurotoxicity.

7.1.4 Non-glycosylated clusterin species do not mediate Aβ induced toxicity

Stress increases the expression of *CLU* variant 1 exon 2 in cells leading to an increased abundance of non-glycosylated clusterin species (Leskov et al., 2003; O'Sullivan et al., 2003; Prochnow et al., 2013), which has been demonstrated to promote cell death (Leskov et al., 2003; Scaltriti, Santamaria, et al., 2004; C.-R. Yang et al., 1999, 2000). However, it has not been established whether non-glycosylated clusterin species facilitate cell death in neurons. Aβ did not alter the expression of *CLU* variant 1 Δ exon 2 transcripts in either control or exon 2 +/- iPSC-neurons, nor did Aβ alter the abundance of non-glycosylated clusterin species. In the absence of these changes, cell death was still demonstrated in iPSC-neurons indicating that an increase in non-glycosylated clusterin species is not required for Aβ induced cell death. This, of course does not rule out a role for non-glycosylated clusterin in mediating Aβ induced cell death; simply that an increase in its expression is not required. Furthermore, increased levels of *CLU* variant 1 Δ exon 2 and non-glycosylated clusterin species did not confer sensitivity to Aβ in exon 2 -/- iPSC-neurons. Together, these experiments show that increased levels of both *CLU* variant 1 Δ

exon 2 transcripts and non-glycosylated clusterin species are neither necessary nor sufficient to mediate Aβ mediated neurotoxicity. Given the relevance of $A\beta_{1-42}$ in AD, further exploration should determine if the abundance of non-glycosylated clusterin species is altered by $A\beta_{1-42}$.

In this thesis, a role for non-glycosylated clusterin species was not identified. To further rule out their contribution to Aβ induced neurotoxicity, a total *CLU* KO iPSC line could be generated, which does not express any clusterin proteins. The response of control, exon 2 -/- and *CLU* KO iPSC-neurons to Aβ could be compared to identify if total *CLU* KO iPSC-neurons exhibit more protection than exon 2 -/- iPSC-neurons. If this was the case, it would suggest a role of non-glycosylated clusterin species in mediating Aβ toxicity that was not identified in this thesis. In contrast, if these species do not contribute, then *CLU* KO and exon 2 -/- iPSC-neurons would have comparable responses. The development of a *CLU* KO iPSC-neuron model would facilitate the understanding of the roles played by non-glycosylated clusterin species in Aβ toxicity, complementing the work achieved in this thesis.

7.1.5 RNA-Seq analysis can be used to identify novel genes and pathways mediating Aβ toxicity

Although not included in this thesis, RNA-Seq data has been generated to identify gene expression changes in exon 2 -/- and control iPSC-neurons following Aβ treatment. This dataset can be utilised to identify genes and pathways that could potentially represent a novel therapeutic strategy for AD. Firstly, comparisons can be made between untreated exon 2 +/- and untreated control iPSC-neurons to identify gene expression changes arising because of *CLU* exon 2 knockout and *CLU* knockdown. This may identify genes conferring the neuroprotection demonstrated in exon 2 -/- iPSC-neurons. Secondly, comparisons can

be made between Aβ treated exon 2 -/- and control iPSC-neurons to identify genes that may be involved in mediating Aβ toxicity in iPSC-neurons. This would facilitate the identification of genes that may contribute to the altered response of exon 2 -/- iPSC-neurons to Aβ. This work can be supported and guided by use of other available transcriptomic data sets such as those identifying genes with altered expression in AD brains (Patel et al., 2019) or those altered by Aβ in other cell types (Killick et al., 2014). Furthermore, previous studies can be used to facilitate the identifications of genes (L. Bertram & Tanzi, 2009; Harold et al., 2009; Lambert et al., 2009, 2013; Tanzi & Bertram, 2005) and known pathways (Bagyinszky et al., 2020; Lars Bertram et al., 2007; Jones et al., 2010; Rosenthal et al., 2014; van Rooij et al., 2019) in our dataset, that could be explored as therapeutic targets. For example, *EGR1* was demonstrated to be upregulated following Aβ treatment in both control and exon 2 +/- iPSC-neurons, in agreement with data from rodent neurons (Killick et al., 2014). It would be interesting to determine if *EGR1* is also altered in exon 2 -/- iPSC-neurons, this could elucidate if *EGR1* has a central role in mediating Aβ induced neurotoxicity in iPSC-neurons. Previously, *EGR1* knockdown in rodent neurons was demonstrated to prevent $A\beta_{25-35}$ induced toxicity (Killick et al., 2014). Knockdown of *EGR1* may provide neuroprotection in control iPSC-neurons following Aβ treatment and may enhance the observed protection in exon 2 -/- iPSC-neurons.

7.1.6 Using neuron models to study clusterin in AD

Purely neuronal cultures were used in this thesis and although these do not reflect the complexity of the networks present in the human brain, they provide a solid foundation on which further work can be expanded. Astrocytes are the primary source of clusterin in the human brain (Morgan et al., 1995; Pasinetti et al., 1994) and therefore it would be crucial to determine if the loss of glycosylated clusterin in astrocytes alters their response to Aβ

and how this may impact on the health of neurons. Studies have demonstrated clusterin may facilitate the uptake of Aβ by astrocytes resulting in altered clusterin trafficking (Nuutinen et al., 2007). However, others have demonstrated Aβ uptake may be hampered by clusterin (Mulder et al., 2014; Nielsen et al., 2010). Therefore, it remains unclear whether clusterin is an important mediator of Aβ uptake and clearance by astrocytes. This can be explored by comparing Aβ uptake by control and exon 2 -/- iPSC-astrocytes. Furthermore, imaging could be used to determine if clusterin binds to Aβ and cell surface receptors expressed by astrocytes, and whether this interaction facilitates the uptake of Aβ by astrocytes. Astrocytes alter neuronal health and viability; Paradisi et al., demonstrated neuroprotection in neuron cultures in the presence of untreated astrocytes, which was lost when astrocytes were treated with Aβ (Paradisi et al., 2004). However, astrocytes may contribute to neurotoxicity too. Cell death is enhanced in cultures when neurons were co-cultured with astrocytes compared when they were cultured in a purely neuronal environment (Allaman et al., 2011; Domenici et al., 2002; Malchiodi-Albedi et al., 2001; Söllvander et al., 2016), suggesting that astrocytes may themselves contribute to neurotoxicity. These studies have primarily focused on the use of neurons and astrocytes of rodent origin but the role of clusterin in human iPSC-astrocytes is unexplored. An astrocyte conditioned medium (ACM) study can be established where control and exon 2 -/- iPSC-astrocytes are treated with Aβ and their conditioned medium collected. This ACM can then be added to cultures of iPSC-neurons to examine the effect of ACM on neuron health. Changes in cell death and neurite length following exposure to untreated and Aβ treated ACM can be quantified and compared. Firstly, this would examine how astrocytic response to Aβ may influence neuron health and secondly, how this is altered by the loss of clusterin. If clusterin plays a role in mediating Aβ uptake by astrocytes, promoting its

degradation and clearance, it would be reasonable to predict the loss of glycosylated clusterin species in exon 2 -/- iPSC-astrocytes would result in increased neurotoxicity. Neurotoxicity would be enhanced due to the increased abundance of Aβ in the media, and potentially by the altered response of exon 2 -/- iPSC-astrocytes to Aβ.

7.1.7 Limitations of using iPSCs to study AD

The study of complex human diseases affecting the brain is hampered by the lack of access to living tissue and cells. The development of human iPSC technology provides the unique opportunity to generate human cells in large numbers that can be used to model a specific disease. These cells can be used to probe the function and contribution of specific genes and proteins in disease as well as in drug discovery. In this thesis, neurons were generated from iPSCs to study the contribution of clusterin in AD, specifically, how clusterin trafficking may mediate Aβ induced toxicity. Although iPSC models have been generated to study AD, these are largely based on cells derived from fAD patients (Arber et al., 2020; Sproul et al., 2014; Woodruff et al., 2013; Yagi et al., 2011). As mentioned previously, most AD animal models are primarily based on fAD genetics. Although these are useful in elucidating the role of Aβ in AD and the development of fAD, they are unlikely to replicate the changes observed in sAD. Mutations in fAD genes are known to directly cause the development of AD, in comparison, sAD genes are risk linked and may influence the probability of an individual developing AD but are not deterministic. There is therefore a need to build better models that recapitulate sAD, given most AD cases are sporadic. A number of genes have been identified to alter sAD risk (Corder et al., 1994; Harold et al., 2009; Lambert et al., 2009; Naj et al., 2011; Seshadri et al., 2010) but few models incorporate sAD genes (Duan et al., 2014; Huang et al., 2017; Young et al., 2015). In fact,

there is no iPSC model that examines how *CLU* SNPs or mutations influence molecular or cellular phenotypes of neurons.

At present there are no effective preventatives or therapeutic interventions to slow or stop the progression of AD, and the identification of new drug targets for AD is a major challenge. Part of this challenge is the failure in translating drugs that showed efficacy in animal models into human patients. Therefore, the use of human iPSC-neurons presents two major advantages for drug discovery. Firstly, iPSC-neurons represent a more disease relevant model for studying AD, since they can be generated from human patients, and secondly, human neurons can be generated from iPSCs in large amounts making the model scalable. In drug screening and discovery, iPSC-derived cells can be used to develop assays relevant to AD phenotypes. CRISPR/Cas9 gene editing can also be used to introduce specific gene mutations to understand the consequence of risk altering gene mutations and SNPs on these phenotypes. Compounds can then be screened to identify those that prevent disease associated phenotypes e.g., compounds could be screened to identify those that prevent neurite retraction induced by Aβ. New drugs can then be developed based on these compounds, which can be tested in human patients during clinical trials to determine their efficacy *in vivo*. For example, murine studies demonstrated that the stabilisation of retromer may have beneficial effects on Aβ production (Chu & Praticò, 2017; Mecozzi et al., 2014). Young et al., identified retromer stabilising compounds as a potential drug candidate and tested this using iPSC-neurons *in vitro* (Young et al 2018). Retromer stabilisation was demonstrated to reduce *APP* processing and Aβ generation in iPSC-neurons generated from both fAD and sAD patients, as well in an isogenic control line in which the *APP* Swedish mutation had been introduced by CRISPR/Cas9 gene editing. Thereby, demonstrating that this drug target reduces cellular AD phenotypes and should

be explored *in vivo* (Young et al., 2018). This is just one example of how therapeutic targets can be identified and validated using iPSC-neuron models. The exon 2 -/- iPSC-neuron model generated in this thesis can be utilised for identifying compounds which may provide further protection from Aβ induced toxicity; RNA-Seq data provided from these cells will facilitate the identification of novel gene targets that may confer neuroprotection *in vivo* and represent a target for drug discovery platforms.

Although iPSC technology presents a great opportunity for researchers to not only study genes and proteins in disease and in drug discovery, but there are also several limitations and concerns associated with their use. Variability among iPSC lines due to differences in genetic backgrounds of donors has been demonstrated following cellular reprogramming (Kilpinen et al., 2017). Specifically, variability has been demonstrated between iPSC-neurons generated from cells obtained from different sAD patients (Israel et al., 2012), highlighting both the heterogeneity of sAD but also the influence of donor genetic backgrounds on cellular phenotypes, therefore adding to the complexity of modelling sAD *in vitro* using human iPSC-neurons. In this thesis, a single parental line was used to generate both the exon 2 +/- and exon 2 -/- iPSC lines, enabling comparisons to be made between all lines due to their shared genetic backgrounds. It is unclear if the results reported in this thesis would be consistent among iPSC-neuron lines generated from other donors. Therefore, further validation would involve the generation of several iPSC-neuron lines from healthy individuals and sAD patients to determine if the neuroprotection observed in exon 2 -/- iPSC-neurons is observed in cells of different origin and genetic backgrounds. To complement the work done previously in HEK293T cells (Bettens et al., 2915), it would be interesting to determine if clusterin trafficking is altered by sAD associated *CLU* variants in human iPSC-neurons *in vitro*. This could include *CLU* mutations

identified by Bettens et al., such as p.I303NfsX13 and p.I360N, which altered clusterin trafficking in HEK293T (Bettens et al., 2012, 2015) or CRISPR/Cas9 could be used to introduce *CLU* SNPs such as rs11136000 and rs9331896 (Lambert et al., 2009, 2013).

Furthermore, iPSC-neurons could be generated from control and sAD patients to compare their sensitivities to Aβ *in vitro.* CRISPR/Cas9 gene editing could then be used to remove *CLU* exon 2 from sAD iPSC-neurons and neuronal response to Aβ recorded again, to determine if *CLU* exon 2 knockout is sufficient to confer neuroprotection to disease lines as well as those obtained from a healthy individual. As demonstrated by Jackson et al., clusterin may mediate synapse loss induced by Aβ (R. J. Jackson et al., 2019). The use of iPSC-neuron lines generated from *APOE E4* carriers or *APOE E4* sAD patients would enable the exploration of clusterin's role in AD, and the use of CRISPR/Cas9 to alter *CLU* expression would elucidate the relationship between Aβ, clusterin and APOE in AD.

The need for appropriate controls in iPSC-based projects is crucial and it is not often clear what the most appropriate control may be. CRISPR/Cas9 gene editing can be used to revert risk mutations back to wildtype, thereby reducing variability between lines and generating an isogenic control. However, in many cases, there may not be a risk mutation present, or indeed, several AD SNPs may be present making gene editing more technically challenging. Furthermore, as demonstrated in this thesis, the use of CRISPR/Cas9 to edit iPSCs is not trivial and must be optimised for each line, gene, and mutation. This increases the complexity and the time frame of a project. Indeed, data obtained in this thesis was used in publication to demonstrate how CRISPR/Cas9 gene editing to excise a single exon was much less efficient in human iPSCs compared to a several other cell types suggesting editing of human iPSCs may be more difficult (Blayney et al., 2020). Additionally, off targets and random alterations induced by CRISPR/Cas9

appears to occur more commonly in iPSCs than in other cell types (Fu et al., 2013), making it essential to screen for alterations that may not be present in the parental line.

A crucial issue with the use of iPSC-derived neurons to model age related diseases is the age and maturity of iPSC-neurons. Ageing is the most significant risk factor for sAD and symptoms typically present in later life (after the age of 60 years). Cells afflicted in AD present pathology and hallmarks of AD decades prior to the onset of symptoms, indicating slow and gradual progression of the disease (Lloret et al., 2019). Neurons cultured *in vitro* do not share the maturity of the neurons afflicted in AD brains and reflect neurons observed during development *in vivo* (Patani et al., 2012), highlighting the immaturity of these cells. Furthermore, cellular reprogramming results in a loss of cellular ageing signatures such as DNA damage, increased mitochondrial reactive oxygen species, loss of heterochromatin markers such as H3K9Me3 and the shortening of telomere length (J. D. Miller et al., 2013). iPSC reprogramming also results in the 'resetting' of the epigenetic ageing signature resulting in iPSCs with the epigenic signature of embryonic stem cells (Choi et al., 2015; Guenther et al., 2010; G. Liang & Zhang, 2013). Therefore, attempts have been made to accelerate or mimic the ageing process and signature in iPSCs to ensure better models can be generated to study age-related diseases *in vitro*. For example, neuronal maturity can be increased by a combination of longer culturing times and co-culturing with astrocytes, which accelerate iPSC-neuron development and maturity (Hedegaard et al., 2020). iPSC-derived cells from patients with premature ageing diseases such as Hutchinson-Gilford progeria syndrome (HGPS) have enabled the identification of *in vitro* ageing markers (Scaffidi & Misteli, 2005, 2006). HGPS is characterised by the premature ageing of cells and tissues (Hennekam, 2006). HGPS is caused by a mutation in the *LMNA* gene that causes a truncation of the lamin A protein generating a variant called

progeria. Miller et al., demonstrated that the overexpression of lamin A in iPSC-fibroblasts and iPSC-neurons induces age related markers and characteristics (J. D. Miller et al., 2013). These studies demonstrate that age related signatures can be induced in iPSC-derived cells to accelerate the ageing process and generate disease related phenotypes.

The traditional method of generating neurons from somatic cells involves the reprogramming of adult somatic cells into iPSCs, which are then differentiated into neurons (***Figure 7.1***) (Shi, Kirwan, & Livesey, 2012; Shi, Kirwan, Smith, Robinson, et al., 2012; Takahashi et al., 2007; Takahashi & Yamanaka, 2006). Direct differentiation can now be used to generate neurons (iNeurons) directly from adult fibroblasts, bypassing the cellular reprogramming of somatic cells into iPSCs. There are several methods that can be used to generate induced iNeurons from somatic cells (Carter et al., 2020; Vierbuchen et al., 2010). iNeurons have been shown to retain the ageing profiles of the donor cells from which they originate (Mertens et al., 2015) and may provide an alternative to iPSC-derived neurons to study neurodegenerative diseases including AD (Hu et al., 2015). However, a major issue with these cells is that unlike iPSCs, they are not self-renewing and therefore provide a limited resource.

The neurons generated in this thesis are immature and were cultured *in vitro* for 35 days before treatment with Aβ and experiments conducted. Therefore, these cells do not reflect the neurons in the human brain afflicted by AD both in functional and morphological maturity. Neuronal and cortical lineage markers were used to confirm that the cells generated in this thesis were neuronal, however, no functional characteristics were recorded since they were not cultured for sufficient time *in vitro*. This includes the recording of electrophysiological properties such as the expression of glutamate receptors and the firing of action potentials.

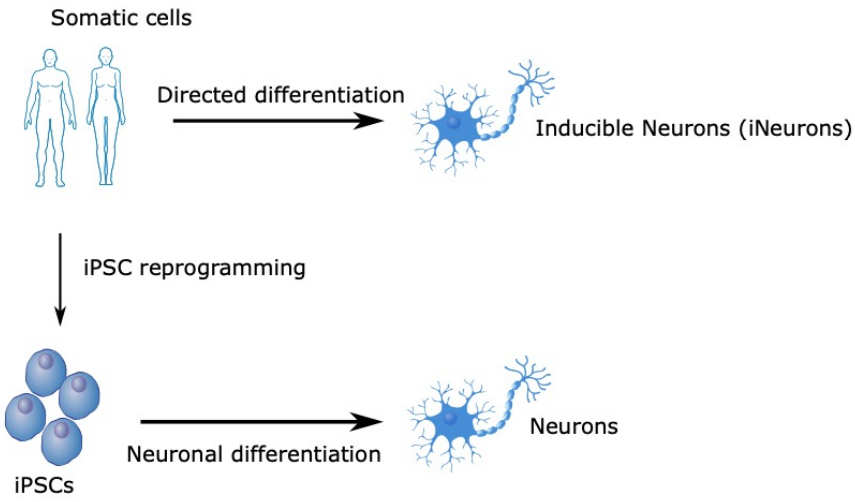


Figure 7.1. Schematic diagram for the generation of iNeurons directly from somatic cells and the programming of iPSCs followed by neuronal differentiation.

Somatic cells from healthy controls or patients can be converted directly into inducible neurons (iNeurons) bypassing the iPSC reprogramming stage. The alternative method is the reprogramming of somatic cells into iPSCs, which must then be differentiated into neurons. This figure was produced using icons provided in the Reactome database that are free to download and modify: (https://reactome.org/icon-lib); (Sidiropoulos et al., 2017).

7.1.8 Concluding remarks and summary diagram

In this thesis I have generated human iPSC-derived cortical neurons from iPSCs lacking exon 2 in one or both *CLU* alleles. Heterozygous exon 2 knockout iPSC-neurons exhibited comparable responses to $A\beta_{25-35}$ treatment as control, healthy iPSC-neurons. In comparison, homozygous exon 2 knockout iPSC-neurons exhibited partial protection against $A\beta_{25-35}$ treatment displaying significantly less death than control neurons, and no retraction of their neurite processes. The results obtained from ***Chapter 7*** provide direct evidence for a role of clusterin, specifically glycosylated clusterin species and their trafficking, in mediating neuronal response to Aβ. In contrast to previous literature, the data provided in this thesis did not identify a role for non-glycosylated clusterin proteins in facilitating the response of cells to stress and in cell death. Therefore, no role for the non-

glycosylated clusterin proteins in mediating neuronal response to Aβ was identified. This is summarised in ***figure 7.2***. Furthermore, the work conducted on homozygous exon 2 knockout neurons demonstrates a major role of clusterin in mediating neurite damage following Aβ treatment, which should be explored further. This work has extended on a range of studies previously demonstrating altered clusterin trafficking in response to stress, including Aβ treatment, and the models generated here provide a foundation for future investigation into clusterin's contribution to neurodegeneration and AD.

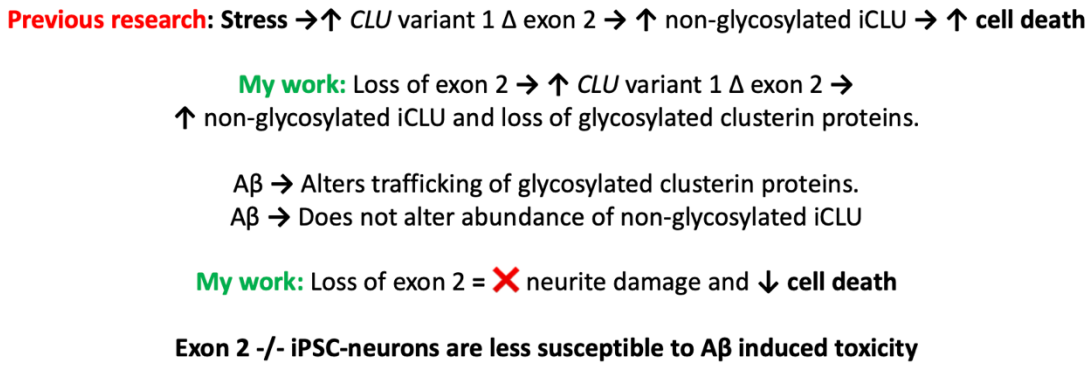


Figure 7.2. Diagram summarising results obtained in Chapter 7.

The loss of exon 2 from both CLU alleles increases the expression of CLU variant 1 Δ exon 2 transcripts and abundance of non-glycosylated intracellular clusterin proteins. While the treatment of iPSC-neurons with Aβ altered the trafficking of glycosylated clusterin proteins in control iPSC-neurons, the abundance of non-glycosylated intracellular clusterin proteins was not altered by Aβ. This is in comparison to previous studies, which demonstrated stress induces an increase in abundance of non-glycosylated clusterin proteins that facilitate cell death. The data obtained in Chapter 7 provides evidence for a role of glycosylated clusterin proteins in contributing to Aβ induced toxicity in iPSC-neurons, while no role for non-glycosylated clusterin proteins was identified.

References

Allaman, I., Bélanger, M., & Magistretti, P. J. (2011). Astrocyte-neuron metabolic relationships: For better and for worse. *Trends in Neurosciences*, *34*(2), 76–87. https://doi.org/10.1016/j.tins.2010.12.001

Andersen, C. L., Schepeler, T., Thorsen, K., Birkenkamp-Demtröder, K., Mansilla, F., Aaltonen, L. A., Laurberg, S., & Ørntoft, T. F. (2007). Clusterin expression in normal mucosa and colorectal cancer. *Molecular & Cellular Proteomics: MCP*, *6*(6), 1039–1048. https://doi.org/10.1074/mcp.M600261-MCP200

Anderson, E. M., Haupt, A., Schiel, J. A., Chou, E., Machado, H. B., Strezoska, Ž., Lenger, S., McClelland, S., Birmingham, A., Vermeulen, A., & Smith, A. van B. (2015). Systematic analysis of CRISPR–Cas9 mismatch tolerance reveals low levels of off-target activity. *Journal of Biotechnology*, *211*, 56–65. https://doi.org/10.1016/j.jbiotec.2015.06.427

Arber, C., Toombs, J., Lovejoy, C., Ryan, N. S., Paterson, R. W., Willumsen, N., Gkanatsiou, E., Portelius, E., Blennow, K., Heslegrave, A., Schott, J. M., Hardy, J., Lashley, T., Fox, N. C., Zetterberg, H., & Wray, S. (2020). Familial Alzheimer's disease patient-derived neurons reveal distinct mutation-specific effects on Aβ. *Molecular Psychiatry*, *25*(11), 2919–2931. https://doi.org/10.1038/s41380-019-0410-8

Armijo, E., Gonzalez, C., Shahnawaz, M., Flores, A., Davis, B., & Soto, C. (2017). Increased susceptibility to Aβ toxicity in neuronal cultures derived from familial Alzheimer's disease (PSEN1-A246E) induced pluripotent stem cells. *Neuroscience Letters*, *639*, 74–81. https://doi.org/10.1016/j.neulet.2016.12.060

Bae, S., Park, J., & Kim, J.-S. (2014). Cas-OFFinder: A fast and versatile algorithm that searches for potential off-target sites of Cas9 RNA-guided endonucleases.

Bioinformatics (Oxford, England), *30*(10), 1473–1475. https://doi.org/10.1093/bioinformatics/btu048

Bagyinszky, E., Giau, V. V., & An, S. A. (2020). Transcriptomics in Alzheimer's Disease: Aspects and Challenges. *International Journal of Molecular Sciences*, *21*(10). https://doi.org/10.3390/ijms21103517

Baldwin, K. T., & Eroglu, C. (2017). Molecular mechanisms of astrocyte-induced synaptogenesis. *Current Opinion in Neurobiology*, *45*, 113–120. https://doi.org/10.1016/j.conb.2017.05.006

Barrangou, R., Fremaux, C., Deveau, H., Richards, M., Boyaval, P., Moineau, S., Romero, D. A., & Horvath, P. (2007). CRISPR Provides Acquired Resistance Against Viruses in Prokaryotes. *Science*, *315*(5819), 1709–1712. https://doi.org/10.1126/science.1138140

Bartl, M. M., Luckenbach, T., Bergner, O., Ullrich, O., & Koch-Brandt, C. (2001). Multiple Receptors Mediate apoJ-Dependent Clearance of Cellular Debris into Nonprofessional Phagocytes. *Experimental Cell Research*, *271*(1), 130–141. https://doi.org/10.1006/excr.2001.5358

Behl, C., Davis, J. B., Klier, F. G., & Schubert, D. (1994). Amyloid β peptide induces necrosis rather than apoptosis. *Brain Research*, *645*(1), 253–264. https://doi.org/10.1016/0006-8993(94)91659-4

Bell, R. D., Sagare, A. P., Friedman, A. E., Bedi, G. S., Holtzman, D. M., Deane, R., & Zlokovic, B. V. (2007). Transport Pathways for Clearance of Human Alzheimer's Amyloid β-Peptide and Apolipoproteins E and J in the Mouse Central Nervous System. *Journal of Cerebral Blood Flow & Metabolism*, *27*(5), 909–918. https://doi.org/10.1038/sj.jcbfm.9600419

Bertram, L. (2005). The genetic epidemiology of neurodegenerative disease. *Journal of Clinical Investigation*, *115*(6), 1449–1457. https://doi.org/10.1172/JCI24761

Bertram, L., & Tanzi, R. E. (2009). Genome-wide association studies in Alzheimer's disease. *Human Molecular Genetics*, *18*(R2), R137–R145. https://doi.org/10.1093/hmg/ddp406

Bertram, Lars, McQueen, M. B., Mullin, K., Blacker, D., & Tanzi, R. E. (2007). Systematic meta-analyses of Alzheimer disease genetic association studies: The AlzGene database. *Nature Genetics*, *39*(1), 17–23. https://doi.org/10.1038/ng1934

Bettens, K., Brouwers, N., Engelborghs, S., Lambert, J.-C., Rogaeva, E., Vandenberghe, R., Le Bastard, N., Pasquier, F., Vermeulen, S., Van Dongen, J., Mattheijssens, M., Peeters, K., Mayeux, R., St George-Hyslop, P., Amouyel, P., De Deyn, P. P., Sleegers, K., & Van Broeckhoven, C. (2012). Both common variations and rare non-synonymous substitutions and small insertion/deletions in *CLU* are associated with increased Alzheimer risk. *Molecular Neurodegeneration*, *7*(1), 3. https://doi.org/10.1186/1750-1326-7-3

Bettens, K., Sleegers, K., & Van Broeckhoven, C. (2010). Current status on Alzheimer disease molecular genetics: From past, to present, to future. *Human Molecular Genetics*, *19*(R1), R4–R11. https://doi.org/10.1093/hmg/ddq142

Bettens, K., Vermeulen, S., Van Cauwenberghe, C., Heeman, B., Asselbergh, B., Robberecht, C., Engelborghs, S., Vandenbulcke, M., Vandenberghe, R., De Deyn, P. P., Cruts, M., Van Broeckhoven, C., & Sleegers, K. (2015). Reduced secreted clusterin as a mechanism for Alzheimer-associated *CLU* mutations. *Molecular Neurodegeneration*, *10*. https://doi.org/10.1186/s13024-015-0024-9

Blasko, I., Wagner, M., Whitaker, N., Grubeck-Loebenstein, B., & Jansen-Du, P. (2000). The amyloid β peptide (25-35) induces apoptosis independent of p53. *FEBS Letters*, 5.

Blayney, J., Foster, E. M., Jagielowicz, M., Kreuzer, M., Morotti, M., Reglinski, K., Xiao, J. H., & Hublitz, P. (2020). Unexpectedly High Levels of Inverted Re-Insertions Using Paired sgRNAs for Genomic Deletions. *Methods and Protocols*, *3*(3). https://doi.org/10.3390/mps3030053

Bolotin, A., Quinquis, B., Sorokin, A., & Ehrlich, S. D. (2005). Clustered regularly interspaced short palindrome repeats (CRISPRs) have spacers of extrachromosomal origin. *Microbiology*, *151*(8), 2551–2561. https://doi.org/10.1099/mic.0.28048-0

Braak, H., & Braak, E. (1991). Neuropathological staging of Alzheimer-related changes. *Acta Neuropathologica*, *82*(4), 239–259. https://doi.org/10.1007/BF00308809

Braak, H., & Braak, E. (1996). Evolution of the neuropathology of Alzheimer's disease. *Acta Neurologica Scandinavica*, *94*(S165), 3–12. https://doi.org/10.1111/j.1600-0404.1996.tb05866.x

Braak, H, Alafuzoff, I., Arzberger, T., Kretzschmar, H., & Del Tredici, K. (2006). Staging of Alzheimer disease-associated neurofibrillary pathology using paraffin sections and immunocytochemistry. *Acta Neuropathologica*, *112*(4), 389–404. https://doi.org/10.1007/s00401-006-0127-z

Brouns, S. J. J., Jore, M. M., Lundgren, M., Westra, E. R., Slijkhuis, R. J. H., Snijders, A. P. L., Dickman, M. J., Makarova, K. S., Koonin, E. V., & van der Oost, J. (2008). Small CRISPR RNAs Guide Antiviral Defense in Prokaryotes. *Science*, *321*(5891), 960–964. https://doi.org/10.1126/science.1159689

Brousseau, T., Legrain, S., Berr, C., Gourlet, V., Vidal, O., & Amouyel, P. (1994). Confirmation of the ϵ4 allele of the apolipoprotein E gene as a risk factor for late-

onset Alzheimer's disease. *Neurology*, *44*(2), 342–342. https://doi.org/10.1212/WNL.44.2.342

Burdick, D., Soreghan, B., Kwon, M., Kosmoski, J., Knauer, M., Henschen, A., Yates, J., Cotman, C., & Glabe, C. (1992). Assembly and aggregation properties of synthetic Alzheimer's A4/ β amyloid peptide analogs. *Journal of Biological Chemistry*, *267*(1), 546–554.

Bussière, T., Giannakopoulos, P., Bouras, C., Perl, D. P., Morrison, J. H., & Hof, P. R. (2003a). Progressive degeneration of nonphosphorylated neurofilament protein-enriched pyramidal neurons predicts cognitive impairment in Alzheimer's disease: Stereologic analysis of prefrontal cortex area 9. *Journal of Comparative Neurology*, *463*(3), 281–302. https://doi.org/10.1002/cne.10760

Byrne, S. M., & Church, G. M. (2015). Crispr-mediated Gene Targeting of Human Induced Pluripotent Stem Cells. *Current Protocols in Stem Cell Biology*, *2015*(Suppl 35), 5A.8.1-5A.8.22. https://doi.org/10.1002/9780470151808.sc05a08s35

Bystron, I., Blakemore, C., & Rakic, P. (2008). Development of the human cerebral cortex: Boulder Committee revisited. *Nature Reviews Neuroscience*, *9*(2), 110–122. https://doi.org/10.1038/nrn2252

Cahoy, J. D., Emery, B., Kaushal, A., Foo, L. C., Zamanian, J. L., Christopherson, K. S., Xing, Y., Lubischer, J. L., Krieg, P. A., Krupenko, S. A., Thompson, W. J., & Barres, B. A. (2008). A transcriptome database for astrocytes, neurons, and oligodendrocytes: A new resource for understanding brain development and function. *The Journal of Neuroscience: The Official Journal of the Society for Neuroscience*, *28*(1), 264–278. https://doi.org/10.1523/JNEUROSCI.4178-07.2008

Cai, R., Han, J., Sun, J., Huang, R., Tian, S., Shen, Y., Dong, X., Xia, W., & Wang, S. (2016). Plasma Clusterin and the *CLU* Gene rs11136000 Variant Are Associated with Mild Cognitive Impairment in Type 2 Diabetic Patients. *Frontiers in Aging Neuroscience*, *8*. https://doi.org/10.3389/fnagi.2016.00179

Caricasole, A. (2004). Induction of Dickkopf-1, a Negative Modulator of the Wnt Pathway, Is Associated with Neuronal Degeneration in Alzheimer's Brain. *Journal of Neuroscience*, *24*(26), 6021–6027. https://doi.org/10.1523/JNEUROSCI.1381-04.2004

Carlson-Stevermer, J., & Saha, K. (2017). Genome Editing in Human Pluripotent Stem Cells. *Methods in Molecular Biology (Clifton, N.J.)*, *1590*, 165–174. https://doi.org/10.1007/978-1-4939-6921-0_12

Carrasquillo, M. M., Belbin, O., Hunter, T. A., Ma, L., Bisceglio, G. D., Zou, F., Crook, J. E., Pankratz, V. S., Dickson, D. W., Graff-Radford, N. R., Petersen, R. C., Morgan, K., & Younkin, S. G. (2010). Replication of *CLU*, *CR1* and *PICALM* associations with Alzheimer's disease. *Archives of Neurology*, *67*(8), 961–964. https://doi.org/10.1001/archneurol.2010.147

Carter, J. L., Halmai, J. A. N. M., & Fink, K. D. (2020). The iNs and Outs of Direct Reprogramming to Induced Neurons. *Frontiers in Genome Editing*, *2*. https://doi.org/10.3389/fgeed.2020.00007

Cascella, R., Conti, S., Tatini, F., Evangelisti, E., Scartabelli, T., Casamenti, F., Wilson, M. R., Chiti, F., & Cecchi, C. (2013). Extracellular chaperones prevent Aβ42-induced toxicity in rat brains. *Biochimica et Biophysica Acta (BBA) - Molecular Basis of Disease*, *1832*(8), 1217–1226. https://doi.org/10.1016/j.bbadis.2013.04.012

Cataldo, A. M., Petanceska, S., Terio, N. B., Peterhoff, C. M., Durham, R., Mercken, M., Mehta, P. D., Buxbaum, J., Haroutunian, V., & Nixon, R. A. (2004). Aβ localization in abnormal endosomes: Association with earliest Aβ elevations in AD and Down syndrome. *Neurobiology of Aging*, *25*(10), 1263–1272. https://doi.org/10.1016/j.neurobiolaging.2004.02.027

Chambers, S. M., Fasano, C. A., Papapetrou, E. P., Tomishima, M., Sadelain, M., & Studer, L. (2009). Highly efficient neural conversion of human ES and iPS cells by dual inhibition of SMAD signaling. *Nature Biotechnology*, *27*(3), 275–280. https://doi.org/10.1038/nbt.1529

Chen, S., Guttridge, D. C., You, Z., Zhang, Z., Fribley, A., Mayo, M. W., Kitajewski, J., & Wang, C.-Y. (2001). WNT-1 Signaling Inhibits Apoptosis by Activating β-Catenin/T Cell Factor–Mediated Transcription. *Journal of Cell Biology*, *152*(1), 87–96. https://doi.org/10.1083/jcb.152.1.87

Chen, X.-Q., & Mobley, W. C. (2019). Alzheimer Disease Pathogenesis: Insights From Molecular and Cellular Biology Studies of Oligomeric Aβ and Tau Species. *Frontiers in Neuroscience*, *13*, 659. https://doi.org/10.3389/fnins.2019.00659

Chen, Y.-C., Farzadfard, F., Gharaei, N., Chen, W. C. W., Cao, J., & Lu, T. K. (2017). Randomized CRISPR-Cas Transcriptional Perturbation Screening Reveals Protective Genes against Alpha-Synuclein Toxicity. *Molecular Cell*, *68*(1), 247-257.e5. https://doi.org/10.1016/j.molcel.2017.09.014

Chen, Y.-H., & Pruett-Miller, S. M. (2018). Improving single-cell cloning workflow for gene editing in human pluripotent stem cells. *Stem Cell Research*, *31*, 186–192. https://doi.org/10.1016/j.scr.2018.08.003

Choi, Jiho, Soohyun Lee, William Mallard, Kendell Clement, Guidantonio Malagoli Tagliazucchi, Hotae Lim, In Young Choi, et al. 'A Comparison of Genetically Matched Cell Lines Reveals the Equivalence of Human IPSCs and ESCs'. *Nature Biotechnology* 33, no. 11 (November 2015): 1173–81. https://doi.org/10.1038/nbt.3388.

Choi-Miura, N.-H., & Oda, T. (1996). Relationship between multifunctional protein "clusterin" and Alzheimer disease. *Neurobiology of Aging*, *17*(5), 717–722. https://doi.org/10.1016/0197-4580(96)00106-6

Chu, J., & Praticò, D. (2017). The retromer complex system in a transgenic mouse model of AD: Influence of age. *Neurobiology of Aging*, *52*, 32–38. https://doi.org/10.1016/j.neurobiolaging.2016.12.025

Citron, M., Westaway, D., Xia, W., Carlson, G., Diehl, T., Levesque, G., Johnson-wood, K., Lee, M., Seubert, P., Davis, A., Kholodenko, D., Motter, R., Sherrington, R., Perry, B., Yao, H., Strome, R., Lieberburg, I., Rommens, J., Kim, S., … Selkoe, D. J. (1997). Mutant presenilins of Alzheimer's disease increase production of 42-residue amyloid β-protein in both transfected cells and transgenic mice. *Nature Medicine*, *3*(1), 67–72. https://doi.org/10.1038/nm0197-67

Clancy, B., Darlington, R. B., & Finlay, B. L. (2001). Translating developmental time across mammalian species. *Neuroscience*, *105*(1), 7–17. https://doi.org/10.1016/S0306-4522(01)00171-3

Cocks, G., Curran, S., Gami, P., Uwanogho, D., Jeffries, A. R., Kathuria, A., Lucchesi, W., Wood, V., Dixon, R., Ogilvie, C., Steckler, T., & Price, J. (2014). The utility of patient specific induced pluripotent stem cells for the modelling of Autistic Spectrum Disorders. *Psychopharmacology*, *231*(6), 1079–1088.

https://doi.org/10.1007/s00213-013-3196-4

Colas, Jean-Francois, & Schoenwolf, G. (2001). Towards a cellular and molecular understanding of neurulation. *Developmental Dynamics : An Official Publication of the American Association of Anatomists*, *221*, 117–145. https://doi.org/10.1002/dvdy.1144

Colombo, E., & Farina, C. (2016). Astrocytes: Key Regulators of Neuroinflammation. *Trends in Immunology*, *37*(9), 608–620. https://doi.org/10.1016/j.it.2016.06.006

Cong, L., Ran, F. A., Cox, D., Lin, S., Barretto, R., Habib, N., Hsu, P. D., Wu, X., Jiang, W., Marraffini, L. A., & Zhang, F. (2013). Multiplex Genome Engineering Using CRISPR/Cas Systems. *Science*, *339*(6121), 819–823. https://doi.org/10.1126/science.1231143

Copani, A., Condorelli, F., Caruso, A., Vancheri, C., Sala, A., Stella, A. M. G., Canonico, P. L., Nicoletti, F., & Sortino, M. A. (1999). Mitotic signaling by β-amyloid causes neuronal death. *The FASEB Journal*, *13*(15), 2225–2234. https://doi.org/10.1096/fasebj.13.15.2225

Corder, E. H., Saunders, A. M., Risch, N. J., Strittmatter, W. J., Schmechel, D. E., Gaskell, P. C., Rimmler, J. B., Locke, P. A., Conneally, P. M., Schmader, K. E., Small, G. W., Roses, A. D., Haines, J. L., & Pericak-Vance, M. A. (1994). Protective effect of apolipoprotein E type 2 allele for late onset Alzheimer disease. *Nature Genetics*, *7*(2), 180–184. https://doi.org/10.1038/ng0694-180

Cradick, T. J., Qiu, P., Lee, C. M., Fine, E. J., & Bao, G. (2014). COSMID: A Web-based Tool for Identifying and Validating CRISPR/Cas Off-target Sites. *Molecular Therapy. Nucleic Acids*, *3*, e214. https://doi.org/10.1038/mtna.2014.64

Cruts, M., Theuns, J., & Van Broeckhoven, C. (2012). Locus-Specific Mutation Databases for Neurodegenerative Brain Diseases. *Human Mutation*, *33*(9), 1340–1344. https://doi.org/10.1002/humu.22117

Dawson, H. N., Ferreira, A., Eyster, M. V., Ghoshal, N., Binder, L. I., & Vitek, M. P. (2001). Inhibition of neuronal maturation in primary hippocampal neurons from τ deficient mice. *Journal of Cell Science*, *114*(6), 1179–1187.

Dawson, Hana N., Cantillana, V., Vitek, M. P., Wilcock, D. M., Lynch, J. R., & Laskowitz, D. T. (2010). Loss of Tau Elicits Axonal Degeneration in a Mouse Model of AD. *Neuroscience*, *169*(1), 516–531. https://doi.org/10.1016/j.neuroscience.2010.04.037

De Jonghe, C., Esselens, C., Kumar-Singh, S., Craessaerts, K., Serneels, S., Checler, F., Annaert, W., Van Broeckhoven, C., & De Strooper, B. (2001). Pathogenic APP mutations near the γ-secretase cleavage site differentially affect Aβ secretion and APP C-terminal fragment stability. *Human Molecular Genetics*, *10*(16), 1665–1671. https://doi.org/10.1093/hmg/10.16.1665

de Silva, H. V., Stuart, W. D., Duvic, C. R., Wetterau, J. R., Ray, M. J., Ferguson, D. G., Albers, H. W., Smith, W. R., & Harmony, J. A. (1990). A 70-kDa apolipoprotein designated ApoJ is a marker for subclasses of human plasma high density lipoproteins. *Journal of Biological Chemistry*, *265*(22), 13240–13247.

Debure, L., Vayssière, J.-L., Rincheval, V., Loison, F., Dréan, Y. L., & Michel, D. (2003). Intracellular clusterin causes juxtanuclear aggregate formation and mitochondrial alteration. *Journal of Cell Science*, *116*(15), 3109–3121. https://doi.org/10.1242/jcs.00619

DeKosky, S. T., & Scheff, S. W. (1990). Synapse loss in frontal cortex biopsies in Alzheimer's disease: Correlation with cognitive severity. *Annals of Neurology*, *27*(5), 457–464. https://doi.org/10.1002/ana.410270502

Deltcheva, E., Chylinski, K., Sharma, C. M., Gonzales, K., Chao, Y., Pirzada, Z. A., Eckert, M. R., Vogel, J., & Charpentier, E. (2011). CRISPR RNA maturation by trans -encoded small RNA and host factor RNase III. *Nature*, *471*(7340), 602–607. https://doi.org/10.1038/nature09886

DeMattos, R., Cirrito, J., Parsadanian, M., May, P., O'Dell, M., Taylor, J., Harmony, J., Aronow, B., Bales, K., Paul, S., & Holtzman, D. (2004). ApoE and Clusterin Cooperatively Suppress Aβ Levels and Deposition: Evidence that ApoE Regulates Extracellular Aβ Metabolism In Vivo.

DeMattos, R., O'dell, M., Parsadanian, M., Taylor, J. W., Harmony, J., Bales, K., Paul, S., Aronow, B., & Holtzman, D. (2002). Clusterin promotes amyloid plaque formation and is critical for neuritic toxicity in a mouse model of Alzheimer's disease. *Proceedings of the National Academy of Sciences*, *99*(16), 10843–10848. https://doi.org/10.1073/pnas.162228299

Domenici, M. R., Paradisi, S., Sacchetti, B., Gaudi, S., Balduzzi, M., Bernardo, A., Ajmone-Cat, M. A., Minghetti, L., & Malchiodi-Albedi, F. (2002). The presence of astrocytes enhances β-amyloid-induced neurotoxicity in hippocampal cell cultures. *Journal of Physiology, Paris*, *96*(3–4), 313–316. https://doi.org/10.1016/s0928-4257(02)00021-9

Doran, E., Keator, D., Head, E., Phelan, M. J., Kim, R., Totoiu, M., Barrio, J. R., Small, G. W., Potkin, S. G., & Lott, I. T. (2017). Down Syndrome, Partial Trisomy 21, and Absence of Alzheimer's Disease: The Role of APP. *Journal of Alzheimer's Disease: JAD*, *56*(2),

459–470. https://doi.org/10.3233/JAD-160836

Drummond, E., & Wisniewski, T. (2017). Alzheimer's disease: Experimental models and reality. *Acta Neuropathologica*, *133*(2), 155–175. https://doi.org/10.1007/s00401-016-1662-x

Duan, L., Bhattacharyya, B. J., Belmadani, A., Pan, L., Miller, R. J., & Kessler, J. A. (2014). Stem cell derived basal forebrain cholinergic neurons from Alzheimer's disease patients are more susceptible to cell death. *Molecular Neurodegeneration*, *9*(1), 3. https://doi.org/10.1186/1750-1326-9-3

Dunckley, T., Beach, T. G., Ramsey, K. E., Grover, A., Mastroeni, D., Walker, D. G., LaFleur, B. J., Coon, K. D., Brown, K. M., Caselli, R., Kukull, W., Higdon, R., McKeel, D., Morris, J. C., Hulette, C., Schmechel, D., Reiman, E. M., Rogers, J., & Stephan, D. A. (2006). Gene expression correlates of neurofibrillary tangles in Alzheimer's disease. *Neurobiology of Aging*, *27*(10), 1359–1371. https://doi.org/10.1016/j.neurobiolaging.2005.08.013

Elbashir, S. (2002). Analysis of gene function in somatic mammalian cells using small interfering RNAs. *Methods*, *26*(2), 199–213. https://doi.org/10.1016/S1046-2023(02)00023-3

Flanagan, L., Whyte, L., Chatterjee, N., & Tenniswood, M. (2010). Effects of clusterin over-expression on metastatic progression and therapy in breast cancer. *BMC Cancer*, *10*(1), 107. https://doi.org/10.1186/1471-2407-10-107

Forloni, G. (1993). Beta-amyloid neurotoxicity. *Functional Neurology*, 8(3), 211-25.

Fortin, J.-P., Tan, J., Gascoigne, K. E., Haverty, P. M., Forrest, W. F., Costa, M. R., & Martin, S. E. (2019). Multiple-gene targeting, and mismatch tolerance can confound analysis of genome-wide pooled CRISPR screens. *Genome Biology*, *20*(1), 21.

https://doi.org/10.1186/s13059-019-1621-7

Foster, E. M., Dangla-Valls, A., Lovestone, S., Ribe, E. M., & Buckley, N. J. (2019). Clusterin in Alzheimer's Disease: Mechanisms, Genetics, and Lessons From Other Pathologies. *Frontiers in Neuroscience*, *13*. https://doi.org/10.3389/fnins.2019.00164

Fu, Y., Foden, J. A., Khayter, C., Maeder, M. L., Reyon, D., Joung, J. K., & Sander, J. D. (2013). High-frequency off-target mutagenesis induced by CRISPR-Cas nucleases in human cells. *Nature Biotechnology*, *31*(9), 822–826. https://doi.org/10.1038/nbt.2623

Fujio, K., Sato, M., Uemura, T., Sato, T., Sato-Harada, R., & Harada, A. (2007). 14-3-3 proteins and protein phosphatases are not reduced in tau-deficient mice. *NeuroReport*, *18*(10), 1049–1052. https://doi.org/10.1097/WNR.0b013e32818b2a0b

Garneau, J. E., Dupuis, M.-È., Villion, M., Romero, D. A., Barrangou, R., Boyaval, P., Fremaux, C., Horvath, P., Magadán, A. H., & Moineau, S. (2010). The CRISPR/Cas bacterial immune system cleaves bacteriophage and plasmid DNA. *Nature*, *468*(7320), 67–71. https://doi.org/10.1038/nature09523

Gasiunas, G., Barrangou, R., Horvath, P., & Siksnys, V. (2012). Cas9-crRNA ribonucleoprotein complex mediates specific DNA cleavage for adaptive immunity in bacteria. *Proceedings of the National Academy of Sciences*, *109*(39), E2579–E2586. https://doi.org/10.1073/pnas.1208507109

Ghiso, J., Matsubara, E., Koudinov,B., & Frangione, B. 'The Cerebrospinal-Fluid Soluble Form of Alzheimer's Amyloid Beta Is Complexed to SP-40,40 (Apolipoprotein J), an Inhibitor of the Complement Membrane-Attack Complex'. *Biochemical Journal* 1, no. 293 (1993): 27–30. https://doi.org/10.1042/bj2930027.

Goate, A., Chartier-Harlin, M.-C., Mullan, M., Brown, J., Crawford, F., Fidani, L., Giuffra, L., Haynes, A., Irving, N., James, L., Mant, R., Newton, P., Rooke, K., Roques, P., Talbot, C., Pericak-Vance, M., Roses, A., Williamson, R., Rossor, M., … Hardy, J. (1991). Segregation of a missense mutation in the amyloid precursor protein gene with familial Alzheimer's disease. Nature, 349(6311), 704–706. https://doi.org/10.1038/349704a0

Gomez-Arboledas, A., Davila, J. C., Sanchez-Mejias, E., Navarro, V., Nuñez-Diaz, C., Sanchez-Varo, R., Sanchez-Mico, M. V., Trujillo-Estrada, L., Fernandez-Valenzuela, J. J., Vizuete, M., Comella, J. X., Galea, E., Vitorica, J., & Gutierrez, A. (2018). Phagocytic clearance of presynaptic dystrophies by reactive astrocytes in Alzheimer's disease. *Glia*, *66*(3), 637–653. https://doi.org/10.1002/glia.23270

Götz, J., Bodea, L.-G., & Goedert, M. (2018). Rodent models for Alzheimer disease. *Nature Reviews Neuroscience*, *19*(10), 583–598. https://doi.org/10.1038/s41583-018-0054-8

Green, D. R. (2004). The Pathophysiology of Mitochondrial Cell Death. *Science*, *305*(5684), 626–629. https://doi.org/10.1126/science.1099320

Gregory, J. M., Whiten, D. R., Brown, R. A., Barros, T. P., Kumita, J. R., Yerbury, J. J., Satapathy, S., McDade, K., Smith, C., Luheshi, L. M., Dobson, C. M., & Wilson, M. R. (2017). Clusterin protects neurons against intracellular proteotoxicity. *Acta Neuropathologica Communications*, *5*(1), 81. https://doi.org/10.1186/s40478-017-

0481-1

Grissa, I., Vergnaud, G., & Pourcel, C. (2007). CRISPRFinder: A web tool to identify clustered regularly interspaced short palindromic repeats. *Nucleic Acids Research*, *35*(Web Server), W52–W57. https://doi.org/10.1093/nar/gkm360

Grolla, A. A., Fakhfouri, G., Balzaretti, G., Marcello, E., Gardoni, F., Canonico, P. L., DiLuca, M., Genazzani, A. A., & Lim, D. (2013). Aβ leads to Ca^{2+} signaling alterations and transcriptional changes in glial cells. *Neurobiology of Aging*, *34*(2), 511–522. https://doi.org/10.1016/j.neurobiolaging.2012.05.005

Guenther, Matthew G., Garrett M. Frampton, Frank Soldner, Dirk Hockemeyer, Maya Mitalipova, Rudolf Jaenisch, and Richard A. Young. 'Chromatin Structure and Gene Expression Programs of Human Embryonic and Induced Pluripotent Stem Cells'. *Cell Stem Cell* 7, no. 2 (6 August 2010): 249–57. https://doi.org/10.1016/j.stem.2010.06.015.

Haass, C., Kaether, C., Thinakaran, G., & Sisodia, S. (2012). Trafficking and Proteolytic Processing of APP. *Cold Spring Harbor Perspectives in Medicine*, *2*(5). https://doi.org/10.1101/cshperspect.a006270

Haight, T., Bryan, R. N., Meirelles, O., Tracy, R., Fornage, M., Richard, M., Nasrallah, I., Yaffe, K., Jacobs, D. R., Lewis, C., Schreiner, P., Sidney, S., Davatzikos, C., & Launer, L. J. (2018). Associations of plasma clusterin and Alzheimer's disease-related MRI markers in adults at mid-life: The CARDIA Brain MRI sub-study. *PLoS ONE*, *13*(1). https://doi.org/10.1371/journal.pone.0190478

Hammad, S. M., Ranganathan, S., Loukinova, E., Twal, W. O., & Argraves, W. S. (1997). Interaction of apolipoprotein J-amyloid beta-peptide complex with low density lipoprotein receptor-related protein-2/megalin. A mechanism to prevent

pathological accumulation of amyloid beta-peptide. *The Journal of Biological Chemistry*, *272*(30), 18644–18649. https://doi.org/10.1074/jbc.272.30.18644

Harada, A., Oguchi, K., Okabe, S., Kuno, J., Terada, S., Ohshima, T., Sato-Yoshitake, R., Takei, Y., Noda, T., & Hirokawa, N. (1994). Altered microtubule organization in small-calibre axons of mice lacking tau protein. *Nature*, *369*(6480), 488–491. https://doi.org/10.1038/369488a0

Hardy, J. A., & Higgins, G. A. (1992). Alzheimer's disease: The amyloid cascade hypothesis. *Science*, *256*(5054), 184–185. https://doi.org/10.1126/science.1566067

Harold, D., Abraham, R., Hollingworth, P., Sims, R., Gerrish, A., Hamshere, M. L., Pahwa, J. S., Moskvina, V., Dowzell, K., Williams, A., Jones, N., Thomas, C., Stretton, A., Morgan, A. R., Lovestone, S., Powell, J., Proitsi, P., Lupton, M. K., Brayne, C., … Williams, J. (2009). Genome-wide association study identifies variants at *CLU* and *PICALM* associated with Alzheimer's disease. *Nature Genetics*, *41*(10), 1088–1093. https://doi.org/10.1038/ng.440

Head, E., Powell, D., Gold, B. T., & Schmitt, F. A. (2012). Alzheimer's Disease in Down Syndrome. *European Journal of Neurodegenerative Disease*, *1*(3), 353–364.

Hedegaard, A., Monzón-Sandoval, J., Newey, S. E., Whiteley, E. S., Webber, C., & Akerman, C. J. (2020). Pro-maturational Effects of Human iPSC-Derived Cortical Astrocytes upon iPSC-Derived Cortical Neurons. *Stem Cell Reports*, *15*(1), 38–51. https://doi.org/10.1016/j.stemcr.2020.05.003

Heigwer, F., Kerr, G., & Boutros, M. (2014). E-CRISP: Fast CRISPR target site identification. *Nature Methods*, *11*(2), 122–123. https://doi.org/10.1038/nmeth.2812

Hemmati-Brivanlou, A., & Melton, D. (1997). Vertebrate Embryonic Cells Will Become Nerve Cells Unless Told Otherwise. *Cell*, *88*(1), 13–17.

https://doi.org/10.1016/S0092-8674(00)81853-X

Hennekam, R. C. M. (2006). Hutchinson–Gilford progeria syndrome: Review of the phenotype. *American Journal of Medical Genetics Part A*, *140A*(23), 2603–2624. https://doi.org/10.1002/ajmg.a.31346

Herring, S. K., Moon, H.-J., Rawal, P., Chhibber, A., & Zhao, L. (2019). Brain clusterin protein isoforms and mitochondrial localization. *ELife*, *8*, e48255. https://doi.org/10.7554/eLife.48255

Hesse, R., Hurtado, M. L., Jackson, R. J., Eaton, S. L., Herrmann, A. G., Colom-Cadena, M., Tzioras, M., King, D., Rose, J., Tulloch, J., McKenzie, C.-A., Smith, C., Henstridge, C. M., Lamont, D., Wishart, T. M., & Spires-Jones, T. L. (2019). Comparative profiling of the synaptic proteome from Alzheimer's disease patients with focus on the APOE genotype. *Acta Neuropathologica Communications*, *7*(1), 214. https://doi.org/10.1186/s40478-019-0847-7

Horvath, P., & Barrangou, R. (2010). CRISPR/Cas, the immune system of bacteria and Archaea. *Science (New York, N.Y.)*, *327*, 167–170. https://doi.org/10.1126/science.1179555

Hossini, A. M., Megges, M., Prigione, A., Lichtner, B., Toliat, M. R., Wruck, W., Schröter, F., Nuernberg, P., Kroll, H., Makrantonaki, E., Zouboulis, C. C., Zoubouliss, C. C., & Adjaye, J. (2015). Induced pluripotent stem cell-derived neuronal cells from a sporadic Alzheimer's disease donor as a model for investigating AD-associated gene regulatory networks. *BMC Genomics*, *16*, 84. https://doi.org/10.1186/s12864-015-1262-5

Hsu, P. D., Scott, D. A., Weinstein, J. A., Ran, F. A., Konermann, S., Agarwala, V., Li, Y., Fine, E. J., Wu, X., Shalem, O., Cradick, T. J., Marraffini, L. A., Bao, G., & Zhang, F. (2013).

DNA targeting specificity of RNA-guided Cas9 nucleases. *Nature Biotechnology*, *31*(9), 827–832. https://doi.org/10.1038/nbt.2647

Hu, W., Qiu, B., Guan, W., Wang, Q., Wang, M., Li, W., Gao, L., Shen, L., Huang, Y., Xie, G., Zhao, H., Jin, Y., Tang, B., Yu, Y., Zhao, J., & Pei, G. (2015). Direct Conversion of Normal and Alzheimer's Disease Human Fibroblasts into Neuronal Cells by Small Molecules. *Cell Stem Cell*, *17*(2), 204–212. https://doi.org/10.1016/j.stem.2015.07.006

Huang, Y.-W. A., Zhou, B., Wernig, M., & Südhof, T. C. (2017). ApoE2, ApoE3 and ApoE4 Differentially Stimulate APP Transcription and Aβ Secretion. *Cell*, *168*(3), 427-441.e21. https://doi.org/10.1016/j.cell.2016.12.044

Humphreys, D. T., Carver, J. A., Easterbrook-Smith, S. B., & Wilson, M. R. (1999). Clusterin Has Chaperone-like Activity Similar to That of Small Heat Shock Proteins. *Journal of Biological Chemistry*, *274*(11), 6875–6881. https://doi.org/10.1074/jbc.274.11.6875

Ikegami, S., Harada, A., & Hirokawa, N. (2000). Muscle weakness, hyperactivity, and impairment in fear conditioning in tau-deficient mice. *Neuroscience Letters*, *279*(3), 129–132. https://doi.org/10.1016/S0304-3940(99)00964-7

Ishino, Y., Shinagawa, H., Makino, K., Amemura, M., & Nakata, A. (1987). Nucleotide sequence of the iap gene, responsible for alkaline phosphatase isozyme conversion in Escherichia coli, and identification of the gene product. *Journal of Bacteriology*, *169*(12), 5429–5433. https://doi.org/10.1128/JB.169.12.5429-5433.1987

Israel, M. A., Yuan, S. H., Bardy, C., Reyna, S. M., Mu, Y., Herrera, C., Hefferan, M. P., Van Gorp, S., Nazor, K. L., Boscolo, F. S., Carson, C. T., Laurent, L. C., Marsala, M., Gage, F. H., Remes, A. M., Koo, E. H., & Goldstein, L. S. B. (2012). Probing sporadic and

familial Alzheimer's disease using induced pluripotent stem cells. *Nature*, *482*(7384), 216–220. https://doi.org/10.1038/nature10821

Ittner, L. M., Ke, Y. D., Delerue, F., Bi, M., Gladbach, A., van Eersel, J., Wölfing, H., Chieng, B. C., Christie, M. J., Napier, I. A., Eckert, A., Staufenbiel, M., Hardeman, E., & Götz, J. (2010). Dendritic Function of Tau Mediates Amyloid-β Toxicity in Alzheimer's Disease Mouse Models. *Cell*, *142*(3), 387–397. https://doi.org/10.1016/j.cell.2010.06.036

Jackson, R. J., Rose, J., Tulloch, J., Henstridge, C., Smith, C., & Spires-Jones, T. L. (2019). Clusterin accumulates in synapses in Alzheimer's disease and is increased in apolipoprotein E4 carriers. *Brain Communications*, *1*(fcz003). https://doi.org/10.1093/braincomms/fcz003

Jackson, S. P., & Jeggo, P. A. (1995). DNA double-strand break repair and V(D)J recombination: Involvement of DNA-PK. *Trends in Biochemical Sciences*, *20*(10), 412–415. https://doi.org/10.1016/s0968-0004(00)89090-8

Jacobi, A. M., Rettig, G. R., Turk, R., Collingwood, M. A., Zeiner, S. A., Quadros, R. M., Harms, D. W., Bonthuis, P. J., Gregg, C., Ohtsuka, M., Gurumurthy, C. B., & Behlke, M. A. (2017). Simplified CRISPR tools for efficient genome editing and streamlined protocols for their delivery into mammalian cells and mouse zygotes. *Methods*, *121–122*, 16–28. https://doi.org/10.1016/j.ymeth.2017.03.021

Jansen, R., Embden, J. D. A. van, Gaastra, W., & Schouls, L. M. (2002). Identification of genes that are associated with DNA repeats in prokaryotes. *Molecular Microbiology*, *43*(6), 1565–1575. https://doi.org/10.1046/j.1365-2958.2002.02839.

Jenne, D. E., & Tschopp, J. (1989). Molecular structure and functional characterization of a human complement cytolysis inhibitor found in blood and seminal plasma: Identity to sulfated glycoprotein 2, a constituent of rat testis fluid. *Proceedings of the National Academy of Sciences of the United States of America*, *86*(18), 7123–7127.

Jiang, X., & Nardelli, J. (2016). Cellular and molecular introduction to brain development. *Neurobiology of Disease*, *92*, 3–17. https://doi.org/10.1016/j.nbd.2015.07.007

Jin, Y.-H., Joo, H., Lee, K., Kim, H., Didier, R., Yang, Y., Shin, H., & Lee, C. (2019). Streamlined procedure for gene knockouts using all-in-one adenoviral CRISPR-Cas9. *Scientific Reports*, *9*(1), 277. https://doi.org/10.1038/s41598-018-36736-y

Jinek, M., Chylinski, K., Fonfara, I., Hauer, M., Doudna, J. A., & Charpentier, E. (2012). A Programmable Dual-RNA-Guided DNA Endonuclease in Adaptive Bacterial Immunity. *Science*, *337*(6096), 816–821. https://doi.org/10.1126/science.1225829

Jinek, M, East, A., Cheng, A., Lin, S., Ma, E., & Doudna, J. (2013). RNA-programmed genome editing in human cells. *ELife*, *2*, e00471. https://doi.org/10.7554/eLife.00471

Jones, L., Holmans, P. A., Hamshere, M. L., Harold, D., Moskvina, V., Ivanov, D., Pocklington, A., Abraham, R., Hollingworth, P., Sims, R., Gerrish, A., Pahwa, J. S., Jones, N., Stretton, A., Morgan, A. R., Lovestone, S., Powell, J., Proitsi, P., Lupton, M. K., … Williams, J. (2010). Genetic Evidence Implicates the Immune System and Cholesterol Metabolism in the Aetiology of Alzheimer's Disease. *PLOS ONE*, *5*(11), e13950. https://doi.org/10.1371/journal.pone.0013950

Joung, J. K., & Sander, J. D. (2013). TALENs: A widely applicable technology for targeted genome editing. *Nature Reviews Molecular Cell Biology*, *14*(1), 49–55. https://doi.org/10.1038/nrm3486

Kanehisa, M., Furumichi, M., Sato, Y., Ishiguro-Watanabe, M., & Tanabe, M. (2021). KEGG: Integrating viruses and cellular organisms. *Nucleic Acids Research*, *49*(D1), D545–D551. https://doi.org/10.1093/nar/gkaa970

Kang, S.-W., Shin, Y.-J., Shim, Y.-J., Jeong, S.-Y., Park, I.-S., & Min, B.-H. (2005). Clusterin interacts with SCLIP (SCG10-like protein) and promotes neurite outgrowth of PC12 cells. *Experimental Cell Research*, *309*(2), 305–315. https://doi.org/10.1016/j.yexcr.2005.06.012

Kapron, J. T., Hilliard, G. M., Lakins, J. N., Tenniswood, M. P., West, K. A., Carr, S. A., & Crabb, J. W. (1997). Identification and characterization of glycosylation sites in human serum clusterin. *Protein Science: A Publication of the Protein Society*, *6*(10), 2120–2133.

Killick, R, Ribe, E. M., Al-Shawi, R., Malik, B., Hooper, C., Fernandes, C., Dobson, R., Nolan, P. M., Lourdusamy, A., Furney, S., Lin, K., Breen, G., Wroe, R., To, A. W. M., Leroy, K., Causevic, M., Usardi, A., Robinson, M., Noble, W., … Lovestone, S. (2014). Clusterin regulates β-amyloid toxicity via Dickkopf-1-driven induction of the wnt–PCP–JNK pathway. *Molecular Psychiatry*, *19*(1), 88–98. https://doi.org/10.1038/mp.2012.163

Kilpinen, H., Goncalves, A., Leha, A., Afzal, V., Alasoo, K., Ashford, S., Bala, S., Bensaddek, D., Casale, F. P., Culley, O. J., Danecek, P., Faulconbridge, A., Harrison, P. W., Kathuria, A., McCarthy, D., McCarthy, S. A., Meleckyte, R., Memari, Y., Moens, N., … Gaffney, D. J. (2017). Common genetic variation drives molecular heterogeneity in human iPSCs. *Nature*, *546*(7658), 370–375. https://doi.org/10.1038/nature22403

Kim, N., Yoo, J. C., Han, J. Y., Hwang, E. M., Kim, Y. S., Jeong, E. Y., Sun, C.-H., Yi, G.-S., Roh, G. S., Kim, H. J., Kang, S. S., Cho, G. J., Park, J.-Y., & Choi, W. S. (2012). Human

nuclear clusterin mediates apoptosis by interacting with Bcl-XL through C-terminal coiled coil domain. *Journal of Cellular Physiology*, *227*(3), 1157–1167. https://doi.org/10.1002/jcp.22836

Kim, S., Kim, D., Cho, S. W., Kim, J., & Kim, J.-S. (2014). Highly efficient RNA-guided genome editing in human cells via delivery of purified Cas9 ribonucleoproteins. *Genome Research*, *24*(6), 1012–1019. https://doi.org/10.1101/gr.171322.113

Kirszbaum, L., Bozas, S. E., & Walker, I. D. (1992). SP-40,40, a protein involved in the control of the complement pathway, possesses a unique array of disulphide bridges. *FEBS Letters*, *297*(1–2), 70–76. https://doi.org/10.1016/0014-5793(92)80330-J

Koistinaho, M., Lin, S., Wu, X., Esterman, M., Koger, D., Hanson, J., Higgs, R., Liu, F., Malkani, S., Bales, K. R., & Paul, S. M. (2004). Apolipoprotein E promotes astrocyte colocalization and degradation of deposited amyloid-β peptides. *Nature Medicine*, *10*(7), 719–726. https://doi.org/10.1038/nm1058

Kondo, T., Asai, M., Tsukita, K., Kutoku, Y., Ohsawa, Y., Sunada, Y., Imamura, K., Egawa, N., Yahata, N., Okita, K., Takahashi, K., Asaka, I., Aoi, T., Watanabe, A., Watanabe, K., Kadoya, C., Nakano, R., Watanabe, D., Maruyama, K., … Inoue, H. (2013). Modeling Alzheimer's Disease with iPSCs Reveals Stress Phenotypes Associated with Intracellular Aβ and Differential Drug Responsiveness. *Cell Stem Cell*, *12*(4), 487–496. https://doi.org/10.1016/j.stem.2013.01.009

Kosicki, M., Tomberg, K., & Bradley, A. (2018). Repair of double-strand breaks induced by CRISPR–Cas9 leads to large deletions and complex rearrangements. *Nature Biotechnology*, *36*(8), 765–771. https://doi.org/10.1038/nbt.4192

Kosik, K. S., Joachim, C. L., & Selkoe, D. J. (1986). Microtubule-associated protein tau (tau) is a major antigenic component of paired helical filaments in Alzheimer disease. *Proceedings of the National Academy of Sciences of the United States of America*, *83*(11), 4044–4048.

Kounnas, M. Z., Rebeck, G. W., Bush, A. I., Argraves, W. S., Hyman, B. T., & Stricklandt, D. K. (1995). LDL Receptor-Related Protein, a Multifunctional ApoE Receptor, Binds Secreted I -Amyloid Precursor Protein and Mediates Its Degradation. 10.

Kraft, A. W., Hu, X., Yoon, H., Yan, P., Xiao, Q., Wang, Y., Gil, S. C., Brown, J., Wilhelmsson, U., Restivo, J. L., Cirrito, J. R., Holtzman, D. M., Kim, J., Pekny, M., & Lee, J. (2013). Attenuating astrocyte activation accelerates plaque pathogenesis in APP/PS1 mice. *The FASEB Journal*, *27*(1), 187–198. https://doi.org/10.1096/fj.12-208660

Kususda, Y., Miyake, H., Gleave, M. E., & Fujisawa, M. (2012). Clusterin inhibition using OGX-011 synergistically enhances antitumour activity of sorafenib in a human renal cell carcinoma model. *British Journal of Cancer*, *106*(12), 1945–1952. https://doi.org/10.1038/bjc.2012.209

Kwart, D., Gregg, A., Scheckel, C., Murphy, E. A., Paquet, D., Duffield, M., Fak, J., Olsen, O., Darnell, R. B., & Tessier-Lavigne, M. (2019). A Large Panel of Isogenic APP and PSEN1 Mutant Human iPSC Neurons Reveals Shared Endosomal Abnormalities Mediated by APP β-CTFs, Not Aβ. *Neuron*, *104*(2), 256-270.e5. https://doi.org/10.1016/j.neuron.2019.07.010

Lakins, J., Bennett, S. A. L., Chen, J.-H., Arnold, J. M., Morrissey, C., Wong, P., O'Sullivan, J., & Tenniswood, M. (1998). Clusterin Biogenesis Is Altered during Apoptosis in the Regressing Rat Ventral Prostate. *Journal of Biological Chemistry*, *273*(43), 27887–27895. https://doi.org/10.1074/jbc.273.43.27887

Lambert, J.-C., Genetic and Environmental Risk in Alzheimer's Disease (GERAD), Alzheimer's Disease Genetic Consortium (ADGC), Cohorts for Heart and Aging Research in Genomic Epidemiology (CHARGE), Ibrahim-Verbaas, C. A., Harold, D., Naj, A. C., Sims, R., Bellenguez, C., Jun, G., DeStefano, A. L., Bis, J. C., Beecham, G. W., Grenier-Boley, B., Russo, G., Thornton-Wells, T. A., Jones, N., Smith, A. V., Chouraki, V., … European Alzheimer's Disease Initiative (EADI). (2013). Meta-analysis of 74,046 individuals identifies 11 new susceptibility loci for Alzheimer's disease. *Nature Genetics*, *45*(12), 1452–1458. https://doi.org/10.1038/ng.2802

Lambert, J.-C., Heath, S., Even, G., Campion, D., Sleegers, K., Hiltunen, M., Combarros, O., Zelenika, D., Bullido, M. J., Tavernier, B., Letenneur, L., Bettens, K., Berr, C., Pasquier, F., Fiévet, N., Barberger-Gateau, P., Engelborghs, S., De Deyn, P., Mateo, I., … the European Alzheimer's Disease Initiative Investigators. (2009). Genome-wide association study identifies variants at *CLU* and *CR1* associated with Alzheimer's disease. *Nature Genetics*, *41*(10), 1094–1099. https://doi.org/10.1038/ng.439

Lancaster, T. M., Brindley, L. M., Tansey, K. E., Sims, R. C., Mantripragada, K., Owen, M. J., Williams, J., & Linden, D. E. J. (2015). Alzheimer's disease risk variant in *CLU* is associated with neural inefficiency in healthy individuals. *Alzheimer's & Dementia: The Journal of the Alzheimer's Association*, *11*(10), 1144–1152. https://doi.org/10.1016/j.jalz.2014.10.012

Lawrence, M., Huber, W., Pagès, H., Aboyoun, P., Carlson, M., Gentleman, R., Morgan, M. T., & Carey, V. J. (2013). Software for Computing and Annotating Genomic Ranges. *PLOS Computational Biology*, *9*(8), e1003118. https://doi.org/10.1371/journal.pcbi.1003118

Le, T. T. H., Tran, N. T., Dao, T. M. L., Nguyen, D. D., Do, H. D., Ha, T. L., Kühn, R., Nguyen, T. L., Rajewsky, K., & Chu, V. T. (2019). Efficient and Precise CRISPR/Cas9-Mediated MECP2 Modifications in Human-Induced Pluripotent Stem Cells. *Frontiers in Genetics*, *10*. https://doi.org/10.3389/fgene.2019.00625

Lee, S. E., Mitchell, R. A., Cheng, A., & Hendrickson, E. A. (1997). Evidence for DNA-PK-dependent and -independent DNA double-strand break repair pathways in mammalian cells as a function of the cell cycle. *Molecular and Cellular Biology*, *17*(3), 1425–1433. https://doi.org/10.1128/mcb.17.3.1425

Lei, P., Ayton, S., Finkelstein, D. I., Spoerri, L., Ciccotosto, G. D., Wright, D. K., Wong, B. X. W., Adlard, P. A., Cherny, R. A., Lam, L. Q., Roberts, B. R., Volitakis, I., Egan, G. F., McLean, C. A., Cappai, R., Duce, J. A., & Bush, A. I. (2012). Tau deficiency induces parkinsonism with dementia by impairing APP-mediated iron export. *Nature Medicine*, *18*(2), 291–295. https://doi.org/10.1038/nm.2613

Lejeune, J., Gautier, M., & Turpin, R. (1959). [Study of somatic chromosomes from 9 mongoloid children]. *Comptes Rendus Hebdomadaires Des Seances De l'Academie Des Sciences*, *248*(11), 1721–1722.

Leskov, K. S., Klokov, D. Y., Li, J., Kinsella, T. J., & Boothman, D. A. (2003). Synthesis and Functional Analyses of Nuclear Clusterin, a Cell Death Protein. *Journal of Biological Chemistry*, *278*(13), 11590–11600. https://doi.org/10.1074/jbc.M209233200

Levy-Lahad, E., Wijsman, E.M., Nemens, E., Anderson, L., Goddard, K. A. B., Weber, J. L., Bird, T.B., & Schellenberg, G. D. (1995). A Familial Alzheimer's Disease Locus on Chromosome I. *Science*, *269*(5226), 970-973.

Lewis, D. A., Campbell, M. J., Terry, R. D., & Morrison, J. H. (1987). Laminar and regional distributions of neurofibrillary tangles and neuritic plaques in Alzheimer's disease:

A quantitative study of visual and auditory cortices. *The Journal of Neuroscience: The Official Journal of the Society for Neuroscience*, *7*(6), 1799–1808.

Lewis, J., Dickson, D. W., Lin, W.-L., Chisholm, L., Corral, A., Jones, G., Yen, S.-H., Sahara, N., Skipper, L., Yager, D., Eckman, C., Hardy, J., Hutton, M., & McGowan, E. (2001). Enhanced Neurofibrillary Degeneration in Transgenic Mice Expressing Mutant Tau and APP. *Science*, *293*(5534), 1487–1491. https://doi.org/10.1126/science.1058189

Li, Y. P., A. F. Bushnell, C. M. Lee, L. S. Perlmutter, and S. K. Wong. 'Beta-Amyloid Induces Apoptosis in Human-Derived Neurotypic SH-SY5Y Cells'. *Brain Research* 738, no. 2 (4 November 1996): 196–204. https://doi.org/10.1016/s0006-8993(96)00733-0.

Li, N., Zoubeidi, A., Beraldi, E., & Gleave, M. E. (2013). GRP78 regulates clusterin stability, retrotranslocation and mitochondrial localization under ER stress in prostate cancer. *Oncogene*, *32*(15), 1933–1942. https://doi.org/10.1038/onc.2012.212

Li, X.L., Li, G.-H., Fu, J., Fu, Y.-W., Zhang, L., Chen, W., Arakaki, C., Zhang, J.-P., Wen, W., Zhao, M., Chen, W. V., Botimer, G. D., Baylink, D., Aranda, L., Choi, H., Bechar, R., Talbot, P., Sun, C.-K., Cheng, T., & Zhang, X.-B. (2018). Highly efficient genome editing via CRISPR–Cas9 in human pluripotent stem cells is achieved by transient BCL-XL overexpression. *Nucleic Acids Research*, *46*(19), 10195–10215. https://doi.org/10.1093/nar/gky804

Liang, X., Potter, J., Kumar, S., Zou, Y., Quintanilla, R., Sridharan, M., Carte, J., Chen, W., Roark, N., Ranganathan, S., Ravinder, N., & Chesnut, J. D. (2015). Rapid and highly efficient mammalian cell engineering via Cas9 protein transfection. *Journal of Biotechnology*, *208*, 44–53. https://doi.org/10.1016/j.jbiotec.2015.04.024

Liang, Gaoyang, and Yi Zhang. 'Embryonic Stem Cell and Induced Pluripotent Stem Cell: An Epigenetic Perspective'. *Cell Research* 23, no. 1 (January 2013): 49–69. https://doi.org/10.1038/cr.2012.175.

Lloret, A., Esteve, D., Lloret, M.-A., Cervera-Ferri, A., Lopez, B., Nepomuceno, M., & Monllor, P. (2019). When Does Alzheimer's Disease Really Start? The Role of Biomarkers. *International Journal of Molecular Sciences*, *20*(22). https://doi.org/10.3390/ijms20225536

Love, M. I., Huber, W., & Anders, S. (2014). Moderated estimation of fold change and dispersion for RNA-seq data with DESeq2. *Genome Biology*, *15*(12), 550. https://doi.org/10.1186/s13059-014-0550-8

Mahairaki, V., Ryu, J., Peters, A., Chang, Q., Li, T., Park, T. S., Burridge, P. W., Talbot, C. C., Asnaghi, L., Martin, L. J., Zambidis, E. T., & Koliatsos, V. E. (2014). Induced Pluripotent Stem Cells from Familial Alzheimer's Disease Patients Differentiate into Mature Neurons with Amyloidogenic Properties. *Stem Cells and Development*, *23*(24), 2996–3010. https://doi.org/10.1089/scd.2013.0511

Makarova, K. S., Haft, D. H., Barrangou, R., Brouns, S. J. J., Charpentier, E., Horvath, P., Moineau, S., Mojica, F. J. M., Wolf, Y. I., Yakunin, A. F., van der Oost, J., & Koonin, E. V. (2011). Evolution and classification of the CRISPR–Cas systems. *Nature Reviews Microbiology*, *9*(6), 467–477. https://doi.org/10.1038/nrmicro2577

Malchiodi-Albedi, F., Domenici, M. R., Paradisi, S., Bernardo, A., Ajmone-Cat, M. A., & Minghetti, L. (2001). Astrocytes contribute to neuronal impairment in βA toxicity increasing apoptosis in rat hippocampal neurons. *Glia*, *34*(1), 68–72. https://doi.org/10.1002/glia.1041

Mali, P., Yang, L., Esvelt, K. M., Aach, J., Guell, M., DiCarlo, J. E., Norville, J. E., & Church, G. M. (2013). RNA-Guided Human Genome Engineering via Cas9. *Science (New York, N.Y.)*, *339*(6121), 823–826. https://doi.org/10.1126/science.1232033

Martin-Rehrmann, M. D., Hoe, H.-S., Capuani, E. M., & Rebeck, G. W. (2005). Association of apolipoprotein J-positive β-amyloid plaques with dystrophic neurites in alzheimer's disease brain. *Neurotoxicity Research*, *7*(3), 231–241. https://doi.org/10.1007/BF03036452

Massi, F., Klimov, D., Thirumalai, D., & Straub, J. E. (2002). Charge states rather than propensity for β-structure determine enhanced fibrillogenesis in wild-type Alzheimer's β-amyloid peptide compared to E22Q Dutch mutant. *Protein Science: A Publication of the Protein Society*, *11*(7), 1639–1647.

Mastroiacovo, F., Busceti, C. L., Biagioni, F., Moyanova, S. G., Meisler, M. H., Battaglia, G., Caricasole, A., Bruno, V., & Nicoletti, F. (2009). Induction of the Wnt Antagonist, Dickkopf-1, Contributes to the Development of Neuronal Death in Models of Brain Focal Ischemia. *Journal of Cerebral Blood Flow & Metabolism*, *29*(2), 264–276. https://doi.org/10.1038/jcbfm.2008.111

Matsubara, E., Soto, C., Governale, S., Frangione, B., & Ghiso, J. (1996). Apolipoprotein J and Alzheimer's amyloid β solubility. *Biochemical Journal*, *316*(2), 671–679. https://doi.org/10.1042/bj3160671

Matta, C., Fellows, C. R., Quasnichka, H., Williams, A., Jeremiasse, B., Allaway, D., & Mobasheri, A. (2020). Clusterin secretion is attenuated by pro-inflammatory cytokines in culture models of cartilage degradation. *BioRxiv*, 2020.05.05.078105. https://doi.org/10.1101/2020.05.05.078105

May, P. C., Lampert-Etchells, M., Johnson, S. A., Poirier, J., Masters, J. N., & Finch, C. E. (1990). Dynamics of gene expression for a hippocampal glycoprotein elevated in Alzheimer's disease and in response to experimental lesions in rat. *Neuron*, *5*(6), 831–839. https://doi.org/10.1016/0896-6273(90)90342-D

Mecozzi, V. J., Berman, D. E., Simoes, S., Vetanovetz, C., Awal, M. R., Patel, V. M., Schneider, R. T., Petsko, G. A., Ringe, D., & Small, S. A. (2014). Pharmacological chaperones stabilize retromer to limit APP processing. *Nature Chemical Biology*, *10*(6), 443–449. https://doi.org/10.1038/nchembio.1508

Mederos, S., González-Arias, C., & Perea, G. (2018). Astrocyte–Neuron Networks: A Multilane Highway of Signaling for Homeostatic Brain Function. *Frontiers in Synaptic Neuroscience*, *10*. https://doi.org/10.3389/fnsyn.2018.00045

Mertens, J., Paquola, A. C. M., Ku, M., Hatch, E., Böhnke, L., Ladjevardi, S., McGrath, S., Campbell, B., Lee, H., Herdy, J. R., Gonçalves, J. T., Toda, T., Kim, Y., Winkler, J., Yao, J., Hetzer, M. W., & Gage, F. H. (2015). Directly Reprogrammed Human Neurons Retain Aging-Associated Transcriptomic Signatures and Reveal Age-Related Nucleocytoplasmic Defects. *Cell Stem Cell*, *17*(6), 705–718. https://doi.org/10.1016/j.stem.2015.09.001

Michaelis, M. L., Ranciat, N., Chen, Y., Bechtel, M., Ragan, R., Hepperle, M., Liu, Y., & Georg, G. (1998). Protection against beta-amyloid toxicity in primary neurons by paclitaxel (Taxol). *Journal of Neurochemistry*, *70*(4), 1623–1627. https://doi.org/10.1046/j.1471-4159.1998.70041623.x

Miller, J. C., Holmes, M. C., Wang, J., Guschin, D. Y., Lee, Y.-L., Rupniewski, I., Beausejour, C. M., Waite, A. J., Wang, N. S., Kim, K. A., Gregory, P. D., Pabo, C. O., & Rebar, E. J. (2007). An improved zinc-finger nuclease architecture for highly specific genome

editing. *Nature Biotechnology*, *25*(7), 778–785. https://doi.org/10.1038/nbt1319

Miller, J. C., Tan, S., Qiao, G., Barlow, K. A., Wang, J., Xia, D. F., Meng, X., Paschon, D. E., Leung, E., Hinkley, S. J., Dulay, G. P., Hua, K. L., Ankoudinova, I., Cost, G. J., Urnov, F. D., Zhang, H. S., Holmes, M. C., Zhang, L., Gregory, P. D., & Rebar, E. J. (2011). A TALE nuclease architecture for efficient genome editing. *Nature Biotechnology*, *29*(2), 143–148. https://doi.org/10.1038/nbt.1755

Miller, J. D., Ganat, Y. M., Kishinevsky, S., Bowman, R. L., Liu, B., Tu, E. Y., Mandal, P. K., Vera, E., Shim, J., Kriks, S., Taldone, T., Fusaki, N., Tomishima, M. J., Krainc, D., Milner, T. A., Rossi, D. J., & Studer, L. (2013). Human iPSC-Based Modeling of Late-Onset Disease via Progerin-Induced Aging. *Cell Stem Cell*, *13*(6), 691–705. https://doi.org/10.1016/j.stem.2013.11.006

Mojica, F. J., Díez-Villaseñor, C., Soria, E., & Juez, G. (2000). Biological significance of a family of regularly spaced repeats in the genomes of Archaea, Bacteria and mitochondria. *Molecular Microbiology*, *36*(1), 244–246. https://doi.org/10.1046/j.1365-2958.2000.01838.x

Mojica, F. J., Ferrer, C., Juez, G., & Rodríguez-Valera, F. (1995). Long stretches of short tandem repeats are present in the largest replicons of the Archaea Haloferax mediterranei and Haloferax volcanii and could be involved in replicon partitioning. *Molecular Microbiology*, *17*(1), 85–93. https://doi.org/10.1111/j.1365-2958.1995.mmi_17010085.x

Mojica, F. J, Díez-Villaseñor, C., García-Martínez, J., & Almendros, C. (2009). Short motif sequences determine the targets of the prokaryotic CRISPR defence system. *Microbiology (Reading, England)*, *155*(Pt 3), 733–740. https://doi.org/10.1099/mic.0.023960-0

Mojica, F. J. M., Juez, G., & Rodriguez-Valera, F. (1993). Transcription at different salinities of Haloferax mediterranei sequences adjacent to partially modified PstI sites. *Molecular Microbiology*, *9*(3), 613–621. https://doi.org/10.1111/j.1365-2958.1993.tb01721.x

Mojica, Francisco J.M., Diez-Villasenor, C., Garcia-Martinez, J., & Soria, E. (2005). Intervening Sequences of Regularly Spaced Prokaryotic Repeats Derive from Foreign Genetic Elements. *Journal of Molecular Evolution*, *60*(2), 174–182. https://doi.org/10.1007/s00239-004-0046-3

Moldoveanu, T., Follis, A. V., Kriwacki, R. W., & Green, D. R. (2014). Many players in BCL-2 family affairs. *Trends in Biochemical Sciences*, *39*(3), 101–111. https://doi.org/10.1016/j.tibs.2013.12.006

Moore, S., Evans, L. D. B., Andersson, T., Portelius, E., Smith, J., Dias, T. B., Saurat, N., McGlade, A., Kirwan, P., Blennow, K., Hardy, J., Zetterberg, H., & Livesey, F. J. (2015). APP Metabolism Regulates Tau Proteostasis in Human Cerebral Cortex Neurons. *Cell Reports*, *11*(5), 689–696. https://doi.org/10.1016/j.celrep.2015.03.068

Moretti, R. M., Montagnani Marelli, M., Mai, S., Cariboni, A., Scaltriti, M., Bettuzzi, S., & Limonta, P. (2007). Clusterin isoforms differentially affect growth and motility of prostate cells: Possible implications in prostate tumorigenesis. *Cancer Research*, *67*(21), 10325–10333. https://doi.org/10.1158/0008-5472.CAN-07-0516

Morgan, T. E., Laping, N. J., Rozovsky, I., Oda, T., Hogan, T. H., Finch, C. E., & Pasinetti, G. M. (1995). Clusterin expression by astrocytes is influenced by transforming growth factor/31 and heterotypic cell interactions. *Journal of Neuroimmunology*, 10.

Morishima, Y., Gotoh, Y., Zieg, J., Barrett, T., Takano, H., Flavell, R., Davis, R. J., Shirasaki, Y., & Greenberg, M. E. (2001). β-Amyloid Induces Neuronal Apoptosis Via a Mechanism that Involves the c-Jun N-Terminal Kinase Pathway and the Induction of Fas Ligand. *Journal of Neuroscience*, *21*(19), 7551–7560. https://doi.org/10.1523/JNEUROSCI.21-19-07551.2001

Mountcastle, V. B. (1998). *Perceptual Neuroscience: The Cerebral Cortex*. Harvard University Press.

Mulder, S. D., Nielsen, H. M., Blankenstein, M. A., Eikelenboom, P., & Veerhuis, R. (2014). Apolipoproteins E and J interfere with amyloid-beta uptake by primary human astrocytes and microglia *in vitro*: ApoE and ApoJ Hamper Amyloid-Beta Uptake. *Glia*, *62*(4), 493–503. https://doi.org/10.1002/glia.22619

Mullan, M., Crawford, F., Axelman, K., Houlden, H., Lilius, L., Winblad, B., & Lannfelt, L. (1992). A pathogenic mutation for probable Alzheimer's disease in the APP gene at the N–terminus of β–amyloid. *Nature Genetics*, *1*(5), 345–347. https://doi.org/10.1038/ng0892-345

Muñoz-Sanjuán, I., & Brivanlou, A. H. (2002). Neural induction, the default model and embryonic stem cells. *Nature Reviews. Neuroscience*, *3*(4), 271–280. https://doi.org/10.1038/nrn786

Muratore, C. R., Rice, H. C., Srikanth, P., Callahan, D. G., Shin, T., Benjamin, L. N. P., Walsh, D. M., Selkoe, D. J., & Young-Pearse, T. L. (2014). The familial Alzheimer's disease APPV717I mutation alters APP processing and Tau expression in iPSC-derived neurons. *Human Molecular Genetics*, *23*(13), 3523–3536. https://doi.org/10.1093/hmg/ddu064

Murrell, J., Farlow, M., Ghetti, B., & Benson, M. (1991). A mutation in the amyloid precursor protein associated with hereditary Alzheimer's disease. Science, 254(5028), 97–99. https://doi.org/10.1126/science.1925564

Musiek, E. S., & Holtzman, D. M. (2015). Three Dimensions of the Amyloid Hypothesis: Time, Space, and "Wingmen". *Nature Neuroscience*, *18*(6), 800–806. https://doi.org/10.1038/nn.4018

Mutations | ALZFORUM. (n.d.). Retrieved 2 January 2021, from https://www.alzforum.org/mutations

Nagele, R. G., D'Andrea, M. R., Lee, H., Venkataraman, V., & Wang, H.-Y. (2003). Astrocytes accumulate Ab42 and give rise to astrocytic amyloid plaques in Alzheimer disease brains. *Brain Research*, 13.

Naj, A. C., Jun, G., Beecham, G. W., Wang, L.-S., Vardarajan, B. N., Buros, J., Gallins, P. J., Buxbaum, J. D., Jarvik, G. P., Crane, P. K., Larson, E. B., Bird, T. D., Boeve, B. F., Graff-Radford, N. R., De Jager, P. L., Evans, D., Schneider, J. A., Carrasquillo, M. M., Ertekin-Taner, N., … Schellenberg, G. D. (2011). Common variants at *MS4A4/MS4A6E*, *CD2AP*, *CD33* and *EPHA1* are associated with late-onset Alzheimer's disease. *Nature Genetics*, *43*(5), 436–441. https://doi.org/10.1038/ng.801

Näslund, J., Schierhorn, A., Hellman, U., Lannfelt, L., Roses, A. D., Tjernberg, L. O., Silberring, J., Gandy, S. E., Winblad, B., & Greengard, P. (1994). Relative abundance of Alzheimer A beta amyloid peptide variants in Alzheimer disease and normal aging. *Proceedings of the National Academy of Sciences of the United States of America*, *91*(18), 8378–8382.

National Institute on Aging. (2019). *Alzheimer's Disease Fact Sheet*. http://www.nia.nih.gov/health/alzheimers-disease-fact-sheet

Nelson, P. T., Alafuzoff, I., Bigio, E. H., Bouras, C., Braak, H., Cairns, N. J., Castellani, R. J., Crain, B. J., Davies, P., Tredici, K. D., Duyckaerts, C., Frosch, M. P., Haroutunian, V., Hof, P. R., Hulette, C. M., Hyman, B. T., Iwatsubo, T., Jellinger, K. A., Jicha, G. A., … Beach, T. G. (2012). Correlation of Alzheimer Disease Neuropathologic Changes With Cognitive Status: A Review of the Literature. *Journal of Neuropathology & Experimental Neurology*, *71*(5), 362–381. https://doi.org/10.1097/NEN.0b013e31825018f7

Nielsen, H. M., Mulder, S. D., Beliën, J. A. M., Musters, R. J. P., Eikelenboom, P., & Veerhuis, R. (2010). Astrocytic Aβ1-42 uptake is determined by Aβ-aggregation state and the presence of amyloid-associated proteins: Uptake of Aβ1-42 Oligomers and Fibrils. *Glia*, *58*(10), 1235–1246. https://doi.org/10.1002/glia.21004

Nielsen, H. M., Veerhuis, R., Holmqvist, B., & Janciauskiene, S. (2009). Binding and uptake of Aβ1-42 by primary human astrocytes *in vitro*. *Glia*, *57*(9), 978–988. https://doi.org/10.1002/glia.20822

Nilselid, A.-M., Davidsson, P., Nägga, K., Andreasen, N., Fredman, P., & Blennow, K. (2006). Clusterin in cerebrospinal fluid: Analysis of carbohydrates and quantification of native and glycosylated forms. *Neurochemistry International*, *48*(8), 718–728. https://doi.org/10.1016/j.neuint.2005.12.005

Nishimasu, H., Ran, F. A., Hsu, P. D., Konermann, S., Shehata, S. I., Dohmae, N., Ishitani, R., Zhang, F., & Nureki, O. (2014). Crystal Structure of Cas9 in Complex with Guide RNA and Target DNA. *Cell*, *156*(5), 935–949. https://doi.org/10.1016/j.cell.2014.02.001

Nizard, P., Tetley, S., Le Dréan, Y., Watrin, T., Le Goff, P., Wilson, M. R., & Michel, D. (2007). Stress-Induced Retrotranslocation of Clusterin/ApoJ into the Cytosol. *Traffic*, *8*(5), 554–565. https://doi.org/10.1111/j.1600-0854.2007.00549.x

Nozawa, T., Furukawa, N., Aikawa, C., Watanabe, T., Haobam, B., Kurokawa, K., Maruyama, F., & Nakagawa, I. (2011). CRISPR Inhibition of Prophage Acquisition in Streptococcus pyogenes. *PLoS ONE*, *6*(5), e19543. https://doi.org/10.1371/journal.pone.0019543

Nuutinen, T., Huuskonen, J., Suuronen, T., Ojala, J., Miettinen, R., & Salminen, A. (2007). Amyloid-β 1–42 induced endocytosis and clusterin/apoJ protein accumulation in cultured human astrocytes. *Neurochemistry International*, *50*(3), 540–547. https://doi.org/10.1016/j.neuint.2006.11.002

Oh, S.-B., Kim, M. S., Park, S., Son, H., Kim, S.-Y., Kim, M.-S., Jo, D.-G., Tak, E., & Lee, J.-Y. (2019). Clusterin contributes to early stage of Alzheimer's disease pathogenesis. *Brain Pathology (Zurich, Switzerland)*, *29*(2), 217–231. https://doi.org/10.1111/bpa.12660

Ortiz-Virumbrales, M., Moreno, C. L., Kruglikov, I., Marazuela, P., Sproul, A., Jacob, S., Zimmer, M., Paull, D., Zhang, B., Schadt, E. E., Ehrlich, M. E., Tanzi, R. E., Arancio, O., Noggle, S., & Gandy, S. (2017). CRISPR/Cas9-Correctable mutation-related molecular and physiological phenotypes in iPSC-derived Alzheimer's PSEN2 N141I neurons. *Acta Neuropathologica Communications*, *5*(1), 77. https://doi.org/10.1186/s40478-017-0475-z

O'Sullivan, J., Whyte, L., Drake, J., & Tenniswood, M. (2003). Alterations in the post-translational modification and intracellular trafficking of clusterin in MCF-7 cells during apoptosis. *Cell Death & Differentiation*, *10*(8), 914–927.

https://doi.org/10.1038/sj.cdd.4401254

Padhy, B., Hayat, B., Nanda, G. G., Mohanty, P. P., & Alone, D. P. (2017). Pseudoexfoliation and Alzheimer's associated *CLU* risk variant, rs2279590, lies within an enhancer element and regulates *CLU*, *EPHX2* and *PTK2B* gene expression. *Human Molecular Genetics*, *26*(22), 4519–4529. https://doi.org/10.1093/hmg/ddx329

Padhy, B., Nanda, G. G., Chowdhury, M., Padhi, D., Rao, A., & Alone, D. P. (2014). Role of an extracellular chaperone, Clusterin in the pathogenesis of Pseudoexfoliation Syndrome and Pseudoexfoliation Glaucoma. *Experimental Eye Research*, *127*, 69–76. https://doi.org/10.1016/j.exer.2014.07.005

Palomer, E., Buechler, J., & Salinas, P. C. (2019). Wnt Signaling Deregulation in the Aging and Alzheimer's Brain. *Frontiers in Cellular Neuroscience*, *13*. https://doi.org/10.3389/fncel.2019.00227

Paquet, D., Kwart, D., Chen, A., Sproul, A., Jacob, S., Teo, S., Olsen, K. M., Gregg, A., Noggle, S., & Tessier-Lavigne, M. (2016). Efficient introduction of specific homozygous and heterozygous mutations using CRISPR/Cas9. *Nature*, *533*(7601), 125–129. https://doi.org/10.1038/nature17664

Paradisi, S., Sacchetti, B., Balduzzi, M., Gaudi, S., & Malchiodi-Albedi, F. (2004). Astrocyte modulation of in vitro beta-amyloid neurotoxicity. *Glia*, *46*(3), 252–260. https://doi.org/10.1002/glia.20005

Parr, C., Mirzaei, N., Christian, M., & Sastre, M. (2015). Activation of the Wnt/β-catenin pathway represses the transcription of the β-amyloid precursor protein cleaving enzyme (BACE1) via binding of T-cell factor-4 to BACE1 promoter. *FASEB Journal: Official Publication of the Federation of American Societies for Experimental Biology*, *29*(2), 623–635. https://doi.org/10.1096/fj.14-253211

Pasinetti, G. M., & Finch, C. E. (1991). Sulfated glycoprotein-2 (SGP-2) mRNA is expressed in rat striatal astrocytes following ibotenic acid lesions. *Neuroscience Letters*, *130*(1), 1–4. https://doi.org/10.1016/0304-3940(91)90213-D

Pasinetti, G. M., Johnson, S. A., Oda, T., Rozovsky, I., & Finch, C. E. (1994). Clusterin (SGP-2): A multifunctional glycoprotein with regional expression in astrocytes and neurons of the adult rat brain. *The Journal of Comparative Neurology*, *339*(3), 387–400. https://doi.org/10.1002/cne.903390307

Patani, R., Lewis, P. A., Trabzuni, D., Puddifoot, C. A., Wyllie, D. J. A., Walker, R., Smith, C., Hardingham, G. E., Weale, M., Hardy, J., Chandran, S., & Ryten, M. (2012). Investigating the utility of human embryonic stem cell-derived neurons to model ageing and neurodegenerative disease using whole-genome gene expression and splicing analysis. *Journal of Neurochemistry*, *122*(4), 738–751. https://doi.org/10.1111/j.1471-4159.2012.07825.x

Patel, H., Dobson, R. J. B., & Newhouse, S. J. (2019). A Meta-Analysis of Alzheimer's Disease Brain Transcriptomic Data. *Journal of Alzheimer's Disease*, *68*(4), 1635–1656. https://doi.org/10.3233/JAD-181085

Pattanayak, V., Lin, S., Guilinger, J. P., Ma, E., Doudna, J. A., & Liu, D. R. (2013). High-throughput profiling of off-target DNA cleavage reveals RNA-programmed Cas9 nuclease specificity. *Nature Biotechnology*, *31*(9), 839–843. https://doi.org/10.1038/nbt.2673

Pei, Y., Brun, S. N., Markant, S. L., Lento, W., Gibson, P., Taketo, M. M., Giovannini, M., Gilbertson, R. J., & Wechsler-Reya, R. J. (2012). WNT signaling increases proliferation and impairs differentiation of stem cells in the developing cerebellum. *Development*, *139*(10), 1724–1733. https://doi.org/10.1242/dev.050104

Pekny, M., & Pekna, M. (2014). Astrocyte Reactivity and Reactive Astrogliosis: Costs and Benefits. *Physiological Reviews*, *94*(4), 1077–1098. https://doi.org/10.1152/physrev.00041.2013

Pfaffl, M. W. (2001). A new mathematical model for relative quantification in real-time RT–PCR. *Nucleic Acids Research*, *29*(9), e45.

Pihlaja, R., Koistinaho, J., Kauppinen, R., Sandholm, J., Tanila, H., & Koistinaho, M. (2011). Multiple cellular and molecular mechanisms are involved in human Aβ clearance by transplanted adult astrocytes. *Glia*, *59*(11), 1643–1657. https://doi.org/10.1002/glia.21212

Pihlaja, R., Koistinaho, J., Malm, T., Sikkilä, H., Vainio, S., & Koistinaho, M. (2008). Transplanted astrocytes internalize deposited beta-amyloid peptides in a transgenic mouse model of Alzheimer's disease. *Glia*, *56*(2), 154–163. https://doi.org/10.1002/glia.20599

Pourcel, C., Salvignol, G., & Vergnaud, G. (2005). CRISPR elements in Yersinia pestis acquire new repeats by preferential uptake of bacteriophage DNA, and provide additional tools for evolutionary studies. *Microbiology (Reading, England)*, *151*(Pt 3), 653–663. https://doi.org/10.1099/mic.0.27437-0

Prochnow, H., Gollan, R., Rohne, P., Hassemer, M., Koch-Brandt, C., & Baiersdörfer, M. (2013). Non-Secreted Clusterin Isoforms Are Translated in Rare Amounts from Distinct Human mRNA Variants and Do Not Affect Bax-Mediated Apoptosis or the NF-κB Signaling Pathway. *PLoS ONE*, *8*(9), e75303. https://doi.org/10.1371/journal.pone.0075303

Purro, S. A., Dickins, E. M., & Salinas, P. C. (2012). The Secreted Wnt Antagonist Dickkopf-1 Is Required for Amyloid -Mediated Synaptic Loss. *Journal of Neuroscience*, *32*(10),

3492–3498. https://doi.org/10.1523/JNEUROSCI.4562-11.2012

Qi, X.-M., Wang, C., Chu, X.-K., Li, G., & Ma, J.-F. (2018). Intraventricular infusion of clusterin ameliorated cognition and pathology in Tg6799 model of Alzheimer's disease. *BMC Neuroscience*, *19*(1), 2. https://doi.org/10.1186/s12868-018-0402-7

Ramakrishna, S., Kwaku Dad, A.-B., Beloor, J., Gopalappa, R., Lee, S.-K., & Kim, H. (2014). Gene disruption by cell-penetrating peptide-mediated delivery of Cas9 protein and guide RNA. *Genome Research*, *24*(6), 1020–1027. https://doi.org/10.1101/gr.171264.113

Ran, F. A., Hsu, P. D., Lin, C.-Y., Gootenberg, J. S., Konermann, S., Trevino, A. E., Scott, D. A., Inoue, A., Matoba, S., Zhang, Y., & Zhang, F. (2013). Double nicking by RNA-guided CRISPR Cas9 for enhanced genome editing specificity. *Cell*, *154*(6), 1380–1389. https://doi.org/10.1016/j.cell.2013.08.021

Ranney, M. K., Ahmed, I. S. A., Potts, K. R., & Craven, R. J. (2007). Multiple pathways regulating the anti-apoptotic protein clusterin in breast cancer. *Biochimica et Biophysica Acta (BBA) - Molecular Basis of Disease*, *1772*(9), 1103–1111. https://doi.org/10.1016/j.bbadis.2007.06.004

Rapoport, M., Dawson, H. N., Binder, L. I., Vitek, M. P., & Ferreira, A. (2002). Tau is essential to -amyloid-induced neurotoxicity. *Proceedings of the National Academy of Sciences*, *99*(9), 6364–6369. https://doi.org/10.1073/pnas.092136199

Ray, M., & Zhang, W. (2010). Analysis of Alzheimer's disease severity across brain regions by topological analysis of gene co-expression networks. *BMC Systems Biology*, *4*, 136. https://doi.org/10.1186/1752-0509-4-136

Reddy, K. B., Jin, G., Karode, M. C., Harmony, J. A. K., & Howe, P. H. (1996). Transforming Growth Factor β (TGFβ)-Induced Nuclear Localization of Apolipoprotein J/Clusterin

in Epithelial Cells †. *Biochemistry*, *35*(19), 6157–6163. https://doi.org/10.1021/bi952981b

Ries, M., & Sastre, M. (2016). Mechanisms of Aβ Clearance and Degradation by Glial Cells. *Frontiers in Aging Neuroscience*, *8*. https://doi.org/10.3389/fnagi.2016.00160

Rizzi, F., Coletta, M., & Bettuzzi, S. (2009). Chapter 2 Clusterin (CLU): From One Gene and Two Transcripts to Many Proteins. In *Advances in Cancer Research* (Vol. 104, pp. 9–23). Academic Press. https://doi.org/10.1016/S0065-230X(09)04002-0

Robbins, J. P., Perfect, L., Ribe, E. M., Maresca, M., Dangla-Valls, A., Foster, E. M., Killick, R., Nowosiad, P., Reid, M. J., Polit, L. D., Nevado, A. J., Ebner, D., Bohlooly-Y, M., Buckley, N., Pangalos, M. N., Price, J., & Lovestone, S. (2018). Clusterin Is Required for β-Amyloid Toxicity in Human iPSC-Derived Neurons. *Frontiers in Neuroscience*, *12*. https://doi.org/10.3389/fnins.2018.00504

Roberson, E. D., Scearce-Levie, K., Palop, J. J., Yan, F., Cheng, I. H., Wu, T., Gerstein, H., Yu, G.-Q., & Mucke, L. (2007). Reducing Endogenous Tau Ameliorates Amyloid -Induced Deficits in an Alzheimer's Disease Mouse Model. *Science*, *316*(5825), 750–754. https://doi.org/10.1126/science.1141736

Rohne, P., Prochnow, H., & Koch-Brandt, C. (2016). The CLU-files: Disentanglement of a mystery. *Biomolecular Concepts*, *7*(1), 1–15. https://doi.org/10.1515/bmc-2015-0026

Rohne, P., Prochnow, H., Wolf, S., Renner, B., & Koch-Brandt, C. (2014). The Chaperone Activity of Clusterin is Dependent on Glycosylation and Redox Environment. *Cellular Physiology and Biochemistry*, *34*(5), 1626–1639. https://doi.org/10.1159/000366365

Rosenthal, S. L., Barmada, M. M., Wang, X., Demirci, F. Y., & Kamboh, M. I. (2014).

Connecting the Dots: Potential of Data Integration to Identify Regulatory SNPs in Late-Onset Alzheimer's Disease GWAS Findings. *PLOS ONE*, *9*(4), e95152. https://doi.org/10.1371/journal.pone.0095152

Roses, A. D., & Saunders, A. M. (1994). APOE is a major susceptibility gene for Alzheimer's disease. *Current Opinion in Biotechnology*, *5*(6), 663–667. https://doi.org/10.1016/0958-1669(94)90091-4

Rossner, S., Lange-Dohna, C., Zeitschel, U., & Perez-Polo, J. R. (2005). Alzheimer's disease beta-secretase BACE1 is not a neuron-specific enzyme. *Journal of Neurochemistry*, *92*(2), 226–234. https://doi.org/10.1111/j.1471-4159.2004.02857.x

Sabatte, J., Faigle, W., Ceballos, A., Morelle, W., Rodríguez Rodrígues, C., Remes Lenicov, F., Thépaut, M., Fieschi, F., Malchiodi, E., Fernández, M., Arenzana-Seisdedos, F., Lortat-Jacob, H., Michalski, J.-C., Geffner, J., & Amigorena, S. (2011). Semen Clusterin Is a Novel DC-SIGN Ligand. *The Journal of Immunology*, *187*(10), 5299–5309. https://doi.org/10.4049/jimmunol.1101889

Sander, J. D., & Joung, J. K. (2014). CRISPR-Cas systems for genome editing, regulation and targeting. *Nature Biotechnology*, *32*(4), 347–355. https://doi.org/10.1038/nbt.2842

Sanders, C. R. (2006). How γ-secretase hits a moving target. *ELife*, *5*. https://doi.org/10.7554/eLife.20043

Scaffidi, P., & Misteli, T. (2005). Reversal of the cellular phenotype in the premature aging disease Hutchinson-Gilford Progeria Syndrome. *Nature Medicine*, *11*(4), 440–445. https://doi.org/10.1038/nm1204

Scaffidi, P., & Misteli, T. (2006). Lamin A-Dependent Nuclear Defects in Human Aging. *Science (New York, N.Y.)*, *312*(5776), 1059–1063. https://doi.org/10.1126/science.1127168

Scali, C., Caraci, F., Gianfriddo, M., Diodato, E., Roncarati, R., Pollio, G., Gaviraghi, G., Copani, A., Nicoletti, F., Terstappen, G. C., & Caricasole, A. (2006). Inhibition of Wnt signaling, modulation of Tau phosphorylation and induction of neuronal cell death by DKK1. *Neurobiology of Disease*, *24*(2), 254–265. https://doi.org/10.1016/j.nbd.2006.06.016

Scaltriti, M., Bettuzzi, S., Sharrard, R. M., Caporali, A., Caccamo, A. E., & Maitland, N. J. (2004a). Clusterin overexpression in both malignant and nonmalignant prostate epithelial cells induces cell cycle arrest and apoptosis. *British Journal of Cancer*, *91*(10), 1842–1850. https://doi.org/10.1038/sj.bjc.6602193

Scaltriti, M., Santamaria, A., Paciucci, R., & Bettuzzi, S. (2004b). Intracellular Clusterin Induces G2-M Phase Arrest and Cell Death in PC-3 Prostate Cancer Cells1. *Cancer Research*, *64*(17), 6174–6182. https://doi.org/10.1158/0008-5472.CAN-04-0920

Scheuner, D., Eckman, C., Jensen, M., Song, X., Citron, M., Suzuki, N., Bird, T. D., Hardy, J., Hutton, M., Kukull, W., Larson, E., Levy-Lahad, L., Viitanen, M., Peskind, E., Poorkaj, P., Schellenberg, G., Tanzi, R., Wasco, W., Lannfelt, L., … Younkin, S. (1996). Secreted amyloid β–protein similar to that in the senile plaques of Alzheimer's disease is increased in vivo by the presenilin 1 and 2 and APP mutations linked to familial Alzheimer's disease. *Nature Medicine*, *2*(8), 864–870. https://doi.org/10.1038/nm0896-864

Seki, A., & Rutz, S. (2018). Optimized RNP transfection for highly efficient CRISPR/Cas9-mediated gene knockout in primary T cells. *The Journal of Experimental Medicine*, *215*(3), 985–997. https://doi.org/10.1084/jem.20171626

Selkoe, D. J., & Hardy, J. (2016). The amyloid hypothesis of Alzheimer's disease at 25 years. *EMBO Molecular Medicine*, *8*(6), 595–608.

https://doi.org/10.15252/emmm.201606210

Sellers, K. J., Elliott, C., Jackson, J., Ghosh, A., Ribe, E., Rojo, A. I., Jarosz-Griffiths, H. H., Watson, I. A., Xia, W., Semenov, M., Morin, P., Hooper, N. M., Porter, R., Preston, J., Al-Shawi, R., Baillie, G., Lovestone, S., Cuadrado, A., Harte, M., … Killick, R. (2018). Amyloid β synaptotoxicity is Wnt-PCP dependent and blocked by fasudil. *Alzheimer's & Dementia*, *14*(3), 306–317. https://doi.org/10.1016/j.jalz.2017.09.008

Sepulcre, J., Sabuncu, M. R., Li, Q., El Fakhri, G., Sperling, R., & Johnson, K. A. (2017). Tau and amyloid β proteins distinctively associate to functional network changes in the aging brain. *Alzheimer's & Dementia: The Journal of the Alzheimer's Association*, *13*(11), 1261–1269. https://doi.org/10.1016/j.jalz.2017.02.011

Serrano-Pozo, A., Mielke, M. L., Gómez-Isla, T., Betensky, R. A., Growdon, J. H., Frosch, M. P., & Hyman, B. T. (2011). Reactive Glia not only Associates with Plaques but also Parallels Tangles in Alzheimer's Disease. *The American Journal of Pathology*, *179*(3), 1373–1384. https://doi.org/10.1016/j.ajpath.2011.05.047

Seshadri, S., Fitzpatrick, A. L., Arfan Ikram, M., DeStefano, A. L., Gudnason, V., Boada, M., Bis, J. C., Smith, A. V., Carassquillo, M. M., Charles Lambert, J., Harold, D., Schrijvers, E. M. C., Ramirez-Lorca, R., Debette, S., Longstreth, W. T., Janssens, A. C. J. W., Shane Pankratz, V., Dartigues, J. F., Hollingworth, P., … Breteler, M. M. B. (2010). Genome-wide Analysis of Genetic Loci Associated with Alzheimer's Disease. *JAMA : The Journal of the American Medical Association*, *303*(18), 1832–1840. https://doi.org/10.1001/jama.2010.574

Shepherd, C. E., Affleck, A. J., Bahar, A. Y., Carew-Jones, F., & Halliday, G. M. (2020). Intracellular and secreted forms of clusterin are elevated early in Alzheimer's

disease and associate with both Aβ and tau pathology. *Neurobiology of Aging*, *89*, 129–131. https://doi.org/10.1016/j.neurobiolaging.2019.10.025

Sherrington, R., Rogaev, E. I., Liang, Y., Rogaeva, E. A., Levesque, G., Ikeda, M., Chi, H., Lin, C., Li, G., Holman, K., Tsuda, T., Mar, L., Foncin, J.-F., Bruni, A. C., Montesi, M. P., Sorbi, S., Rainero, I., Pinessi, L., Nee, L., … St George-Hyslop, P. H. (1995). Cloning of a gene bearing missense mutations in early-onset familial Alzheimer's disease. *Nature*, *375*(6534), 754–760. https://doi.org/10.1038/375754a0

Shi, Y., Kirwan, P., Smith, J., MacLean, G., Orkin, S. H., & Livesey, F. J. (2012). A Human Stem Cell Model of Early Alzheimer's Disease Pathology in Down Syndrome. *Science Translational Medicine*, *4*(124), 124ra29-124ra29. https://doi.org/10.1126/scitranslmed.3003771

Shi, Yichen, Kirwan, P., & Livesey, F. J. (2012). Directed differentiation of human pluripotent stem cells to cerebral cortex neurons and neural networks. *Nature Protocols*, *7*(10), 1836–1846. https://doi.org/10.1038/nprot.2012.116

Shi, Yichen, Kirwan, P., Smith, J., Robinson, H. P. C., & Livesey, F. J. (2012). Human cerebral cortex development from pluripotent stem cells to functional excitatory synapses. *Nature Neuroscience*, *15*(3), 477–486. https://doi.org/10.1038/nn.3041

Shipton, O. A., Leitz, J. R., Dworzak, J., Acton, C. E. J., Tunbridge, E. M., Denk, F., Dawson, H. N., Vitek, M. P., Wade-Martins, R., Paulsen, O., & Vargas-Caballero, M. (2011). Tau Protein Is Required for Amyloid β-Induced Impairment of Hippocampal Long-Term Potentiation. *The Journal of Neuroscience*, *31*(5), 1688–1692. https://doi.org/10.1523/JNEUROSCI.2610-10.2011

Shuai, P., Liu, Y., Lu, W., Liu, Q., Li, T., & Gong, B. (2015). Genetic associations of *CLU* rs9331888 polymorphism with Alzheimer's disease: A meta-analysis. *Neuroscience*

Letters, *591*, 160–165. https://doi.org/10.1016/j.neulet.2015.02.040

Sidiropoulos, K., Viteri, G., Sevilla, C., Jupe, S., Webber, M., Orlic-Milacic, M., Jassal, B., May, B., Shamovsky, V., Duenas, C., Rothfels, K., Matthews, L., Song, H., Stein, L., Haw, R., D'Eustachio, P., Ping, P., Hermjakob, H., & Fabregat, A. (2017). Reactome enhanced pathway visualization. *Bioinformatics*, *33*(21), 3461–3467. https://doi.org/10.1093/bioinformatics/btx441

Söllvander, S., Nikitidou, E., Brolin, R., Söderberg, L., Sehlin, D., Lannfelt, L., & Erlandsson, A. (2016). Accumulation of amyloid-β by astrocytes result in enlarged endosomes and microvesicle-induced apoptosis of neurons. *Molecular Neurodegeneration*, *11*(1), 38. https://doi.org/10.1186/s13024-016-0098-z

Sproul, A. A., Jacob, S., Pre, D., Kim, S. H., Nestor, M. W., Navarro-Sobrino, M., Santa-Maria, I., Zimmer, M., Aubry, S., Steele, J. W., Kahler, D. J., Dranovsky, A., Arancio, O., Crary, J. F., Gandy, S., & Noggle, S. A. (2014). Characterization and Molecular Profiling of PSEN1 Familial Alzheimer's Disease iPSC-Derived Neural Progenitors. *PLoS ONE*, *9*(1). https://doi.org/10.1371/journal.pone.0084547

Stewart, E. M., Aquilina, J. A., Easterbrook-Smith, S. B., Murphy-Durland, D., Jacobsen, C., Moestrup, S., & Wilson, M. R. (2007). Effects of glycosylation on the structure and function of the extracellular chaperone clusterin. *Biochemistry*, *46*(5), 1412–1422. https://doi.org/10.1021/bi062082v

Stiles, J., & Jernigan, T. L. (2010). The Basics of Brain Development. *Neuropsychology Review*, *20*(4), 327–348. https://doi.org/10.1007/s11065-010-9148-4

Suzuki, N., Cheung, T. T., Cai, X. D., Odaka, A., Otvos, L., Eckman, C., Golde, T. E., & Younkin, S. G. (1994). An increased percentage of long amyloid beta protein secreted by familial amyloid beta protein precursor (beta APP717) mutants.

Science, *264*(5163), 1336–1340. https://doi.org/10.1126/science.8191290

Symington, L. S., & Gautier, J. (2011). Double-Strand Break End Resection and Repair Pathway Choice. *Annual Review of Genetics*, *45*(1), 247–271. https://doi.org/10.1146/annurev-genet-110410-132435

Szaruga, M., Munteanu, B., Lismont, S., Veugelen, S., Horre, K., Mercken, M., Saido, T.C., Ryan, N.S., De Vos, T., Savvides, S.N., Gallardo, R., Schymkowitz, J., Rousseau, F., Fox, N.C., Hopf, C., De Strooper, B & Chavez-Gutierrez, L. (2017). Alzheimer's causing mutations shift Aβ length by destabilising γ-Secretase-Aβn Interactions. *Cell, 170*(3), 443-456.

Szymanski, M., Wang, R., Bassett, S. S., & Avramopoulos, D. (2011). Alzheimer's risk variants in the clusterin gene are associated with alternative splicing. *Translational Psychiatry*, *1*(7), e18–e18. https://doi.org/10.1038/tp.2011.17

Takahashi, K., Tanabe, K., Ohnuki, M., Narita, M., Ichisaka, T., Tomoda, K., & Yamanaka, S. (2007). Induction of Pluripotent Stem Cells from Adult Human Fibroblasts by Defined Factors. *Cell*, *131*(5), 861–872. https://doi.org/10.1016/j.cell.2007.11.019

Takahashi, K., & Yamanaka, S. (2006). Induction of Pluripotent Stem Cells from Mouse Embryonic and Adult Fibroblast Cultures by Defined Factors. *Cell*, *126*(4), 663–676. https://doi.org/10.1016/j.cell.2006.07.024

Takami, M., Nagashima, Y., Sano, Y., Ishihara, S., Morishima-Kawashima, M., Funamoto., S., & Ihara, Y. (2009). Gamma-secretase: successive tripeptide and tetrapeptide release from the transmembrane domain of beta-carboxyl terminal fragment. *Journal of Neuroscience, 29*(41), 13042-52.

Takase, O., Minto, A. W. M., Puri, T. S., Cunningham, P. N., Jacob, A., Hayashi, M., & Quigg, R. J. (2008). Inhibition of NF-κB-dependent Bcl-xL expression by clusterin promotes

albumin-induced tubular cell apoptosis. *Kidney International*, *73*(5), 567–577. https://doi.org/10.1038/sj.ki.5002563

Takata, M., Sasaki, M. S., Sonoda, E., Morrison, C., Hashimoto, M., Utsumi, H., Yamaguchi-Iwai, Y., Shinohara, A., & Takeda, S. (1998). Homologous recombination and non-homologous end-joining pathways of DNA double-strand break repair have overlapping roles in the maintenance of chromosomal integrity in vertebrate cells. *The EMBO Journal*, *17*(18), 5497–5508. https://doi.org/10.1093/emboj/17.18.5497

Tan, L., Wang, H.-F., Tan, M.-S., Tan, C.-C., Zhu, X.-C., Miao, D., Yu, W.-J., Jiang, T., Tan, L., & Yu, J.-T. (2016). Effect of *CLU* genetic variants on cerebrospinal fluid and neuroimaging markers in healthy, mild cognitive impairment and Alzheimer's disease cohorts. *Scientific Reports*, *6*. https://doi.org/10.1038/srep26027

Tanzi, R. E., & Bertram, L. (2005). Twenty Years of the Alzheimer's Disease Amyloid Hypothesis: A Genetic Perspective. *Cell*, *120*(4), 545–555. https://doi.org/10.1016/j.cell.2005.02.008

Tapia-Rojas, C., Burgos, P. V., & Inestrosa, N. C. (2016). Inhibition of Wnt signaling induces amyloidogenic processing of amyloid precursor protein and the production and aggregation of Amyloid-β (Aβ) $_{42}$ peptides. *Journal of Neurochemistry*, *139*(6), 1175–1191. https://doi.org/10.1111/jnc.13873

Teo, J.-L., & Kahn, M. (2010). The Wnt signaling pathway in cellular proliferation and differentiation: A tale of two coactivators. *Advanced Drug Delivery Reviews*, *62*(12), 1149–1155. https://doi.org/10.1016/j.addr.2010.09.012

Terry, R. D., Masliah, E., Salmon, D. P., Butters, N., DeTeresa, R., Hill, R., Hansen, L. A., & Katzman, R. (1991). Physical basis of cognitive alterations in alzheimer's disease: Synapse loss is the major correlate of cognitive impairment. *Annals of Neurology*,

30(4), 572–580. https://doi.org/10.1002/ana.410300410

Thal, D. R., Rüb, U., Orantes, M., & Braak, H. (2002). Phases of Aβ-deposition in the human brain and its relevance for the development of AD. *Neurology*, *58*(12), 1791–1800. https://doi.org/10.1212/WNL.58.12.1791

Thambisetty, M., An, Y., Kinsey, A., Koka, D., Saleem, M., Güntert, A., Kraut, M., Ferrucci, L., Davatzikos, C., Lovestone, S., & Resnick, S. M. (2012). Plasma clusterin concentration is associated with longitudinal brain atrophy in mild cognitive impairment. *NeuroImage*, *59*(1), 212–217. https://doi.org/10.1016/j.neuroimage.2011.07.056

Thambisetty, M., Simmons, A., Hye, A., Campbell, J., Westman, E., Zhang, Y., Wahlund, L.-O., Kinsey, A., Causevic, M., Killick, R., Kloszewska, I., Mecocci, P., Soininen, H., Tsolaki, M., Vellas, B., Spenger, C., & Lovestone, S. (2011). Plasma Biomarkers of Brain Atrophy in Alzheimer's Disease. *PLoS ONE*, *6*(12). https://doi.org/10.1371/journal.pone.0028527

Thambisetty, M., Simmons, A., Velayudhan, L., Hye, A., Campbell, J., Zhang, Y., Wahlund, L.-O., Westman, E., Kinsey, A., Güentert, A., Proitsi, P., Powell, J., Causevic, M., Killick, R., Lunnon, K., Lynham, S., Broadstock, M., Choudhry, F., Howlett, D. R., … Lovestone, S. (2010). Association of plasma clusterin concentration with severity, pathology, and progression in Alzheimer disease. *Archives of General Psychiatry*, *67*(7), 739–748. https://doi.org/10.1001/archgenpsychiatry.2010.78

Trougakos, I. P., & Gonos, E. S. (2004). Functional Analysis of Clusterin/Apolipoprotein J in Cellular Death Induced by Severe Genotoxic Stress. *Annals of the New York Academy of Sciences*, *1019*(1), 206–210. https://doi.org/10.1196/annals.1297.033

Trougakos, I. P., Lourda, M., Agiostratidou, G., Kletsas, D., & Gonos, E. S. (2005). Differential effects of clusterin/apolipoprotein J on cellular growth and survival. *Free Radical Biology and Medicine*, *38*(4), 436–449. https://doi.org/10.1016/j.freeradbiomed.2004.10.038

Trougakos, I. P., Lourda, M., Antonelou, M. H., Kletsas, D., Gorgoulis, V. G., Papassideri, I. S., Zou, Y., Margaritis, L. H., Boothman, D. A., & Gonos, E. S. (2009). Intracellular Clusterin Inhibits Mitochondrial Apoptosis by Suppressing p53-Activating Stress Signals and Stabilizing the Cytosolic Ku70-Bax Protein Complex. *Clinical Cancer Research*, *15*(1), 48–59. https://doi.org/10.1158/1078-0432.CCR-08-1805

Trougakos, I. P., So, A., Jansen, B., Gleave, M. E., & Gonos, E. S. (2004). Silencing Expression of the Clusterin/Apolipoprotein J Gene in Human Cancer Cells Using Small Interfering RNA Induces Spontaneous Apoptosis, Reduced Growth Ability, and Cell Sensitization to Genotoxic and Oxidative Stress. *Cancer Research*, *64*(5), 1834–1842. https://doi.org/10.1158/0008-5472.CAN-03-2664

Tycko, J., Myer, V. E., & Hsu, P. D. (2016). Methods for Optimizing CRISPR-Cas9 Genome Editing Specificity. *Molecular Cell*, *63*(3), 355–370. https://doi.org/10.1016/j.molcel.2016.07.004

Urban, J., Parczyk, K., Leutz, A., Kayne, M., & Kondor-Koch, C. (1987). Constitutive apical secretion of an 80-kD sulfated glycoprotein complex in the polarized epithelial Madin-Darby canine kidney cell line. *The Journal of Cell Biology*, *105*(6), 2735–2743.

Urnov, F. D., Rebar, E. J., Holmes, M. C., Zhang, H. S., & Gregory, P. D. (2010). Genome editing with engineered zinc finger nucleases. *Nature Reviews Genetics*, *11*(9), 636–646. https://doi.org/10.1038/nrg2842

van Belkum, A., Scherer, S., van Alphen, L., & Verbrugh, H. (1998). Short-Sequence DNA Repeats in Prokaryotic Genomes. *Microbiology and Molecular Biology Reviews*, *62*(2), 275–293.

van Rooij, J. G. J., Meeter, L. H. H., Melhem, S., Nijholt, D. A. T., Wong, T. H., Netherlands Brain Bank, Rozemuller, A., Uitterlinden, A. G., van Meurs, J. G., & van Swieten, J. C. (2019). Hippocampal transcriptome profiling combined with protein-protein interaction analysis elucidates Alzheimer's disease pathways and genes. *Neurobiology of Aging*, *74*, 225–233. https://doi.org/10.1016/j.neurobiolaging.2018.10.023

Vassar, R., Bennett, B. D., Babu-Khan, S., Kahn, S., Mendiaz, E. A., Denis, P., Teplow, D. B., Ross, S., Amarante, P., Loeloff, R., Luo, Y., Fisher, S., Fuller, J., Edenson, S., Lile, J., Jarosinski, M. A., Biere, A. L., Curran, E., Burgess, T., … Citron, M. (1999). β-Secretase Cleavage of Alzheimer's Amyloid Precursor Protein by the Transmembrane Aspartic Protease BACE. *Science*, *286*(5440), 735–741. https://doi.org/10.1126/science.286.5440.735

Veeraraghavalu, K., Zhang, C., Zhang, X., Tanzi, R. E., & Sisodia, S. S. (2014). Age-dependent, non-cell-autonomous deposition of amyloid from synthesis of β-amyloid by cells other than excitatory neurons. *The Journal of Neuroscience: The Official Journal of the Society for Neuroscience*, *34*(10), 3668–3673. https://doi.org/10.1523/JNEUROSCI.5079-13.2014

Vierbuchen, T., Ostermeier, A., Pang, Z. P., Kokubu, Y., Südhof, T. C., & Wernig, M. (2010). Direct conversion of fibroblasts to functional neurons by defined factors. *Nature*, *463*(7284), 1035–1041. https://doi.org/10.1038/nature08797

Wadhwani, A. R., Affaneh, A., Van Gulden, S., & Kessler, J. A. (2019). Neuronal apolipoprotein E4 increases cell death and phosphorylated tau release in alzheimer disease. *Annals of Neurology*, *85*(5), 726–739. https://doi.org/10.1002/ana.25455

Wang, C., Najm, R., Xu, Q., Jeong, D., Walker, D., Balestra, M. E., Yoon, S. Y., Yuan, H., Li, G., Miller, Z. A., Miller, B. L., Malloy, M. J., & Huang, Y. (2018). Gain of toxic apolipoprotein E4 effects in human iPSC-derived neurons is ameliorated by a small-molecule structure corrector. *Nature Medicine*, *24*(5), 647–657. https://doi.org/10.1038/s41591-018-0004-z

Watanabe, K., Ueno, M., Kamiya, D., Nishiyama, A., Matsumura, M., Wataya, T., Takahashi, J. B., Nishikawa, S., Nishikawa, S., Muguruma, K., & Sasai, Y. (2007). A ROCK inhibitor permits survival of dissociated human embryonic stem cells. *Nature Biotechnology*, *25*(6), 681–686. https://doi.org/10.1038/nbt1310

Weggen, S., & Beher, D. (2012). Molecular consequences of amyloid precursor protein and presenilin mutations causing autosomal-dominant Alzheimer's disease. *Alzheimer's Research & Therapy*, *4*(2), 9. https://doi.org/10.1186/alzrt107

Weinstein, D. C., & Hemmati-Brivanlou, A. (1999). Neural induction. *Annual Review of Cell and Developmental Biology*, *15*, 411–433. https://doi.org/10.1146/annurev.cellbio.15.1.411

Westra, E. R., Semenova, E., Datsenko, K. A., Jackson, R. N., Wiedenheft, B., Severinov, K., & Brouns, S. J. J. (2013). Type I-E CRISPR-Cas Systems Discriminate Target from Non-Target DNA through Base Pairing-Independent PAM Recognition. *PLOS Genetics*, *9*(9), e1003742. https://doi.org/10.1371/journal.pgen.1003742

Wilson, Robert S., Beckett, L. A., Bennett, D. A., Albert, M. S., & Evans, D. A. (1999). Change in Cognitive Function in Older Persons From a Community Population: Relation to

Age and Alzheimer Disease. *Archives of Neurology*, *56*(10), 1274. https://doi.org/10.1001/archneur.56.10.1274

Wojtas, A. M., Sens, J. P., Kang, S. S., Baker, K. E., Berry, T. J., Kurti, A., Daughrity, L., Jansen-West, K. R., Dickson, D. W., Petrucelli, L., Bu, G., Liu, C.-C., & Fryer, J. D. (2020a). Astrocyte-derived clusterin suppresses amyloid formation in vivo. *Molecular Neurodegeneration*, *15*(1), 71. https://doi.org/10.1186/s13024-020-00416-1

Wojtas, A. M., Carlomagno, Y., Sens, J. P., Kang, S. S., Jensen, T. D., Kurti, A., Baker, K. E., Berry, T. J., Phillips, V. R., Castanedes, M. C., Awan, A., DeTure, M., De Castro, C. H. F., Librero, A. L., Yue, M., Daughrity, L., Jansen-West, K. R., Cook, C. N., Dickson, D. W., … Fryer, J. D. (2020b). Clusterin ameliorates tau pathology in vivo by inhibiting fibril formation. *Acta Neuropathologica Communications*, *8*(1), 210. https://doi.org/10.1186/s40478-020-01079-1

Wojtas, A. M., Kang, S. S., Olley, B. M., Gatherer, M., Shinohara, M., Lozano, P. A., Liu, C.-C., Kurti, A., Baker, K. E., Dickson, D. W., Yue, M., Petrucelli, L., Bu, G., Carare, R. O., & Fryer, J. D. (2017). Loss of clusterin shifts amyloid deposition to the cerebrovasculature via disruption of perivascular drainage pathways. *Proceedings of the National Academy of Sciences*, *114*(33), E6962–E6971. https://doi.org/10.1073/pnas.1701137114

Wong, P., Pineault, J., Lakins, J., Taillefer, D., Léger, J., Wang, C., & Tenniswood, M. (1993). Genomic organization and expression of the rat TRPM-2 (clusterin) gene, a gene implicated in apoptosis. *The Journal of Biological Chemistry*.

Wood, J. G., Mirra, S. S., Pollock, N. J., & Binder, L. I. (1986). Neurofibrillary tangles of Alzheimer disease share antigenic determinants with the axonal microtubule-associated protein tau (tau). *Proceedings of the National Academy of Sciences of*

the United States of America, *83*(11), 4040–4043.

Woodruff, G., Young, J. E., Martinez, F. J., Buen, F., Gore, A., Kinaga, J., Li, Z., Yuan, S. H., Zhang, K., & Goldstein, L. S. B. (2013). The Presenilin-1 ΔE9 mutation results in reduced γ-secretase activity, but not total loss of PS1 function, in isogenic human stem cells. *Cell Reports*, *5*(4). https://doi.org/10.1016/j.celrep.2013.10.018

Wyss-Coray, T., Loike, J. D., Brionne, T. C., Lu, E., Anankov, R., Yan, F., Silverstein, S. C., & Husemann, J. (2003). Adult mouse astrocytes degrade amyloid-β in vitro and in situ. *Nature Medicine*, *9*(4), 453–457. https://doi.org/10.1038/nm838

Xing, Y.-Y., Yu, J.-T., Cui, W.-Z., Zhong, X.-L., Wu, Z.-C., Zhang, Q., & Tan, L. (2012). Blood Clusterin Levels, rs9331888 Polymorphism, and the Risk of Alzheimer's Disease. *Journal of Alzheimer's Disease*, *29*(3), 515–519. https://doi.org/10.3233/JAD-2011-111844

Xu, X (2009). γ-Secretase Catalyzes Sequential Cleavages of the AβPP Transmembrane Domain. *Journal of Alzheimer's Disease : JAD*, *16*(2), 211–224. https://doi.org/10.3233/JAD-2009-0957

Yagi, T., Ito, D., Okada, Y., Akamatsu, W., Nihei, Y., Yoshizaki, T., Yamanaka, S., Okano, H., & Suzuki, N. (2011). Modeling familial Alzheimer's disease with induced pluripotent stem cells. *Human Molecular Genetics*, *20*(23), 4530–4539. https://doi.org/10.1093/hmg/ddr394

Yang, C.-R., Leskov, K., Hosley-Eberlein, K., Criswell, T., Pink, J. J., Kinsella, T. J., & Boothman, D. A. (2000). Nuclear clusterin/XIP8, an x-ray-induced Ku70-binding protein that signals cell death. *Proceedings of the National Academy of Sciences*, *97*(11), 5907–5912. https://doi.org/10.1073/pnas.97.11.5907

Yang, C.-R., Yeh, S., Leskov, K., Odegaard, E., Hsu, H.-L., Chang, C., Kinsella, T. J., Chen, D. J., & Boothman, D. A. (1999). Isolation of Ku70-binding proteins (KUBs). *Nucleic Acids Research*, *27*(10), 2165–2174. https://doi.org/10.1093/nar/27.10.2165

Yang, L., Guell, M., Byrne, S., Yang, J. L., De Los Angeles, A., Mali, P., Aach, J., Kim-Kiselak, C., Briggs, A. W., Rios, X., Huang, P.-Y., Daley, G., & Church, G. (2013). Optimization of scarless human stem cell genome editing. *Nucleic Acids Research*, *41*(19), 9049–9061. https://doi.org/10.1093/nar/gkt555

Yang, S., Chang, R., Yang, H., Zhao, T., Hong, Y., Kong, H. E., Sun, X., Qin, Z., Jin, P., Li, S., & Li, X.-J. (2017). CRISPR/Cas9-mediated gene editing ameliorates neurotoxicity in mouse model of Huntington's disease. *The Journal of Clinical Investigation*, *127*(7), 2719–2724. https://doi.org/10.1172/JCI92087

Yankner, B. A., Duffy, L. K., & Kirschner, D. A. (1990a). *Neurotrophic and Neurotoxic Effects of Amyloid ,8 Protein: Reversal by Tachykinin Neuropeptides*. *250*, 4.

Yerbury, J. J., Poon, S., Meehan, S., Thompson, B., Kumita, J. R., Dobson, C. M., & Wilson, M. R. (2007). The extracellular chaperone clusterin influences amyloid formation and toxicity by interacting with prefibrillar structures. *The FASEB Journal*, *21*(10), 2312–2322. https://doi.org/10.1096/fj.06-7986com

Young, J. E., Boulanger-Weill, J., Williams, D. A., Woodruff, G., Buen, F., Revilla, A. C., Herrera, C., Israel, M. A., Yuan, S. H., Edland, S. D., & Goldstein, L. S. B. (2015). Elucidating Molecular Phenotypes Caused by the SORL1 Alzheimer's Disease Genetic Risk Factor Using Human Induced Pluripotent Stem Cells. *Cell Stem Cell*, *16*(4), 373–385. https://doi.org/10.1016/j.stem.2015.02.004

Young, J. E., Fong, L. K., Frankowski, H., Petsko, G. A., Small, S. A., & Goldstein, L. S. B. (2018). Stabilizing the Retromer Complex in a Human Stem Cell Model of

Alzheimer's Disease Reduces TAU Phosphorylation Independently of Amyloid Precursor Protein. *Stem Cell Reports*, *10*(3), 1046–1058. https://doi.org/10.1016/j.stemcr.2018.01.031

Yu, X., Liang, X., Xie, H., Kumar, S., Ravinder, N., Potter, J., de Mollerat du Jeu, X., & Chesnut, J. D. (2016). Improved delivery of Cas9 protein/gRNA complexes using lipofectamine CRISPRMAX. *Biotechnology Letters*, *38*(6), 919–929. https://doi.org/10.1007/s10529-016-2064-9

Zhang, F., Kumano, M., Beraldi, E., Fazli, L., Du, C., Moore, S., Sorensen, P., Zoubeidi, A., & Gleave, M. E. (2014). Clusterin facilitates stress-induced lipidation of LC3 and autophagosome biogenesis to enhance cancer cell survival. *Nature Communications*, *5*(1), 5775. https://doi.org/10.1038/ncomms6775

Zhang, H., Kim, J. K., Edwards, C. A., Xu, Z., Taichman, R., & Wang, C.-Y. (2005). Clusterin inhibits apoptosis by interacting with activated Bax. *Nature Cell Biology*, *7*(9), 909–915. https://doi.org/10.1038/ncb1291

Zhang, S., Li, X., Ma, G., Jiang, Y., Liao, M., Feng, R., Zhang, L., Liu, J., Wang, G., Zhao, B., Jiang, Q., Li, K., & Liu, G. (2016). CLU rs9331888 Polymorphism Contributes to Alzheimer's Disease Susceptibility in Caucasian But Not East Asian Populations. *Molecular Neurobiology*, *53*(3), 1446–1451. https://doi.org/10.1007/s12035-015-9098-1

Zhang, S., Zhang, D., Jiang, Y., Wu, L., Shang, H., Liu, J., Feng, R., Liao, M., Zhang, L., Liu, Y., Liu, G., & Li, K. (2015). CLU rs2279590 polymorphism contributes to Alzheimer's disease susceptibility in Caucasian and Asian populations. *Journal of Neural Transmission*, *122*(3), 433–439. https://doi.org/10.1007/s00702-014-1260-9

Zhang, Y., Thompson, R., Zhang, H., & Xu, H. (2011). APP processing in Alzheimer's disease. *Molecular Brain*, *4*, 3. https://doi.org/10.1186/1756-6606-4-3

Zhou, Y., Hayashi, I., Wong, J., Tugusheva, K., Renger, J. J., & Zerbinatti, C. (2014). Intracellular Clusterin Interacts with Brain Isoforms of the Bridging Integrator 1 and with the Microtubule-Associated Protein Tau in Alzheimer's Disease. *PLOS ONE*, *9*(7), e103187. https://doi.org/10.1371/journal.pone.0103187

Zhu, B., Wang, R. M., Wang, J. T., Chen, R. L., Zheng, Y. F., Zhang, L., & Zhao, Z. G. (2017). Correlation of rs9331888 polymorphism with Alzheimer's disease among Caucasian and Chinese populations: A meta-analysis and systematic review. *Metabolic Brain Disease*, *32*(4), 981–989. https://doi.org/10.1007/s11011-017-9957-8

Zlokovic, V. (1996). Cerebrovascular transport of Alzheimer's amyloid-beta and apolipoproteins j and e: possible anti-amyloidogenic role of the blood-brain barrier. 59(18), 15.